Modeling, Estimation, and Feedback Techniques in Type 2 Diabetes

Ahdab, Mohamad Al

DOI (link to publication from Publisher):
10.54337/aau614554303

Publication date:
2023

Document Version
Publisher's PDF, also known as Version of record

MODELING, ESTIMATION, AND FEEDBACK TECHNIQUES IN TYPE 2 DIABETES

BY
MOHAMAD AL AHDAB

DISSERTATION SUBMITTED 2023

AALBORG UNIVERSITY
DENMARK

Modeling, Estimation, and Feedback Techniques in Type 2 Diabetes

Ph.D. Dissertation

Mohamad Al Ahdab

Aalborg University
Department of Electronic Systems
Fredrik Bajers Vej 7B
DK-9220 Aalborg

Dissertation submitted: August 2023

PhD supervisor:: Associate Professor John-Josef Leth
Aalborg University

PhD committee: Associate Professor Anders La Cour-Harbo (chairman)
Aalborg University, Denmark

Associate Professor Chiara Dalla Man
Padova University, Italy

Senior Scientist Hans-Michael Kaltenbach
Eidgenössische Technische Hochschule Zürich, Switzerland

PhD Series: Technical Faculty of IT and Design, Aalborg University

Department: Department of Electronic Systems

ISSN (online): 2446-1628
ISBN (online): 978-87-7573-651-5

Published by:
Aalborg University Press
Kroghstræde 3
DK – 9220 Aalborg Ø
Phone: +45 99407140
aauf@forlag.aau.dk
forlag.aau.dk

Printed in Denmark by Stibo Complete, 2023

To my parents, for their endless sacrifices and support.

Abstract

Type 2 Diabetes (T2D) is a growing global health concern, with an alarming increase in prevalence worldwide. It affects millions of individuals, placing a tremendous burden on healthcare systems and individuals alike. Effective T2D management is essential to prevent complications such as cardiovascular diseases, neuropathy, and kidney damage, which can significantly impact subjects' health and well-being. Managing T2D requires a multifaceted approach that encompasses lifestyle modifications, dietary interventions, medication adherence, and insulin therapy. However, achieving good glucose control and maintaining a balanced lifestyle can be intricate and demanding for individuals with T2D. Factors such as individual variations in response to treatment, fluctuating dietary patterns, the inaccuracies of glucose measuring devices, and the challenges associated with medication adherence present challenges in diabetes management. To tackle these challenges, this PhD thesis explores the development and application of algorithmic tools and models to enhance T2D management.

Firstly, a detailed mathematical model is developed to simulate the glucose-insulin dynamics in T2D subjects. The model incorporates various factors such as physical activity, stress levels, oral medications, and different types of injected insulin. The model is intended to aid medical staff in evaluating treatment plans, and in the education and training of medical students.

In addition, the thesis proposes a stochastic model that can be individualized using typical data gathered during the treatment of individuals with T2D. This model incorporates both behavioral parameters, such as patterns of meal consumption, and physiological parameters, including insulin sensitivity and secretion. The thesis explores various estimation and fitting methods, primarily relying on Markov Chain Monte Carlo and Sequential Monte Carlo strategies, to estimate these parameters and the states of the proposed model. The aim of the model and the fitting approaches is to enhance the personalization of treatment plans and provide valuable additional information for managing glucose levels, benefiting both the medical staff and individuals with T2D.

Moreover, two strategies are proposed to enhance the readings from glucose sensors. These enhancements aid in more accurate monitoring and help individuals in making informed decisions regarding their treatment.

Furthermore, the thesis introduces physiological-model-free algorithms for calculating long-acting insulin doses in T2D subjects. These algorithms are compared against standard of care and state-of-the-art methods using simulations with different T2D models. The developed strategies demonstrated better performance with the simulation studies, offering potential advancements in insulin dosing practices.

Lastly, the thesis explores a method for scheduling nudges to promote medication adherence among subjects with T2D. This approach shows promise in encouraging individuals to follow their treatment plans, thereby enhancing the overall management outcomes of T2D.

Overall, this thesis investigates various avenues to improve the management of T2D and offers different frameworks for future tool development. The presented frameworks and methodologies pave the way for future developments in the field, providing valuable resources for medical professionals and offering a better quality of life for individuals with T2D.

Resumé

Type 2 diabetes (T2D) er en voksende global sundhedsproblem med en bekymrende stigning i forekomsten på verdensplan. Det påvirker millioner af mennesker og lægger en enorm byrde på både sundhedssystemer og enkeltpersoner. Effektiv T2D-styring er afgørende for at forebygge komplikationer som kardiovaskulære sygdomme, neuropati og nyreskader, der kan have betydelig indflydelse på personers sundhed og velbefindende. Styring af T2D kræver en mangefacetteret tilgang, der omfatter ændringer i livsstilen, kosttilpasninger, medicinoverholdelse og insulinterapi. Dog kan opnåelse af god glukosekontrol og opretholdelse af en afbalanceret livsstil være komplekst og krævende for personer med T2D. Faktorer som individuelle variationer i behandlingsrespons, svingende kostmønstre, unøjagtigheder ved måling af glukose og udfordringer ved medicinoverholdelse udgør udfordringer i diabetesstyring. For at tackle disse udfordringer udforsker denne ph.d.-afhandling udviklingen og anvendelsen af algoritmiske værktøjer og modeller til forbedring af T2D-styring. Først udvikles en detaljeret matematisk model til at simulere glukose-insulin-dynamikken hos T2D-patienter. Modellen inkorporerer forskellige faktorer som fysisk aktivitet, stressniveauer, orale medicin og forskellige typer af injiceret insulin. Modellen er beregnet til at hjælpe sundhedspersonale med at evaluere behandlingsplaner samt i uddannelsen af medicinstuderende. I afhandlingen er der også udviklet en stokastisk model, der kan individualiseres ved hjælp af typiske data indsamlet under behandlingen af personer med T2D. Denne model inkorporerer både adfærdsparametre som mønstre for måltidsindtagelse og fysiologiske parametre, herunder insulinfølsomhed og sekretion. Afhandlingen udforsker forskellige estimations- og tilpasningsmetoder, primært baseret på Markov Chain Monte Carlo og Sequential Monte Carlo-strategier, til at estimere disse parametre og tilstandene i den foreslåede model. Formålet med modellen og tilpasningsmetoderne er at forbedre individualiseringen af behandlingsplaner og give værdifuld supplerende information til håndtering af glukoseniveauer, til gavn både for sundhedspersonalet og personer med T2D. Derudover foreslås to strategier til at forbedre aflæsningerne fra glukosesensorer. Disse forbedringer hjælper med mere præcis overvågning og hjælper enkeltpersoner med at træffe informerede beslutninger om deres behandling. Envidere introducerer afhandlingen fysiologimodelfrie algoritmer til beregning af dosering af langttidsvirkende insulin hos personer med T2D. Disse algoritmer sammenlignes med standardpleje og state-of-the-art-metoder ved hjælp af simuleringer med forskellige T2D-modeller. De udviklede strategier demonstrerede bedre resultater i simuleringerne og tilbyder potentielle fremskridt inden for insulin-doseringspraksis. Endelig udforsker afhandlingen en metode til planlægning af "nudges" for at fremme medicinoverholdelse hos personer med T2D. Denne tilgang kan potentielt at opmuntre enkeltpersoner til at følge deres behandlingsplaner

og dermed forbedre de overordnede resultater af T2D-styring. Samlet set undersøger denne afhandling forskellige måder at forbedre T2D-styring på og udvikler forskellige koncepter for fremtidig værktøjsudvikling. De præsenterede koncepter og metoder baner vejen for fremtidige fremskridt på området og giver værdifulde ressourcer til sundhedspersonale samt tilbyder en bedre livskvalitet for personer med T2D.

Contents

Thesis Details

Thesis Title:	Modeling, Estimation, and Feedback Techniques in Type 2 Diabetes
Ph.D. Student:	Mohamad Al Ahdab
Supervisors:	Assoc. Prof. John-Josef Leth, Aalborg University
	Assoc. Prof. Torben Knudsen, Aalborg University
	Prof. Jakob Stoustrup, Aalborg University

The main body of this thesis consist of the following papers.

[A] Ahdab, M. A., Leth, J., Knudsen, T., Vestergaard, P., & Clausen, H. G., "Glucose-Insulin Mathematical Model for the Combined Effect of Medications and Life Style of Type 2 Diabetic Patients," *Biochemical Engineering Journal*, vol. 176, no. 108170, 2021.

[B] Ahdab, M. A., Clausen, H. G., Knudsen, T., Björk Araddóttir, T., Schmidt, S., Nørgaard, K., & Leth, J-J. , " Parameter Estimation in Type 2 Diabetes in the Presence of Unannounced Meals and Unmodelled Disturbances," *2021 European Control Conference (ECC)*, pp. 1278-1282, 2021.

[C] Ahdab, M. A., Papež, M., Knudsen, T., Bjork Aradóttir, T., Schmidt, S., Nørgaard, K., & Leth, J-J., " Parameter Estimation for a Jump Diffusion Model of Type 2 Diabetic Patients in the Presence of Unannounced Meals," *2021 IEEE Conference on Control Technology and Applications (CCTA)*, pp. 176-183, 2021.

[D] Ahdab, M. A., Papež, M., Knudsen, T., Bjork Aradóttir, T., Schmidt, S., Nørgaard, K., & Leth, J-J., " Stochastic Modeling and Inference for Type 2 Diabetes," *IEEE Transactions of Biomedical Engineering*, (Submitted, 2023).

[E] Ahdab, M. A., Knudsen, T., & Leth, J-J., "State Space Temporal Gaussian Processes for Glucose Measurements," *2022 European Control Conference (ECC)* , pp. 284-290, 2022.

[F] Ahdab, M. A., Benam, K. D., Khoshamadi, H., Fougner, A. L., & Gros, S., "Sensor Fusion for Glucose Monitoring Systems," *IFAC World Congress 2023*, (Accepted/In Press, 2023).

[G] Ahdab, M. A., Knudsen, T., Stoustrup, J., & Leth, J-J., "An Online Stochastic Optimization Approach for Insulin Intensification in Type 2 Diabetes with Attention to Pseudo-Hypoglycemia," *2022 61th IEEE Conference on Decision and Control (CDC)*, pp. 2572-2579, 2023.

[H] Ahdab, M. A., Knudsen, T., Stoustrup, J., & Leth, J-J., "Blood Glucose Reference Personalization for Subjects with Type 2 Diabetes," *2023 IEEE Conference on Control Technology and Applications (CCTA)*, (Accepted/In Press, 2023).

[I] Ahdab, M. A., Knudsen, T., Stoustrup, J., & Leth, J-J., "Online Optimization Approach for Calculating Insulin Doses for Individuals with Type 2 Diabetes," *IEEE Transactions on Control Systems Technology*, (Submitted, 2023).

[J] Ahdab, M. A., Knudsen, T., Stoustrup, J., & Leth, J-J., "Entropy for Optimal Control on a Simplex with an Application to Behavioral Nudging," *IEEE Control Systems Letters*, vol. 7, pp. 2797-2802, 2023.

This thesis has been submitted for assessment in partial fulfillment of the PhD degree. The thesis is based on the submitted or published scientific papers which are listed above. Parts of the papers are used directly or indirectly in the extended summary of the thesis. As part of the assessment, co-author statements have been made available to the assessment committee and are also available at the Faculty. The thesis is not in its present form acceptable for open publication but only in limited and closed circulation as copyright may not be ensured.

Preface

This thesis is submitted as a collection of papers in partial fulfilment of the requirements for the degree of Doctor of Philosophy at the Department of Electronic Systems, Automation and Control, Aalborg University, Denmark. The work covered by this thesis has been carried out in the period from January 2020 to July 2023 under the Adherence through cloud-based Personalised Treatment for Type 2 Diabetes (ADAPT-T2D) funded by the Innovation Fund Denmark (IFD) Grand Solutions. The thesis is structured in two parts, the first part gives an introduction and a summary for the contributions, and the second part consists of ten published or submitted papers.

I would like to express my heartfelt gratitude to my supervisors, Associate Professor John-Josef Leth, Associate Professor Torben Knudsen, and Professor Jakob Stoustrup, for their guidance and support throughout this project. In particular, I am deeply grateful to Associate Professor John-Josef Leth, who has been an exceptional mentor, providing invaluable career advice and staying up late with me on numerous nights to discuss and refine my research. His dedication and expertise have been instrumental in shaping my academic journey.

I am also indebted to my supervisors for their compassion and understanding during the challenging period when my father's health was compromised. Their unwavering support and flexibility allowed me to navigate this difficult time while maintaining my progress in my research.

Additionally, I would like to express my gratitude for my colleagues at the Control and Automation section at Aalborg University, namely Aitor Ramirez Gomez, Henrik Glavind Clausen, Simon Thorsteinsson, Deividas Eringis, Saruch Satishkumar Rathore, Mirhan Ürkmez, Rahul Misra, Salahuddin Abdul Rahman, Chandramouli Santhanam, and the entire staff at the section. Their stimulating conversations over the numerous shared coffee breaks have made my time at the university enjoyable and memorable.

I am also grateful to Tatjana for her unwavering patience and support. She has been a constant source of encouragement, always willing to lend an ear for my complaints and discussions about my research. Her genuine interest and efforts to understand my work have meant the world to me.

Lastly, I would like to express my deepest gratitude to my parents, Thakwan and Nadra, and my sister, Durdana. Their endless support has been the cornerstone of my achievements. Their unwavering presence, listening to me every day over phone calls, sharing in the highs and lows of my PhD journey, has been immeasurable. I sincerely hope for my father Thakwan's swift recovery to good health and for the well-being of both of my parents.

Mohamad Al Ahdab
Aalborg University, August 16, 2023

Part I

Summary

Chapter 1

Introduction

1 Motivation

Diabetes is a global health issue, with an estimated 537 million adults affected worldwide and a prevalence of 10.5 percent among adults aged 20 to 79 years (see figure 1.1, [33]). Among those, type 2 diabetes (T2D) accounts for approximately 98 percent of all diabetes diagnoses globally [29]. Moreover, the Center for Disease Control and Prevention Diabetes Surveillance System reported in 2022 that approximately 11.3 percent of adults (37.3 million people) had diagnosed diabetes, with an estimated 8.5 million cases undiagnosed, and 95 percent of them having T2D [27]. Furthermore, the rise in childhood obesity has raised concerns about a substantial increase in the prevalence of diabetes. Global data supports this concern, as the worldwide incidence rate of T2D among adolescents and young adults (aged 15 to 39 years) has increased from 117 to 183 per 100,000 population between 1990 and 2019 [58]. Given the widespread impact of T2D and its projected increase for the upcoming years, it is important to develop tools and strategies to help T2D subjects with managing their diabetes. T2D is characterized by high glucose concentration in the blood due to insulin resistance and insufficient insulin production.

Insulin is a hormone produced by the pancreas that plays a crucial role in regulating blood glucose (BG) levels. In T2D, the body's cells become resistant to the effects of insulin, leading to impaired glucose uptake. As a result, the pancreas tries to compensate by producing more insulin to overcome this resistance.

Over time, however, the pancreas may become unable to maintain adequate insulin production, leading to a deficiency in insulin levels. This stage is often referred to as "beta-cell dysfunction." As a consequence, BG levels remain high, leading to the diagnosis of T2D.

As T2D progresses, the combination of insulin resistance and diminished insulin secretion can result in persistent hyperglycemia (high BG concentrations). This chronic elevation in BG can lead to the development of complications affecting various organs and systems, including the cardiovascular system, eyes, kidneys, nerves, and others.

Managing T2D involves a comprehensive approach, starting with lifestyle changes such as

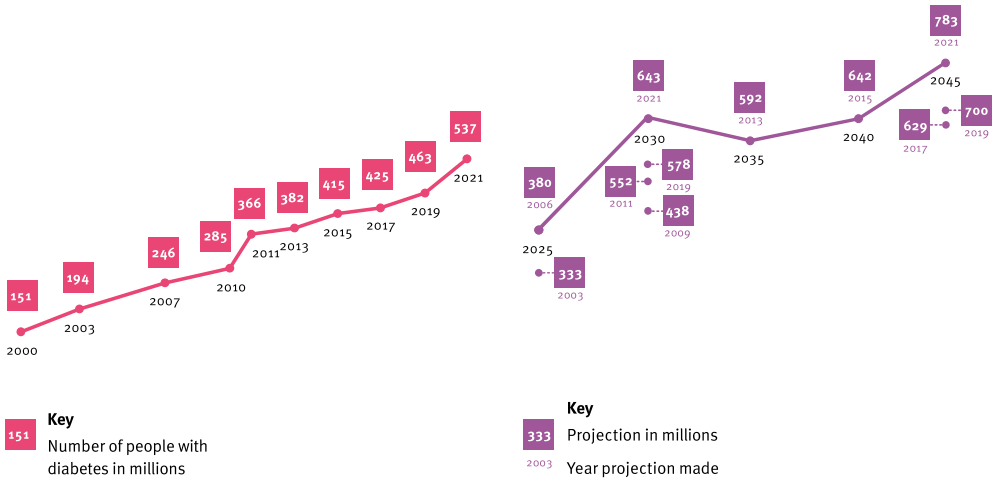

Fig. 1.1: Estimates and projections of the global prevalence of diabetes in the 20–79 year age group (millions) [33].

adopting a healthy diet, engaging in regular physical activity, maintaining a healthy weight, oral medications, and monitoring BG levels with glucose sensors. If these initial methods are ineffective in reducing high BG concentrations, long-acting (basal) insulin therapy can be initiated. This involves administering insulin once daily using insulin pens, with the dosage adjusted based on BG measurements. The process of determining the appropriate insulin dosage, known as insulin titration, is crucial. Insufficient insulin dosage can result in persistent hyperglycemia, which can lead to various complications as mentioned previously. On the other hand, an excessive insulin dosage can lower BG concentrations to unsafe levels (hypoglycemia), posing risks such as fainting, brain damage, or even death. Regular monitoring, adherence to treatment plans, and ongoing healthcare support are crucial in successfully managing this condition.

Effective management of the glucose concentration is crucial in order to prevent or delay the onset of complications such as cardiovascular diseases, kidney disease, nerve damage, and eye problems. However, achieving the optimal basal insulin doses can be challenging in clinical practice, often resulting in prolonged periods of uncontrolled hyperglycemia until a safe glucose level is reached [3, 56]. Several factors contribute to this difficulty. While consistent attention from medical staff is beneficial, the limited number of healthcare professionals compared to the large population of individuals with T2D poses a significant hurdle. Furthermore, the

high variability among T2D subjects and the varying effects of diet and lifestyle on insulin resistance make it challenging to determine the optimal insulin dosage. Consequently, many individuals experience hypoglycemia as a result of unintentional overdosing on basal insulin due to inaccuracies in dose calculations.

Additionally, imperfect glucose monitoring devices further complicate the management process. Inaccurate readings and inconsistent data make it harder to fine-tune insulin dosages and maintain glucose levels within the target range. This technological limitation adds another layer of complexity to achieving optimal glucose management.

Moreover, adherence to prescribed insulin and medication regimens can be problematic for many individuals with T2D. Economic constraints, the burden of daily insulin injections, fear of hypoglycemia, and concerns about weight gain are among the reasons that contribute to difficulties in adhering to the prescribed treatment plans.

Therefore, it is clear that developing tools and automatic techniques to aid health professionals and individual with T2D in the management of their condition is necessary and will make it easier for many individuals with T2D.

Thus, this thesis aims to address these limitations by developing different feedback and modeling techniques specifically tailored for T2D management. The proposed research encompasses several key areas: modeling, stochastic modeling and estimation, improving glucose measurements, developing feedback algorithms for long-acting insulin dose recommendations, and designing feedback techniques to discourage non-adherence to medication.

The outcomes of this research have the potential to impact the management of T2D by offering effective tools for teaching and testing, personalized feedback mechanisms, improving glucose measurements, and guiding insulin dose recommendations. Ultimately, the author hope that this research will be used in the future to improve the treatment outcomes for T2D subjects, reduce healthcare costs, and enhance the quality of life for individuals living with T2D.

2 Background and State of the Art

This section will delve into various facets and state-of-the-art tools that aid in the management of T2D.

2.1 Modeling

Generally, models used to study insulin-glucose dynamics in individuals with T2D can be classified into two different categories [16]. The first category covers complex models capable of simulating a wide range of real-life scenarios and can incorporate the effects of oral medications, stress, and physical activity. These models are not designed to be personalized with data to a specific subject; rather, their purpose is to test various treatment plans and provide educational resources for medical students and healthcare professionals. By utilizing these complex models, one can gain insights into different therapeutic strategies and broaden their understanding of insulin-glucose dynamics.

In contrast, the second category comprises simpler models that focus on the fundamental aspects of glucose-insulin dynamics. The defining characteristic of these models is their ability

to be personalized to a specific individual with the typical data that T2D subjects provide during treatment. This personalization feature allows them to offer valuable insights into an individual's glucose management and behavior. Moreover, these simpler models can be integrated with automatic insulin titration schemes, which leverage the model's personalized parameters to compute insulin doses.

Complex Models

Having a model to simulate the combined effect of oral medications, insulin doses, and lifestyle changes can be beneficial for medical staff involved in studying and designing different treatment plans for individuals with T2D. Additionally, these models can assist in the teaching and training of medical personnel in managing T2D. Moreover, the models can contribute to the understanding of how medications and lifestyle choices work together to manage T2D effectively.

It is worth noting that while complex models are more detailed and can account for a larger set of variables than simple models, the amount of different data, which is required to estimate parameters for these models and fit them for a specific subject, is large and difficult to obtain from subjects undergoing typical treatment plans.

Various complex mathematical structures have been developed to study the glucose-insulin dynamics in individuals with T2D. Some of these models focus on specific variables and effects, such as investigating brain glucose homeostasis and the effect of stress, as the one in [28], or studying the influence of physical activity, such as the one in [19]. Other complex models aim to be more general, like the ones proposed in [21, 52].

The model presented in [52] has been proposed and validated using detailed patient data. It incorporates a glucose ingestion model that considers glucose meals consumed after fasting conditions. Additionally, an insulin Degludec linear pharmacokinetic model has been incorporated into the model as described in [55]. Moreover, a version of this model has been implemented in a Graphical User Interface (GUI) to assist medical professionals in treatment plan design and in the training of medical students [54]. On the other hand, the model described in [21] is based on the work by [48], and it accounts for the effects of oral medications (metformin and vildagliptin), Glucagon, and Glucagon-Like Peptide-1 (GLP-1). This model utilizes the same glucose ingestion model as the one in [52].

The work in [28] focused on the glucose dynamics in the brain and provided a mathematical description for the effect of stress in diabetic individuals. Physical activity has been modelled before but mainly for T1D subjects. It has been included in models such as the ones in [10, 19, 46] with heart rate as an input, and [20] with accelerometer counts as an input.

Having a model to simulate the combined effect of different types of treatments together with the impact of stress and physical activity can enhance the process of evaluating and developing treatment plans for subjects with T2D and help in the training of medical staff to handle more realistic scenarios.

Simple Models

Fitting and personalizing mathematical models for specific individuals with T2D can be a challenging task due to the limited amount and type of data typically provided by T2D subjects. When it comes to individuals undergoing insulin-based treatment, the available data often

includes the amount of injected insulin and the measured glucose concentration, obtained through either Continuous Glucose Monitors (CGMs) devices, or Self-Monitored Blood Glucose values (SMBG).

CGM devices utilize a small sensor placed under the skin to continuously measure glucose levels in the interstitial fluid every few minutes. This provides a real-time view of a person's glucose levels and trends over time. However, T2D subjects find it difficult and burdensome to accurately provide data on their meal times, meal sizes, physical activity, and other factors that influence their BG levels.

SMBG devices provide blood glucose measurements at specific times of the day, usually before and after meals and before bedtime, which provide a snapshot of a person's blood glucose level at that moment in time.

As a result, fitting mathematical models and estimating physiological factors like insulin sensitivity and behavioral factors like the average number of meals per day become challenging with the limited data typically provided by T2D subjects.

In the context of T1D, several papers have addressed parameter estimation with known meal times and sizes [6, 7]. For unannounced meals, [47] employed sliding mode disturbance observers to estimate the states of a deterministic T2D model, along with the rate of appearance of glucose in the blood during meal consumption. Similarly, different techniques based on Kalman Filters (KFs) were applied for state estimation in T2D [45, 57]. Additionally, a least-squares approach was used in [18] with the inclusion of Fourier series. The model was then used in [17] to be personalized with specific T1D subjects through a web interface in order to provide treatment insights to the subjects themselves.

Regarding T2D specifically, [53] fitted physiological parameters of a T2D model using data obtained from a triple-tracer meal test, which included measurements of plasma glucose, insulin, and C-peptide concentrations. The work in [15] demonstrated the possibility of using the unscented KF to estimate three physiological parameters in a T2D model when the meal intake is known, utilizing CGM data. Furthermore, [14] proposed a stochastic model that accounted for unannounced meals and other disturbances, successfully estimating the states only for the proposed stochastic model but not the parameters. There are no works in the literature, at the time of writing this thesis, which estimates both physiological and behavioral related parameters for T2D subjects utilizing only CGM readings and insulin injection doses.

2.2 Algorithms for Glucose Sensors

Subjects with diabetes employ different methods to monitor their BG concentration during treatment, such as SMBG measurements and CGM devices. SMBG measurements provide sparse readings and are typically obtained three to four times per day, while CGM devices offer more frequent measurements and better glucose variability description [13, 37]. However, CGM devices measure the interstitium glucose (IG) concentration, leading to a time lag between CGM measurements and BG concentrations. Moreover, CGM devices are prone to systematic and random errors [38]. To address these issues, subjects often use SMBG measurements to calibrate their CGM devices [1].

Common off-the-shelf CGMs utilize wireless transmitters, such as Bluetooth, to connect with an artificial pancreas (AP) or a smart phone. Nevertheless, these communication methods can lose connection if the CGM and the receiver/pump are on opposite sides of the body,

e.g. when the subjects are sleeping. Additionally, external pressure on the CGM can cause compression artifacts, rapidly decreasing the measured BG level. These factors make single-sensor APs and dose calculators unreliable, necessitating the supervision of the CGM readings [23].

These challenges in the literature have been tackled through various approaches. One strategy is to use redundant sensors. For example, [34] used two sensors in their AP, where one would replace the active sensor in case of a failure.

Another approach is to obtain and fit models for CGM device errors, enabling better understanding for the sources of error in CGM devices [4, 5].

Several models exist in the literature for CGM measurement errors with varying degrees of complexity. Some models, such as the one in [9], perform a posteriori recalibration of CGM using BG references and estimate the measurement noise as the residual between CGM and estimated IG. Other models, like the refined version in [43], consider forcing functions and estimate time constants for BG to IG kinetics. More detailed models, such as those in [24, 25, 49, 50], incorporate polynomial models for gain and drift errors on CGM measurements. However, these models rely on more frequent reference BG values obtained in a clinical setting, which makes them difficult to use in subject-specific settings.

Several models have also been proposed for SMBG errors with different levels of complexity. Some models assume the relative error of SMBG measurements to be an identically and independently distributed Gaussian process with a bias term [8, 51]. Others model the error as Gaussian distributed with zero mean and variances dependent on the BG concentration [11]. Recently, [50] considered two different skew normal distributions for SMBG errors, depending on BG concentrations, and estimated parameters for the distributions along with parameters for exponential distributions accounting for outlier measurements. However, fitting these models require highly accurate reference BG data obtained in parallel with SMBG measurements.

Another approach to improving glucose sensor readings is to apply filtering methods. Works such as [26, 36, 40] aim to enhance CGM measurements using KFs and SMBG data. These methods incorporate extended KFs or dual rate KFs to estimate BG concentrations from SMBG and CGM measurements. However, these methods are still prone to failures in the CGM device or losses of connection.

2.3 Automatic Insulin Titration Strategies

Insulin titration, is the process of determining the optimal dosage of long-acting insulin for a diabetic subject. Inadequate insulin doses can result in persistently high BG levels, leading to hyperglycemia. Conversely, excessive insulin dosage can cause BG levels to drop dangerously low, resulting in hypoglycemia, which can lead to severe consequences like fainting, brain damage, or even death. Recognizing the challenges associated with manual titration methods, researchers have explored automated insulin dose calculators for individuals with T2D.

Traditional insulin guidance schemes, such as those described in [35], rely on SMBG measurements once a week to determine a fixed insulin dose. However, these titration strategies can be time-consuming and may take a relatively long time to bring fasting blood glucose (FBG) concentrations to a safe level. To address these limitations, alternative titration algorithms based on control theory have been proposed and studied in the literature.

One such approach, discussed in [2], utilizes a physiological model to guide the insulin titration process within a Model Predictive Control (MPC) setup. This strategy incorporates SMBG measurements and leverages a model-based framework. While this method has shown promise when compared to standard of care strategies. It relied on precise parameter values for the prediction model, which could be a limitation when considering a wide range of T2D subjects. The study also assumed an ideal scenario where the prediction model in the MPC is the same simulated model with the physiological parameters being the same at the start. In reality, the MPC approach would require personalizing the prediction model for each individual first by using historical data and keep updating it in real-time with state and parameter estimation methods. The diverse characteristics and variations among individuals with T2D make it inherently challenging to effectively utilize MPC approaches for insulin titration.

In contrast, the work presented in [39] introduces a "model-free" insulin titration approach using an Extremum Seeking Control (ESC) strategy. This method does not rely on a physiological model but instead optimizes the insulin dosage based on feedback from SMBG measurements. The effectiveness of this approach was demonstrated in the study, although it should be acknowledged that the strategy was tested against only one model with limited parameter variation and without accounting for measurement noise.

These strategies only consider fasting SMBG measurement as feedback. However, in reality, glucose levels throughout the day can vary and may fall into either the hypoglycemic or hyperglycemic range. For individuals with T1D, this issue has been addressed by developing methods that utilize CGM data as feedback within an AP system to calculate insulin doses, see [22] as an example. Nevertheless, the use of CGM data for calculating doses of long-acting insulin injections in T2D has not been explored in the literature before.

2.4 Nudging Towards Adherence to Medication

Adherence refers to the extent to which individuals follow their prescribed treatment regimen. It encompasses factors such as taking medications as prescribed, adhering to dietary and exercise guidelines, and attending regular healthcare appointments. Poor adherence to T2D management can have serious consequences, including worsening glycemic control, increased risk of complications, and reduced quality of life [32, 44]. Numerous factors contribute to non-adherence in T2D management. These can range from forgetfulness and lack of motivation to complex socio-economic and psychological barriers.

Recognizing the need for innovative strategies to improve adherence, researchers and healthcare professionals have turned to "nudging" techniques as a potential solution for non-adherence problems in the management of diabetes [41].

Nudging techniques leverage principles from behavioral economics and psychology to subtly influence individual behaviors and decision-making. By employing gentle prompts, reminders, and incentives, nudging aims to encourage positive behaviors without limiting individuals' freedom of choice. In the context of T2D management, nudging techniques can play a valuable role in helping individuals adhere to their prescribed treatment plans and make healthier lifestyle choices [41].

Recognizing the effectiveness of nudging techniques for different applications, several research studies have explored the optimization and automation of designing and selecting nudges for specific individuals or groups. One notable example is the work by [31], in which machine

learning techniques were used to develop a tool aimed at designing and delivering tailored nudges to enhance medication adherence among general cardiology patients participating in a clinical trial. The nudge content, timing, frequency, and delivery route were personalized by utilizing various types of feedback data obtained from individual patients. The results of the trial demonstrated a clinically relevant increase in adherence, highlighting the potential of personalized nudges in adherence to medication. Additionally, the work in [12] considered the optimal design of nudges for general applications within a Markov decision process framework derived from a resource-rational analysis based model. The framework is based on a resource-rational analysis-based model, aiming to determine the optimal types of nudges to employ. However, the frequency of nudges, an important factor in their effectiveness, is not explicitly considered in this approach. It is important to note that the frequency of nudges is typically desired to be kept at a moderate level to mitigate the risk of alert fatigue [42]. Alert fatigue happens when the rate of nudges becomes high enough to diminish the effectiveness of the nudges.

Nudging techniques offer promising avenues for enhancing adherence by gently influencing individual behaviors and decision-making processes. By optimizing and automating these techniques for subjects with T2D, healthcare professionals can support the T2D individuals in adopting and maintaining healthy habits, ultimately leading to better disease management and improved quality of life.

3 Research Objectives

Based on the previous discussion in the motivation, background, and state-of-the-art, this thesis aims to address several research objectives that contribute to improving the management of T2D. The research objectives are categorized into four focus areas: Modeling, Enhancing Glucose Sensors, Automatic Insulin Titration Strategies, and Nudging for Adherence. Under the Modeling focus area, the thesis aims to develop complex and simple models for T2D management. For complex models, the research objective is

Research Objective 1: To create a detailed comprehensive model that considers various variables and medications. This model will be utilized for testing treatment plans, educating medical staff, and evaluating dosing strategies.

On the other hand, simple models personalized for individual subjects using CGM data and insulin injections are investigated. The research objective here is

Research Objective 2: To propose a simple T2D model that includes physiological parameters in addition to parameters related to the behavior of the subject. In addition, the model should be fitted to CGM readings and insulin injection data. The fitted parameters of the model should be able to reflect information regarding the behaviour and the physiology of T2D individuals. The model can be used to detect unannounced meals, predicting glucose fluctuations, or identifying individuals who may benefit from specific behavioral interventions.

Enhancing Glucose Sensors is another focus area of the research. The main research objective in this domain is

Research Objective 3: To develop algorithmic tools that improve the quality of CGM readings. These tools will be designed to enhance the readings based on either SMBG readings or multiple CGM devices, contributing to more accurate and reliable glucose monitoring.

The research in this thesis also considers Automatic Insulin Titration Strategies. The main research objective here is

Research Objective 4: To develop new dosing strategies for long-acting insulin that are model-free, simple to implement, computationally light, and easily understandable for medical staff. These strategies should outperform the existing standard of care methods while ensuring safety. Moreover, these strategies should handle individual variability among the populations of T2D subjects. Furthermore, the developed strategies will be tested on different T2D models in conjunction with other dosing strategies, providing a comprehensive evaluation of their effectiveness.

Lastly, this thesis explores Nudging for Adherence. The research objective in this focus area is

Research Objective 5: To develop a method for scheduling and controlling the frequency of different types of nudges aimed at encouraging adherence to medication. These nudges will be designed to assist both medical staff and T2D individuals in effectively managing their BG levels.

By addressing these interconnected research objectives, this thesis aims to contribute to the advancement of T2D management by improving modeling techniques, enhancing glucose monitoring, optimizing insulin dosing strategies, and promoting adherence to medication.

4 Papers and Outline

In this section, the papers which constitutes the thesis and investigates the research objectives are listed with a short summery first. Afterwards, the outline for the rest of the thesis is provided in which the papers are discussed more thoroughly with some extensions.

Paper A

Ahdab, M. A., Leth, J., Knudsen, T., Vestergaard, P., & Clausen, H. G. (2021). Glucose-Insulin Mathematical Model for the Combined Effect of Medications and Life Style of Type 2 Diabetic Patients. In Biochemical Engineering Journal, vol. 176, no. 108170, 2021.

Summary: This paper introduces a mathematical model which captures the combined impact of various treatments and lifestyles on the dynamics of glucose and insulin in individuals with T2D. The model incorporates physical activity, stress, meals, and medications. For medications, the model considers metformin and DPP4-inhibitors as oral medications. In addition, the model incorporate long-acting insulin injection and fast-acting insulin injections. By incorporating these factors and medications, this model enables the evaluation and development of

treatment plans for T2D patients. The model builds upon existing literature by combining and modifying established models. Simulation experiments were carried out in the paper to check that it aligns with findings reported in T2D research. Furthermore, a discussion on how the model can be used in the assessment of treatment plans is carried out. Moreover, in Chapter 2, we provide a detailed summary of the paper, including extensions and improvements that were incorporated into a web-based GUI version accessible at `www.t2d.aau.dk`. This interactive platform has been successfully utilized by medical doctors at Aalborg University Hospital to educate and train medical students in the management of T2D.

The model presented in this paper with its extensions in Chapter 2 addresses **Research Objective 1** by developing a model which considers various medications and effects. The testing of dosing strategies part with the model in Paper A has been accomplished with Paper G, Paper H, and Paper I.

Paper B

Ahdab, M. A., Glavind Clausen, H., Knudsen, T., Bjork Aradottir, T., Schmidt, S., Norgaard, K., & Leth, J. (2021). Parameter Estimation in Type 2 Diabetes in the Presence of Unannounced Meals and Unmodelled Disturbances. In 2021 European Control Conference (ECC), pp. 1278-1282, 2021.

Summary: This paper presents a least squares approach to estimate the states and parameters of a simple model for the glucose-insulin dynamics of T2D subjects. The estimation is performed solely based on CGM and injected insulin. To evaluate the effectiveness of the method, clinical data and simulated data generated using proposed jump diffusion models for meals and disturbances were employed. Along with the estimation of the T2D subject model's states, unannounced meals, and disturbances, three parameters were also estimated. The estimated meal states were observed to accurately track the patterns of unannounced meals. This strategy enables the creation of a model which can be utilized for designing dosing strategies. Moreover, it facilitates the testing of various insulin and meal plans using the estimated disturbances and parameters for the specific T2D subject. Additionally, the study highlights the capability of jump diffusion models in simulating meals and disturbances. However, it is important to note that the method solely estimates the disturbances and meals as time-series data, without providing explicit parameters or a model that can be directly utilized by medical professionals or individuals with T2D to reflect on their management of glucose concentration.

This paper contributes to **Research Objective 2** by proposing a simple model with a least-squares approach that allows for the estimation of states and physiological parameters using only CGM data and information on injected insulin. The model is also personalized for the subject in the sense that it can be used to assess the validity of unannounced meals and detect unannounced ones.

Paper C

Ahdab, M. A., Papez, M., Knudsen, T., Aradottir, T. B., Schmidt, S., Norgaard, K., & Leth, J. (2021). Parameter Estimation for a Jump Diffusion Model of Type 2 Diabetic Patients in the Presence of Unannounced Meals. In 2021 IEEE Conference on Control Technology and Applications (CCTA), pp. 176-183, 2021.

Summary: In this paper, the jump diffusion model which is used for simulations in Paper B is considered for state and parameter estimation. Since the model is stochastic with non-gaussian process noise being the jump part of the model, a strategy based on the combination of Markov Chain Monte Carlo (MCMC) methods and Sequential Monte Carlo (SMC) is proposed. The estimation strategy was applied both on clinical data and simulation data consisting of CGM readings and injected insulin doses. The proposed stochastic model with the estimation strategy provided the possibility to estimate behavior related parameters for each T2D subject. The parameters are statistical parameters related to the size of meals and the frequency of them. In addition, a diffusion parameter on BG is estimated to represent unmodeled disturbances on the BG concentration. The strategy was successful in estimating the parameters related to the stochastic part of the model with CGM and insulin injection data. However, parameters related to the deterministic part of the model (drift part) such as insulin sensitivity are not estimated in the proposed strategy. Moreover, the estimation strategy with the proposed model struggled in fitting low values of BG.

This paper contributes to **Research Objective 2** by considering a jump diffusion model for parameter estimation and providing means to estimate parameters related to the behavior of T2D subjects.

Paper D

Ahdab, M. A., Knudsen, T., Stoustrup, J., & Leth, J-J. Stochastic Modeling and Inference for Type 2 Diabetes. In IEEE Transactions on Biomedical Engineering, Submitted, 2021.

Summary: In this paper, a jump diffusion model based on the one from Paper C is propsed. The model differs from the one in Paper C by including a term that allows the sizes of the meals to be correlated. In addition, the unmodeled disturbances in the model are included as the output of an Ornstein–Uhlenbeck (OU) process to consider that the unmodeled disturbances are also correlated. Moreover, a different MCMC with SMC estimation strategy is proposed and tested for the new model with CGM and insulin injection data. With the estimation strategy and the proposed stochastic model, parameters from both the stochastic and the deterministic part of the model were able to be estimated. Behavioral (statistics for meal sizes and frequency) together with physiological (e.g., parameters related to insulin sensitivity and insulin secretion) were able to be estimated. Moreover, unlike the model with the estimation method in Paper C, the model with the newly proposed method performs well for low BG values.

This paper contributes to **Research Objective 2** by proposing a stochastic model which contains both physiological and behavior related parameters. The model with an estimation strategy was shown to be able to be used for estimating physiological and behavior related parameters based on only CGM and insulin injection data. In addition, the model can be used to confirm announced meals and detect unannounced ones.

Paper E

Ahdab, M. A., Knudsen, T., & Leth, J. (2022). State Space Temporal Gaussian Processes for Glucose Measurements. In 2022 European Control Conference (ECC), pp. 284-290, 2022.

Summary: This paper investigates the possibility of obtaining a model for the error of CGM devices based on a single CGM device and SMBG measurements. The use of Temporal Gaussian Processes (TGP) as a potential solution is proposed and discussed. Various TGP models are suggested, and an MCMC algorithm with SMC strategy is employed to fit the models using simulated data of one CGM device and SMBG readings generated from detailed models of CGM and SMBG errors. The method demonstrates favorable performance and exhibits promise for utilizing TGP models as data-driven approaches for modeling the error of CGM devices.

This research contributes to **Research Objective 3** by presenting a model structure and fitting approach to derive personalized CGM error models using CGM readings and SMBG data. Although the method is computationally intensive, the approach proposed in this paper demonstrates the potential of investigating TGP models for CGM device errors. Developing a TGP model for CGM readings facilitates a better understanding of the errors associated with CGM measurements, enabling post-processing of CGM data to enhance its quality for other applications.

Paper F

Ahdab, M. A., Benam, K. D., Khoshamadi, H., Fougner, A. L., & Gros, S. Sensor Fusion for Glucose Monitoring Systems. In IFAC World Congress 2023, Accepted/In press, 2023.

Summary: In this paper, the Multiple Model Kalman Filter (MMKF) setup is introduced for fusing the readings of multiple CGM devices to obtain BG readings, which can be employed in automated insulin dosing systems such as AP systems. Furthermore, an MMKF with a Forgetting Factor (MMFKF) is proposed to address cases where the performance of CGM sensors varies over time. The proposed method and framework are evaluated using two distinct datasets acquired from separate animal experiments involving APs. The obtained results exhibit promising outcomes for the proposed setup and methods, indicating the potential of employing them to enhance the management of BG for subjects with diabetes.

The research presented in this paper contributes to **Research Objective 3** by putting forth a setup for obtaining reliable BG readings through the fusion of multiple CGM devices.

Paper G

Ahdab, M. A., Knudsen, T., Stoustrup, J., & Leth, J. (2022). An Online Stochastic Optimization Approach for Insulin Intensification in Type 2 Diabetes with Attention to Pseudo-Hypoglycemia. In 2022 61th IEEE Conference on Decision and Control (CDC), pp. 2572-2579, 2022.

Summary: This paper proposes a physiological model-free approach for determining optimal doses of long-acting insulin for individuals with T2D based on SMBG measurements to maintain their BG concentration within a safe range. The proposed strategy fine-tunes the parameters of a control law by employing an online optimization technique, optimizing a predefined cost function. The technique utilizes cost function evaluations only (zeorth-order) to obtain estimates of the gradient using a Recursive Least Square (RLS) scheme with directional forgetting. The estimated gradients are then used with an adaptive moment estimation-based

approach known as AdaBelief to tune the parameters of the control law. Furthermore, the proposed strategy is demonstrated to be able to account for a phenomenon called relative hypoglycemia or pseudo-hypoglycemia (PHG) by considering feedback ratings from the subjects regarding their hypoglycemia symptoms. PHG refers to instances where individuals experience hypoglycemia symptoms based on the rate at which their BG concentration decreases. The effectiveness of the insulin calculation strategy is showcased through simulations involving three different models, and its performance is compared against both standard of care insulin dosing strategies and the state-of-the-art model-free insulin dosing method in [39]. The proposed strategy was demonstrated to outperform the other dosing strategies under different simulations. Moreover, the propsed strategy is simple to compute and computationally light.

This paper contributes to **Research Objective 4** by proposing a simple physiological-model-free method which was demonstrated to have better glucose management metrics, defined in [30], when compared to current state-of-the-art titration methods on virtual subjects generated by three different physiological models.

Paper H

Ahdab, M. A., Knudsen, T., Stoustrup, J., & Leth, J-J. Blood Glucose Reference Personalization for Subjects with Type 2 Diabetes. In 2021 IEEE Conference on Control Technology and Applications (CCTA), Accepted/In press, 2023.

Summary: This paper investigates the concept of adapting the target glucose value or the reference glucose value for long-acting insulin titration strategies, including standard of care strategies. Two simple approaches for adapting the glucose reference are proposed. The first approach is based on an Integral-Derivative (ID) controller with a nonlinear error function, while the second approach involves a weighted average of outputs from multiple ID controllers, with the weights being adapted online. Both of these approaches rely on CGM data to adapt a glucose target, which is then used in the insulin titration strategy. The proposed methods are tested with various insulin titration strategies and simulated T2D subjects generated using three different models. The results demonstrate how adapting the reference glucose value for titration strategies based on CGM readings can reduce instances of hypoglycemia. By raising the reference glucose values for individuals who are more prone to hypoglycemia, these approaches provide a potential solution for improving safety in insulin titration strategies for T2D subjects.

This paper contributes to **Research Objective 4** by introducing the idea of adapting the glucose target based on CGM readings in long-acting insulin titration strategies for individuals with T2D. Additionally, it describes two simple methods to achieve this adaptation. The demonstrated reduction in instances of hypoglycemia with the proposed methods showcases their potential to enhance insulin titration strategies for T2D subjects, providing greater safety against hypoglycemic events.

Paper I

Ahdab, M. A., Knudsen, T., Stoustrup, J., & Leth, J-J. . Online Optimization Approach for Calculating Insulin Doses for Individuals with Type 2 Diabetes. In IEEE Transactions on Control Systems Technology, Submitted, 2023.

Summary: This paper presents a framework which combines the ideas presented in Paper G and Paper H. The paper introduces a framework for tuning the parameters of an insulin titration control law alongside a reference glucose value, employing an online optimization framework. This method can utilizes CGM data and/or SMBG data. The paper also proposes two distinct gradient estimation methods. The first method is a RLS approach with directional forgetting, similar to the one described in Paper G. The second method, termed the one-point residual feedback method, offers a computationally simpler alternative to RLS. Additionally, two different control laws are tested with the proposed online optimization framework. The framework, together with various titration strategies from existing literature, is assessed using virtual T2D subjects generated by three different models.

The proposed framework was shown to have better glucose management metrics, defined in [30], when compared to the other titration strategies from the literature. The paper addresses **Research Objective 4** by proposing a setup for tuning and adapting the parameters and glucose reference in various insulin titration methods for individuals with T2D. It was shown through simulations that the proposed method reduces instances of hypoglycemia, thereby highlighting its safety features and potential to mitigate hypoglycemic events.

Paper J

Ahdab, M. A., Knudsen, T., Stoustrup, J., & Leth, J-J. Entropy for Optimal Control on a Simplex with an Application to Behavioral Nudging. IEEE Control Systems Letters, vol. 7, pp. 2797-2802, 2023.

Summary: This paper focuses on the application of behavioral nudging, specifically in the context of discouraging non-adherence to medication in diabetes management through the lens of optimal control. By adopting an optimal control framework, the problem of scheduling different types of nudges with varying frequencies is addressed. The dynamical model employed in the paper is based on behavioral momentum theory, where the inputs represent the probability of selecting a particular type of nudge together with the average rate of nudges. The paper formulates an Optimal Control Problem (OCP) that belongs to a class of OCPs with inputs constrained to a variable-sized simplex, where the size is an additional input to be optimized over. Moreover, it is shown in the paper that the inclusion of the entropy function into the objective functional of this class of OCPs enables the derivation of closed-form solutions for it. Multiple examples are provided in the paper to illustrate the practical application of the OCP framework in conjunction with behavioral momentum theory. These examples demonstrate how the closed-form solutions can be utilized to schedule different types of nudges and their frequencies for a hypothetical scenario involving the encouragement of medication adherence in a diabetic individual.

This work contributes to **Research Objective 5** by offering a foundational framework for scheduling nudging strategies with their frequencies within the context of T2D management. It serves as a starting point for future research endeavors aimed at optimizing behavioral interventions and improving the management of T2D.

The papers in full can be found in the second part of the thesis. As for the remaining of this part, the following chapters will provide an extended summary for the topics these papers are addressing:

- Chapter 2 is concerned with the complex model proposed in Paper A. It provides more details on the model together with some extension on it. It also highlights how it has been used for teaching at Aalborg University Hospital.
- Chapter 3 is concerned with stochastic modeling and estimation for a simple model for T2D subjects. It summarizes the work from Paper B, Paper C, and Paper D.
- Chapter 4 is concerned with enhancing readings from CGM devices and it summarizes the work from Paper E, and Paper F.
- Chapter 5 is concerned with long-acting insulin dosing strategies. It summarizes the work from Paper G, Paper H, and Paper I.
- Chapter 6 is concerned with scheduling nudges for adherence. It summarizes the work in Paper J.

In addition, Chapter 7 will include concluding remarks for the work in this thesis.

5 Notations

This section will contain the notations used in the first part of the thesis, unless stated otherwise for a specific expression.

Let $[a, b]$ denote the closed interval from a to b, and $[a\ b]$ denote the row vector with coordinates a and b. For a random variable X, $X \sim \mu$ denotes either that X is distributed according to μ or sampled from μ. The notation $X \sim p_X(x)$ when $p_X(x)$ is the density for the random variable X. For random variables X and Y, the notation $p_{Y|X}(Y = y \mid X = x)$ or simply $p_{Y|X}(y \,|\, x)$ is used to denote the (conditional) density of the conditional distribution of Y given $X = x$. Additionally, the subscripts X, $Y \,|\, X$ are dropped in $p(x), p(y \,|\, x)$ for cases when it is clear from the context for ease of notation. Let two successive time instants t_k and t_{k+j} be such that $t_{k+j} - t_k = jT,\ j \in \mathbb{Z}$ with $T \in \mathbb{R}$, then variables $x(t_k), x(t_{k+j})$ are denoted as $x(k), x(k+j)$. Moreover, for a sequence of integers $k_1, \ldots, k_N$, the following notation is used $\boldsymbol{x}\,(k_1 : k_N) \coloneqq \begin{bmatrix} x(k_1) & \ldots & x(k_N) \end{bmatrix}^{\mathrm{T}}$. For integers $k_\ell < k_u$, the notation $\boldsymbol{x}\,[k_\ell : k_u] \coloneqq \begin{bmatrix} x(k_1) & \ldots & x(k_N) \end{bmatrix}^{\mathrm{T}}$ is used with $k_i \in [k_\ell, k_u]$ for all $i \in \{1, \ldots, N\}$. The notations $\mathcal{U}[a, b]$, $\mathcal{U}\left(\mathbb{B}^d\right)$, $\mathcal{U}\left(\mathbb{S}^{d-1}\right)$, $\mathrm{Exp}(\mu_e)$, $\mathcal{N}\left(\boldsymbol{\mu_n}, \boldsymbol{\Sigma}\right)$, $Ber(p_b)$, $Beta(\alpha, \beta)$, and $\mathrm{LogNormal}(\mu_\ell, \sigma_\ell)$ are for the uniform probability distribution on an interval $[a, b]$, the uniform distribution over the unit ball $\mathbb{B}^d \coloneqq \left\{\boldsymbol{x} \in \mathbb{R}^d : \|\boldsymbol{x}\|_2 \leq 1\right\}$, the uniform distribution over the unit sphere $\mathbb{S}^{d-1} \coloneqq \left\{\boldsymbol{x} \in \mathbb{R}^d : \|x\|_2 = 1\right\}$, the exponential distribution with mean μ_e, the normal distribution with mean $\boldsymbol{\mu}_n$ and variance $\boldsymbol{\Sigma}$, the Bernolli distribution with probability p_b, the Beta distribution with parameters α, β, and the log-normal distribution with parameters μ_ℓ and σ_ℓ, respectively.

The writing $p \propto q$ is to denote that p is proportional to q with a proportionality constant equal to the normalization constant. For a vector $\boldsymbol{x}$, $\mathrm{diag}\,(\boldsymbol{x})$ is written for the diagonal matrix with diagonal elements being the elements of $\boldsymbol{x}$. The symbols $\boldsymbol{I}_n$ and $\boldsymbol{0}_{n\times m}$ are used to denote the $n\times n$ identity and the $n\times m$ zero matrix, respectively. The symbol $\boldsymbol{1}_n$ is used to denote the n-dimensional column vector of 1s. The symbols $\geq_e, >_e, <_e, \leq_e$ are used for element-wise $\geq, >, <$, and $\leq$. For $\boldsymbol{u} \in \triangle_n^v \coloneqq \left\{\boldsymbol{u} \in \mathbb{R}^n_{\geq 0} \mid \|\boldsymbol{u}\|_1 = v\right\}$, the entropy function is defined as as $\phi\,(\boldsymbol{u}) \coloneqq -\sum_{i=1}^n u_i \ln\,(u_i)$ with $0\ln(0) \coloneqq 0$. For $\boldsymbol{u} \in \triangle_n^v$ and $\boldsymbol{w} >_e 0$, the Kullback–Leibler (KL) divergence (relative entropy) is denoted as $D_{KL}(\boldsymbol{u} \,||\, \boldsymbol{w}) = \sum_{i=1}^n u^i \ln\left(u^i/w^i\right)$. The symbols $\exp_e(\boldsymbol{x})$

and $\ln_e(\boldsymbol{x})$ are used for the element-wise exponential and logarithm of a vector $\boldsymbol{x}$, respectively. A projection operator is defined as $\Pi_{\Theta,\boldsymbol{\Sigma}}(\boldsymbol{x}) := \operatorname{argmin}_{\boldsymbol{\theta}\in\Theta}\|\boldsymbol{\Sigma}^{1/2}(\boldsymbol{\theta}-\boldsymbol{x})\|^2$ with $\boldsymbol{\Sigma}$ a positive definite matrix and Θ a compact set. For a vector $\boldsymbol{x} = [x_1 \ \dots \ x_N]^{\mathrm{T}}$, a vector of moving averages with a window $H \leq N$ is defined as $\boldsymbol{\mu}_H(\boldsymbol{x}) := 1/H \begin{bmatrix} \sum_{i=1}^{H} x_i & \dots & \sum_{i=N-H+1}^{N} x_i \end{bmatrix}^{\mathrm{T}}$. For $x \in \mathbb{R}$, the softplus function with parameter $\alpha > 0$ is defined as $\mathrm{s}_\alpha(x) := 1/\alpha \log\big(1+\exp(\alpha x)\big)$. Additionally, if $\boldsymbol{x}$ is a vector, then $\mathrm{s}_\alpha(\boldsymbol{x})$ is to be understood element-wise.

References

[1] G. Acciaroli, M. Vettoretti, A. Facchinetti, and G. Sparacino, "Chapter 9 - calibration of cgm systems," in *Glucose Monitoring Devices*, C. Fabris and B. Kovatchev, Eds. Academic Press, 2020, pp. 173–201.

[2] T. B. Aradóttir, D. Boiroux, H. Bengtsson, J. Kildegaard, M. L. Jensen, J. B. Jørgensen, and N. K. Poulsen, "Model predictive control for dose guidance in long acting insulin treatment of type 2 diabetes," *IFAC Journal of Systems and Control*, vol. 9, p. 100067, 2019.

[3] S. Arnolds, T. Heise, F. Flacke, and J. Sieber, "Common standards of basal insulin titration in t2dm," *Journal of Diabetes Science and Technology*, vol. 7, no. 3, pp. 771–788, 2013, pMID: 23759411.

[4] L. Biagi, A. Hirata Bertachi, I. Conget, C. Quirós, M. Giménez, F. J. Ampudia-Blasco, P. Rossetti, J. Bondia, and J. Vehí, "Extensive assessment of blood glucose monitoring during postprandial period and its impact on closed-loop performance," *Journal of diabetes science and technology*, vol. 11, no. 6, pp. 1089–1095, 2017.

[5] C. Boettcher *et al.*, "Accuracy of blood glucose meters for self-monitoring affects glucose control and hypoglycemia rate in children and adolescents with type 1 diabetes," *Diabetes technology & therapeutics*, vol. 17, no. 4, pp. 275–282, 2015.

[6] D. Boiroux, Z. Mahmoudi, and J. B. Jørgensen, "Parameter estimation in type 1 diabetes models for model-based control applications," in *2019 American Control Conference (ACC)*, 2019, pp. 4112–4117.

[7] D. Boiroux, M. Hagdrup, Z. Mahmoudi, N. K. Poulsen, H. Madsen, and J. B. Jørgensen, "Model identification using continuous glucose monitoring data for type 1 diabetes," *IFAC-PapersOnLine*, vol. 49, no. 7, pp. 759–764, 2016.

[8] J. C. Boyd and D. E. Bruns, "Quality specifications for glucose meters: assessment by simulation modeling of errors in insulin dose," *Clinical Chemistry*, vol. 47, no. 2, pp. 209–214, 2001.

[9] M. Breton and B. Kovatchev, "Analysis, modeling, and simulation of the accuracy of continuous glucose sensors," *Journal of diabetes science and technology*, vol. 2, no. 5, pp. 853–862, 2008.

[10] M. D. Breton, "Physical activity—the major unaccounted impediment to closed loop control," *Journal of Diabetes Science and Technology*, vol. 2, no. 1, pp. 169–174, 2008.

[11] M. D. Breton and B. P. Kovatchev, "Impact of blood glucose self-monitoring errors on glucose variability, risk for hypoglycemia, and average glucose control in type 1 diabetes: an in silico study," *Journal of Diabetes Science and Technology*, vol. 4, no. 3, pp. 562–570, 2010.

[12] F. Callaway, M. Hardy, and T. Griffiths, "Optimal nudging for cognitively bounded agents: A framework for modeling, predicting, and controlling the effects of choice architectures," Jan 2022. [Online]. Available: psyarxiv.com/7ahdc.

[13] S. Clarke and J. Foster, "A history of blood glucose meters and their role in self-monitoring of diabetes mellitus," *British journal of biomedical science*, vol. 69, no. 2, pp. 83–93, 2012.

[14] H. G. Clausen, T. Knudsen, M. Al Ahdab, T. B. Aradottir, S. Schmidt, K. Nrgaard, and J.-J. Leth, "A new stochastic approach for modeling glycemic disturbances in type 2 diabetes," *IEEE Transactions on Biomedical Engineering*, 2021.

[15] H. G. Clausen, J.-J. Leth, T. Knudsen, and H. Schiøler, "State estimation in type 2 diabetes using the continuous-discrete unscented Kalman filter," *IFAC-PapersOnLine*, vol. 53, no. 2, pp. 16 500–16 505, 2020.

[16] C. Cobelli, C. Dalla Man, G. Sparacino, L. Magni, G. De Nicolao, and B. P. Kovatchev, "Diabetes: models, signals, and control," *IEEE reviews in biomedical engineering*, vol. 2, pp. 54–96, 2009.

[17] P. Colmegna, A. Bisio, R. McFadden, C. Wakeman, M. C. Oliveri, R. Nass, and M. Breton, "Evaluation of a web-based simulation tool for self-management support in type 1 diabetes: A pilot study," *IEEE Journal of Biomedical and Health Informatics*, vol. 27, no. 1, pp. 515–525, 2023.

[18] P. Colmegna, K. Wang, J. Garcia-Tirado, and M. D. Breton, "Mapping data to virtual patients in type 1 diabetes," *Control Engineering Practice*, vol. 103, p. 104605, 2020.

[19] C. Dalla Man, M. D. Breton, and C. Cobelli, "Physical activity into the meal glucose—insulin model of type 1 diabetes: In silico studies," pp. 56–67, 2009.

[20] J. Deichmann, S. Bachmann, M.-A. Burckhardt, M. Pfister, G. Szinnai, and H.-M. Kaltenbach, "New model of glucose-insulin regulation characterizes effects of physical activity and facilitates personalized treatment evaluation in children and adults with type 1 diabetes," *PLOS Computational Biology*, vol. 19, no. 2, p. e1010289, 2023.

[21] M. Eftekhari and O. Vahidi, "Mechanism based pharmacokinetic pharmacodynamic modeling of vildagliptin as an add-on to metformin for subjects with type 2 diabetes," *Computer Modeling in Engineering & Sciences*, vol. 114, no. 2, pp. 153–171, 2018.

[22] A. El Fathi, C. Fabris, and M. D. Breton, "Titration of long-acting insulin using continuous glucose monitoring and smart insulin pens in type 1 diabetes: A model-based carbohydrate-free approach," *Frontiers in Endocrinology*, vol. 12, 2021.

[23] A. Facchinetti, "Continuous glucose monitoring sensors: past, present and future algorithmic challenges," *Sensors*, vol. 16, no. 12, p. 2093, 2016.

[24] A. Facchinetti, S. Del Favero, G. Sparacino, J. R. Castle, W. K. Ward, and C. Cobelli, "Modeling the glucose sensor error," *IEEE Transactions on Biomedical Engineering*, vol. 61, no. 3, pp. 620–629, 2013.

[25] A. Facchinetti, S. Del Favero, G. Sparacino, and C. Cobelli, "Model of glucose sensor error components: identification and assessment for new dexcom g4 generation devices," *Medical & biological engineering & computing*, vol. 53, no. 12, pp. 1259–1269, 2015.

[26] A. Facchinetti, G. Sparacino, and C. Cobelli, "Enhanced accuracy of continuous glucose monitoring by online extended kalman filtering," *Diabetes technology & therapeutics*, vol. 12, no. 5, pp. 353–363, 2010.

[27] M. Fang, D. Wang, J. Coresh, and E. Selvin, "Undiagnosed diabetes in us adults: prevalence and trends," *Diabetes care*, vol. 45, no. 9, pp. 1994–2002, 2022.

[28] L. Gaohua and H. Kimura, "A mathematical model of brain glucose homeostasis." *Theoretical biology and medical modelling*, vol. 6, no. 26, 2009.

[29] A. Green, S. M. Hede, C. C. Patterson, S. H. Wild, G. Imperatore, G. Roglic, and D. Beran, "Type 1 diabetes in 2017: global estimates of incident and prevalent cases in children and adults," *Diabetologia*, vol. 64, pp. 2741–2750, 2021.

[30] R. I. Holt, J. H. DeVries, A. Hess-Fischl, I. B. Hirsch, M. S. Kirkman, T. Klupa, B. Ludwig, K. Nørgaard, J. Pettus, E. Renard *et al.*, "The management of type 1 diabetes in adults. a consensus report by the american diabetes association (ada) and the european association for the study of diabetes (easd)," *Diabetes Care*, vol. 44, no. 11, pp. 2589–2625, 2021.

[31] B. D. Horne, J. B. Muhlestein *et al.*, "Behavioral nudges as patient decision support for medication adherence: the encourage randomized controlled trial," *American Heart Journal*, vol. 244, pp. 125–134, 2022.

[32] J. Huang, S. Ding, S. Xiong, and Z. Liu, "Medication adherence and associated factors in patients with type 2 diabetes: A structural equation model," *Frontiers in Public Health*, vol. 9, 2021. [Online]. Available: https://www.frontiersin.org/articles/10.3389/fpubh.2021.730845

[33] International Diabetes Federation, "IDF Diabetes Atlas, 10th edn," https://diabetesatlas.org/atlas/tenth-edition/, 2021 (accessed June 23th, 2023).

[34] P. G. Jacobs, J. El Youssef, J. Castle *et al.*, "Automated control of an adaptive bihormonal, dual-sensor artificial pancreas and evaluation during inpatient studies," *IEEE Trans Biomed Eng*, vol. 61, no. 10, pp. 2569–2581, 2014.

[35] T. Kadowaki, H. Jinnouchi, K. Kaku, M. L. Hersløv, J. Hyllested-Winge, and S. Nakamura, "Insulin degludec in a simple or stepwise titration algorithm in a japanese population of patients with type 2 diabetes: a randomized, 26-week, treat-to-target trial," *Diabetology international*, vol. 8, no. 1, pp. 87–94, 2017.

[36] E. J. Knobbe and B. Buckingham, "The extended kalman filter for continuous glucose monitoring," *Diabetes technology & therapeutics*, vol. 7, no. 1, pp. 15–27, 2005.

[37] B. Kovatchev and C. Cobelli, "Glucose variability: timing, risk analysis, and relationship to hypoglycemia in diabetes," *Diabetes Care*, vol. 39, no. 4, pp. 502–510, 2016.

[38] B. P. Kovatchev, S. D. Patek, E. A. Ortiz, and M. D. Breton, "Assessing sensor accuracy for non-adjunct use of continuous glucose monitoring," *Diabetes technology & therapeutics*, vol. 17, no. 3, pp. 177–186, 2015.

[39] D. Krishnamoorthy, D. Boiroux, T. B. Aradóttir, S. E. Engell, and J. B. Jørgensen, "A model-free approach to automatic dose guidance in long acting insulin treatment of type 2 diabetes," *IEEE Control Systems Letters*, vol. 5, no. 6, pp. 2030–2035, 2020.

[40] M. Kuure-Kinsey, C. C. Palerm, and B. W. Bequette, "A dual-rate kalman filter for continuous glucose monitoring," in *2006 International Conference of the IEEE Engineering in Medicine and Biology Society*. IEEE, 2006, pp. 63–66.

[41] Y. Kwan, T. Cheng, S. Yoon, L. Ho, C. Huang, E. Chew, J. Thumboo, T. Østbye, and L. Low, "A systematic review of nudge theories and strategies used to influence adult health behaviour and outcome in diabetes management," *Diabetes & Metabolism*, vol. 46, no. 6, pp. 450–460, 2020. [Online]. Available: https://www.sciencedirect.com/science/article/pii/S1262363620300574

[42] B. S. Last, A. M. Buttenheim *et al.*, "Systematic review of clinician-directed nudges in healthcare contexts," *BMJ open*, vol. 11, no. 7, p. e048801, 2021.

[43] D. Lunn, C. Wei, and R. Hovorka, "Fitting dynamic models with forcing functions: application to continuous glucose monitoring in insulin therapy," *Statistics in medicine*, vol. 30, no. 18, pp. 2234–2250, 2011.

[44] W. H. Polonsky and R. R. Henry, "Poor medication adherence in type 2 diabetes: recognizing the scope of the problem and its key contributors," *Patient preference and adherence*, pp. 1299–1307, 2016.

[45] C. M. Ramkissoon, P. Herrero, J. Bondia, and J. Vehi, "Unannounced meals in the artificial pancreas: Detection using continuous glucose monitoring," *Sensors (Basel, Switzerland)*, vol. 18, no. 3, p. 884, Mar 2018.

[46] M. Rashid, S. Samadi, M. Sevil, I. Hajizadeh, P. Kolodziej, N. Hobbs, Z. Maloney, R. Brandt, J. Feng, M. Park *et al.*, "Simulation software for assessment of nonlinear and adaptive multivariable control algorithms: Glucose–insulin dynamics in type 1 diabetes," *Computers & Chemical Engineering*, vol. 130, p. 106565, 2019.

[47] I. Sala-Mira, J.-L. Díez, B. Ricarte, and J. Bondia, "Sliding-mode disturbance observers for an artificial pancreas without meal announcement," *Journal of Process Control*, vol. 78, pp. 68 – 77, 2019.

[48] J. T. Sorensen, "A physiologic model of glucose metabolism in man and its use to design and assess improved insulin therapies for diabetes," Ph.D. dissertation, Massachusetts Institute of Technology, 1985.

[49] M. Vettoretti, C. Battocchio, G. Sparacino, and A. Facchinetti, "Development of an error model for a factory-calibrated continuous glucose monitoring sensor with 10-day lifetime," *Sensors*, vol. 19, no. 23, p. 5320, 2019.

[50] M. Vettoretti, A. Facchinetti, G. Sparacino, and C. Cobelli, "A model of self-monitoring blood glucose measurement error," *Journal of diabetes science and technology*, vol. 11, no. 4, pp. 724–735, 2017.

[51] N. S. Virdi and J. J. Mahoney, "Importance of blood glucose meter and carbohydrate estimation accuracy," *Journal of diabetes science and technology*, vol. 6, no. 4, pp. 921–926, 2012.

[52] R. Visentin, C. Cobelli, and C. Dalla Man, "The padova type 2 diabetes simulator from triple-tracer single-meal studies: in silico trials also possible in rare but not-so-rare individuals," *Diabetes technology & therapeutics*, vol. 22, no. 12, pp. 892–903, 2020.

[53] ——, "The padova type 2 diabetes simulator from triple-tracer single-meal studies: In silico trials also possible in rare but not-so-rare individuals," *Diabetes technology & therapeutics*, vol. 22, no. 12, pp. 892–903, 2020.

[54] ——, "A software interface for in silico testing of type 2 diabetes treatments," *Computer Methods and Programs in Biomedicine*, vol. 223, p. 106973, 2022.

[55] R. Visentin, M. Schiavon, and C. Dalla Man, "In silico cloning of target type 2 diabetes population for treatments development and decision support," in *2020 42nd Annual International Conference of the IEEE Engineering in Medicine & Biology Society (EMBC)*. IEEE, 2020, pp. 5111–5114.

[56] K. Wong, D. Glovaci, S. Malik, S. S. Franklin, G. Wygant, U. Iloeje, H. Kan, and N. D. Wong, "Comparison of demographic factors and cardiovascular risk factor control among u.s. adults with type 2 diabetes by insulin treatment classification," *Journal of Diabetes and its Complications*, vol. 26, no. 3, pp. 169 – 174, 2012.

[57] J. Xie and Q. Wang, "A variable state dimension approach to meal detection and meal size estimation: In silico evaluation through basal-bolus insulin therapy for type 1 diabetes," *IEEE Transactions on Biomedical Engineering*, vol. 64, no. 6, pp. 1249–1260, 2017.

[58] J. Xie, M. Wang, Z. Long, H. Ning, J. Li, Y. Cao, Y. Liao, G. Liu, F. Wang, and A. Pan, "Global burden of type 2 diabetes in adolescents and young adults, 1990-2019: systematic analysis of the global burden of disease study 2019," *bmj*, vol. 379, 2022.

Chapter 2

Complex Model

This chapter presents a summary on the structure of the model presented in Paper A [1]. In addition, it provides a description on some extensions to the model. Finally, it discusses how the model is used for testing treatment plans and teaching at Aalborg University Hospital.

1 Model Structure

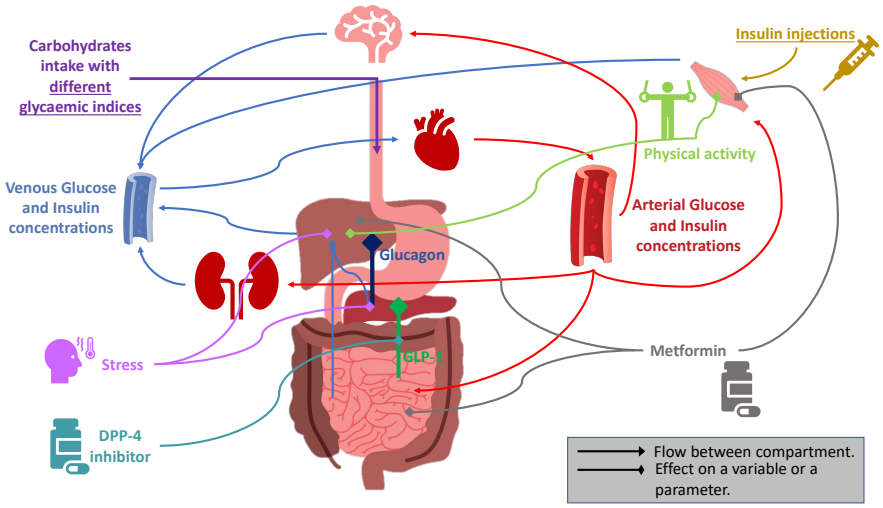

Fig. 2.1: Summary for the structure of the model. The underlined text denotes compartments that have undergone additional modifications to what is described in Paper A..

The model presented in Paper A builds upon the model proposed in [2], incorporating four main subsystems: the glucose subsystem, insulin subsystem, glucagon subsystem, and incretins hormone subsystem. Figure 2.1 provides an overview of the model. The glucose and insulin subsystems are represented by a series of compartments that simulate various parts of the human body, including the brain, heart and lungs, guts, liver, kidney, and the peripherals. The flow of substances between these compartments mimics the circulation of blood in the human body. Conversely, the glucagon and incretins subsystems are represented by single compartments, assuming equal concentration throughout the body. To capture the metabolic dynamics, the model incorporates metabolic production and uptake rates specific to each compartment. These rates are generally defined as the product of their basal values and scaling variables, which depend on the concentrations of insulin, glucose, and/or glucagon. The pancreas is modeled using a distinct nonlinear and hybrid model. Additionally, the model includes a glucose ingestion model based on [3] and modified to accommodate multiple meals throughout the day. Furthermore, oral treatment models for metformin and DPP-4 inhibitors are included, based on [4] and [5], respectively. However, modifications are made to the oral metformin model to handle different oral doses during the treatment. Moreover, a physical activity model, derived from [6], is incorporated into the model. Furthermore, models for long-acting and fast-acting insulin injections are included, based on [7]. Finally, stress is considered as a factor $\alpha_s \in [0, 1]$, following the approach described in [8]. The main model parameters were chosen by [9] for a healthy 70 kg male. In the case of diabetic scenarios, a subset of these parameters was estimated as described in [10]. Parameters for the additional models incorporated in this study are sourced from their respective literature references.

In addition to the model in Paper A, two main modifications were made to the model. The first one is to consider different types of carbohydrate meals in terms of Glycaemic Index (GI) and the second one is to modify the long-acting insulin injection model and calculate new parameters for it to consider the pharmacokinetics (the time profile for the absorption and clearance) of insulin Degludec. These modifications will be descried in section 2 and section 3. In 4, a description of how the model can be used for testintg treatment plans and teaching will be mentioned.

2 Including Meals with Different GI

The Glycaemic Index (GI) is a nutritional rating system which provides valuable insights into how carbohydrates in different foods affect BG concentrations. It is a measure of how quickly a particular food raises BG levels after consumption compared to a standard reference, usually pure sugar. The GI scale ranges from 0 to 100, with higher values indicating a more rapid increase in BG levels. Incorporating these different types of meals with different parameters for the ingestion model can be beneficial to simulate a more realistic scenario of an individual with T2D. Additionally, it can help the medical staff who is undergoing treatment and T2D individuals to understand how important it is to consider the GI when planning the diet. The ingestion model used in Paper A, which is based on the one from [3] with parameters from [10], is considered for meals with GI of 100 (reference meal) since it is based on an oral glucose test. To include meals with different GIs, several copies of the ingestion model structure are made for different values of GI. In more detail, consider $M \in \mathbb{Z}_{>0}$ different types of meals with

different GIs, then for each type of meal $j \in \{1, \dots, M\}$, the following dynamics are defined

$$\dot{q}^j_{Ss} = -k^j_{12q} q_{Ss} + \sum_{i=1}^{N^j_q(t)} u^j_{q_i} \delta(t - t_i),\ i \in \mathbb{Z}_+, \tag{2.1a}$$

$$\dot{q}^j_{Sl} = -k_{\text{empt}} q^j_{Sl} + k^j_{12q} q^j_{Ss}, \tag{2.1b}$$

$$\dot{q}^j_{\text{int}} = -k^j_{\text{abs}} q^j_{\text{int}} + k_{\text{empt}} q^j_{Sl}, \tag{2.1c}$$

$$\tag{2.1d}$$

where $u^j_{q_i}$ [mg] is the amount of carbohydrates of meal type j, $N^j_q(t)$ is the number of meals of type j up until time t, q^j_{Ss} [mg] is first stomach compartment for meal type j, q^j_{Sl} [mg] is the second stomach compartment for meal type j, and q^j_{int} [mg] is the intestines compartment for meal type j. The parameters k^j_{12q} [min^{-1}] and k^j_{abs} [min^{-1}] are absorption rate parameters related to the type of meal j and are tuned based on the GI of type meal j. Parameter k_{empt} [min^{-1}] is the stomach emptying rate parameter and it is related to the amount of carbohydrates ingested from the different meals as following

$$\begin{aligned} &k_{\text{empt}} = k_{\min} + \\ &\frac{k_{\max} - k_{\min}}{2} \left(\tanh\left(\varphi_1 \left(q_{Ss} + q_{Sl} - k_{\varphi_1} D_q\right)\right) - \tanh\left(\varphi_2 \left(q_{Ss} + q_{Sl} - k_{\varphi 2} D_q\right)\right) + 2 \right) \end{aligned} \tag{2.2a}$$

$$\dot{D}_e = -k_q D_e + \sum_{i=1}^{N_q(t)} u_{q_i} \delta(t - t_i) \tag{2.2b}$$

$$\dot{D}_q = k_q \left(u_{q_{N_q(t)}} - D_q \right) + D_m \sum_{i=1}^{N_q(t)} \delta(t - t_i) \tag{2.2c}$$

$$D_m = \begin{cases} D_e - D_q & u_{q_{N_q(0)}} \neq 0 \\ 1 & u_{q_{N_q(0)}} = 0 \end{cases} \tag{2.2d}$$

with $q_{Ss} = \sum_{j=1}^{M} q^j_{Ss}$, $q_{Sl} = \sum_{j=1}^{M} q^j_{Sl}$, $u_{q_i} = \sum_{j=1}^{M} u^j_{q_i}$, and $\varphi_1 = \frac{5}{2(1-k_{\varphi_1})D_q}, \varphi_2 = \frac{5}{k_{\varphi_2} D_q}$. The equation (2.1a) is to adjust the emptying rate of the stomach between k_{min} [min^{-1}] and k_{max} [min^{-1}] based on D_q [mg] which is related to the amount of accumulated meals. The state D_e [mg] in equation (2.2b) is to consider the accumulation of carbohydrates meals with a rate k_q [min^{-1}] in order to diminish the effect of meals with time. More details for these states and parameters can be found in Paper A. The notable part here which extends the ingestion model in Paper A is that there are M types of different meals with different rate constants k^j_{12q} [min^{-1}] and k^j_{abs} [min^{-1}] for $j = \{1, \dots, M\}$. The model from Paper A can be recovered by choosing the number of different meals to be $M = 1$ and using the same k_{12q} [mg] and k_{abs} [mg] for Paper A. The parameters for five different meal types, presented in table 2.1, were tuned. The parameters for the "Very High GI" meals were taken to be the same as the ones in Paper A. Considering the "Very High GI" meal type as the reference meal (GI of 100), the parameters for the other meal types are tuned such that the area under the BG curve after

two hours of consuming a 50 [g] meal of type j (AUC_j) is

$$\text{AUC}_j \approx \frac{\text{GI}_j \text{AUC}_1}{100}, \ \forall j \in \{2, \dots, M\}, \tag{2.3}$$

where GI_j is the GI for meal type j. The formula in (2.3) is based on the definition of the GI [11]. It is important to remark that this method of modeling the effect of different types of meals is simple and it is made as an extension for the ingestion model in Paper A with the aim to preserve its structure. For example, different types of meals will have a different effect on the emptying rate of the stomach, which is not captured in the model in (2.2).

Meal Type	GI
Very High GI	100
High GI	Approximately 80
Medium GI	Approximately 60
Low GI	Approximately 40
Very Low GI	Approximately 20

Table 2.1: Different Types of Meals with their Range of IG

3 Modifying the Insulin Injection Model

In this section, a modification to the long-acting insulin injection model from Paper A is provided. Moreover, a method to fit the parameters of the new model for a specific type of long-acting insulin will be discussed. The dynamics for the long-acting insulin injections in Paper A are based on the dynamics from [7] and modified to be the following

$$\dot{B}_{la} = \sum_{i=1}^{N_{la}(t)} \delta(t - t_i) \frac{10}{V_{PF}^I} u_{l_i} - k_{la} B_{la} \frac{C_{\max}}{1 + H_{la}}, \tag{2.4a}$$

$$\dot{H}_{la} = k_{la} B_{la} \frac{C_{\max}}{1 + H_{la}} - p_{la} \left(H_{la} - q_{la} D_{la}^3 \right), \tag{2.4b}$$

$$\dot{D}_{la} = p_{la} \left(H_{la} - q_{la} D_{la}^3 \right) - \frac{b_{la} D_{la}}{1 + I_{la}}, \tag{2.4c}$$

$$\dot{I}_{la} = r_{la} \frac{b_{la} D_{la}}{1 + I_{la}} - c_{la} I_{la}, \tag{2.4d}$$

where $N_{la}(t)$ is the number of injected long-acting insulin doses up until time t, u_{l_i} [mU] is the long-acting insulin dose at time t_i, and the states B_{la}, H_{la}, D_{la} [$\text{mU}\,\text{dL}^{-1}$] are states represent the different stages for injected long-insulin, see Paper A for more details. The modification to what is in Paper A is the equation (2.4d) for the state I_{la} [$\text{mU}\,\text{dL}^{-1}$] and the inclusion of the parameter c_{la}. In Paper A, the term D_{la} [$\text{mU}\,\text{dL}^{-1}$] enters the periphery insulin compartment. On the other hands, with the modification, the term I_{la} [$\text{mU}\,\text{dL}^{-1}$] enters the periphery insulin

compartment. This modification is done to make it more similar to the model presented in [7] in order to introduce a clearance parameter c_{la} [min^{-1}] specific to the type of injected insulin. In addition to the modifications, the parameters $k_{la}, q_{la}, b_{la}, p_{la}, r_{la}$, and c_{la} were fitted using an optimization procedure for insulin Degludec. To describe the optimization procedure, let $\boldsymbol{x} = [B_{la}\ H_{la}\ D_{la}\ I_{la}\ x_I]^{\mathrm{T}}$ with $\dot{x}_I = I_{la}$. Additionally, let $\boldsymbol{\theta} = [k_{la}\ q_{la}\ b_{la}\ p_{la}\ r_{la}\ c_{la}]^{\mathrm{T}}$. Then the optimization procedure to estimate the parameters $\boldsymbol{\theta}$ for a specific insulin profile is as following

$$\min_{\boldsymbol{\theta}} \quad \left(x_I\left(t_N\right) - AUC_{0-120}\right)^2 + \left(I_{la}(t_{hf}) - 0.5u_{l_0}\right)^2 \tag{2.5a}$$

$$\text{s.t.} \quad \boldsymbol{x}(t_{i+1}) = F(\boldsymbol{x}(t_i), \boldsymbol{\theta}),\ \forall i \in \{0, \ldots, N-1\}, \tag{2.5b}$$

$$I_{la}(t_i) \leq C_{\max}, \forall i \in \{0, \ldots, N\}, \tag{2.5c}$$

$$\boldsymbol{x}(t_i) \geq 0, \forall i \in \{0, \ldots, N\}, \tag{2.5d}$$

where F is a discretization to the continuous mode in (2.4) together with the integral state x_I, t_{hf} [hour] is the half-life time for insulin Degludec, AUC_{0-120} is the area under the insulin Degludec curve for 120 hours since injection u_{l_0}, and $C_{\max}$ is the maximum concentration of insulin Degludec. The parameters t_{hf}, AUC_{0-120}, and $C_{\max}$ are taken from [12]. Figure 2.2 shows the I_{la} state for an insulin Degludec dose of 0.4 [U/Kg] for a 70 [Kg] subject.

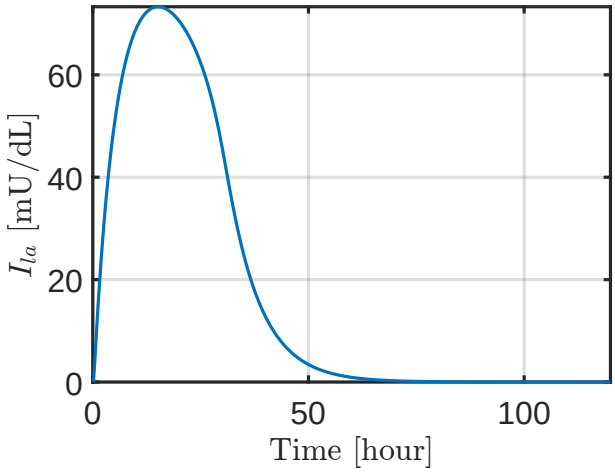

Fig. 2.2: The state I_{la} [mU/dL] for the model in (2.4) fitted to insulin Degludec using the method in (2.5).

4 Applications of the Model

The developed model can be utilized to assess different treatment plans under different medications and conditions. For example, medical professionals or medical students can evaluate

the impact of different diet styles on a diabetic individual, as depicted in figure 2.3. By analyzing figure 2.3, it can be deduced that when implementing a treatment plan that only relies on long-acting insulin, individuals who adhere to a low GI diet are more likely to consistently stay within the target range, as defined in [13], compared to those consuming meals with a high GI. Moreover, the model is used in the thesis and Paper G, H, and I to test different

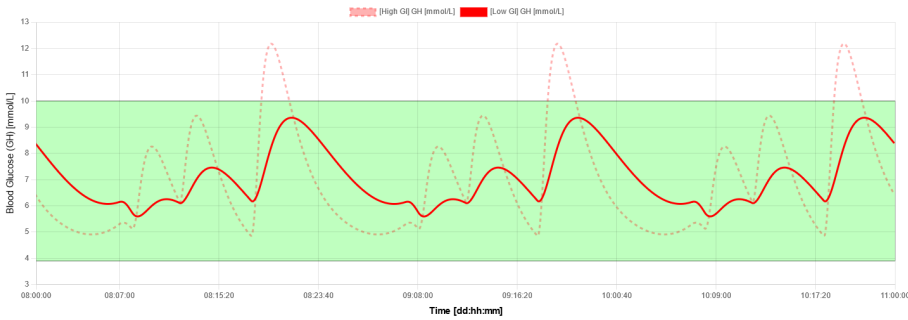

Fig. 2.3: A Subject taking a 30 [U] of insulin Degludec daily before breakfast. The solid line shows when the subject is eating meals with low GI compared to the dotted line in which the subject is consuming high GI meals. The range in green is the target range according to [13].

long-acting dosing algorithms. Additionally, an extended version of the model that includes various types of fast-acting insulin along with GLP-1 agonist medications[1] has been utilized in conjunction with a web-based GUI, accessible at `https://www.t2d.aau.dk/`. The GUI was used for teaching third semester medical students at Aalborg University Hospital in 2023. The user-friendly web-based GUI includes three distinct instances of the model, each representing a unique subject with varying levels of insulin sensitivity and secretion. Students were guided on how to approach treatment for the three subjects under a range of scenarios.

References

[1] M. A. Ahdab, J.-J. Leth, T. Knudsen, and H. Clausen, "Glucose-insulin dynamical model for type 2 diabetic patients," 2020, arXiv:2008.01614.

[2] M. Eftekhari and O. Vahidi, "Mechanism based pharmacokinetic pharmacodynamic modeling of vildagliptin as an add-on to metformin for subjects with type 2 diabetes," *Computer Modeling in Engineering & Sciences*, vol. 114, no. 2, pp. 153–171, 2018.

[3] C. Dalla Man, R. A. Rizza, and C. Cobelli, "Meal simulation model of the glucose-insulin system," *IEEE Transactions on Biomedical Engineering*, vol. 54, no. 10, pp. 1740–1749, Oct 2007.

[1]The inclusion of GLP-agonists and different fast-acting insulin types has not been detailed in the thesis as the ongoing research associated with these components is not yet sufficiently matured to be included in the thesis. The reference to the GUI is intended to showcase how the model can be used as a tool to help with the teaching of medical students.

[4] L. Sun, E. Kwok, B. Gopaluni, and O. Vahidi, "Pharmacokinetic-pharmacodynamic modeling of metformin for the treatment of type ii diabetes mellitus," *The open biomedical engineering journal*, vol. 5, p. 1, 2011.

[5] C. B. Landersdorfer, Y.-L. He, and W. J. Jusko, "Mechanism-based population modelling of the effects of vildagliptin on glp-1, glucose and insulin in patients with type 2 diabetes," *British journal of clinical pharmacology*, vol. 73, no. 3, pp. 373–390, 2012.

[6] M. D. Breton, "Physical activity—the major unaccounted impediment to closed loop control," *Journal of Diabetes Science and Technology*, vol. 2, no. 1, pp. 169–174, 2008.

[7] J. Li and J. D. Johnson, "Mathematical models of subcutaneous injection of insulin analogues: a mini-review," *Discrete and continuous dynamical systems. Series B*, vol. 12, no. 2, p. 401, 2009.

[8] L. Gaohua and H. Kimura, "A mathematical model of brain glucose homeostasis." *Theoretical biology and medical modelling*, vol. 6, no. 26, 2009.

[9] J. T. Sorensen, "A physiologic model of glucose metabolism in man and its use to design and assess improved insulin therapies for diabetes," Ph.D. dissertation, Massachusetts Institute of Technology, 1985.

[10] O. Vahidi, K. E. Kwok, R. B. Gopaluni, and F. K. Knop, "A comprehensive compartmental model of blood glucose regulation for healthy and type 2 diabetic subjects," *Medical & Biological Engineering & Computing*, vol. 54, no. 9, pp. 1383–1398, 2016.

[11] D. J. Jenkins, T. Wolever, R. H. Taylor, H. Barker, H. Fielden, J. M. Baldwin, A. C. Bowling, H. C. Newman, A. L. Jenkins, and D. V. Goff, "Glycemic index of foods: a physiological basis for carbohydrate exchange," *The American journal of clinical nutrition*, vol. 34, no. 3, pp. 362–366, 1981.

[12] H. Haahr and T. Heise, "A review of the pharmacological properties of insulin degludec and their clinical relevance," *Clinical pharmacokinetics*, vol. 53, pp. 787–800, 2014.

[13] R. I. Holt, J. H. DeVries, A. Hess-Fischl, I. B. Hirsch, M. S. Kirkman, T. Klupa, B. Ludwig, K. Nørgaard, J. Pettus, E. Renard *et al.*, "The management of type 1 diabetes in adults. a consensus report by the american diabetes association (ada) and the european association for the study of diabetes (easd)," *Diabetes Care*, vol. 44, no. 11, pp. 2589–2625, 2021.

Chapter 3

Stochastic Modeling and Estimation

In this section, a short summary for the work in Paper B [1], Paper C [2], and Paper D [3] will be presented and discussed.

1 The Stochastic Model

The general form for the stochastic model used for simulation in Paper B, and for simulation and fitting in Paper C and Paper D is a jump diffusion model and can be summarized as follows

$$d\boldsymbol{X} = \boldsymbol{f}\left(\boldsymbol{X}(t), u(t), t\right) dt + \boldsymbol{g}(\boldsymbol{X}(t), t) dW(t) + \boldsymbol{h}(\boldsymbol{X}(t), t) d\mathcal{J}(\boldsymbol{X}(t), t), \tag{3.1}$$

in which

- $\boldsymbol{X} \in \mathbb{R}^{n_X}$ is a random state vector with the variables related to blood glucose concentration, insulin concentration, and others states for disturbances, meals, or dynamics.
- $u(t) \in \mathbb{R}_{\geq 0}$ is representing long-acting insulin. Note that the input can be a vector if one desires to include other relevant variables such as fast-acting insulin and heart rate.
- $W(t) \in \mathbb{R}$ is a Wiener process, representing uncertainties and unmodelled disturbances.
- $\mathcal{J}(t) \in \mathbb{R}$ is a compound Poisson process, representing uncertain events causing rapid changes in BG such as eating. Note that multiple compound Poisson processes can be used in the same model to account for different types of meals or meals occurring at different times, see Paper D for more details on how they can be used.
- $\boldsymbol{f} : \mathbb{R}^{n_X} \times \mathbb{R}^{n_u} \times \mathbb{R}_{\geq 0} \to \mathbb{R}^{n_X}$ is the drift function, containing injected insulin pharmacokinetics, insulin-glucose dynamics, dynamics related to ingested meals, dynamics related to CGM readings, and disturbances.

- $\boldsymbol{g} : \mathbb{R}^{n_X} \times \mathbb{R}_{\geq 0} \to \mathbb{R}^{n_X}$ is the diffusion term, relating the Wiener process to the overall dynamics.
- $\boldsymbol{h} : \mathbb{R}^{n_X} \times \mathbb{R}_{\geq 0} \to \mathbb{R}^{n_X}$ is the jump term, accounting for the effect of uncertain events on the overall dynamics.

In Paper B and Paper C, the drift part of the model $\boldsymbol{f}$ is based on the one from [4] with $n_X = 6$ states. The first two states are for the pharmocokinitiks of injected insulin, the third one is for the effective insulin in the blood, the fourth one is for BG, and the last two are for ingested carbohydrates. The diffusion term is $\boldsymbol{g} = \begin{bmatrix} \mathbf{0}_3^{\mathrm{T}} & \sigma & \mathbf{0}_2^{\mathrm{T}} \end{bmatrix}^{\mathrm{T}}$ with $\sigma > 0$ for the Wiener process affecting the BG state directly. Moreover, the jump term is $h = \begin{bmatrix} \mathbf{0}_4^{\mathrm{T}} & 1 & 0 \end{bmatrix}^{\mathrm{T}}$ with the meals affecting the first meal ingestion state. Additionally, the compound Poisson process in Paper B and Paper C is as follows

$$\mathcal{J}(t) = \sum_{i=1}^{\mathcal{P}(t)} Z(i) \tag{3.2}$$

where $\mathcal{P}(t)$ is a Poisson point process with a constant intensity λ_c, and $Z(i)$ is the ith mark (or jump size). The Poisson point process is a stochastic process with the random variable $\mathcal{P}(t) \in \mathbb{Z}_{\geq 0}$ representing the number of events (or jumps) happening on the interval $[0, t]$. More specifically, the random variable $\mathcal{P}(t) \in \mathbb{Z}_{\geq 0}$ is Poisson distributed with mean $\lambda_c t$. Additionally, for the time points $t_0 < t_1 < \cdots < t_{k-1} < t_k \in \mathbb{R}_{\geq 0}$, the random variables $\mathcal{P}(t_1) - \mathcal{P}(t_0), \ldots, \mathcal{P}(t_k) - \mathcal{P}(t_{k-1})$ are independent. See figure 3.1 for an example of a Poisson point process with the corresponding Poisson compound process. The Jump sizes in the Pois-

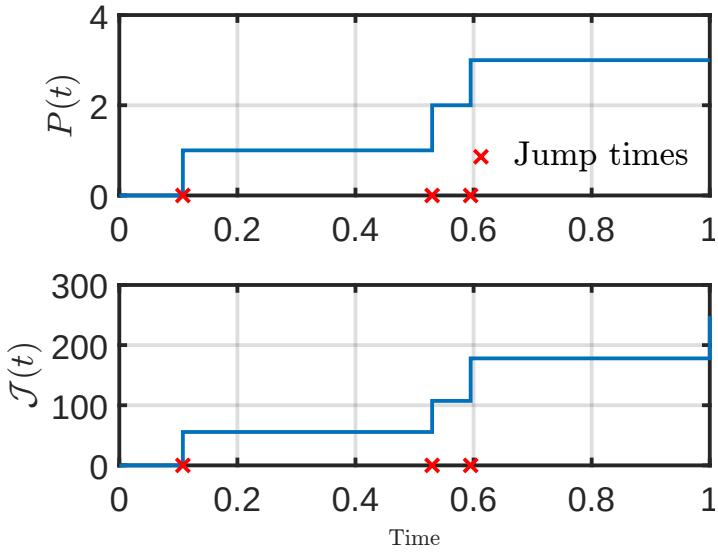

Fig. 3.1: An example of a Poisson point process $\mathcal{P}(t)$ with intensity $\lambda_c = 3$ and a compound Poisson process $\mathcal{J}(t)$ with jump sizes $Z(i) \overset{\text{i.i.d.}}{\sim} \text{LogNormal}\left(\log(60), 0.3\right)$.

son compound process in Paper C and Paper D are for the meal sizes. The jump sizes $Z(i)$ are assumed independent of $\mathcal{P}(t)$, mutually independent, and identically distributed for both Paper C and Paper D. For Paper C, the jump sizes are assumed to be distributed according to the lognormal distribution

$$Z(i) \overset{\text{i.i.d.}}{\sim} \text{LogNormal}\left(\mu_z, \sigma_z\right).$$

The parameters λ_c, μ_z, and σ_z represent behavioral parameters since they are related to the eating pattern of a subject. In Paper B, the model was used for simulation only. As for Paper C, an estimation method based on MCMC and SMC is used to estimate the parameters λ_c, μ_z, and σ_z together with the diffusion parameter σ. In paper C, the estimation of these parameters yielded successful results for both simulated and clinical data. However, when dealing with clinical data, the accuracy of estimated BG values was unsatisfactory when the CGM readings were low. This suggests that the model struggles to handle low BG values, which poses limitations on the validation of the estimated parameters. Moreover, the proposed estimation method in Paper C fails to account for the estimation of parameters in the drift part $\boldsymbol{f}$. This fact can also be a reason for the challenges faced in accurately estimating low BG values.

In Paper D, these limitations were addressed by considering a modified version of the model in Paper C together with a different estimation approach. The first modification on the model is the introduction of two extra states: a seventh state representing an Ornstein–Uhlenbeck (OU) process, and an eighth state to account for the fact that CGM devices measure the interstitial glucose (IG) and not the BG directly. Thus, the diffusion term in Paper D is $\boldsymbol{g} = \begin{bmatrix}\mathbf{0}_6^{\mathrm{T}} & \sigma & 0\end{bmatrix}^T$. The OU modification in the model implies that the BG dynamics are influenced by the OU process as opposed to the direct effect of the Wiener process in Paper B and Paper C. Since disturbances on the BG are more likely to be correlated in time, the use of an OU process is more realistic than a Wiener process directly affecting the dynamics of BG. In addition to these modifications, the jump term is modified to be $\boldsymbol{h} = \begin{bmatrix}\mathbf{0}_4^{\mathrm{T}} & \exp\left(-\alpha_z X_5\right) & \mathbf{0}_3^{\mathrm{T}}\end{bmatrix}^{\mathrm{T}}$, with the jump sizes of the compound Poisson process being mutually independent, and identically distributed according to

$$Z(i) \overset{\text{i.i.d.}}{\sim} \text{Exp}\left(\mu_z\right).$$

The term $\exp\left(-\alpha_z X_5(t)\right)$ is utilized to incorporate dependency into meal sizes with a parameter α_z with $X_5(t)$ being the state for the first compartment of ingested glucose. See figure 3.2 for a comparison between a case when $\alpha_z = 0$ (no dependency between the meal sizes) and a case when $\alpha_z = 0.01$.

The choice of an exponential distribution for the jumps is motivated by its positive support and the convenience of it being defined by a single parameter. The choice of using an exponential distribution with one parameter over the lognormal distribution as done in Paper C is to reduce the number of estimated parameters with the new model to avoid problems with identifibility. With the new model in Paper D, another MCMC strategy with SMC method is proposed to estimate various parameters associated with meal consumption, namely μ_z, α_z, and λ_c, in addition to the drift parameter within the OU process. Furthermore, it extends its scope to include the estimation of physiological parameters linked to insulin sensitivity, insulin secretion, and a time constant representing the injected insulin.

Note that in Paper B and Paper C, the CGM measurement model is assumed to be in the

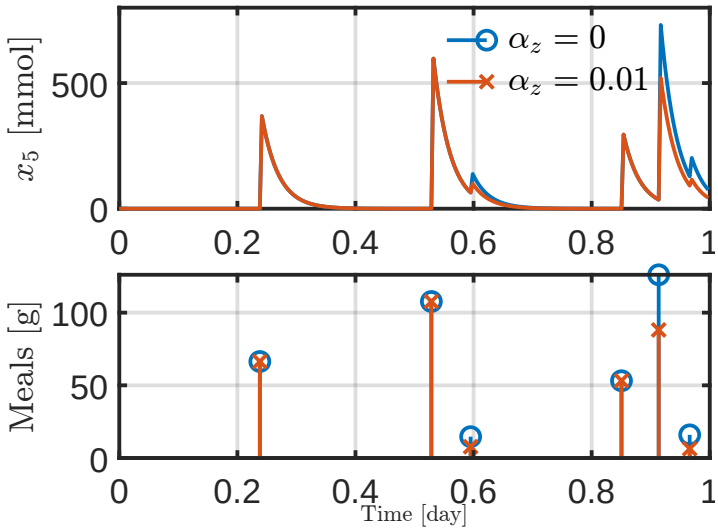

Fig. 3.2: Compound Poisson process for carbohydrate meals with no meal size dependency ($\alpha_z = 0$) and with meal size dependency ($\alpha_z = 0.01$).

form of

$$y_c(k) = x_g(k) + \sigma_y \epsilon(k),\ \epsilon(k) \sim \mathcal{N}(0,1), \tag{3.3}$$

with $x_g(k)$ [mmol/L] being the BG concentration. This model is too simple for CGM measurement even with the assumption that the CGM measurements are calibrated (see [5]). In Paper D, a slightly more accurate model is used for CGM. The model is of the following form

$$y_c(k) = x_c(k) + x_c(k)\sigma_y \epsilon(k),\ \epsilon(k) \sim \mathcal{N}(0,1), \tag{3.4}$$

where $x_c(k)$ [mmol/L] is the IG concentration state. This model is more accurate as it considers the IG concentration state and measurement errors with a standard deviation σ_y proportional to $x_c(k)$. In paper D (also in papers G,H, and I for generating simulated subjects), it is reported that a value $\sigma_y = 0.42$ is chosen to consider a mean absolute relative difference (MARD) value of 10%. This value is reported in [6] to be based on [5]. However, this value actually corresponds to a MARD of 33% instead of a 10% [1]. For a MARD value of 10%, the value of σ_y is $\sigma_y = 0.125$ instead which agrees with [5]. This means that for Paper D, the estimates could have been more pessimistic about the CGM errors than they should have been for some subjects. Nevertheless, since the model is still a simplified approximation, the results should not be drastically different if a value of $\sigma_y = 0.125$ is chosen instead. Moreover, (3.3) is still a simple approximation for the errors of calibrated CGM readings [5]. In [5], it was demonstrated that the MARD value is different for different ranges of glucose. A more accurate model would

[1] With the assumption that $x_c(k) \geq 0$ for all $k \in \mathbb{Z}$, the MARD value according to (3.3) can be found as $\mathbb{E}\left[\frac{|y_c(k)-x_c(k)|}{x_c(k)}\right] = \mathbb{E}\left[|\sigma_y \epsilon(k)|\right] = \sigma_y \sqrt{2/\pi}$.

then be to consider different values of σ_y based on $x_c(k)$ or $x_g(k)$. A fourth-order polynomial was used in [5] to fit different MARD values for different glucose values. For simplicity and better numerical robustness, a softplus approximation is proposed to be used instead of the fourth-order polynomial

$$\sigma_y(x_c(k)) = 0.025 \log\left(1 + \mathrm{e}^{-2(x_c(k)-7)}\right) + 0.1125, \tag{3.5a}$$

$$y_c(k) = x_c(k) + x_c(k)\sigma_y(x_c(k))\epsilon(k). \tag{3.5b}$$

Figure 3.3 shows the different choices of σ_y as a function of glucose. In table 3.1, the average fitting and prediction results from Paper D are presented with a choice of $\sigma_y = 0.125$ (corresponding to a constant MARD of 10%), $\sigma_y = 0.42$ (corresponding to a constant MARD of 33%), and the softplus model in (3.5). It can be observed from the results that there is no significant difference for the reported averages. The results for the choice of σ_y as in (3.5) are close to the ones when $\sigma_y = 0.125$ since the CGM readings for most of the subjects were above 6 [mmmol/L] and the softplus function in that range is approximately constant and close to a value of 0.125.

Table 3.1: Average Root Mean Square Error (RMSE) in [mmol/L] with clinical data of 8 subjects and the prediction of the fitted model for different time horizons and different choices of σ_y.

	Fitting	Pred.10 [min]	Pred.30 [min]	Pred.40 [min]
$\sigma_y = 0.42$	0.114	0.412	1.058	1.418
$\sigma_y = 0.125$	0.11	0.398	1.049	1.403
σ_y as in (3.5)	0.11	0.4	1.052	1.414

2 Estimation Strategies

In this section, the different estimation strategies will be summarized for Paper B, Paper C, and Paper D.

In Paper B, the estimation method is based on a least-square strategy minimizing the error between the BG state in the model and the CGM readings. The strategy estimates the states of the model, three physiological parameters, ingested meals as a time-series, and a disturbance time-series on BG. The strategy is simple and it yields time-series estimates of meals and disturbances. However, no parameters related to meal consumption are estimated. Additionally, the model cannot be used for predictions since there is no model for the estimated disturbances and meals.

In both Paper C and Paper D, the employed estimation strategy is based on an MCMC method with an SMC strategy. The estimation method in both Paper C and Paper D aims at drawing samples from the posterior distribution $p\left(\boldsymbol{x}(1:K), \boldsymbol{\theta} \mid \boldsymbol{y}_c[1:K]\right)$, with $\boldsymbol{y}_c[1:K]$ being a vector of the available CGM measurements form time sample 1 until time sample K, and $\boldsymbol{\theta}$ are the parameters which are desired to be estimated. For the next three subsections, MCMC and SMC strategies will be summarized and a summary on the differences between the estimation strategies of papers B, C, and D will be provided.

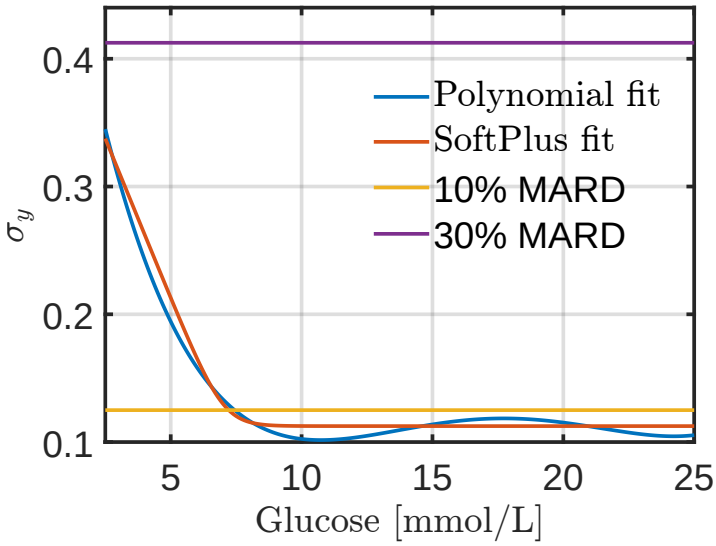

Fig. 3.3: Different choices of σ_y for a CGM error model.

2.1 MCMC methods

MCMC methods are algorithms utilized for sampling a desired probability distribution p which is challenging to evaluate. They involve constructing a Markov chain which has a desired distribution p as its stationary distribution, allowing for the generation of a sequence of samples from the desired distribution. More specifically, consider a Markov chain on the space $\mathcal{Z}$ consisting of a sequence of random variables $\{\boldsymbol{Z}_0, \boldsymbol{Z}_1, \boldsymbol{Z}_2 \dots\} \in \mathcal{Z}$ such that $\boldsymbol{Z}_{k+1} \sim \mathcal{K}(\boldsymbol{z} \mid \boldsymbol{z}_k)$. The idea of MCMC is to construct an ergodic Markov chain kernel $\mathcal{K}$ with a unique stationary distribution being the desired distribution p. With this construction, the marginal distribution of the Markov chain will approach p in the limit. That is, for sufficiently large k, the realization $\{\boldsymbol{Z}_k, \boldsymbol{Z}_{k+1}, \dots, \} \in \mathcal{Z}$ represent samples from p. In papers C and D, the desired distribution is chosen to be the posterior distribution $p\left(\boldsymbol{x}(1:K), \boldsymbol{\theta} \mid \boldsymbol{y}_c[1:K]\right)$.

2.2 SMC methods

SMC methods are simulation based methods relying on importance sampling to approximate the posterior of the state given the available observations in state-space models. In summary, a single run of an SMC method, such as the particle filter, gives the empirical estimate $\hat{p}(\boldsymbol{x}(1:K) \mid \boldsymbol{\theta}, \boldsymbol{y}[1:K])$ of the posterior $p(\boldsymbol{x}(1:K) \mid \boldsymbol{\theta}, \boldsymbol{y}[1:K])$:

$$\hat{p}(\boldsymbol{x}(1:K) \mid \boldsymbol{\theta}, \boldsymbol{y}[1:K]) = \sum_{i=1}^{N} w^i \delta_{\boldsymbol{X}^i(1:K)}(\boldsymbol{x}(1:K)), \tag{3.6}$$

where N is the number of particle trajectories $\left\{\boldsymbol{X}^1(1:K), \ldots, \boldsymbol{X}^N(1:K)\right\}$ used in the SMC method, and $\left\{w^1, \ldots, w^N\right\}$ are the normalized importance weights associated with each of the particle trajectories.

2.3 Particle MCMC

Particle MCMC (PMCMC) methods utilize SMC techniques, such as the particle filter, to construct efficient and high-dimensional Markov chain kernels within the context of MCMC for state space models. One specific PMCMC strategy is the Particle Gibbs (PG), proposed by [7]. It constructs the Markov kernel by running an SMC method, such as the conditional particle filter (CPF), given a fixed reference trajectory. In the CPF, one particle trajectory is fixed (set deterministically) as a reference $\boldsymbol{x}^r(1:K)$. After running the CPF with the fixed reference trajectory, a trajectory $\boldsymbol{X}^*(1:K)$ is sampled according to the importance weights of the CPF $\mathbb{P}\left(\boldsymbol{X}^*(1:K) = \boldsymbol{X}^i(1:K)\right) = w^i$ for $i \in \{1, \ldots, N\}$. In other words, the CPF maps the reference trajecotry $\boldsymbol{x}^r(1:K)$ into a probability distribution on the space of state trajectories. Thus, it implicitly defines a Markov kernel on the space of state trajectories. In [8], the Markov kernel defined by the CPF is shown to be ergodic with a unique target distribution being $p\left(\boldsymbol{x}(1:K) \mid \boldsymbol{\theta}, \boldsymbol{y}_c[1:K]\right)$.

However, the CPF experiences path degeneracy (the loss of trajectory diversity due to resampling) which makes the mixing of the CPF as a Markov kernel poor. To address this issue, PG with Ancestor Sampling (PGAS) was introduced by [8]. The Ancestor Sampling step partitions the fixed particle trajectory by sampling new ancestor indices at different time steps. Both Paper C and Paper D adopt a strategy based on PGAS to estimate the states of the stochastic model in (3.1).

2.4 Estimating Parameters with PMCMC

In Paper C, the state vector is augmented with the sufficient statistics of the parameters to be estimated, following a method called Particle Learning (PL) [9]. However, PL is only applicable to parameters for which the closed-form posterior can be determined given a specific prior. Consequently, this limitation prevented the estimation of physiological parameters in the drift part of Paper C. Additionally, increasing the dimension of the model by augmenting the sufficient statistics of the parameters in the state vector increases the Monte Carlo error for the same number of particles.

In contrast, Paper D estimates the parameters using Gibbs Sampling, another MCMC strategy. Gibbs Sampling enables the generation of approximate samples from the joint posterior of the states and parameters given the measurements. It achieves this by iteratively sampling from the posterior of the states given fixed parameters and measurements $p\left(\boldsymbol{x}(1:K) \mid \boldsymbol{\theta}, \boldsymbol{y}_c[1:K]\right)$ (using a strategy based on PGAS with CPF), followed by sampling from the posterior of the parameters given the fixed sampled trajectory and measurements $p\left(\boldsymbol{\theta} \mid \boldsymbol{x}(1:K), \boldsymbol{y}_c[1:K]\right)$. To sample from the posterior of the parameters $p\left(\boldsymbol{\theta} \mid \boldsymbol{x}(1:K), \boldsymbol{y}_c[1:K]\right)$, a Metropolis-Hastings method, which is also an MCMC approach, is utilized. This strategy allows for the estimation of both physiological and behavioral parameters.

In summary, table 3.2 provides the differences between the three estimation approaches

	Paper B	Paper C	Paper D
Strategy	Least-Squares	PMCMC + PL	PMCMC + Gibbs Sampling
# of Est. Param.	3	5	7
Est. Behavioral Param.	No	Yes	Yes
Est. Physiological Param.	Yes	No	Yes
Prediction	Not Possible	Possible	Possible
Missing CGM	Can Handle	Cannot Handle	Can Handle

Table 3.2: Summary for the different estimation approaches in Paper B, Paper C, and Paper D. Est. and Param. are abbreviations for estimated and parameters, respectively.

3 Summary of the Results

The method and the model in Paper D provide the best results with clinical data.

The clinical data utilized in Papers B, C, and D is from the study conducted by [10]. This dataset comprises both CGM and SMBG measurements obtained over a duration ranging from 30 to 80 days. The data pertains to eight distinct insulin-naïve T2D subjects who initiated insulin treatment using long-acting insulin Degludec.

In Paper D, both physiological and behavioural parameters were estimated for all the 8 subjects. The estimated average number of meals per day λ_c [day^{-1}] and the mean size of meals μ_z [g] are observed to be close for all subjects and align with the recommended statistics for individuals with T2D [11].

Furthermore, the estimates of the parameter α_z, which determines how much the size of subsequent meals is correlated, exhibits variability among the subjects. This suggests individual variations in meal patterns and highlights the personalized nature of the proposed model in Paper D.

In addition, lower estimates of the insulin sensitivity parameter p_4 are consistent with lower estimates of the insulin secretion parameter p_7, aligning with the pathophysiology of T2D. This supports the physiological validity of the estimated parameters. Moreover, estimates of the time constant for the injected insulin p_I were all consistently close to the expected value of the insulin Degludec, which further validates the accuracy of the estimated parameters.

Furthermore, an interesting observation was made when one of the subjects provided their meal times for a short period during the study. The estimated meal compartment state for that specific subject exhibited a consistency with the reported meal times. Additionally, the meal compartment state exhibited relatively large peaks in close proximity to the reported meal times. However, other meals are also estimated between the reported meals. These meals could be due to some uncertainties in the model, such as the effect of different types of ingested carbohydrates, or imperfections in the subject's meal time reporting process, such as unreported small snacks.

Moreover, it is important to highlight that the accuracy of the model's predictions gradually decreases, on average, within a time frame of 40 minutes when all the subjects are considered. This is consistent with the prediction results reported in [12] for different CGM prediction approaches for T1D subjects. This decrease in accuracy is to be expected as the model encounters

limitations in accounting for all the uncertainties inherent in human subjects over long periods of time. However, the fitted model was shown to still possesses the ability to predict potential meals within minutes of the point of prediction. Furthermore, when CGM predictions were generated for the different eight subjects, the majority of the CGM readings fell within the $10_{th} - 90_{th}$ percentile range of the predicted trajectories for a prediction period of around 200 minutes. This showcases the model's ability to capture the glucose concentration trend of the studied T2D subjects for an extended period of times.

References

[1] M. Al Ahdab, H. Glavind Clausen, T. Knudsen, T. Björk Aradóttir, S. Schmidt, K. Nørgaard, and J.-J. Leth, "Parameter estimation in type 2 diabetes in the presence of unannounced meals and unmodelled disturbances," in *2021 European Control Conference (ECC)*, 2021, pp. 1278–1282.

[2] M. A. Ahdab, M. Papež, T. Knudsen, T. B. Aradóttir, S. Schmidt, K. Nørgaard, and J.-J. Leth, "Parameter estimation for a jump diffusion model of type 2 diabetic patients in the presence of unannounced meals," in *2021 IEEE Conference on Control Technology and Applications (CCTA)*, 2021, pp. 176–183.

[3] ——, "Stochastic modeling and inference for type 2 diabetes," *IEEE Transactions on Biomedical Engineering*, 2023 (Submitted).

[4] T. Aradóttir, D. Boiroux, H. Bengtsson, J. Kildegaard, B. Orden, and J. Jørgensen, "Model for simulating fasting glucose in type 2 diabetes and the effect of adherence to treatment." in *IFAC-PapersOnLine*, vol. 50, no. 1. Elsevier, 2017, pp. 15 086–15 091.

[5] D. Rodbard, "Characterizing accuracy and precision of glucose sensors and meters," *Journal of diabetes science and technology*, vol. 8, no. 5, pp. 980–985, 2014.

[6] P. Colmegna, K. Wang, J. Garcia-Tirado, and M. D. Breton, "Mapping data to virtual patients in type 1 diabetes," *Control Engineering Practice*, vol. 103, p. 104605, 2020.

[7] C. Andrieu, A. Doucet, and R. Holenstein, "Particle markov chain monte carlo methods," *Journal of the Royal Statistical Society: Series B (Statistical Methodology)*, vol. 72, no. 3, pp. 269–342, 2010.

[8] F. Lindsten, M. I. Jordan, and T. B. Schon, "Particle gibbs with ancestor sampling," *Journal of Machine Learning Research*, vol. 15, pp. 2145–2184, 2014.

[9] C. M. Carvalho, M. S. Johannes, H. F. Lopes, and N. G. Polson, "Particle learning and smoothing," *Statistical Science*, vol. 25, no. 1, pp. 88–106, Feb. 2010, publisher: Institute of Mathematical Statistics.

[10] T. B. Aradóttir, H. Bengtsson, M. L. Jensen, N. K. Poulsen, D. Boiroux, L. L. Jensen, S. Schmidt, and K. Nørgaard, "Feasibility of a new approach to initiate insulin in type 2 diabetes," *Journal of diabetes science and technology*, vol. 15, no. 2, pp. 339–345, 2021.

[11] A. Gray and R. J. Threlkeld, "Nutritional recommendations for individuals with diabetes," 2015.

[12] F. Prendin, S. Del Favero, M. Vettoretti, G. Sparacino, and A. Facchinetti, "Forecasting of glucose levels and hypoglycemic events: head-to-head comparison of linear and nonlinear data-driven algorithms based on continuous glucose monitoring data only," *Sensors*, vol. 21, no. 5, p. 1647, 2021.

Chapter 4

Enhancing Glucose Sensors

In this section, a summary for the works in Paper E [1] and Paper F [2] will be described in details.

CGM devices do not measure BG directly. Instead, they measure the glucose concentrations in the interstitium (IG), which results in a time lag between the measurements of CGM and BG. Furthermore, CGM devices have shown susceptibility to both systematic and random errors [3]. As a result, diabetic subjects often use SMBG measurements to calibrate their CGM devices throughout the day [4].

Multiple models have been proposed in academic literature to understand and address the errors in CGM measurements [5–10]. However, these methods often rely on BG values taken more frequently than typical SMBG measurements, which makes them less practical for individual use. Additionally, they use data from multiple CGM devices to develop their models.

Several researches [11–13] have attempted to enhance CGM measurements using KFs and the standard SMBG data provided by the diabetic subjects. These methods typically employ models with various assumptions, such as a time constant between IG and BG, a random walk model for BG, and additive Gaussian noise for SMBG and CGM measurements. These methods focus on improving CGM measurements rather than obtaining an individual-specific CGM model.

Paper E aims to explore the application of Temporal Gaussian Processes (TGP) to derive an individual-specific CGM error model, which can be determined using readings from a single CGM device and SMBG measurements. In contrast, Paper F aims to construct a framework to integrate data from multiple CGM devices, if available, to derive a reliable fused CGM signal. The works in these two papers take distinct approaches to address the issue of CGM device quality. Paper E focuses on obtaining individualized CGM error models, similar to those in [5–10], but with a minimal requirement for devices and measurements. Conversely, Paper F aims to develop a method to enhance CGM readings, similar to those in [11–13], but through the fusion of multiple CGM devices.

1 CGM Error Models

Paper E investigates the use of TGP with an estimation framework similar to the one in Paper D using MCMC methods together with SMC strategies (PMCMC). To explain the work in Paper E further, a short description of state space TGP will be provided first and then a discussion on the different TGPs and how they were evaluated will be provided.

1.1 State Space Temporal Gaussian Processes

A TGP is a stochastic process $F(t)$ indexed by time $t \in \mathbb{R}_{\geq 0}$ such that any finite collection of the random variables $F(t_1), \ldots, F(t_n)$ possesses an n-dimensional Gaussian distribution [14]. TGPs, or general Gaussian processes, are entirely determined by their second order statistics. Therefore, defining the mean and the covariance functions of a TGP will be enough to define the TGP completely. TGP process are typically denoted as

$$F(t) \sim \mathcal{GP}\left(\mu(t), \mathrm{c}\left(t, t^{'}, \boldsymbol{\theta}_{\mathrm{c}}\right)\right) \tag{4.1}$$

where $\mu(t)$ is the mean function and $\mathrm{c}\left(t, t^{'}, \boldsymbol{\theta}_{\mathrm{c}}\right)$ being the covariance function between time points t and $t^{'}$, parameterized by $\boldsymbol{\theta}_{\mathrm{c}}$. The mean and covariance functions encapsulate prior information about the process. For Paper E, the mean is assumed to be $\mu(t) = 0$ for simplicity. Given the set $\{t_1, \ldots, t_n\}$ with $\{F(t_1), \ldots, F(t_n)\}$, then the joint distribution of $\left[F(t_1), \ldots, F(t_n)\right]^{\mathrm{T}}$ is $\left[F(t_1), \ldots, F(t_n)\right]^{\mathrm{T}} \sim \mathcal{N}(0, \mathbf{C})$ where the ijth element of the covariance matrix $\mathbf{C}$ is $\mathrm{C}_{ij} = \mathrm{c}\left(t_i, t_j, \boldsymbol{\theta}_{\mathrm{c}}\right)$. The regression of TGP aims at estimating the statistics of $F(t^*)$ with t^* being an arbitrary point given the observations $\{f(t_1), \ldots, f(t_n)\}$ or noisy measurements of them $\{y(t_1), \ldots, y(t_n)\}$ (e.g., $Y(t_i) = f(t_i) + E_i,\ E_i \sim \mathcal{N}(\mu_e, \sigma_e)$ for $i \in \{1, \ldots, n\}$).

The computational complexity for the regression of TGPs can escalate to $\mathcal{O}(n^3)$ for all types of output processes $Y(t)$, as discussed in [14]. This presents a significant challenge for large datasets, particularly when time serves as an input and the sampling frequency is high, as is the case with CGM measurements. One potential solution involves using state space representation for TGPs. In [15, 16], precise or approximate methods to attain state space representations for TGPs with stationary covariance function ($\mathrm{c}(t, t^{'}, \boldsymbol{\theta}_{\mathrm{c}}) = \mathrm{c}(\tau, \boldsymbol{\theta}_{\mathrm{c}}),\ \tau = t - t^{'}$) have been illustrated and examined. Furthermore, the regression problem for TGPs in (4.1) can be considered a smoothing problem for the following linear system

$$d\boldsymbol{X}_{gp}(t) = \boldsymbol{A}_{gp}\boldsymbol{X}_{gp}(t)\mathrm{d}t + \boldsymbol{L}_{gp}\mathrm{d}W \tag{4.2a}$$

$$F(t) = \boldsymbol{H}_{gp}\boldsymbol{X}_{gp}(t), \tag{4.2b}$$

where W is the Wiener process. The stationary covariance functions define the matrices $\boldsymbol{A}_{gp}, \boldsymbol{L}_{gp}$, and $\boldsymbol{H}_{gp}$ along with the state dimension.

For certain covariance functions, exact state space representation can be computed as demonstrated in [15, 16]. For instance, a TGP with an exponential covariance function can be represented by an OU process. Other examples having closed-form state space representation include TGPs with half-integer Matérn covariance functions. As for other kinds of stationary

covariance functions, such as the squared exponential function, approximations can be achieved using Taylor series or Padé approximation for their spectral density to obtain an approximate linear state space representation, as performed in [15, 17].

1.2 The CGM Error Model

The CGM error model used in Paper E is of the following form

$$Y_c(k) = \big(1 + G(k)\big)\, x_c(k) + V(k) + E_c(k),\;\; E_c(k) \sim \mathcal{N}(0, \sigma_c^2), \tag{4.3}$$

where $t_{k+j} - t_k = jT_m, j \in \mathbb{Z}$ with T_m being the sampling time of the CGM device and $y_c(k)$ is a notation for $Y_c(t_k)$. Here, the state $x_c(k)$ [mmol/L] is for the IG concentration. The process $G(k)$ is the gain error of the sensor due to calibration. As for the process $V(k)$ and $E_c(k)$, they represent the additive calibration and the random measurement errors of the sensor. The IG concentration is linked to the BG through the following first order model (similar to [7, 13])

$$\dot{x}_c(t) = \frac{1}{\tau_c}\left(x_g(t) - x_c(t)\right), \tag{4.4}$$

where $\tau_c > 0$ is a time constant to represent the lag between BG and IG. Three different models are investigated for $G(k)$ and $V(k)$ in Paper E as demonistrated in table 4.1. In addition, the

Model Number	$G(k)$	$V(k)$
Model 1	Exponential (OU)	AR(2)
Model 2	Exponential (OU)	Squared Exponential
Model 3	Matérn 5/2	Matérn 5/2

Table 4.1: Different models of CGM considered in the paper

following model is considered for the SMBG readings

$$Y_s(t_s) = x_g(t_s) + \sigma_s\left(x_g(t_s)\right) E_s(t_s), \tag{4.5a}$$

$$\sigma_s\left(x_g\right) = \frac{1}{\kappa}\sigma_2 \log\left(1 + \mathrm{e}^{\kappa\left(x_g - 4.2\right)}\right) + \sigma_1, \tag{4.5b}$$

where t_s is the time point of which the measurement is recorded, and $\kappa > 0$. The model for the standard deviation (4.5b) is chosen such that it provides a smooth transition between the two zones which simulates the ISO standard for SMBG devices [18]. The model is then used in a PMCMC approach, similar to the one used for Paper D, to estimate $\boldsymbol{\theta}_g$ (parameters for $G(t)$), $\boldsymbol{\theta}_v$ (parameters for $V(t)$), σ_c, σ_1, and σ_2.

1.3 Estimation and Regression

The models outlined in the previous section are utilized in a PMCMC approach, similar to the one described for Paper D. This PMCMC method serves as a smoothing technique, which is equivalent to the regression of TGPs, as discussed earlier.

The models incorporating the PMCMC methodology are tested in Paper E with the use of simulated data, generated based on the model from Paper A [19]. BG and IG concentrations obtained from the simulated data were used to create CGM data by utilizing the detailed models from [7–10, 20]. For simulating SMBG readings, the two zones skew normal distributions specific to the One Touch Ultra 2 (OTU2) device was employed [9]. CGM and SMBG data were generated for 100 distinct simulated subjects. Each of these subjects' CGM and SMBG data was then processed with the PMCMC method in conjunction with the three different models proposed in table 4.1.

The first model's performance was noticeably poor in accurately estimating the actual simulated BG concentration. Conversely, the second and third models exhibited comparable performances which were better than the performance of the first model. The chosen covariance functions for these latter models facilitated the generation of highly correlated time series, which are suitable for handling the biases and drifts inherent in CGM errors. Furthermore, the uncertainty associated with the fits for the second and third models was substantially less compared to that of the first model.

The application of TGP in Paper E, combined with the proposed smoothing strategy, demonstrates promising potential for modeling correlated, time-dependent CGM errors with the aid of a single CGM device and SMBG measurements. The models and strategies, given their applicability with just one CGM device and SMBG measurements, seem well-suited for subject-specific modeling.

However, it is critical to highlight that this method is computationally demanding. It is also important to compare the method and the models with other strategies using actual CGM data from T2D subjects. Nevertheless, the work in Paper E showcases the potential of TGP for modeling CGM errors using a single CGM device and SMBG measurements.

2 Fusing CGM Readings

The technique explained in Paper F fuses the readings from different CGM devices by using the Multi-Model Kalman Filter (MMKF) framework. This framework works by combining the estimates of multiple KFs, each using a different prediction model. This is particularly helpful in situations where the quality of the different sensors changes overtime. In Paper F, the number of KFs is decided by the number of CGM devices used. Each KF model differs only in the assumed measurement error covariance matrix. For instance, the first KF has a lower variance for the first CGM device, the second KF has a lower variance for the second CGM device, and so on. In this way, each KF for each CGM device assumes that its device is the best among the others. Apart from this, all models share the same linear dynamics which were chosen to be the dynamics of a discrete triple integrator of white noise. This choice was made for simplicity and it is common in time series estimation of physiological processes (see [21] as an example). The approach could also work for more accurate models which could consider different available information such as insulin.

The estimates from the different KFs are then combined into one estimate based on weights (probabilities) assigned for each KF and updated according to the innovation likelihood of their assumed model and predictions. To explain it more, if the innovation, or output residual, for the i_{th} KF is represented as $\tilde{\boldsymbol{y}}^i(k{+}1 \mid k)$ for the prediction at time step $k{+}1$ given measurements

up to k, then the weight $\beta^i(k|k)$ for the i_{th} KF is updated according to the following equation:

$$\beta^i(k+1|k+1) = \frac{p\left(\tilde{\boldsymbol{y}}^i(k+1|k) \mid \mathrm{m}^i_{k+1}\right)}{\sum_{i=1}^{N} \beta^i(k+1|k) p\left(\tilde{\boldsymbol{y}}^i(k+1|k) \mid \mathrm{m}^{\mathrm{i}}_{\mathrm{k+1}}\right)} \beta^i(k|k), \tag{4.6}$$

where $p\left(\tilde{\boldsymbol{y}} \mid \mathrm{m}^i_{k+1}\right)$ is the innovation density for the i_{th} KF, and N is the number of available KFs.

This setup can have issues if the quality of one sensor changes overtime to become the best or the worst among the other sensors, which is expected when using multiple CGM devices. To handle this, Paper F introduces and investigates the Multiple Model Kalman Filter with Forgetting Factor (MMKFF). In the MMKFF, An additional step is added to the equation for updating the weights in (4.6) to make it as follows

$$\beta^i(k+1|k) = (1-\alpha)\beta^i(k|k) + \alpha\bar{\beta}^i, \tag{4.7a}$$

$$\beta^i(k+1|k+1) = \frac{p\left(\tilde{\boldsymbol{y}}^i(k+1|k) \mid \mathrm{m}^i_{k+1}\right)}{\sum_{i=1}^{N} \beta^i(k+1|k) p\left(\tilde{\boldsymbol{y}}^i(k+1|k) \mid \mathrm{m}^{\mathrm{i}}_{\mathrm{k+1}}\right)} \beta^i(k+1|k), \tag{4.7b}$$

where $\alpha \in [0,1]$ is a forgetting factor, and $\bar{\beta}^i$ is a default value. The default value can be chosen to be $\bar{\beta}^i = 1/N$ for all $i \in \{1,\ldots,N\}$, or to be a discrete distribution that reflects our prior knowledge about the quality of the sensors. The added step in (4.7a) works as a regularization for the weights to bring them closer to a default value. To understand it more, if the weights are kept updated for $l > 0$ step ahead from step k without measurements (prediction), then $\beta^i(k+l|k) = (1-\alpha)^l\beta^i(k|k) + \alpha^l\bar{\beta}^i$, and $\lim_{l\to\infty} \beta^i(k+l|k) = \bar{\beta}^i$ for all $i \in \{1,\ldots,N\}$. Meaning that the information contained in $\beta^i(k|k)$ has been replaced with the default value $\bar{\beta}^i$ for all $i \in \{1,\ldots,N\}$ in the absence of measurements.

Both of these methods were tested using data from two different animal experiments. The results showed that both methods produce a reliable fused CGM signal. It was also shown that the MMKFF can respond to changes in the quality of the different CGM devices better than other KF methods, including MMKF. However, it was noticed that the MMKFF's ability to adapt resulted in a slower response to sudden changes. Future studies could improve this by using an adaptive forgetting factor for the MMKFF. Also, testing the method on more data from different experiments could give us a better understanding of its potential applicability in a real-world, human setting.

References

[1] M. Ahdab, T. Knudsen, and J.-J. Leth, "State space temporal gaussian processes for glucose measurements," in *2022 European Control Conference (ECC)*. United States: IEEE, 2021, pp. 1277–1282.

[2] M. Ahdab, K. Benam, H. Khoshamadi, A. Fougner, and S. Gros, "Sensor fusion for glucose monitoring systems," in *IFAC World Congress 2023*, 2023 (In press).

[3] B. P. Kovatchev, S. D. Patek, E. A. Ortiz, and M. D. Breton, "Assessing sensor accuracy for non-adjunct use of continuous glucose monitoring," *Diabetes technology & therapeutics*, vol. 17, no. 3, pp. 177–186, 2015.

[4] G. Acciaroli, M. Vettoretti, A. Facchinetti, and G. Sparacino, "Chapter 9 - calibration of cgm systems," in *Glucose Monitoring Devices*, C. Fabris and B. Kovatchev, Eds. Academic Press, 2020, pp. 173–201.

[5] M. Breton and B. Kovatchev, "Analysis, modeling, and simulation of the accuracy of continuous glucose sensors," *Journal of diabetes science and technology*, vol. 2, no. 5, pp. 853–862, 2008.

[6] D. Lunn, C. Wei, and R. Hovorka, "Fitting dynamic models with forcing functions: application to continuous glucose monitoring in insulin therapy," *Statistics in medicine*, vol. 30, no. 18, pp. 2234–2250, 2011.

[7] A. Facchinetti, S. Del Favero, G. Sparacino, J. R. Castle, W. K. Ward, and C. Cobelli, "Modeling the glucose sensor error," *IEEE Transactions on Biomedical Engineering*, vol. 61, no. 3, pp. 620–629, 2013.

[8] A. Facchinetti, S. Del Favero, G. Sparacino, and C. Cobelli, "Model of glucose sensor error components: identification and assessment for new dexcom g4 generation devices," *Medical & biological engineering & computing*, vol. 53, no. 12, pp. 1259–1269, 2015.

[9] M. Vettoretti, A. Facchinetti, G. Sparacino, and C. Cobelli, "A model of self-monitoring blood glucose measurement error," *Journal of diabetes science and technology*, vol. 11, no. 4, pp. 724–735, 2017.

[10] M. Vettoretti, C. Battocchio, G. Sparacino, and A. Facchinetti, "Development of an error model for a factory-calibrated continuous glucose monitoring sensor with 10-day lifetime," *Sensors*, vol. 19, no. 23, p. 5320, 2019.

[11] E. J. Knobbe and B. Buckingham, "The extended kalman filter for continuous glucose monitoring," *Diabetes technology & therapeutics*, vol. 7, no. 1, pp. 15–27, 2005.

[12] M. Kuure-Kinsey, C. C. Palerm, and B. W. Bequette, "A dual-rate kalman filter for continuous glucose monitoring," in *2006 International Conference of the IEEE Engineering in Medicine and Biology Society*. IEEE, 2006, pp. 63–66.

[13] A. Facchinetti, G. Sparacino, and C. Cobelli, "Enhanced accuracy of continuous glucose monitoring by online extended kalman filtering," *Diabetes technology & therapeutics*, vol. 12, no. 5, pp. 353–363, 2010.

[14] C. E. Rasmussen, "Gaussian processes in machine learning," in *Summer school on machine learning*. Springer, 2003, pp. 63–71.

[15] J. Hartikainen and S. Särkkä, "Kalman filtering and smoothing solutions to temporal gaussian process regression models," in *2010 IEEE international workshop on machine learning for signal processing*. IEEE, 2010, pp. 379–384.

[16] S. Sarkka, A. Solin, and J. Hartikainen, "Spatiotemporal learning via infinite-dimensional bayesian filtering and smoothing: A look at gaussian process regression through kalman filtering," *IEEE Signal Processing Magazine*, vol. 30, no. 4, pp. 51–61, 2013.

[17] S. Särkkä and R. Piché, "On convergence and accuracy of state-space approximations of squared exponential covariance functions," in *2014 IEEE International Workshop on Machine Learning for Signal Processing (MLSP)*. IEEE, 2014, pp. 1–6.

[18] *In vitro diagnostic test systems: requirements for blood-glucose monitoring systems for self-testing in managing diabetes mellitus.* International Organization for Standardization, 2003.

[19] M. A. Ahdab, J.-J. Leth, T. Knudsen, and H. Clausen, "Glucose-insulin dynamical model for type 2 diabetic patients," 2020, arXiv:2008.01614.

[20] L. Biagi, C. M. Ramkissoon, A. Facchinetti, Y. Leal, and J. Vehi, "Modeling the error of the medtronic paradigm veo enlite glucose sensor," *Sensors*, vol. 17, no. 6, p. 1361, 2017.

[21] G. De Nicolao, G. Sparacino, and C. Cobelli, "Nonparametric input estimation in physiological systems: Problems, methods, and case studies," *Automatica*, vol. 33, no. 5, pp. 851–870, 1997.

Chapter 5

Automatic Insulin Titration Strategies

This chapter discusses the works in Paper G [1], Paper H [2], and Paper I [3]. Those paper are concerned with developing long-acting insulin dose calculators for subjects with T2D. In Paper G and Paper I, the method is based on the concept of online optimization to tune the parameters of a proposed control law which updates the size of the insulin doses. On the other hand, Paper H focuses on adapting the BG reference, which insulin dosing strategies uses to calculate insulin, based on CGM readings. The setup considered in these works is summarized in figure 5.1. Each time instant $kT_K,\ k \in \mathbb{Z}_{\geq 0}$ with T_K being in the order of days (e.g. $T_K = 1$ [day] or $T_K = 7$ [day]), the T2D individual will provide BG related measurements which will then be used to calculate a new long-acting insulin dose recommendation for the subject to administer once daily until the $(k+1)T_K$ day. In particular, Papers G, H, and I focus on adjusting insulin doses utilizing a control law, denoted as π, which is defined as follows

$$\Delta u(k) = \pi\left(y_g(k), \boldsymbol{\theta}(j(k))\right), j(k) = \left\lfloor \frac{T_K k}{T_J} \right\rfloor, \tag{5.1}$$

$$u(k) = \max\left(0, u(k-1) + \Delta u(k)\right) \tag{5.2}$$

Here, $u(k)$ [U] is the recommended long-acting insulin dose at day kT_K, which is to be administered once daily until day $(k+1)\,T_K$. The parameters for the control law π are denoted as $\boldsymbol{\theta}(j(k))$ (or $\boldsymbol{\theta}(j)$ for the ease of notations), where $j(k)$ is an index representing the updated parameter set every $T_J \geq T_K$ days, with $T_J \in \mathbb{Z}_{>0}$. These parameters can include a gain (as in Paper G), a BG reference (as in Paper H), or a combination of both (as in Paper I). For instance, if $T_K = 1$ [day] and $T_J = 7$ [day], then $\Delta u(0) = \pi\left(y_g(0), \boldsymbol{\theta}(0)\right), \Delta u(1) = \pi\left(y_g(1), \boldsymbol{\theta}(0)\right), \ldots, \Delta u(7) = \pi\left(y_g(7), \boldsymbol{\theta}(1)\right)$, and so on. The value $y_g(k)$ represents a calculated glucose value based on the available glucose measurements. If SMBG measurements of fasting BG (FBG) are available, then $y_g(k)$ corresponds to the SMBG measurement of FBG. Alternatively, if CGM measurements are available, then $y_g(k)$ in Paper I is $y_g(k) = \min\left(\boldsymbol{\mu}_H\left(\boldsymbol{y}_c(k)\right)\right)$

(see the notation section 5 from chapter 1), where $\boldsymbol{y}_c(k) = \begin{bmatrix} y(m_{k_1}) & \dots & y(m_{k_q}) \end{bmatrix}$ is a vector containing the q available CGM measurements $y(m_{k_1}), \dots, y(m_{k_q})$ from day $(k-1)\,T_K$ until day kT_K such that $T_m m_{k_i} \in \left[(k-1)\,T_K, kT_K\right]$ for $i \in \{1, \dots, q\}$ with T_m being the sampling time of the CGM device, and $H = 3$ [hour]. On the other hand, in Paper H, $y_g(k)$ is chosen depending on T_K. If $T_K < 3$, then y_g, when CGM is considered, is computed the same way as descried previously for Paper I. Otherwise, the last three days of $\boldsymbol{y}_c(k)$ are extracted into $\boldsymbol{y}_{c_1}(k)$ for the first day ($[kT_K - 1, kT_K]$), $\boldsymbol{y}_{c_2}(k)$ for the second day ($[kT_K - 2, kT_K - 1]$), and $\boldsymbol{y}_{c_3}(k)$ for the third day ($[kT_K - 3, kT_K - 2]$). Afterwards, an average quantity is calculated $y_g(k) = (1/3)\sum_{i=1}^{3} \min\left(\boldsymbol{\mu}_H\left(\boldsymbol{y}_{c_i}(k)\right)\right)$[1]. These minimum values obtained from a moving average provides an estimate of the lowest BG concentration during a specific period, as introduced in a clinical trial [4]. The average quantity over the last three days is done in Paper H to mirror how one of the standard of care dosing algorithm computes y_g by averaging over the last three days of SMBG measurements.

In Papers G and I, the parameters $\boldsymbol{\theta}(j)$ are updated using an online optimization method. In contrast, Paper H updates the BG reference using either an Integral-Derivative (ID) controller or a weighted average of the outputs from multiple ID controllers.

In Paper G, it was also shown how the online optimization strategy can be extended to additional feedback signals. More specifically, a scenario in which T2D can provide ratings on how they feel in terms of hypoglycemia symptoms is considered. These ratings are used in the control law for the long-acting insulin dose calculation. The feedback ratings are used to handle what is known as Pseudo-Hypoglycemia (PHG) [5, 6], which is when T2D subjects experience hypoglycemia symptoms when their BG concentration is reduced quickly after being consistently high for a certain duration.

It is important to note that in the simulation studies for Paper G, Paper H, and Paper I, the model for simulating CGM errors corresponds to a MARD value of 33% instead of 10% as reported in the papers. Check the discussion in section 1 from chapter 3 for more details about this discrepancy.

It is worth noting that a MARD of 33% presents a more challenging scenario than a MARD of 10%. Nevertheless, despite the increased measurement noise in the CGM readings, the dosing methods which employ CGM readings demonstrated robust capability and managed to yield good results. This highlights the robustness of these dosing strategies to measurement noise in CGM readings. Note also that the other dosing strategies from the literature, which were compared to the dosing strategies presented in this thesis, do not rely on CGM readings. Therefore, the MARD value do not affect their performance.

1 Online Optimization for Insulin Dosing

The goal of online optimization is to tune the parameters $\boldsymbol{\theta} \in \Theta \subset \mathbb{R}^{n_\theta}$ for a control law π based on the available glucose measurements. The online optimization scheme works by finding

[1] This fact has not been explained correctly in Paper I. In addition, in Paper I a notation for the average is used as $\bar{y}_g(k)$ to distinguish it from $y_g(k)$ without averaging. This choice was not made in the thesis to make the notation fit the general framework in equation I.1.

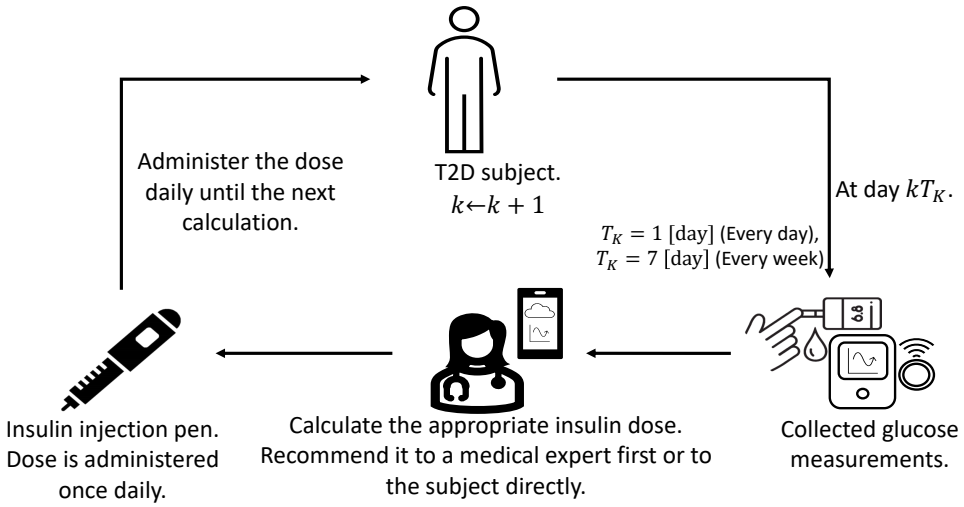

Fig. 5.1: Overview of the setup. At each kT_K days, the T2D individuals provides glucose measurements for the insulin calculation method. The insulin calculation method then computes a new long-acting insulin dose and recommend it either to a medical professional so they can communicate it to the subject, or to the subject directly. Afterwards, The subject administer the recommended dose every day until the next time for a new computation.

estimates $\hat{\boldsymbol{\theta}}$ tracking the following

$$\boldsymbol{\theta}^*(j) = \underset{\boldsymbol{\theta}\in\Theta}{\operatorname{argmin}}\ \eta(j)\bar{c}(j,\theta) + \alpha\frac{\|\boldsymbol{\theta} - \boldsymbol{\theta}^*(j-1)\|^2}{2}, \tag{5.3}$$

where $\bar{c}\,(j,\boldsymbol{\theta}) := c\left(y_g(j;\boldsymbol{\theta}), \boldsymbol{y}_c(j;\boldsymbol{\theta})\right)$ is an objective function chosen with $y_g(j;\boldsymbol{\theta}), \boldsymbol{y}_c(j;\boldsymbol{\theta})$ being the glucose measurements obtained using parameters $\boldsymbol{\theta}$ from day $(j-1)\,T_J$ until day jT_J, $\eta(j) > 0$, and $\alpha > 0$. For each $\hat{\boldsymbol{\theta}}(j)$, an inexact gradient $\hat{\boldsymbol{g}}(j+1) \approx \nabla\bar{c}(j+1,\hat{\theta}(j)))$ will be estimated. After that, $\hat{\boldsymbol{g}}(j+1)$ is used to obtain an estimate $\hat{\boldsymbol{\theta}}(j+1)$.

The term $\alpha\frac{\|\boldsymbol{\theta}-\boldsymbol{\theta}^*(j-1)\|^2}{2}$ is added to ensure that the parameters $\boldsymbol{\theta}^*$ do not change abruptly between iterations. Additionally, the values $\eta(j)$ and α are included to help balance between the cost $\bar{c}(j,\boldsymbol{\theta})$ and $\frac{\|\boldsymbol{\theta}-\boldsymbol{\theta}^*(j-1)\|^2}{2}$. Gradient estimates in Paper G and Paper I are obtained either by using the One-Point Residual Feedback (OPRF) method in [7], or by assuming a local linear model for the objective function $\bar{c}\,(j,\boldsymbol{\theta})$ and then use a Recursive Least Squares (RLS) approach with directional forgetting to obtain estimates of the gradient. The gradient

estimate of the OPRF method is simply given by

$$\hat{\boldsymbol{g}}(j) = n_\theta \Delta\bar{c}(j, \hat{\boldsymbol{\theta}}(j-1), \hat{\boldsymbol{\theta}}(j-2))\boldsymbol{\gamma}^{-1}(j-1)\boldsymbol{\nu}(j-1), \tag{5.4a}$$

$$\begin{aligned}&\Delta\bar{c}(j, \hat{\boldsymbol{\theta}}(j-1), \hat{\boldsymbol{\theta}}(j-2)) \coloneqq \\ &\bar{c}\left(j, \hat{\boldsymbol{\theta}}(j-1) + \boldsymbol{\gamma}(j-1)\boldsymbol{\nu}(j-1)\right) - \bar{c}\left(j-1, \hat{\boldsymbol{\theta}}(j-2) + \boldsymbol{\gamma}(j-2)\boldsymbol{\nu}(j-2)\right),\end{aligned} \tag{5.4b}$$

where $\boldsymbol{\nu}(j) \sim \mathcal{U}\left(\mathbb{S}^{n_\theta - 1}\right)$, and $\boldsymbol{\gamma}(j) \in \mathbb{R}^{n_\theta}_{>0}$. Note that all the operations on the vectors in (5.4) are to be understood element-wise. It is worth noting that the OPRF method is actually very similar to the extremum seeking control setup in which $\hat{\boldsymbol{g}}(j)$ is the output of a specific high-pass filter on the objective function. The main difference here is that the perturbations are stochastic. Similar to the OPRF method, perturbations are also used on the parameters in the RLS with directional forgetting to ensure persistent excitation. In both of these methods, the gain on the perturbations $\boldsymbol{\gamma}(j)$ and the weight $\eta(j)$ are made to decay with time to remove their effect as the BG is converging to a safe range. To avoid problems with the conditional number of the covariance matrix within the RLS method in the absence of persistent excitation, a directional forgetting method is employed, see Paper G or Paper I for more details. With the estimated gradient, the parameters are updated through a Quasi-Newton method called AdaBelief [8]. In Paper I, a derivation on how the Quasi-Newton method updates the parameters constrained to a set Θ is provided. Table 5.1 summarizes the differences between the online-optimization approaches and how they were used in Paper G and Paper I.

It is important to note that these approaches have decaying $\eta(j)$ and $\boldsymbol{\gamma}(j)$ over time to reduce the impact of perturbations and measurement noise in the long run. By doing so, it effectively reduces exploration over time, particularly when the BG is expected to be within a safe range. However, if a subject undergoes a significant change in their behavior or physiology after their BG has converged to the safe range for a while, such as a drastic weight loss, then the current setup described here will not adapt new parameters $\boldsymbol{\theta}$ after the change. One way to address this issue is to re-initiate the tuning process (reset $\boldsymbol{\gamma}$ and η) when a significant change in the CGM or the SMBG data is observed. In Paper I, $\eta(j) = \frac{\bar{\eta}}{1+j^{0.5}}$ and $\boldsymbol{\gamma}(j) = \frac{\bar{\boldsymbol{\gamma}}}{1+j^{0.5}}$ with $\bar{\boldsymbol{\gamma}} \in \mathbb{R}^{\theta}_{>0}$, $\bar{\eta} \in \mathbb{R}$, and $T_J = 7$ [day].

Papers	Paper G	Paper I
Param.	Two gains	One gain and a reference
# of Control Laws	1	2
Grad. Est.	RLS	RLS and OPRF
Meas.	SMBG and PHG ratings	SMBG/CGM

Table 5.1: Differences between Paper G and Paper I. Param., Grad, Est, and Meas. correspond to Parameters, Gradient, Estimation, and Measurements, respectively. The # of Control Laws refers to the number of different control laws investigated in the paper.

2 Integral Derivative Controllers

In Paper H, only the BG reference is updated and it is updated using simpler approaches to the ones in Paper G and Paper I. The reference is adapted for each subject using ID controllers driven by an averaged "nonlinear error" quantity $\bar{\phi}(\boldsymbol{y}_c(j))$ computed based on CGM readings $\boldsymbol{y}_c(j)$ as follows

$$\bar{\phi}(\boldsymbol{y}_c(j)) := \frac{1}{q}\sum_{i=1}^{q} \gamma_{y_\ell, y_u}(y(m_{j_i}))\phi(y(m_{j_i})), \tag{5.5}$$

where the cutoff function γ_{y_ℓ, y_u} is defined as

$$\gamma(y)_{y_\ell, y_u} := \begin{cases} 0, & y \in [y_\ell + 1, y_u - 1] \\ 1, & \text{Otherwise,} \end{cases} \tag{5.6}$$

with $y_\ell = 4$ [mmol/L] and $y_u = 7$ [mmol/L]. The nonlinear error function is defined as

$$\phi_\ell(y) := K_1 s_a(-(y - y_\ell)) \tag{5.7a}$$
$$\phi_u(y) := -K_2 s_b(y - y_u) \tag{5.7b}$$
$$\phi(y) := \phi_u(y) + \phi_\ell(y) \tag{5.7c}$$

where $s_\alpha(x) := \frac{1}{\alpha}\log(1 + \mathrm{e}^{\alpha x})$ is the softplus function, $K_1, K_2 \in \mathbb{R}_{>0}$ are gain constants, and $a, b \in \mathbb{R}$ are shape parameters. This nonlinear error function "weighs" different regions of BG according with different gains, see Figure 5.2.

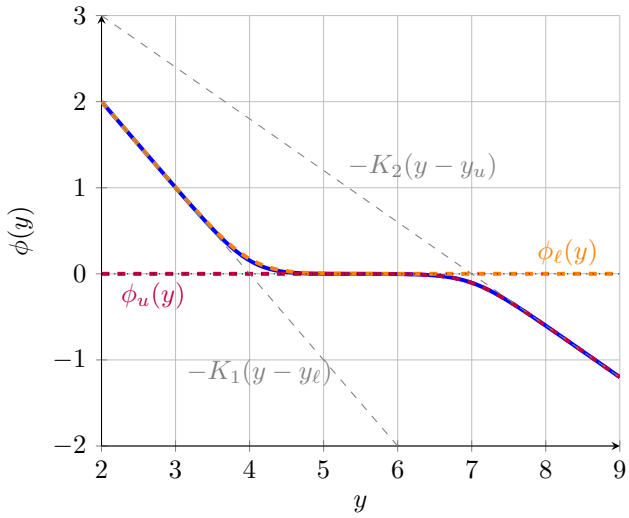

Fig. 5.2: The nonlinear error function.

The BG references are then updated for each subject by either using a simple ID controller

$$r(j) = \Pi_{\Omega,\boldsymbol{I}}\Big(r(j-1) + T_J K_I \bar{\phi}\left(\boldsymbol{y}_c(j)\right) + K_D\left(\bar{\phi}\left(\boldsymbol{y}_c(j)\right) - d_r(j-1)\right)\Big), \tag{5.8a}$$

$$d_r(j) = (1-\beta)d_r(j-1) + \beta\bar{\phi}\left(\boldsymbol{y}_c(j)\right),\ d_r(0) = 0. \tag{5.8b}$$

where $K_I > 0$ is the integral gain, $K_D \geq 0$ is the derivative gain, $0 < \beta \leq 1$, and $\Omega = [r_\ell, r_u]$ with $r_\ell = 4$ [mmol/L] and $r_u = 10$ [mmol/L], or by using weighted average for the output of several ID controllers in which the weights are adapted online based on ϕ, see Paper H for more details.

Remark 2.1. *The ID controller name*
The reasoning behind the naming of the controller in (5.8) to be an ID controller can be understood if a simpler version of it is considered. Namely, if $\beta = 1$ and the projection $\Pi_{\Omega,\boldsymbol{I}}$ is not used, then (5.8) becomes

$$r(j) - r(j-1) = T_J K_I \bar{\phi}\left(\boldsymbol{y}_c(j)\right) + K_D\left(\bar{\phi}\left(\boldsymbol{y}_c(j)\right) - \bar{\phi}\left(\boldsymbol{y}_c(j-1)\right)\right). \tag{5.9}$$

Dividing by T_J and taking $T_J \to 0$

$$\dot{r}(t) = K_I \bar{\phi}\left(\boldsymbol{y}_c(t)\right) + K_D \dot{\bar{\phi}}\left(\boldsymbol{y}_c(t)\right).$$

Integrating with respect to time

$$r(t) - r(0) = K_I \int_0^t \bar{\phi}\left(\boldsymbol{y}_c(s)\right) ds + K_D\left(\bar{\phi}\left(\boldsymbol{y}_c(t)\right) - \bar{\phi}\left(\boldsymbol{y}_c(0)\right)\right).$$

The term $\int_0^t \bar{\phi}\left(\boldsymbol{y}_c(s)\right) ds$ is the reason behind the "Integral" part of the name. While one could call the difference $K_D\left(\bar{\phi}\left(\boldsymbol{y}_c(t)\right) - \bar{\phi}\left(\boldsymbol{y}_c(0)\right)\right)$ as a proportional term, the "Derivative" name is used instead to emphasize that it is implemented as a difference in (5.9) and it has the characteristic of a derivative term (sensitive to noise).

3 Comparing the Strategies

This section presents a comparison between three strategies: the strategy proposed in Paper G without considering PHG ratings, the most effective strategy devised in Paper H, and the most effective strategy developed in Paper I. The purpose of this comparison is to evaluate their respective performance. The comparison is made by generating 1500 virtual T2D subjects according to three different simulation models, including the model in Paper A [9]. The simulation setup is the same one as in Paper I and the details for it can be found there. In addition to the simulation setup in Paper I, subjects simulated with the model in Paper A are assumed to perform a physical activity two hours before dinner everyday for a period drawn randomly for each subject according to a uniform distribution of $\mathcal{U}[30, 60]$ [mins]. In that period, the heart rate of the subjects is increased by 30 beats per minute from the base heart rate.

Table 5.2: Glucose management metrics from [10]. The unit for the ranges and glucose values is [mmol/L].

Measure	% of time of BG in	Target
Time in Range (TIR)	$[3.9, 10)$	$> 70\%$
Time Above Range 1 (TAR1)	$[10, 13.9)$	$< 25\%$
Time Above Range 2 (TAR2)	$[13.9, \infty)$	$< 5\%$
Time Below Range 1 (TBR1)	$[3, 3.9)$	$< 4\%$
Time Below Range 2 (TBR2)	$[0, 3)$	$< 1\%$
Average Glucose (AG)		< 8.6
Glucose Variability (GV)		36%
Glucose Management Index (GMI)		7%

Table 5.3 demonstrate some statistics for the calculated glucose management metrics, defined in table 5.2, for each subject. Analysis of the results presented in Table 5.3 reveals some key observations. To begin with, the strategy from Paper G demonstrates the highest mean Time in Range (TIR) value, accompanied by the lowest standard deviation in TIR. However, it is important to note that this strategy is the only one among the dosing methods that exhibits a non-zero mean Time Below Range 1 (TBR1). This discrepancy can be explained according to the fact that the approach described in Paper G relies only on SMBG measurements as feedback, unlike the other methods that incorporate CGM readings. The incorporation of CGM readings as feedback enables the other methods to adjust the BG reference, thus reducing the occurrence of hypoglycemic events. Comparing the strategies presented in Paper I and Paper H, it is evident that Paper I exhibits better statistics. Nonetheless, the method described in Paper H possesses certain advantages, such as its simplicity and the absence of perturbations. These characteristics render it more practical and appealing for real-world implementation.

Table 5.3: Statistics for the different methods from the different papers. The abbreviation std. stands for the standard deviation.

	Mean TIR	std. TIR	Mean TBR1	std. TBR1
Target [10]	$> 70\%$		$< 4\%$	
Paper I	96.6%	4%	0%	0%
Paper H	94.82%	3.5%	0%	0%
Paper G	96.8%	3%	0.8%	2.11%

	Mean TBR2	std. TBR2	Mean AG	std. AG
Target [10]	$< 1\%$		< 8.6 [mmol/L]	
Paper I	0%	0%	7	0.7
Paper H	0%	0%	7.3	0.8
Paper G	0%	0%	5.8	0.65

	Mean TAR1	std TAR1	Mean TAR2	std TAR2
Target [10]	$< 25\%$		$< 5\%$	
Paper I	3.4%	2.5%	0.5%	0.4%
Paper H	4.9%	2.4%	0.4%	0.34%
Paper G	1.86%	1.33%	0.4%	0.4%

	Mean GV	std GV	Mean GMI	std GMI
Target [10]	$< 36\%$		$< 7\%$	
Paper I	18.2%	5.2%	6.3%	0.3%
Paper H	19%	3.7%	6.5%	0.43%
Paper G	22.77%	5.23%	5.83%	0.3%

References

[1] M. Al Ahdab, T. Knudsen, J. Stoustrup, and J.-J. Leth, "An online stochastic optimization approach for insulin intensification in type 2 diabetes with attention to pseudo-hypoglycemia," in *2022 IEEE 61st Conference on Decision and Control (CDC)*, 2022, pp. 2572–2579.

[2] M. Ahdab, T. Knudsen, J. Stoustrup, and J.-J. Leth, "Blood glucose reference personalization for subjects with type 2 diabetes," in *2021 IEEE Conference on Control Technology and Applications (CCTA)*. United States: IEEE, 2023 (In press).

[3] ——, "Online optimization approach for calculating insulin doses for individuals with type 2 diabetes," in *IEEE Transactions on Control Systems Technology*. United States: IEEE, 2023 (Submitted).

[4] T. B. Aradóttir, H. Bengtsson, M. L. Jensen, N. K. Poulsen, D. Boiroux, L. L. Jensen, S. Schmidt, and K. Nørgaard, "Feasibility of a new approach to initiate insulin in type 2 diabetes," *Journal of diabetes science and technology*, vol. 15, no. 2, pp. 339–345, 2021.

[5] M. T. McDermott, "Pseudopheochromocytoma," *Management of Patients with Pseudo-Endocrine Disorders: A Case-Based Pocket Guide*, p. 193, 2019.

[6] E. R. Seaquist, J. Anderson, B. Childs, P. Cryer, S. Dagogo-Jack, L. Fish, S. R. Heller, H. Rodriguez, J. Rosenzweig, and R. Vigersky, "Hypoglycemia and diabetes: a report of a workgroup of the american diabetes association and the endocrine society," *The Journal of Clinical Endocrinology & Metabolism*, vol. 98, no. 5, pp. 1845–1859, 2013.

[7] Y. Zhang, Y. Zhou, K. Ji, and M. M. Zavlanos, "A new one-point residual-feedback oracle for black-box learning and control," *Automatica*, vol. 136, p. 110006, 2022. [Online]. Available: https://www.sciencedirect.com/science/article/pii/S000510982100532X

[8] J. Zhuang, T. Tang, Y. Ding, S. C. Tatikonda, N. Dvornek, X. Papademetris, and J. Duncan, "Adabelief optimizer: Adapting stepsizes by the belief in observed gradients," *Advances in neural information processing systems*, vol. 33, pp. 18 795–18 806, 2020.

[9] M. A. Ahdab, J.-J. Leth, T. Knudsen, and H. Clausen, "Glucose-insulin dynamical model for type 2 diabetic patients," 2020, arXiv:2008.01614.

[10] R. I. Holt, J. H. DeVries, A. Hess-Fischl, I. B. Hirsch, M. S. Kirkman, T. Klupa, B. Ludwig, K. Nørgaard, J. Pettus, E. Renard *et al.*, "The management of type 1 diabetes in adults. a consensus report by the american diabetes association (ada) and the european association for the study of diabetes (easd)," *Diabetes Care*, vol. 44, no. 11, pp. 2589–2625, 2021.

Chapter 6

Nudging Towards Adherence

In this chapter, a description on how behavioral momentum theory can be used to obtain a dynamical model for the effect of nudges on discouraging a certain behavior will be provided. Afterwards, an OCP will be formulated with the developed model to schedule different types of nudges and their frequencies. Finally, a discussion on how this can be used for scheduling nudges for T2D subjects to encourage them to adhere to medications. This chapter is based on Paper J [1].

1 Behavioral Momentum Model

Behavioral momentum theory offers a quantitative framework to support the notion that behaviors, reinforced frequently in the past, exhibit greater resistance to change when faced with disruptions compared to behaviors with less frequent past reinforcement [2, 3]. The works in [2, 3] introduced and validated mathematical models for behavioral momentum theory using data from various experiments. Those mathematical models were used to obtain a simplified averaged continuous-time version in Paper J. To present the model, define $\beta(t) \in \mathbb{R}_{\geq 0}$ as the average rate of occurrence for a specific behavior per unit time and represent it as $x(t) := \log_{10}\big(\beta(t)\big)$. Then the change $x(t) - x(t_1)$ over a time interval $\Delta t := t - t_1 \geq 0$ is modeled, according to behavioral momentum theory, in relation to disruptions and reinforcers as

$$x(t) - x(t_1) = \frac{-\delta(t)}{\sqrt{r(t)}}\Delta t.$$

Here, $r(t) \in \mathbb{R}_{\geq 0}$ denotes the average rate of a reinforcer, and $\delta(t) = b(t)v(t)$, where $v(t) \in \mathbb{R}_{\geq 0}$ represents the average rate of disruption events and $b(t) \in \mathbb{R}_{\geq 0}$ serves as a factor determining the effect of these disruption events. The value $\sqrt{r}$ corresponds to "behavioral inertia," indicating that a higher average reinforcer rate necessitates a higher average rate of disruption δ to induce a change in behavior. By dividing by Δt and taking the limit as $\Delta t \to 0$, we obtain

the differential equation:

$$\dot{x}(t) = \frac{-1}{\sqrt{r(t)}}\delta(t). \tag{6.1}$$

Now consider that disruptions occur at an average rate of $v(t)$. These disruptions can fall into n_u different types, each with a probability of $\bar{u}_i$ and an effect factor of b_i. In this case, the expression for $\delta(t)$ in Equation (6.1) can be written as follows:

$$\delta(t) = v(t)\boldsymbol{b}(t)^{\mathrm{T}}\bar{\boldsymbol{u}}(t), \tag{6.2}$$

where $\bar{\boldsymbol{u}}(t) \in \triangle^1_{n_u}$ and $\boldsymbol{b}(t) \in \mathbb{R}^{n_u}_{\geq 0}$. Here, each component $\bar{u}_i(t)$ of $\bar{\boldsymbol{u}}(t)$ can be viewed as the average rate of a specific disruption type relative to the other types in $\delta(t)$ (average rate ratio). It is important to note that the sum $\sum_{i=1}^{n_u} v(t)\bar{u}_i(t) = v(t)$. Ideally, the value of $v(t)$ should be kept relatively small to avoid alert fatigue, which refers to the phenomenon where the effectiveness of disruptions diminishes due to their high average rate [4]. With the model in (6.1) with (6.2), an OCP can be defined to decide on $\bar{\boldsymbol{u}}(t)$ for the different types of disruptions together with $v(t)$.

2 Optimal Control Problem

The behavioral momentum model can be used in an OCP as following

$$\max_{\boldsymbol{u},v} \int_{t_0}^{t_f} L\left(x(t), \boldsymbol{u}(t), v(t), t\right)dt + S\left(x(t_f)\right) \tag{6.3a}$$

$$\dot{x} = \frac{-1}{\sqrt{r(t)}}\boldsymbol{b}^{\mathrm{T}}(t)\boldsymbol{u}(t),\ x(t_0) = x_0, \tag{6.3b}$$

$$\mathbf{1}^{\mathrm{T}}\boldsymbol{u}(t) = v(t),\ \boldsymbol{u}(t) \geq_e 0,\ v(t) \geq 0, \tag{6.3c}$$

where $\boldsymbol{u}(t) = v(t)\bar{\boldsymbol{u}}(t)$. The functions L and S are defined as

$$L\left(x, \boldsymbol{u}, v, t\right) := \frac{1}{\eta}\phi(\boldsymbol{u}) + \boldsymbol{c}^{\mathrm{T}}(t)\boldsymbol{u} + dx + qv^2,\ S(x) := ex,$$

with $\phi(\boldsymbol{u})$ being the Shannon's entropy in $\boldsymbol{u}$, $\eta > 0$, $\boldsymbol{c}(t) \in \mathbb{R}^{n_u}$ being continuously differentiable, $d \in \mathbb{R}$, $e \in \mathbb{R}$, and $q < 0$. The entropy term $\phi(\boldsymbol{u})$ encourages the diversity of using different types of disruptions. This is particularly advantageous because it allows for a wider range of disruptive strategies to be explored and incorporated into the solution. Moreover, unlike using a quadratic term for the regularization of $\boldsymbol{u}$, the inclusion of an entropy term facilitates the derivation of a closed-form solution for (6.3), as demonstrated in Paper J. The availability of a closed-form solution enhances the efficiency and practical implementation of the approach, making it more feasible for real-world applications.

3 Example for Nudging to Adherence

In this section, an abstract example of how the OCP in (6.3) can be used to schedule different types of nudges to discourage non-adherence to medications is presented.

Nudges can be considered as disruptions that can change the reinforcement contingencies associated with an undesired behavior, such as non-adherence to medication. Now consider a scenario where an individual with diabetes is not adhering to their prescribed medication regimen with an initial average rate of $\beta(0) = 5$ [week^{-1}]. For example, the diabetic individual is not administrating the exact prescribed dose of insulin due to some average rate of a reinforcer $r = 7$ [week^{-1}]. The reinforcer could be inconveniences associated with dose administration and economic constraints. With this setup, consider that there are three different types of nudges which can be used to encourage the individual to adhere better to their treatment despite the reinforcers.

The first type of nudges involves sending dose reminder text messages to the subject. This nudge is characterized by a probability $\bar{u}_1(t)$ with an effect $b_1(t)$ on disrupting the non-adherence behaviour. The dose reminder text messages serve as gentle reminders to the individual, encouraging them to stay on track with their treatment regimen.

The second type of nudges is personalized encouraging text messages directed at the individual. These messages are tailored specifically to the individual's circumstances and are intended to motivate and inspire them to adhere to their prescribed doses. The probability of employing this type of nudge is denoted as $\bar{u}_2(t)$ with an effect $b_2(t)$ on disrupting the undesired behavior of non-adherence.

Lastly, the third type of nudges involves personal phone calls made by the medical staff. These calls serve as direct communication with the individual, emphasizing the importance of following their prescribed doses. The probability of implementing this type of nudge is represented by $\bar{u}_3(t)$ with an effect $b_3(t)$ on the non-adherence behavior. These personal phone calls aim to create a stronger impact and enhance the individual's understanding of the significance of treatment adherence. The effect of phone calls can be set to be the highest and the effect of the dose reminder text can be set to be the lowest. The value $v(t)$ then represent the average rate at which a nudge is implemented. The parameters in the objective of the OCP (6.3a) can be chosen such that $d < 0$ and $e < 0$ to penalize non-adherence (minimizing $\beta(t) = 10^{x(t)}$), $\boldsymbol{c}(t) = \begin{bmatrix} c_1(t) & c_2(t) & c_3(t) \end{bmatrix}^{\mathrm{T}} \leq_e 0$ with $c_3(t) < c_2(t) < c_1(t)$ for all $t > 0$ to put more cost on using medical phone calls than text reminders, and $q < 0$ representing how much it is desired to lower the frequency of nudges to avoid alert fatigue. In Paper J, different scenarios were investigated for this example with different values for $\boldsymbol{b}(t)$ and when the solution of the OCP in (6.3a) is applied in a receding horizon fashion in which it is assumed that only noisy estimates of the true $\boldsymbol{b}(t)$ are available. The code for all the simulations of the examples can be found at `https://gitlab.com/aau-adapt-t2d/nudging_entropyocp`. The following figure represent a case in which $b_1 < b_2 < b_3$ and $c_3 < c_2 < c_1$

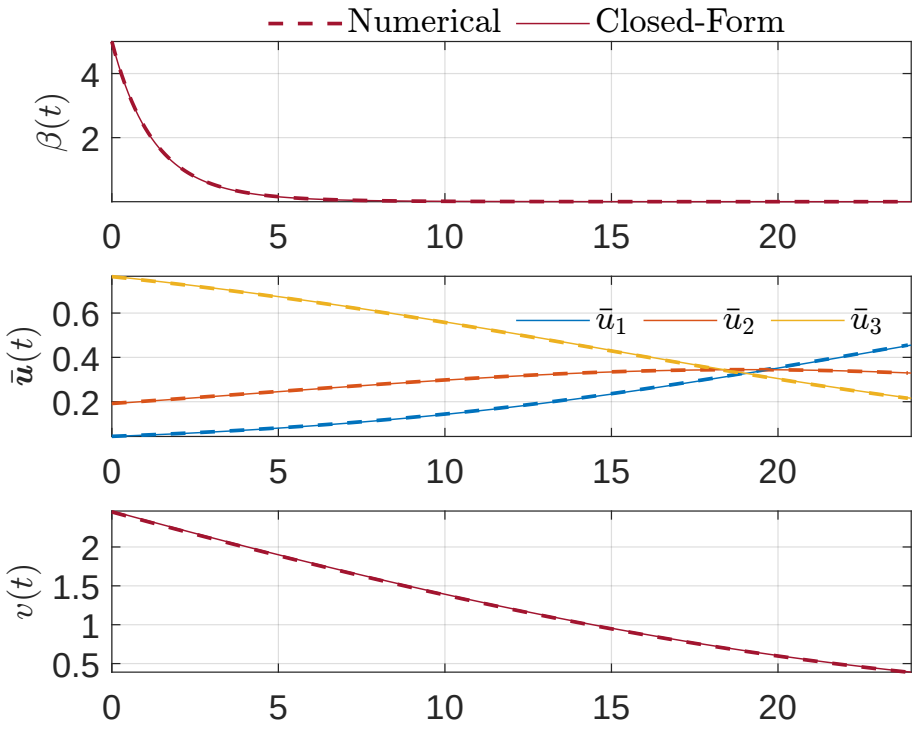

Fig. 6.1: A numerical solution for OCP in (6.3a) against the closed-form solution derived in Paper J [1].

References

[1] M. A. Ahdab, T. Knudsen, J. Stoustrup, and J.-J. Leth, "Entropy for optimal control on a simplex with an application to behavioral nudging," *IEEE Control Systems Letters*, vol. 7, pp. 2797–2802, 2023.

[2] J. A. Nevin and T. A. Shahan, "Behavioral momentum theory: Equations and applications," *Journal of Applied Behavior Analysis*, vol. 44, no. 4, pp. 877–895, 2011.

[3] B. D. Greer, W. W. Fisher, P. W. Romani *et al.*, "Behavioral momentum theory: A tutorial on response persistence," *The Behavior Analyst*, vol. 39, pp. 269–291, 2016.

[4] B. S. Last, A. M. Buttenheim *et al.*, "Systematic review of clinician-directed nudges in healthcare contexts," *BMJ open*, vol. 11, no. 7, p. e048801, 2021.

Chapter 7

Concluding Remarks

In this chapter, concluding remarks regarding the contribution of this theses with regards to the research objective will be provided and discussed. This thesis aims to provide tools and feedback strategies to support both the medical professionals and individuals with T2D in the management of diabetes. The thesis explores different avenues of possible tools which can help with the management of T2D. These different directions are identified as research objectives which the thesis aims to contribute to. The conclusions for the different avenues with possible directions of future work for each one of them is provided in the sections of this chapter.

1 Complex Modeling

In Paper A and for some part of this thesis, a detailed model for the glucose-insulin dynamics of T2D subjects has been developed. The model is able to account for different types of medications, different types of meals, physical activity, and stress. This comprehensive model serves multiple purposes, including the assessment of treatment plans and the education of medical students. It has been specifically used at Aalborg University Hospital as a teaching tool for medical students. Moreover, the model has been utilized within the thesis to assess algorithms for long-acting insulin dose calculators.

Given the complexity of the model's functionalities, it is challenging to obtain data that can validate all of its aspects simultaneously. Nevertheless, it remains important to pursue the collection of data related to different parts of the model and individually validate them. This approach serves as a crucial avenue for future work. Moreover, this validation process allows for a detailed understanding of the functionality for each part of the model.

2 Stochastic Modeling and Estimation

The works presented in Paper B, C, and D have resulted in the development of a simple, in the sense discussed in the introduction chapter, stochastic model along with a method to estimate

its parameters. This stochastic model offers the opportunity to estimate not only physiological parameters but also behavioral parameters, such as the average number of meals consumed by the subject per day. Additionally, methods to estimate and fit this class of stochastic models were investigated and developed. Furthermore, the models have demonstrated their capability to identify meal events when fitted to specific subjects. Moreover, The potential of these stochastic models for short-term prediction and meal detection has also been evaluated, showing promise for their practical application to help with the managment of T2D.

It is necessary to point that the estimation methods, especially in Paper C and Paper D, are computationally intensive. Future work should consider making these estimation methods more efficient. In addition, it is essential to conduct a more comprehensive assessment and validation of the models using a larger set of clinical data in order to validate their generalizability. Moreover, it is crucial to develop and test algorithms that directly utilize the stochastic model as a tool for clinical trials. For example, developing a tool which utilizes the fitted models to simulate and test alternative scenarios and compare them with the available CGM data. In terms of the stochastic models themselves, an interesting direction for future work is to study the utilization of different jump processes to consider various types of meals or variations in the average number of meals throughout the day. This would enhance the models' ability to capture and represent different meal patterns effectively.

3 Enhancing Glucose Sensors

The research conducted in Paper E and Paper F within this thesis addresses the objective of enhancing glucose sensors through distinct approaches. In Paper E, the focus lies in investigating the use of TGPs to derive a subject-specific model for the errors in CGM devices. The paper aims to demonstrate the potential of using different TGP models to capture correlated and time-dependent CGM errors by incorporating data from a single CGM device and SMBG measurements. The results in Paper E showcases the potential of TGPs for modeling CGM errors with data obtained from one CGM device and SMBG measurements.

While the results presented in Paper E are promising for future implementation in glucose sensor enhancement, it is important to note that the method described in the paper is computationally heavy. Furthermore, it is crucial for future research to compare the performance of the method and models in Paper E with alternative methods, utilizing actual CGM and SMBG readings from individuals with T2D.

On the other hand, Paper F introduces a framework to fuse the readings of multiple CGM devices to generate a more reliable fused CGM signal. The framework's effectiveness was evaluated using real data from two distinct animal experiments, where the results showcased its ability to produce a reliable fused CGM signal. To further improve the framework, a potential research direction is to explore the integration of an adaptive forgetting factor for the MMKFF strategy. Additionally, it is important to test the framework on additional data from different experiments to gain deeper insights into its potential applicability in real-world, human settings.

4 Automatic Insulin Titration Strategies

The papers G, H, and I present different strategies for recommending long-acting insulin doses, utilizing different types of feedback signals. These dosing strategies can incorporate feedback signals unrelated to BG measurement devices, such as PHG scores, as demonstrated in Paper G. The performance of these strategies is compared against standard of care methods and state-of-the-art techniques through simulations using three different models. The results demonstrate that the strategies outperform the existing methods in terms of glucose management metrics defined in [1].

Notably, all these strategies do not rely on a physiological model and are computationally lightweight and easy to implement. Additionally, when comparing the strategies presented in Papers G, H, and I, it is evident that the method described in Paper I achieves better statistical performance when compared to the other methods. However, despite the method in Paper H not performing as well as the one in Paper I, the method in Paper H offers a simpler approach without stochastic perturbations, making it more attractive for application in a clinical setting.

It is important to note that the online optimization methods utilize both a decaying perturbation gain and a step size on the tuned parameters. Additionally, the adaptive weights method discussed in Paper H employs a decaying step size. These methods may face challenges when sudden changes occur in T2D individuals after their BG has stabilized within the safe zone for a certain period. To overcome this issue, one potential approach is to re-initiate the online optimization process when either the perturbation gain and/or the step size drop below a predetermined threshold, and specific changes are identified in the BG data.

5 Nudging Towards Adherence

Paper J focuses on the implementation of behavioral nudging to address non-adherence to medication in diabetes management using an optimal control approach. Within this framework, the scheduling of different types of nudges, each with varying frequencies, is examined. The dynamical model employed in this study is based on behavioral momentum theory, with inputs representing the probability of selecting a specific nudge type and the average rate of nudges.

To address this, the paper formulates an OCP belonging to a class of OCPs with inputs constrained to a variable-sized simplex, in which the size of the simplex itself is an additional input. Furthermore, the paper demonstrates that by incorporating the entropy function into the objective functional of this class of OCPs, a closed-form solution can be derived for the OCP. The paper provides several examples illustrating the practical application of the OCP framework in conjunction with behavioral momentum theory. These examples demonstrates the potential of the closed-form solution to be utilized to schedule different types of nudges and their frequencies in a hypothetical scenario involving medication adherence encouragement for an individual with diabetes.

This work serves as a foundational step towards utilizing control theory techniques in conjunction with behavioral momentum theory for the design of effective nudging strategies. Future work will concentrate on incorporating more detailed behavioral momentum models into the framework. Additionally, the proposed method need to be compared with alternative

approaches, such as the one outlined in [2]. Another direction for future work is the identification techniques for behavioral momentum models so that they can be used effectively with the method outlined in Paper J. These research directions aim to advance the understanding and application of behavioral nudging in diabetes management, optimizing the adherence of T2D individuals and their overall treatment outcomes.

References

[1] R. I. Holt, J. H. DeVries, A. Hess-Fischl, I. B. Hirsch, M. S. Kirkman, T. Klupa, B. Ludwig, K. Nørgaard, J. Pettus, E. Renard *et al.*, "The management of type 1 diabetes in adults. a consensus report by the american diabetes association (ada) and the european association for the study of diabetes (easd)," *Diabetes Care*, vol. 44, no. 11, pp. 2589–2625, 2021.

[2] F. Callaway, M. Hardy, and T. Griffiths, "Optimal nudging for cognitively bounded agents: A framework for modeling, predicting, and controlling the effects of choice architectures," Jan 2022. [Online]. Available: psyarxiv.com/7ahdc.

Part II

Papers

Paper A

Glucose-Insulin Mathematical Model for the Combined Effect of Medications and Life Style of Type 2 Diabetic Patients

Mohamad Al Ahdab, John Leth, Torben Knudsen, Peter Vestergaard, and Henrik Glavind Clausen.

The paper has been published in the Biochemical Engineering Journal, vol. 176, no. 108170, 2021.

The layout has been revised.

Abstract

The goal of this paper is to propose a new mathematical model for the combined effect of different treatments and lifestyles on the glucose-insulin dynamics of Type 2 diabetes (T2D) patients. The model gives the possibility to take into consideration physical activity, stress, meals, and medications while evaluating or designing treatment plans for T2D patients. The model is proposed by combining and modifying some of the available models in the literature. Simulations were performed for the modifications to show how the model confirm with literature on T2D patients. Additionally, a discussion is provided to demonstrate the ability of the model to be used in the assessment of treatment plans and in the design for robust insulin dose guidance algorithms. An open source code for the model is additionally provided.

1 Introduction

One of the greatest health challenges which faces humanity in the 21st century is the emergence of type 2 diabetes (T2D) as a global pandemic. More than 463 million were reported to suffer from diabetes in 2019 and the number is expected to reach 700 million by 2045 [1]. Moreover, the global expenses related to diabetes are estimated to be 760 billion USD in 2019 and they are expected to increase [1]. T2D is characterized by high levels of glucose concentration in the blood. This increase in glucose levels can cause cardiovascular, kidney, and eye diseases and, if left untreated, will lead to organ failures. For T2D patients, low sensitivity to insulin, which is the hormone responsible for lowering glucose concentration in the blood, causes the beta cells in the pancreas to produce insulin to compensate. This will eventually weaken the cells and damage them, which in turn will make the body fail to regulate glucose concentration [2]. Insulin based treatment is initiated at later stages of the T2D disease when changes in diets and physical activities accompanied with oral medications have failed. Clinically, it is difficult to calculate suitable insulin doses and oral medication treatment plans for each specific patient. Therefore, many patients experience uncontrolled hyperglycemia for a long period of time until they reach a safe level of glucose [3]. Having a model to simulate the combined effect of oral medications, insulin doses, and lifestyle changes can help medical professionals in the evaluation of different treatment plans. Moreover, such models can be used together with robust control methods to design automatic insulin guidance algorithms that ensure safe reach to the desired glucose concentrations.

In general, there are two main categories of methods to model systems: first principles methods, or data driven methods derived by fitting data to general mathematical structures such as ARMAX models.

The glucose-insulin dynamical models for T2D patients based on first principles can vary with different degrees of complexity. In the literature, there exist two main categories of such models: minimal models and maximal models [4]. Maximal models are very detailed models, which model metabolic functions at a molecular level. On the other hand, minimal models are less detailed and rely mostly on compartments and mass balance equations. While maximal models provide a great level of accuracy, the amount of different data, which is required to estimate parameters for these models is large and difficult to obtain from patients undergoing typical treatment plans. Moreover, the high accuracy of maximal models provides

little relevance to the accuracy of the general glucose-insulin dynamics within the human body [4].

In contrast, minimal models consist of compartments to represent the distribution, diffusion, and production of glucose and insulin in the body with terms to represent the interaction between them. Furthermore, these models include pharmacokinetic equations to describe exogenous insulin injections and the intake of other medications. Several mathematical structures have been developed for the glucose-insulin dynamics in T2D patients. Some of them have a simple structure with less than ten states such as the ones presented in [5, 6]. These models consider simple insulin injections and meal models. Their simplicity make them good candidates for patient specific parameter estimation and control design. Nevertheless, the few number of states force them to consider generic insulin and glucose states without considering other metabolic hormones (e.g. glucagon). Thus, making the process of augmenting them with oral medications and stress difficult. On the other hands, the models in [7, 8] are larger and more complex. The model in [7] has recently been proposed and confirmed with patient data. Parameters were estimated as mean and covariance matrices of a normal distribution from patients' data. Only the mean and the diagonal elements of the covariance matrices were reported. The model includes a glucose ingestion model that takes into account only glucose meal given after fasting conditions. The model was also augmented with an insulin degludec linear pharmacokinetic model in [9]. As for the model in [8], it is based on [10] and includes the effect of oral medications (metformin and vildagliptin), Glucagon, and Glucagon-like peptide-1. The model uses the same glucose ingestion model from [7] and it is only for glucose meals after fasting conditions. Only mean parameters were reported. The work in [11] focused on the glucose dynamics in the brain and provided a mathematical description for the effect of stress in diabetic patients. Physical activity has been modelled before but mainly for type 1 diabetes patients. It has been included in simple models such as the one in [12, 13] or more complicated ones such as the one in [14].

Heart beat rate data from smart watches [15] and data regarding stress levels from self-assessment questionnaires [16, 17] are becoming more feasible to be obtained from patients during treatment. Therefore, having a model to simulate the combined effect of different types of treatments together with the effect of stress and physical activity can improve the process of evaluating and developing treatment plans for diabetic patients.

Therefore, in this work, it is intended to present a mathematical structure for the combined effect of multiple glucose meals with no fasting conditions, insulin injections, multiple oral doses of metformin with different sizes, physical activity, and stress. Additionally, a Matlab [18] toolbox is developed to simulate patients with this mathematical structure is provided as an open source code on GitLab (Link will be included in the final draft if the manuscript is accepted) for others to use the model easily and have a better chance to contribute on the development of the model. This structure can help with analyzing treatment plans depending on lifestyle conditions. Moreover, the structure can be used with robust control strategies to obtain algorithmic insulin dose calculators. The structure is based on the one in [19] with modifications and inclusions as following (see figure A.1):

- Modifying the model to account for multiple meals (see section 2.1).
- Including a model for insulin injections based on [20] (see section 2.2).
- Modifying the metformin model to account for multiple different doses in section 2.3.

- Including the effect of physical activity based on [12] (see section 2.4).
- Including the effect of stress based on [11] (see section 2.5).

In addition, a discussion on how the developed model can be used, and what type of data is needed to fit the model is provided in Section 3. All simulations are performed using the toolbox from GitLab. The model parameters, which are used in the simulations, are found in Table A.3.

2 Model Description

The model is mainly based on the one from [19] with the following four main subsystems:

- Glucose subsystem.
- Insulin subsystem.
- Glucagon subsystem.
- Incretins hormone subsystem.

See Figure A.1 for an overview of the model. The glucose and insulin subsystems are modelled as a set of compartments representing different main parts of the human body: brain, heart and lungs, guts, liver, kidney, and peripherals. The flow between these compartments follows the human blood cycle. As for the glucagon and the incretins, a single compartment is used for each one of them as it is assumed that glucagon and incretins have equal concentration in all the body parts. In addition, the model contains metabolic production and uptake rates for different compartments. These metabolic rates are generally defined as their basal values multiplied with scaling variables that depend on the concentrations of insulin, glucose, and/or glucagon (see (A.11)). The pancreas has a different nonlinear and hybrid model. In addition, a glucose ingestion model based on [21] is included as in [8] but modified to handle multiple meals along the day. Moreover, metformin and vildagliptin oral treatment models are included based on [22] and [23] respectively, as in [19] but with a modification on the oral metformin model to handle different oral doses along the treatment. Additionally, a physical activity model based on [12] is added to the model. Furthermore, long acting and fast acting insulin injection models based on [20] are added. Finally, stress is included as a factor $\alpha_s \in [0, 1]$ as in [11]. The main model includes parameters that were estimated by [10] for a healthy 70 kg male. The work in [8] considered a subset of these parameters to be estimated for the diabetic cases. Parameters for the different added models are taken from their corresponding literature. In the following subsections, the added and modified models and states will be discussed. The full model equations are provided in appendix A.

2.1 Glucose Absorption Model

In this section, a modification is introduced to account for multiple glucose meal sizes. The model is based on the one used in [8] which is based on [21]. The model takes into account that the gastric emptying of the stomach is correlated with the stomach content; which is supported by the study in [24]. The model in [8] and [21], however, are used for oral glucose

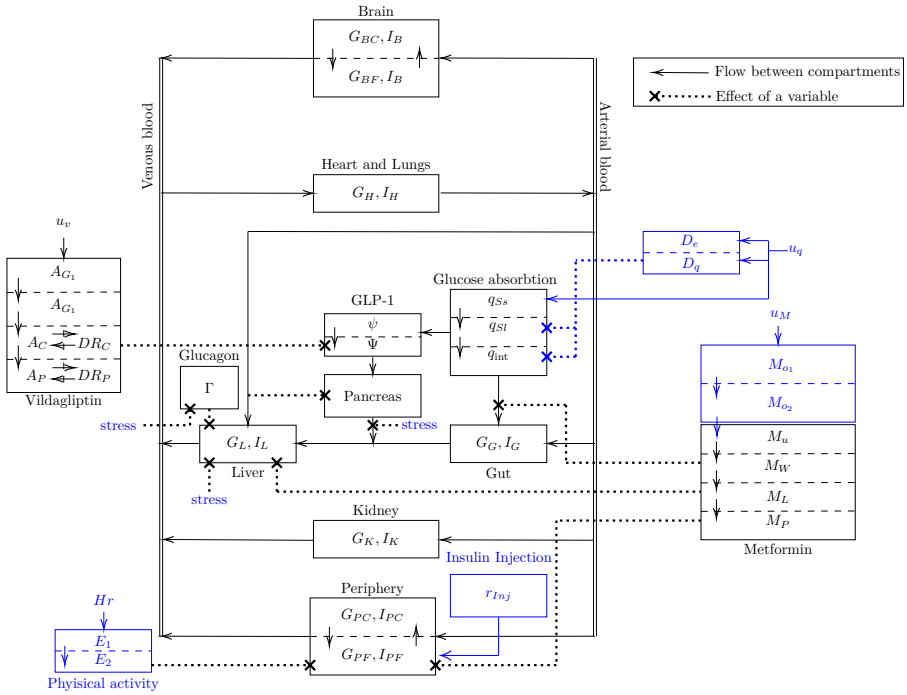

Fig. A.1: A summary of the overall model with blue indicating the modified or added models compared to [19]

tolerant tests only. The aim in this section is to make the model to take into account the effect of accumulated glucose meals on gastric emptying. It is acknowledged that gastric emptying depends on many factors other than the size of the meal as described in [25] and there exist models, which focus primarily on meal ingestion such as [26]. However, the model provided in this paper is a simplification by considering meals as glucose ingestions, as done in [5], and taking only the effect of the size of the meals for gastric emptying.

The model used for glucose absorption in [8] considers only one glucose meal and was used for oral glucose tests in which the patients were given an oral glucose dose and asked to fast

while data is collected. The model is given as:

$$\frac{dq_{Ss}}{dt} = -k_{12q} q_{Ss} \tag{A.1a}$$

$$\frac{dq_{Sl}}{dt} = -k_{\text{empt}} q_{Sl} + k_{12q} q_{Ss} \tag{A.1b}$$

$$\frac{dq_{\text{int}}}{dt} = -k_{\text{abs}} q_{\text{int}} + k_{\text{empt}} q_{Sl} \tag{A.1c}$$

$$\begin{aligned} k_{\text{empt}} = k_{\min} + \frac{k_{\max} - k_{\min}}{2} \Big(& \\ & \tanh\left[\varphi_1 \left(q_{Ss} + q_{Sl} - k_{\varphi_1} D_q\right)\right] \\ & - \tanh\left[\varphi_2 \left(q_{Ss} + q_{Sl} - k_{\varphi 2} D_q\right)\right] + 2 \Big) \end{aligned} \tag{A.1d}$$

$$\varphi_1 = \frac{5}{2D_q(1 - k_{\varphi_1})} \tag{A.1e}$$

$$\varphi_2 = \frac{5}{2D_q(k_{\varphi_2})} \tag{A.1f}$$

$$Ra = f_q k_{\text{abs}} q_{\text{int}} \tag{A.1g}$$

Where $q_{Ss}(0) = D_q$ [mg] is the oral glucose quantity, Ra is the rate of glucose appearance in the blood, f_q is an absorption factor, k_{12} [min^{-1}] and k_{abs} [min^{-1}] are the rate constants for glucose transfer to stomach and glucose absorption in the intestines respectively, k_{empt} [min^{-1}] is a rate parameter for emptying the stomach of glucose to the intestines. This parameter can have values between $k_{\min}$ and $k_{\max}$ depending on the oral glucose quantity D_q. In order to make the model handle different meals with different time instants, the parameter D_q needs to be modified according to the meal sizes and time. The following are the proposed modifications:

$$\frac{dq_{Ss}}{dt} = -k_{12q} q_{Ss} + \sum_{i=1}^{N_q(t)} u_{q_i} \delta(t - t_i), \; i \in \mathbb{Z}_+ \tag{A.2a}$$

$$\frac{dD_e}{dt} = -k_q D_e + \sum_{i=1}^{N_q(t)} u_{q_i} \delta(t - t_i) \tag{A.2b}$$

$$\frac{dD_q}{dt} = k_q \left(u_{q_{N_q(t)}} - D_q\right) + D_m \sum_{i=1}^{N_q(t)} \delta(t - t_i) \tag{A.2c}$$

$$D_m = \begin{cases} D_e - D_q & u_{q_{N_q(0)}} \neq 0 \\ 1 & u_{q_{N_q(0)}} = 0 \end{cases} \tag{A.2d}$$

Where $q_{Ss}(0) = 0$, $D_e(0) = 0$ [mg], $\delta(t - t_i)$ is the Dirac delta distribution, t_i is the time instance for meal i, $N_q(t)$ is the integer number of meals until time t starting from time $t = 0$, that is $N_q(t)$ takes into account all meals up until t, u_{q_i} [mg] is the amount of oral carbohydrates intake for meal i. The state D_e is introduced to handle the accumulation of carbohydrates

meals with a decay factor k_q [min^{-1}] in order to remove the effect of meals with time. With that, parameter D_q is now a state updated by D_e each time a new meal is consumed and made to converge to the last given meal amount u_{q_i} with the same rate factor k_q such that it converges to the original model through time if no meal is consumed afterwards. Note that $D_q(0) = 0$ [mg] when a zero carbohydrates meal ($u_{q_{N_q(0)}} = 0$) is assumed at time $t = 0$, which leads to (A.1d) being undefined ($\varphi_1 q_{Ss} = \infty\, 0$). To avoid this, the state $D_m(0)$ [mg] is set to 1 [mg] when $u_{q_{N_q(0)}} = 0$. Note also that the value $D_m(0)$ can have any nonzero value in the case of zero carbohydrates meal at $t = 0$. The value $D_m(0)$ will not affect the rate of glucose appearance in the plasma since the states q_{Ss} for ingested carbohydrates, and D_e for the effect of accumulation of meals depend on $u_{q_{N_q(0)}}$ and not D_m. Parameters f_q, $k_{\varphi 1}$, and $k_{\varphi 2}$ are known and taken from [21]. The rest of the parameters, k_{12q}, k_{min}, $k_{\text{max}}, k_{\text{abs}}$, and k_q are taken to be the mean parameters which were estimated in [8]. The introduced parameter k_q has no estimate. Therefore, it is assumed to be equal to k_{min}.

A simulation of a patient with the modified meals model compared against the unmodified one is shown in Figure A.2. The patient is consuming a breakfast meal of 30 [g] carbohydrates, a second breakfast meal of 10 [g] carbohydrates, a lunch meal of 50 [g] carbohydrates, an afternoon snack of 10 [g] carbohydrates, and a dinner meal of 110 [g] carbohydrates. The simulated patient has a basal value of $G_{PC}(0) = 8$ [$\text{mmol}\,\text{L}^{-1}$] for glucose concentration in the central periphery compartment and $I_{PF}(0) = 1$ [$\text{mU}\,\text{L}^{-1}$] for the insulin concentration in the interstitial fluid periphery compartment. No insulin injections or oral medications, physical activity, or stress are included in this simulation. It can be seen from the simulation results that the glucose appearance in plasma is distributed in a larger window of time with lower peaks for meals that are close to each other. This is due to the reduction of the stomach emptying rate k_{empt} in response to increased accumulation of ingested carbohydrates captured by the state D_q. Additionally, glucose appearance in plasma for the modified model in response to meals after hours of fasting closely resembles the glucose appearance in plasma for the unmodified model as can be seen for the dinner and breakfast meal. This is intended since the unmodified model was proposed for fasting conditions. These observations agree with clinical data such as [27] and [28].

2.2 Insulin Injection Model

In this section, a model for long acting and fast acting insulin injections based on the one from [20] is introduced to the base model from [19]. Both fast and long acting insulin analogues treatments are considered for the model. When analogue insulin is injected, it dissociates from its hexameric form to dimers and monomers which then can penetrate the capillary membrane and get absorbed into the plasma. For fast acting insulin, only two compartments are considered: a compartment for insulin in its hexameric form, and a compartment for insulin

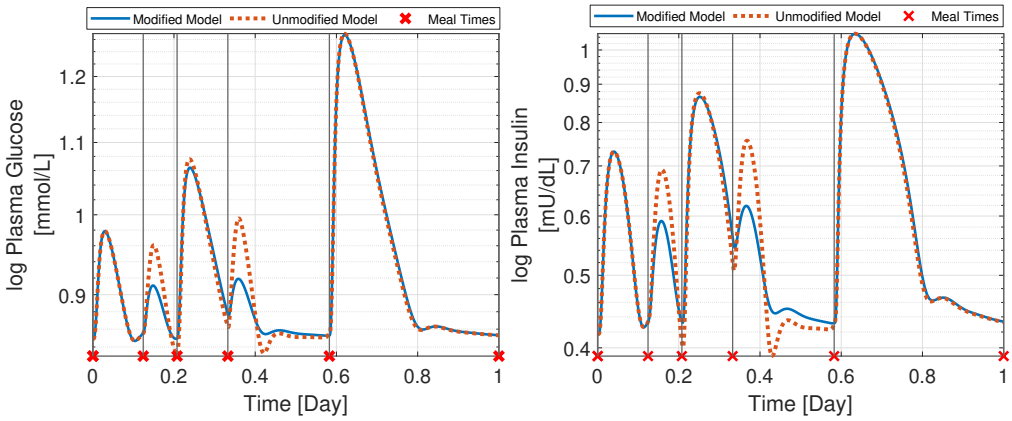

Fig. A.2: Simulation results for the modified glucose absorption model against the unmodified one. Note the log scale on the second axis

in its dimeric and monomeric form. The following are the equations for fast acting insulin:

$$\frac{dH_{fa}}{dt} = \sum_{i=1}^{N_{fa}(t)} \delta\left(t - t_i\right) \frac{10}{V_{PF}^{I}} u_{f_i} - p_{fa}\left(H_{fa} - q_{fa} D_{fa}^{3}\right) \tag{A.3a}$$

$$\frac{dD_{fa}}{dt} = p_{fa}\left(H_{fa} - q_{fa} D_{fa}^{3}\right) - \frac{b_{fa} D_{fa}}{1 + I_{PF}} \tag{A.3b}$$

Where H_{fa} [mU dL^{-1}] is the concentration of injected fast acting insulin in its hexameric form, D_{fa} [mU dL^{-1}] is the concentration of insulin in its diameric and monomeric form, $N_{fa}(t)$ is the number of injected fast acting insulin doses until time t starting from time $t = 0$, that is $N_{fa}(t)$ takes into account all doses up until t, u_{f_i} [mU] is the amount of injected fast acting insulin, b_{fa} [min^{-1}] is a constant for the infusion of fast acting insulin into the body, p_{fa} [min^{-1}] is a constant diffusion parameter, q_{fa} [dL^2 mU^{-2}] is a constant such that $p_{fa}q_{fa}$ is the parameter for fast acting insulin dimers converting back to hexamers, and I_{PF} [mU dL^{-1}] is the insulin concentration in the interstitial periphery compartment. Parameters for Lispo and Aspart insulin injection are reported in [20]. For long acting insulin, an extra state B_{la} is added in [20] to take into account the increased delay in the dissociation of hexameric insulin

to dimers and monomers:

$$\frac{dB_{la}}{dt} = \sum_{i=1}^{N_{la}(t)} \delta\left(t - t_i\right) \frac{10}{V_{PF}^I} u_{l_i} - k_{la} B_{la} \frac{C_{\max}}{1 + H_{la}} \tag{A.4a}$$

$$\frac{dH_{la}}{dt} = k_{la} B_{la} \frac{C_{\max}}{1 + H_{la}} - p_{la}\left(H_{la} - q_{la} D_{la}^3\right) \tag{A.4b}$$

$$\frac{dD_{la}}{dt} = p_{la}\left(H_{la} - q_{la} D_{la}^3\right) - \frac{b_{la} D_{la}}{1 + I_{PF}} \tag{A.4c}$$

Where B_{la} [mU dL^{-1}] is the added bound state for the concentration of hexameric insulin before diffusing, H_{la} [mU dL^{-1}] is the concentration of injected long acting insulin in its hexameric form, D_{la} [mU dL^{-1}] is the concentration of injected insulin in its diameric and monomeric form, $N_{la}(t)$ is the number of injected long acting insulin doses until time t starting from time $t = 0$, that is $N_{la}(t)$ takes into account all doses up until t, u_{l_i} [mU] is the amount of long acting insulin dose at time t_i, b_{la} [min^{-1}] is a constant for the infusion of long acting insulin into the body, p_{la} [min^{-1}] is a constant diffusion parameter for long acting insulin, q_{la} [dL^2 mU^{-2}] is a constant such that $p_{la} q_{la}$ is the parameter for long acting insulin dimers converting back to hexamers, k_{la} [min^{-1}] is a constant absorption rate, and $C_{\max}$ is a dimensionless maximum transmission capacity constant. Parameters for insulin Glargin are reported in [20]. The injected insulin enters the interstitial periphery compartment (A.20g) with the following rate r_{Inj}:

$$r_{Inj} = V_{PF}^I \frac{r_{la} b_{la} D_{la}}{1 + I_{PF}} + V_{PF}^I \frac{r_{fa} b_{fa} D_{fa}}{1 + I_{PF}} \tag{A.5}$$

Where $r_{la}, r_{fa} \leq 1$ are the fractions of long acting and fast acting insulin that get to the periphery compartment, and V_{PH}^I [L] is the volume of the interstitial compartment. Figure A.3 shows a simulation for a patient having the same basal values and following the same meal plan as the simulation discussed in section 2.1. The patient takes a long acting insulin dose of 50 [U] everyday an hour before the breakfast meal. Additionally, the patient takes a 30 [U] of fast acting insulin 15 minutes before dinner. Oral medications, physical activity, and stress are not included in the simulation. Long acting insulin lower the glucose concentration over a large window of time. Moreover, the fast acting insulin helps at reducing the glucose peak after dinner [29]. Quantitative Insulin Sensitivity Check Index (QISCI) [30] is a test performed on fasting glucose and insulin concentrations to assess insulin sensitivity. Healthy patients will typically have values around 0.382 while diabetic patients will have values around 0.304. The QISCI is calculated as:

$$\text{QISCI} = \frac{1}{\log(G_{H_f}) + \log(I_{H_f})} \tag{A.6}$$

Where G_{H_f} and I_{H_f} are the fasting plasma glucose and fasting plasma insulin concentrations respectively. The QISCI was calculated for the case of taking insulin injection doses and for the case in which the patient was not taking any insulin doses. The QISCI with no insulin injections was found to be 0.3717 while the QISCI with insulin injections was found to be 0.3369. The decrease in QISCI agrees with clinical studies [31]. Additionally, the gradual decrease of the glucose concentration during the days with long acting insulin agrees with the data collected in the study in [32].

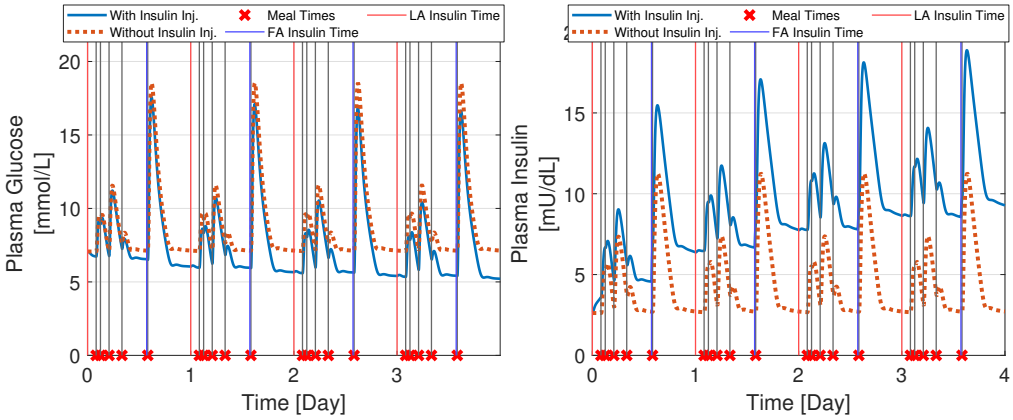

Fig. A.3: Simulation showing the effect of injected fast acting (FA) and long acting (LA) insulin on glucose and insulin concentrations.

2.3 Metformin

In this section, a modification for the metformin model in [19] is carried out to account for multiple doses of oral metfromin with different amounts. The metformin model used in [19], including the pharmacokinetic and its interaction with full glucose-insulin dynamical models, is based on the model in [22] which was fitted with data from the study in [33] and confirmed with the clinical study in [34]. The pharmacokinetic model of metformin in [22] is given as follows:

$$\frac{dM_{GL}}{dt} = -M_{GL}\left(k_{go} + k_{gg}\right) + M_O \tag{A.7a}$$

$$\frac{dM_{GW}}{dt} = M_{GL}k_{gg} + M_P k_{pg} - M_{GW}k_{gl} \tag{A.7b}$$

$$\frac{dM_L}{dt} = M_{GW}k_{gl} + M_P k_{pl} - M_L k_{lp} \tag{A.7c}$$

$$\frac{dM_P}{dt} = M_L k_{lp} - M_P\left(k_{pl} + k_{pg} + k_{po}\right) + M_{GL} \tag{A.7d}$$

Where M_{GL} [μg] is the metformin amount in the gastrointestina lumen, parameters $k_{go}, k_{gg}, k_{pg}, k_{gl}, k_{pl}$, k_{lp}, k_{po} [min^{-1}] are transfer rate constants between the compartments, and M_O is the flow rate of orally ingested metformin which is modelled as:

$$M_O = Ae^{-\alpha_M t} + Be^{-\beta_M t} \tag{A.8}$$

Where A, B [$\mu\text{g}\,\text{min}^{-1}$] and α_M, β_M [min^{-1}] are constant parameters that were identified in [22]. These parameters were identified with data in which patients were taking only a 500 [mg] oral

dose of metformin. Therefore, the model is modified in this work to take into account different amount of doses at different times by introducing the following:

$$\frac{dM_{O1}}{dt} = -\alpha_M M_{O1} + \sum_{i=1}^{N_M(t)} \delta\left(t - t_i\right) u_{M_i} \tag{A.9a}$$

$$\frac{dM_{O2}}{dt} = -\beta_M M_{O2} + \sum_{i=1}^{N_M(t)} \delta\left(t - t_i\right) u_{M_i} \tag{A.9b}$$

$$M_O = \rho_\alpha M_{01} + \rho_\beta M_{02} \tag{A.9c}$$

with $N_M(t)$ being the number of consumed doses of metformin until time t starting from time $t = 0$, that is $N_M(t)$ takes into account all doses up until t, u_{M_i} [μg] is the amount of metformin consumed at time t_i, and the constants $\rho_\alpha = A/(500000\ [\mu g])$ [min^{-1}] and $\rho_\beta = B/(500000\ [\mu g])$ [min^{-1}] are rate parameters. Figure A.4 shows a simulation result of the same patient as section 2.1 taking metformin doses of 500 [mg] for the first two days and then a metformin dose of 1000 [mg] for the remaining days. Insulin injections, Vildagliptin oral medication, physical activity, and stress are not included in this simulation. The 1000 [mg] dose prolong the effect of metformin on lowering the glucose concentration when compared to the dose of 500 [mg].The effect of metformin on both glucose and insulin concentrations matches the study in [34] that was used to confirm the model in [22]. The QISCI with no metformin doses was found to be 0.3717 while the QISCI with metformin was found to be 0.3921. This shows the effect of metformin improving insulin sensitivity over time.

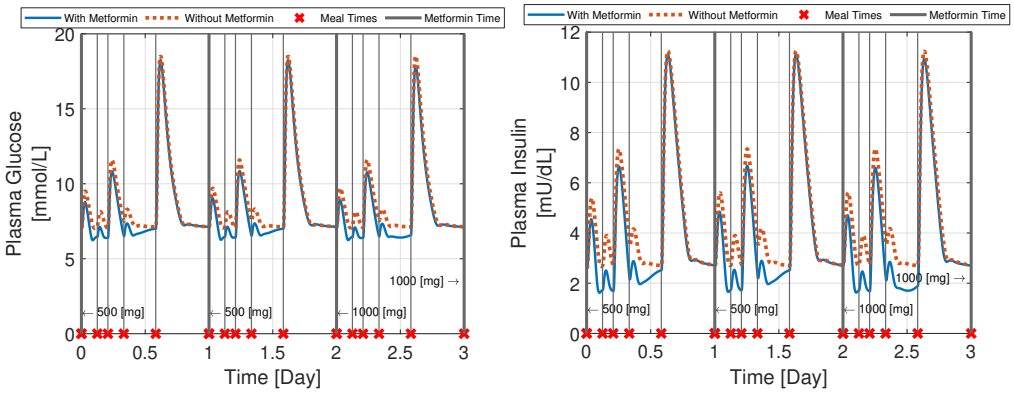

Fig. A.4: Simulation showing the effect of metformin on glucose and insulin concentrations.

2.4 Physical Activity Model

In this section, a physical activity model based on [12] is added to the model in [19]. The model in [12] was developed for a T1D model based on [35]. The model considers the change of the heart beat rate following a physical activity to be the stimulus of two states E_1 and E_2, which are dimensionless:

$$\frac{dE_1}{dt} = -\frac{1}{\tau_{\mathrm{HR}}} E_1 + \frac{1}{\tau_{\mathrm{HR}}} \left(\mathrm{HR} - \mathrm{HR}_b\right) \tag{A.10a}$$

$$\frac{dE_2}{dt} = -\left(g_e(E_1) + \frac{1}{\tau_e}\right) E_2 + g_e(E_1) \tag{A.10b}$$

$$g(E_1) = \frac{\left(\frac{E_1}{a_e \mathrm{HR}_b}\right)^{n_e}}{1 + \left(\frac{E_1}{a_e \mathrm{HR}_b}\right)^{n_e}} \tag{A.10c}$$

Where t_{HR}, τ_e [min] are time constants, HR, HR_b [bpm] are the current and rest heart rates respectively, and the parameters a_e, n_e are dimensionless parameters. The first state E_1 is used directly as a stimulus to increase the insulin-independent glucose uptake in response to a physical activity while the state E_2 is used for the longer lasting change of insulin action on glucose. The glucose and insulin model structure in [12] is simpler than the one considered in this work. Nevertheless, the inclusion of the physical activity for the model in this work is similar to how other models include physical activity, e.g., see [14]. With that, the effect of the state E_1 is included as an increase in the clearance rate of glucose in the periphery interstitial fluid compartment with a constant parameter β_e [bpm^{-1}] as $\frac{1}{T_P^G}(1 + \beta_e E_1)$ where $\frac{1}{T_P^G}$ [min^{-1}] is the clearance rate for glucose in the periphery interstitial fluid compartment in (A.13h). The effect of E_1 can be removed to obtain the original model by setting $\beta_e = 0$. As for the effect on insulin action, the state E_2 is introduced on the glucose metabolic rates, which depend on insulin as follows:

- An increase in the periphery glucose uptake rate r_{PGU} in the interstitial fluid periphery compartment (A.13h) by a constant α_e as $(1 + \alpha_e E_2)\, r_{PGU}$.
- An increase in the hepatic glucose uptake rate r_{HGU} in the liver compartment (A.13e) with a constant α_e as $(1 + \alpha_e E_2)\, r_{HGU}$.
- A decrease in the hepatic glucose production rate r_{PGH} in the liver compartment (A.13e) with a constant α_e as $(1 + \alpha_e E_2)\, r_{HGP}$.

The effect of E_2 can be removed to obtain the original model by setting $\alpha_e = 0$. The parameters for the physical activity model are taken from [12] except for α_e and β_e, which were tuned to have a similar effect to the ones demonstrated in [12, 14]. Figure A.5 shows a simulation for the patient described in section 2.1 when the patient exercise every day before dinner raising the heart beat rate from a rest value of 80 [bpm] to a value of 140 [bpm] for 30 minutes. Insulin injections, oral medications, and stress are not considered in this simulation. The immediate effect of physical activity is seen in the simulation results. In addition, the prolonged effect of physical activity on insulin action on glucose is seen in the figure. The QISCI with no physical activity was found to be 0.3717 while the QISCI with physical activity was found to be 0.385. This shows the effect of physcial activity on improving the insulin sensitivity.

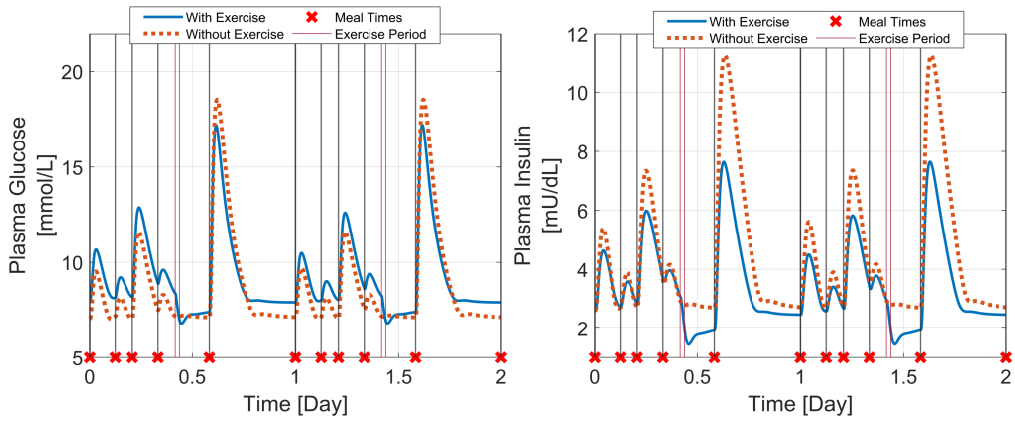

Fig. A.5: Simulation showing the effect of physical activity on plasma glucose and plasma insulin concentrations.

2.5 Stress Effect

In this section, the effect of stress is included in the model [19]. In [11], the effect of stress was included as a multiplicative factor $1 + \alpha_s$, with $\alpha_s \in [0, 1]$, to the glucose and glucagon production rates. This is because stress causes a direct increase in the pancreatic glucagon production through an increase in catecholamines, which in turns drives an increase of glucose production in the liver [36]. In addition, stress was also included as a multiplicative factor $1 - \alpha_s$ to the pancreatic insulin secretion rate based on [36]. Similarly, in this work, the effect of stress is included in the model as follows:

- An increase in the plasma glucagon release rate $r_{P\Gamma R}$ in the glucagon compartment (A.19a) as $(1 + \alpha_s)\, r_{P\Gamma R}$.
- An increase in the hepatic glucose production rate r_{HGP} in the glucose liver compartment (A.13e) as $(1 + \alpha_s)\, r_{HGP}$.
- A decrease in the pancreatic insulin release rate r_{PIR} in the insulin liver compartment (A.20d) as $(1 - \alpha_s)\, r_{PIR}$

Figure A.6 shows the effect of stress in a simulation for the same patient discussed in section 2.1 when the patient is stressed on the second day with α_s ramping up from 0 to 0.4 in 6 hours, staying at 0.4 for 12 hours, and then ramping down to 0 for the rest of the day. Insulin injections, oral medications, and physical activity are not considered in the simulation. Stress manages to increase glucose concentration together with a decrease in insulin concentration. The QISCI was calculated at fasting conditions after the day in which stress is present. The QISCI with no stress was found to be 0.3717 while the QISCI with stress was found to be 0.3416. This shows a decrease in insulin sensitivity when stress is present for one day.

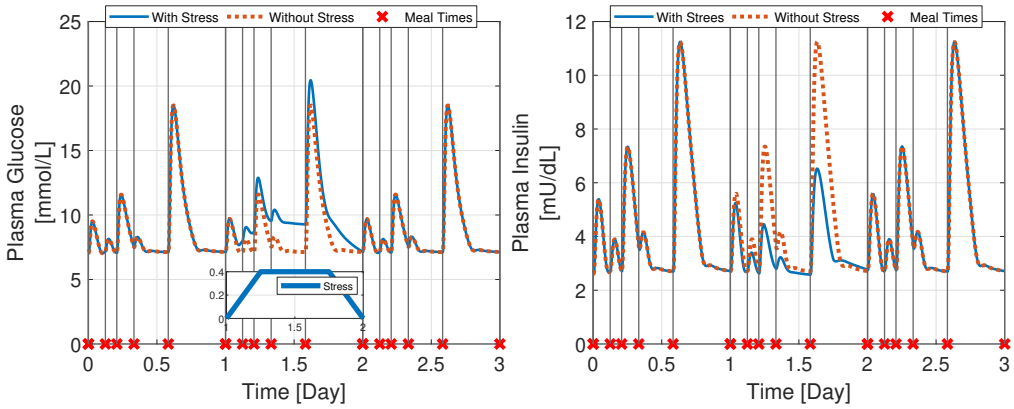

Fig. A.6: Simulation showing the effect of stress on glucose and insulin concentrations.

3 Discussion

3.1 Fitting the Model with Data

The model has more than 120 parameters and it is, without a doubt, challenging to obtain clinical data that can be used to estimate all the parameters for the model. Nevertheless, the authors in [8], which the model in this paper is based on, performed a sensitivity analysis for the model's parameters and determined a set of specific parameters that are more influential on the response of the model than other. The authors then carried out a least square nonlinear optimization problem to estimate the parameters based on a 50 [g] oral glucose tolerance test data in which peripheral glucose and insulin concentrations are measured together with incretin concentration. Since the model in this paper is based on the one in [8], patients can perform oral glucose tolerance test occasionally to obtain data which, can be used to estimate personalized parameters for the base model. Subsequently, the estimated parameters for the base model can be fixed for each patient while the parameters for the extensions of the base model can be estimated using data that can be collected during the treatment process of the patients. Data for stress can be collected using the Perceived Stress Scale (PSS) as done in the studies [16, 17] in which a self-administered questionnaire is filled by the patients. Afterwards, a stress level can be deduced from the answers by mapping them to be between 0 and 1 to match the model presented in this paper. As for the physical activity model, heart beat rate data can be acquired using wearable smart watches as discussed in [15]. Together with these data, continues glucose measurement data with registered insulin injections and oral medications data can be used to estimate more parameters of the augmented models other than the base model parameters.

3.2 Usage of the model

In this section, it is intended to discuss examples on how the model can be used to help subjects with Type 2 diabetes. Consider a patient who performed oral glucose tolerance test to estimate the base model parameters and has been providing data during treatment to estimate parameters of the augmented sub-models. Assume now a case in which the patient is expected to have a stressful period of 4 days. For examples, a school exam period. From previously gathered data about stress, the patient is expected to have stress levels ranging from 0.4 to 0.8 during these days. Moreover, the eating patterns of the patients are fitted from previously collected meal registered data according to the following for each meal of the day: with $\mathcal{U}(a, b)$

Meal	Time [Hours]	Glucose [g]
Breakfast	$\mathcal{U}(7, 8)$	$\mathcal{U}(5, 40)$
Lunch	$\mathcal{U}(11.5, 13)$	$\mathcal{U}(50, 100)$
Dinner	$\mathcal{U}(17, 19)$	$\mathcal{U}(100, 130)$

Table A.1: Meals model for the hypothetical patient

being a continues uniform distribution between a and b. In addition, the patient is known to have physical activity every day from to 16:00 to 16:30 raising their heart beat rate by 40 [bpm]. With all these information, a medical professional can test different treatment plans for the patient using the model by performing a Monte Carlo simulation with the given information about the patient. Figure A.7 shows a Monte Carlo simulation for a treatment plan consisting of long acting insulin doses of 40[U] at the beginning of each day together with metformin doses of 500 [mg] each day. The patient has a basal value of $G_{PC}(0) = 8$ [mmol L^{-1}] for glucose concentration in the central periphery compartment and $I_{PF}(0) = 1$ [mU L^{-1}] for the insulin concentration in the interstitial fluid periphery compartment. It is seen from the figure that the fasting glucose is brought to a safe glucose concentration region between 4 and 6 for some simulations. Nevertheless, it is seen that for some cases the patient can experience high glucose concentration levels during the meals. The medical professional now test a different treatment plan where the metformin dose is increased to 1000 [mg] and the long acting insulin dose is increased to 50 [U]. Figure A.8 shows the results. It can be seen now that the new treatment plan produces simulations with lower glucose concentration peaks. The example shows how the model gives the opportunity for a medical professional to test different treatment plans against the combined effect of different factors such as stress and physical activity for patients.

The model can also be used to evaluate the performance of dose finding algorithms for insulin injections or oral medications against different kinds of patients and different lifestyles with stress, physical activity, and meals. For example, consider the rule based strategy for determining long acting insulin doses based on fasting glucose measurement in [37]. The dose finder's goal is to bring and keep fasting glucose concentrations within a safe region between 4 [mmol/L] and 5 [mmol/L]. Figure A.9 shows the results of applying the rule based long acting insulin dose finding strategy to three different hypothetical patients to test the robustness of the strategy. The first patient having the same parameters as in Table A.3. The second patient is chosen to have the same parameters as in Table A.3 except with parameters c_1 and c_4 increased by 90% and c_2 decreased by 90%. This was done to increase the effect of insulin on

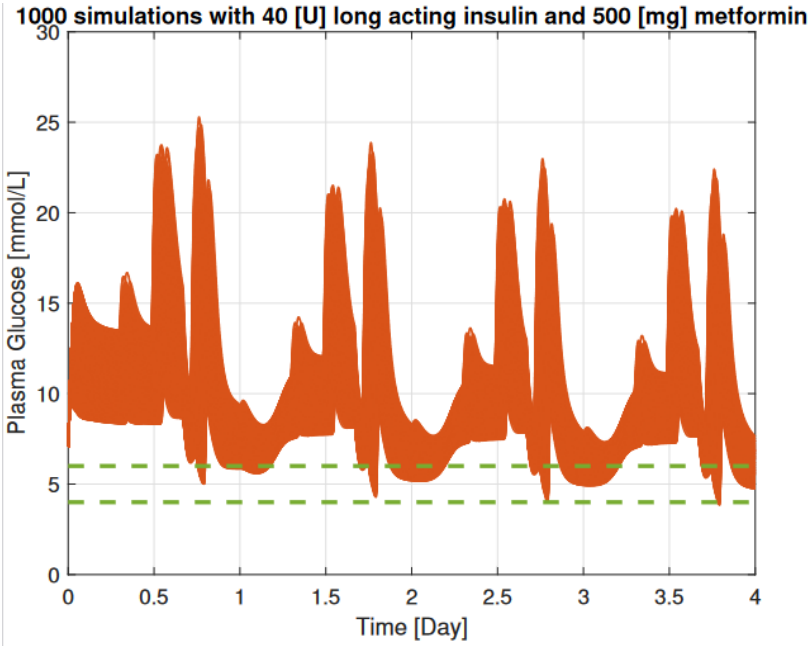

Fig. A.7: 1000 Simulations of the patient with stress levels drawn uniformly between 0.4 and 0.8 for each simulation and a meal plan according to table A.1. The patient is taking a long acting insulin dose of 40 [U] and a metformin dose of 500 [mg] each day of the simulation

the metabolic glucose uptake and glucose production rates. Finally, the third patient is chosen to have the same parameters as in Table A.3 except with parameters c_1 and c_4 decreased by 90% and c_2 increased by 90%. This was done to decrease the effect of insulin on the metabolic glucose uptake and glucose production rates. Note that the 90% increase or decrease on the parameters is chosen arbitrary. The parameter perturbation range in which one can use for the parameters of the model and still obtain a model that represent a real life patient is uncertain. Nevertheless, ensuring a strategy to be robust under extreme cases is still an advantage. All the patients have meal plans identical to Table A.1. In addition, all the patients are taking a metformin dose of 500 [mg] and having physical activity each day from 16 to 16:30 increasing their heart beat rate during that period to 40 [bpm]. The aim of these simulations is to test the robustness of the dose finding algorithm against physiologically different patients. It can be seen from the figure that the strategy managed to bring the fasting glucose concentrations for patient 1 to be within a safe range in less than 10 days. For patient 3, the strategy needed more time to bring the fasting glucose concentrations to the safe region. As for patient 2, the strategy undershooted below the safe region and then converged to a value on the lower limit of the safe region. This is dangerous since the risk of hypoglycemic episodes are higher for patient 2. In conclusion, the strategy can handle a variety of patients with different insulin resistivity. Nevertheless, the strategy can take a long period to have the fasting glucose concentrations

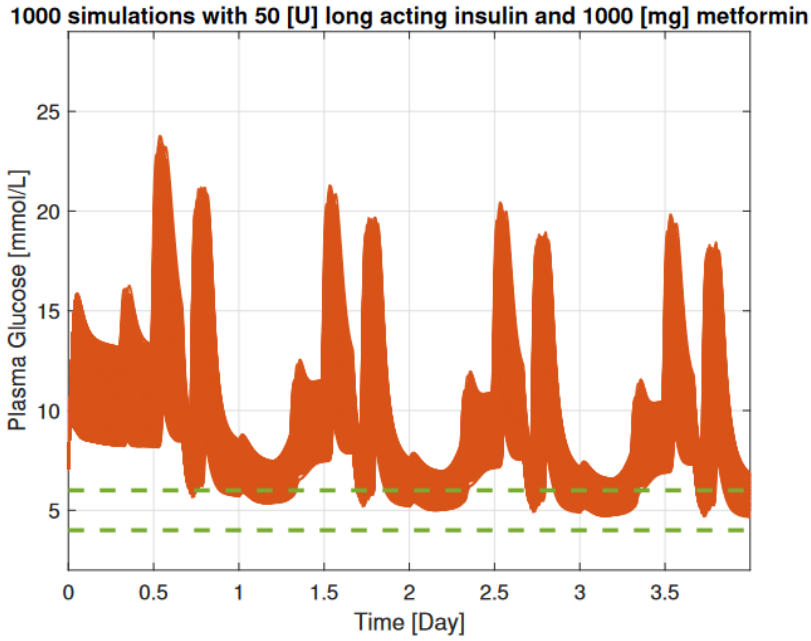

Fig. A.8: 1000 Simulations of the patient with stress levels drawn uniformly between 0.4 and 0.8 for each simulation and a meal plan according to Table A.1. The patient is taking a long acting insulin dose of 50 [U] and a metformin dose of 1000 [g] each day of the simulation

converging for some cases. Moreover, it can cause patients to experience hypoglycemia by undershooting or converging to a concentration on the lower limit for the safe region, which is dangerous.

This evaluation study was tested with the effect of physical activity considerations and metformin medication. Consider now testing the same strategy with the same patients but without the consideration of physical activity and metformin. Figure A.10 shows the results. It is clear from the figure that the strategy performs differently. While none of the patients risk experiencing hypoglycemia, the strategy takes more time to converge for all of them. Another point to notice here is that patient 2 now takes more time to converge to the safe region than patient 3. The possibility to perform evaluations of treatment plans against physical activity and stress together with other medications is what distinguish this model from the current state of the art models.

The model can also be used to design insulin and oral medication dose finders for patients. For example, similarly to how the model is used in the first example to test and evaluate treatment plans, the model can be used in an optimization algorithm to decide on the insulin, oral medication doses, or even physical activity conditions. Such strategies are refereed to as optimal predictive controllers or model predictive controller (MPC). One can use robust MPC techniques such as [38] by choosing a compact set in which some of the model parameters

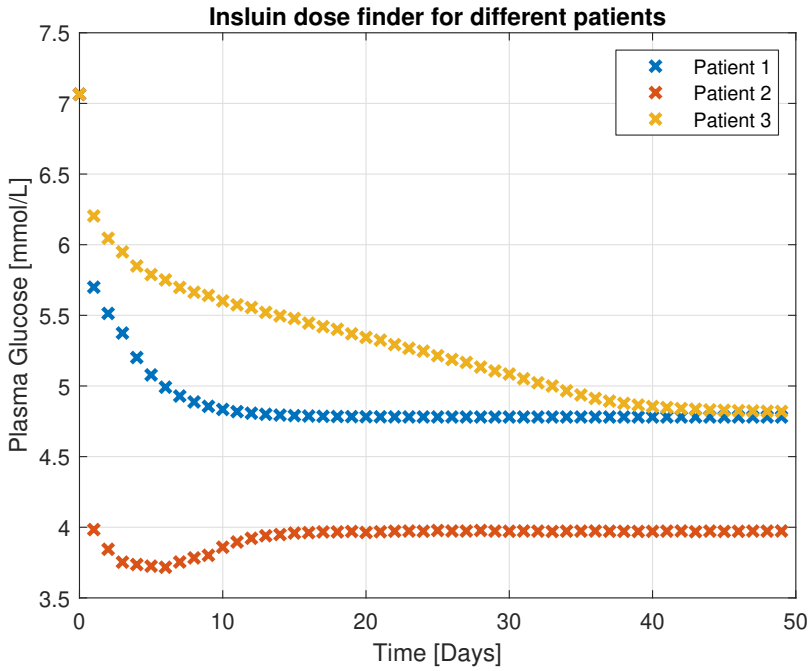

Fig. A.9: Fasting Glucose for three different patients. Physical activity and a dose of 500 [mg] metformin are considered.

can take values from. In this case, one can optimize for certain objectives, e.g. bringing glucose concentrations to a safe region, or minimizing the use of injected insulin, while insuring satisfaction of some constraints, e.g. limited amounts of insulin, allowed time for physical activity, or constraining glucose concentrations to a specific region, for all possible values of the chosen parameters in the compact set. Moreover, one can have a more relaxed and realistic version by choosing a probability for the parameters to be inside the chosen compact set (Robust with probability MPC), and thus, ensuring the constraint satisfaction with a specific probability value. Another option is to consider stochastic MPC techniques [39] to handle stochastic disturbances or inputs similar to the meal plan example in Table A.1. Stochastic MPC techniques offers the chance to optimize for the expected values of objectives or the probabilities of objective while ensuring the satisfaction of some constraints with some chosen probability.

4 Conclusion and Future Work

A model for glucose-insulin dynamics, which incorporates the effect of multiple glucose meal

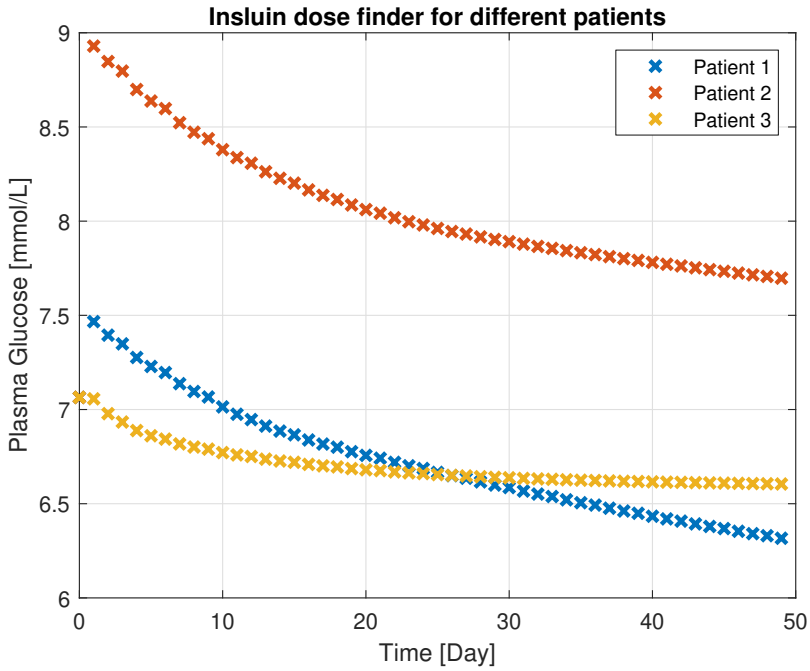

Fig. A.10: Fasting Glucose for three different patients. Physical activity and metformin are not considered.

sizes, different metformin doses, physical activity, insulin injections, and stress, is proposed by combining and modifying different available models in the literature. The effect of the different added and modified models is demonstrated by different simulations and was aimed to match studies from the literature on T2D patients. A discussion on the data needed to fit the model is provided. Additionally, a discussion is provided on how the model can be used to evaluate treatment plans and possibly develop some treatment plans with robust and stochastic control techniques. The model, however, need to be confirmed with real patients data. Moreover, real patient data can be used to estimate joint probability distribution to simulate a population of T2D patients.

A Full Model Equations

The compartments include metabolic production rates r_{CXP} and metabolic uptake rates r_{CXU} for substance X in compartment C generally defined as following:

$$r_{CXP,U} = M^I M^G M^\Gamma r^b_{CXP,U} \tag{A.11}$$

Where M^I,M^G, and M^Γ are multiplicative quantities for the effect of insulin I, glucose G, and glucagon Γ respectively, and $r^b_{CXP,U}$ is the basal metabolic rate of substance X in compartment C. The general form for the multiplicative quantities representing the effect of a substance Y in compartment C with concentration Y_C is given as:

$$M^Y = \frac{a + b\tanh\left[c\left(Y_C/Y^b_C - d\right)\right]}{a + b\tanh[c(1-d)]} \tag{A.12}$$

Where Y^b_C is the basal concentration of substance Y in compartment C, and a, b, c, and d are model parameters.

A.1 Glucose Sub-Model

Applying mass balance equations over the compartments for glucose, the following equations are obtained:

$$V^G_{BC}\frac{dG_{BC}}{dt} = Q^G_B\left(G_H - G_{BC}\right) - \frac{V^G_{BF}}{T^G_B}\left(G_{BC} - G_{BF}\right) \tag{A.13a}$$

$$V^G_{BF}\frac{dG_{BF}}{dt} = \frac{V^G_{BF}}{T^G_B}\left(G_{BC} - G_{BF}\right) - r_{BGU} \tag{A.13b}$$

$$\begin{aligned} V^G_H\frac{dG_H}{dt} &= Q^G_B G_{BC} + Q^G_L G_L + Q^G_K G_K \\ &\quad + Q^G_P G_{PC} + Q^G_H G_H - r_{RBCU} \end{aligned} \tag{A.13c}$$

$$V^G_G\frac{dG_G}{dt} = Q^G_G\left(G_H - G_G\right) - r^m_{GGU} + Ra \tag{A.13d}$$

$$\begin{aligned} V^G_L\frac{dG_L}{dt} &= Q^G_A G_H + Q^G_G G_G - Q^G_L G_L \\ &\quad + \left((1+\alpha_s)\left(1-\alpha_e E_2\right) r^m_{HGP} - \left(1+\alpha_e E_2\right) r_{HGU}\right) \end{aligned} \tag{A.13e}$$

$$V^G_K\frac{dG_K}{dt} = Q^G_K\left(G_H - G_K\right) - r_{KGE} \tag{A.13f}$$

$$V^G_{PC}\frac{dG_{PC}}{dt} = Q^G_P\left(G_H - G_{PC}\right) - \frac{V^G_{PF}}{T^G_P}\left(G_{PC} - G_{PF}\right) \tag{A.13g}$$

$$\begin{aligned} V^G_{PF}\frac{dG_{PF}}{dt} &= \frac{V^G_{PF}}{T^G_P}\left(G_{PC}\right. \\ &\quad \left. - \left(1+\beta_e E_1\right) G_{PF}\right) - \left(1+\alpha_e E_2\right) r^m_{PGU} \end{aligned} \tag{A.13h}$$

Where G_i [mg dL^{-1}] is glucose concentration for each compartment i, Q^G_i [dL min^{-1}] is the vascular blood flow for the glucose compartment i, V^G_i [dL] is the volume of compartment i, T^G_i [min] is the transcapillary diffusion time for compartment i, and r_{xP}, r_{xU} are metabolic glucose production and uptake rates respectively. The following are the meanings of each subscript in the model: The metabolic rates for the glucose subsystem are given as:

B	Brain	BC	Brain capillary space
BF	Brain interstitial fluid	H	Heart
G	Guts	L	Liver
K	Kidney	P	Periphery
PC	Periphery capillary space	PF	Periphery interstitial fluid
BGU	Brain glucose uptake	RBCU	Red blood cell glucose uptake
GGU	Gut glucose uptake	HGP	Hepatic glucose production
HGU	Hepatic glucose uptake	KGE	Kidney glucose excretion
PGU	Peripheral glucose uptake		

Table A.2: Subscripts abbreviations

$$r_{PGU} = M^I_{PGU} M^G_{PGU} r^b_{PGU},\ r^b_{PGU} = 35 \tag{A.14a}$$

$$r_{HGP} = M^I_{HGP} M^G_{HGP} M^\Gamma_{HGP} r^b_{HGP},\ r^b_{HGP} = 35 \tag{A.14b}$$

$$r_{HGU} = M^I_{HGU} M^G_{HGU} r^b_{HGU},\ r^b_{HGU} = 20 \tag{A.14c}$$

$$r_{KGE} = \begin{cases} 71 + 71 \tanh\left[0.11\,(G_K - 460)\right] & G_K < 460 \\ -330 + 0.872 G_K & G_K \geq 460 \end{cases} \tag{A.14d}$$

$$r_{BGU} = 70,\ r_{RBCU} = 10,\ r_{GGU} = 20 \tag{A.14e}$$

Where:

$$M^{I}_{PGU} = \frac{7.03 + 6.52 \tanh\left[c_1\left(I_{PF}/I^{B}_{PF} - d_1\right)\right]}{7.03 + 6.52 \tanh[c_1(1-d_1)]} \tag{A.15a}$$

$$M^{G}_{PGU} = G_{PF}/G^{b}_{PF} \tag{A.15b}$$

$$\frac{d}{dt}M^{I}_{HGP} = 0.04\left(M^{I\infty}_{HGP} - M^{I}_{HGP}\right) \tag{A.15c}$$

$$M^{I\infty}_{HGP} = \frac{1.21 - 1.14 \tanh\left[c_2\left(I_L/I^{B}_{L} - d_2\right)\right]}{1.21 - 1.14 \tanh[c_2(1-d_2)]} \tag{A.15d}$$

$$M^{G}_{HGP} = \frac{1.42 - 1.41 \tanh\left[c_3\left(G_L/G^{B}_{L} - d_3\right)\right]}{1.42 - 1.41 \tanh[c_3(1-d_3)]} \tag{A.15e}$$

$$M^{\Gamma}_{HGP} = 2.7 \tanh\left[0.39\Gamma/\Gamma^{B}\right] - f \tag{A.15f}$$

$$\frac{d}{\mathrm{d}t}f = 0.0154\left[\left(\frac{2.7 \tanh\left[0.39\Gamma/\Gamma^{B}\right] - 1}{2}\right) - f\right] \tag{A.15g}$$

$$\frac{d}{dt}M^{I}_{HGU} = 0.04\left(M^{I\infty}_{HGU} - M^{I}_{HGU}\right) \tag{A.15h}$$

$$M^{I\infty}_{HGU} = \frac{2.0 \tanh\left[c_4\left(I_L/I^{B}_{L} - d_4\right)\right]}{2.0 \tanh[c_4(1-d_4)]} \tag{A.15i}$$

$$M^{G}_{HGU} = \frac{5.66 + 5.66 \tanh\left[c_5\left(G_L/G^{B}_{L} - d_5\right)\right]}{5.66 + 5.66 \tanh[c_5(1-d_5)]} \tag{A.15j}$$

Note that some of these rates have a constant numerical value. In addition, parameters a and b for the multiplicative quantities are substituted with numerical values. These numerical values are the ones estimated for a healthy 70 kg male. Parameters c and d were left for the estimation in case of a diabetic patient as in [8]. The following rates are modified with the effect of metformin as following:

$$r^{m}_{GGU} = (1 + E_{GW})\, r_{GGU} \tag{A.16a}$$

$$r^{m}_{HGP} = (1 - E_{L})\, r_{HGP} \tag{A.16b}$$

$$r^{m}_{PGU} = (1 + E_{P})\, r_{PGU} \tag{A.16c}$$

Where E_{GW}, E_L, and E_P are positives coefficients which depend on the amount of metformin in the gastrointestina wall (GI) M_{GW} [μg], liver M_L [μg], and peripherals M_p [μg] respectively. These coefficients increase (or decrease) the glucose uptake (or production) as seen in (A.16).

The equations for these coefficients are given as following:

$$E_{GW} = \frac{\nu_{GW,\max} \times (M_{GW})^{n_{GW}}}{(\varphi_{GW,50})^{n_{GW}} + (M_{GW})^{n_{GW}}} \tag{A.17a}$$

$$E_L = \frac{\nu_{L,\max} \times (M_L)^{n_L}}{(\varphi_{L,50})^{n_L} + (M_L)^{n_L}} \tag{A.17b}$$

$$E_P = \frac{\nu_{P,\max} \times (M_P)^{n_P}}{(\varphi_{P,50})^{n_P} + (M_P)^{n_P}} \tag{A.17c}$$

Where $\nu_{GW,\max}$, $\nu_{L,\max}$, $\nu_{P,\max}$ are parameters to represent the maximum effect of metformin in each one of its corresponding compartments, $\varphi_{GW,50}$, $\varphi_{GI,50}$, $\varphi_{GI,50}$ [μg] are the masses of metformin within the different compartments to produce half of its maximum effect, and n_{GW}, n_L, and n_P are shape factors.

A.2 Incretins Sub-Model

The incretins hormones are metabolic hormones released after eating a meal to stimulate a decrease in blood glucose levels. For T2D patients, Glucagon-Like-Peptide-1 (GLP-1) is the most active incretin [40]. GLP-1 is then modelled with the following two compartments as in [19]:

$$\frac{d\psi}{dt} = \zeta k_{\text{empt}} q_{Sl} - \frac{1}{\tau_\psi}\psi \tag{A.18a}$$

$$V^\Psi \frac{d\Psi}{dt} = \frac{1}{\tau_\psi}\psi - \left[K_{out} + (R_{maxC} - DR_c)\, Cf_2\right] \Psi \tag{A.18b}$$

Where τ_ψ [min^{-1}] is a time constant for the release and absorption of GLP-1 to the blood stream upon consuming a meal, V^Ψ [dL] is the volume of the GLP-1 compartment, DR_c [nmol] is the amount of Dipeptidyl peptidase-4 (DPP-4) in the central compartment deactivated by the drug vildagliptin, K_{out} [min^{-1}] is a clearance constant for GLP-1 independently of the amount of DPP-4, and $(R_{maxC} - DR_c)$ is the amount of available activated DPP-4 in the blood plasma with R_{maxC} [nmol] being the maximum amount of active DPP-4 in the absence of the vildagliptin. Cf_2 [min^{-1}nmol^{-1}] is a proportionality factor for the elimination of GLP-1 by active DPP-4 [23]. Parameters τ_ψ and ζ are estimated in [8] when other incretins than GLP-1 are considered and later modified in [8] to account for vildagliptin treatment. Parameters K_{out}, R_{maxC}, and Cf_2 were estimated in [23] together with the parameters for the vildagliptin model described in subsection A.6.

A.3 Glucagon Sub-Model

The glucagon subsystem consists of one compartment as it is assumed to have the same concentration over all the body:

$$V^{\Gamma}\frac{d\Gamma}{dt} = (1+\alpha_s)r_{P\Gamma R} - 9.1\Gamma \tag{A.19a}$$

$$r_{P\Gamma R} = M^{G}_{P\Gamma R} M^{I}_{P\Gamma R} r^{b}_{P\Gamma R},\ r^{b}_{P\Gamma R} = 9.1 \tag{A.19b}$$

$$M^{G}_{P\Gamma R} = 1.31 - 0.61\tanh\left[1.06\left(\frac{G_H}{G^{B}_{H}} - 0.47\right)\right] \tag{A.19c}$$

$$M^{I}_{P\Gamma R} = 2.93 - 2.09\tanh\left[4.18\left(\frac{I_H}{I^{B}_{H}} - 0.62\right)\right] \tag{A.19d}$$

Where $r_{P\Gamma R}$ is the plasma glucagon release rate. The state Γ represent a normalized glucagon state with respect to its basal value. This is done since it is difficult in practice to obtain glucagon measurements for each subject in order to initialize the state. Therefore for this model, the basal glucagon state is 1.

A.4 Insulin Sub-Model

Applying mass balance equations over the insulin compartments will yield the following:

$$V^{I}_{B}\frac{dI_B}{dt} = Q^{I}_{B}\left(I_H - I_B\right) \tag{A.20a}$$

$$\begin{aligned} V^{I}_{H}\frac{dI_H}{dt} &= Q^{I}_{B}I_B + Q^{I}_{L}I_L + Q^{I}_{K}I_K \\ &\quad + Q^{I}_{P}I_{PV} - Q^{I}_{H}I_H \end{aligned} \tag{A.20b}$$

$$V^{I}_{G}\frac{dI_G}{dt} = Q^{I}_{G}\left(I_H - I_G\right) \tag{A.20c}$$

$$\begin{aligned} V^{I}_{L}\frac{dL_L}{dt} &= Q^{I}_{A}I_H + Q^{I}_{G}I_G - Q^{I}_{L}I_L \\ &\quad + (1-\alpha_s)r_{PIR} - r_{LIC} \end{aligned} \tag{A.20d}$$

$$V^{I}_{K}\frac{dI_K}{dt} = Q^{I}_{K}\left(I_H - I_K\right) - r_{KIC} \tag{A.20e}$$

$$V^{I}_{PC}\frac{dI_{PC}}{dt} = Q^{I}_{P}\left(I_H - I_{PC}\right) - \frac{V^{I}_{PF}}{T^{I}_{P}}\left(I_{PC} - I_{PF}\right) \tag{A.20f}$$

$$V^{I}_{PF}\frac{dI_{PF}}{dt} = \frac{V^{I}_{PF}}{T^{I}_{P}}\left(I_{PC} - I_{PF}\right) - r_{PIC} + r_{Inj} \tag{A.20g}$$

Where r_{LIC}, r_{KIC}, and r_{PIC} are the liver, kidney, and peripherals insulin clearance rates respectively and are defined as following:

$$r_{LIC} = 0.4 \left[Q_A^I I_H + Q_G^I I_G - Q_L^I I_L + r_{PIR} \right] \tag{A.21a}$$

$$r_{KIC} = 0.3 Q_K^I I_K \tag{A.21b}$$

$$r_{PIC} = \frac{I_{PF}}{\left[\left(\frac{1-0.15}{0.15 Q_P^I} \right) - \frac{20}{V_{PF}^I} \right]} \tag{A.21c}$$

the pancreas insulin release is calculated by the following:

$$r_{PIR} = \frac{S}{S^b} r_{PIR}^b \tag{A.22}$$

Where S [U min^{-1}] is the pancreas secreted insuln rate, and S^b, r_{PIR}^b are the basal values. The model for S and S^b is described in subsection A.5.

A.5 Pancreas Sub-Model

The model consists of two main compartments: a large insulin storage compartment m_s [μg] and a small labile insulin compartment m_l [μg]. The flow of insulin from the storage compartment to the labile insulin compartment is dependent on a dimensionless factor P with a proportionality constant γ [μg min^{-1}]. The factor P depends on a dimensionless glucose-enhanced excitation factor represented by X and GLP-1 through a linear compartment with constant first order rate α [min^{-1}]. Upon a glucose stimulus, the glucose-enhanced excitation factor X will increase instantaneously depending on the glucose increase in the plasma G_H. In addition, a dimensionless inhibitor R for X will increase in response to X through a linear compartment with a first order constant rate β [min^{-1}]. During that increase, the secreted insulin S will depend directly on both X and its inhibitor R together with GLP-1. Afterwards when R reaches X or X starts decreasing after R reaching it, the insulin secretion rate will

only depend on X and GLP-1. The following are the equations of the model:

$$\frac{dm_s}{dt} = K_l m_l - K_s m_s - \gamma P \tag{A.23a}$$

$$\frac{dm_l}{dt} = K_s m_s - K_l m_l + \gamma P - S \tag{A.23b}$$

$$\frac{dP}{dt} = \alpha(P_\infty - P) \tag{A.23c}$$

$$\frac{dR}{dt} = \beta(X - R) \tag{A.23d}$$

$$S = \begin{cases} \left[N_1 P_\infty + N_2 (X - R) + \zeta_2 \Psi\right] m_l & X > R \\ (N_1 P_\infty + \zeta_2 \Psi) m_l & X \leq R \end{cases} \tag{A.23e}$$

$$P_\infty = X^{1.11} + \zeta_1 \Psi \tag{A.23f}$$

$$X = \frac{G_H^{3.27}}{132^{3.27} + 5.93 G_H^{3.02}} \tag{A.23g}$$

Where K_l [min^{-1}] and K_s [min^{-1}] are the rates for the flow between the labile and storage insulin compartments independently of P, N_1 [min^{-1}] and N_2 [min^{-1}] are constant parameters that represent the effect of P and $(X - R)$ on the insulin secretion rate respectively, and ζ_1 [L pmol^{-1}], ζ_2 [L (pmol min)^{-1}] are constant parameters to represent the effect of GLP-1 on P_∞ and the insulin secretion rate. For initializing the model and calculating the basal values, the storage compartment is assumed to be large enough for it to be constant. Therefore, writing the mass balance for the storage compartment at zero glucose concentration will yield the following:

$$K_s m_s = K_l m_{l_0} \tag{A.24}$$

Where m_{l_0} is the labile insulin concentration at zero glucose concentration. This parameter in [10] is provided with a value of 6.33 [U] for a healthy 70 kg male.

A.6 Vildagliptin

The vildagliptin model is based on [23]. The absorption of orally ingested vildagliptin is modelled by two compartments as following:

$$\frac{dA_{G1}}{dt} = -k_{a1} A_{G1} + \sum_{i=1}^{N_v(t)} \delta(t - t_i) f_v u_{v_i} \tag{A.25a}$$

$$\frac{dA_{G2}}{dt} = k_{a1} \times A_{G1} - k_{a2} \times A_{G2} \tag{A.25b}$$

Where A_{G1}, A_{G2} [nmol] are the amount of vildagliptin in the gut and absorption compartments respectively, $N_v(t)$ is the number of oral vildagliptin doses until time t, u_{v_i} [nmol] is the amount of consumed vildagliptin, f_a is the bioavailability of vlidagliptin, and k_{a1}, k_{a2} [min^{-1}] are rate absorption parameters. After that, the model contains a central and a peripheral compartment

for the vildagliptin and the vildagliptin-DPP-4 complex (deactivated DPP-4):

$$\begin{aligned}\frac{dA_c}{dt} &= k_{a2}A_{G2} - \frac{CL + CL_{ic}}{V_C}A_C + \frac{CL_{ic}}{V_p}A_p \\ &\quad - \frac{(R_{\max C} - DR_C)\, k_{v2}\frac{A_c}{V_C}}{K_{vd} + \frac{A_c}{V_c}} + k_{off}DR_C\end{aligned} \tag{A.26a}$$

$$\begin{aligned}\frac{dA_p}{dt} &= CL_{ic}\left(\frac{A_c}{V_c} - \frac{A_p}{V_p}\right) \\ &\quad - \frac{(R_{\max P} - DR_p)\, k_{v2}\frac{A_p}{V_p}}{K_{vd} + \frac{A_p}{V_p}} + k_{off}DR_p\end{aligned} \tag{A.26b}$$

$$\begin{aligned}\frac{dDR_C}{dt} &= \frac{(R_{\max C} - DR_C)\, k_{v2}\frac{A_C}{V_C}}{K_{vd} + \frac{A_C}{V_C}} \\ &\quad - (k_{off} + k_{deg})\, DR_C\end{aligned} \tag{A.26c}$$

$$\begin{aligned}\frac{dDR_P}{dt} &= \frac{(R_{\max P} - DR_P)\, k_{v2}\frac{A_P}{V_P}}{K_{vd} + \frac{A_P}{V_P}} \\ &\quad - (k_{off} + k_{deg})\, DR_P\end{aligned} \tag{A.26d}$$

Where A_C, A_P [nmol] are the amounts of vildagliptin in the central and peripheral compartments respectively, CL [$\mathrm{L\,min^{-1}}$] is a non-saturable clearance, CL_{ic} [$\mathrm{L\,min^{-1}}$] is the intercompartmental clearance, V_c, V_p [L] are the volumes of the central and peripheral compartments respectively, k_{v2} [$\mathrm{min^{-1}}$] is a parameter added for the slow tight binding of vildagliptin to DPP-4, K_{vd} [$\mathrm{nmol\,L^{-1}}$] is the equilibrium dissociation constant, k_{off} [$\mathrm{min^{-1}}$] is a rate constant for the dissociation of intact vildaglptin from DPP-4, R_{maxP} [nmol] is the maximum possible amount of DPP-4 in the peripheral compartment, k_{deg} [$\mathrm{min^{-1}}$] is a rate constant for the hydrolysis of vildagliptin by DPP-4, and DR_P [nmol] is the amount of deactivated DPP-4 in the peripheral compartments.

B Parameter Mean Values

Table A.3 includes the values of the parameters which were used in the simulation.

Table A.3: Parameter values

Parameter	Value	Parameter	Value	Parameter	Value
V_{BC}^G [dL]	3.5	V_{BF}^G [dL]	4.5	V_H^G [dL]	13.8
V_L^G [dL]	25.1	V_G^G [dL]	11.2	V_K^G [dL]	6.6
V_{PC}^G [dL]	10.4	V_{PF}^G [dL]	67.4	V_B^I [L]	0.26
V_H^I [L]	0.99	V_G^I [L]	0.94	V_L^I [L]	1.14
V_K^I [L]	0.51	V_{PC}^I [L]	0.74	V_{PF}^I [L]	6.74
V^Γ [mL]	6.74	Q_B^G [dL min^{-1}]	5.9	Q_H^G [dL min^{-1}]	43.7
Q_A^G [dL min^{-1}]	2.5	Q_L^G [dL min^{-1}]	12.6	Q_G^G [dL min^{-1}]	10.1
Q_K^G [dL min^{-1}]	10.1	Q_P^G [dL min^{-1}]	15.1	Q_B^I [dL min^{-1}]	0.45
Q_H^I [L min^{-1}]	3.12	Q_A^I [L min^{-1}]	0.18	Q_K^I [L min^{-1}]	0.72
Q_P^I [L min^{-1}]	1.05	Q_G^I [L min^{-1}]	0.72	Q_L^I [L min^{-1}]	0.9
T_B^G [min]	2.1	T_P^G [min]	5.0	T_P^I [min]	20.0
f_q [·]	0.9	$k_{\phi 1}$ [·]	0.68	$k_{\phi 2}$ [·]	0.00236
k_{12_q} [min^{-1}]	0.08	$k_{\min}$ [min^{-1}]	0.005	$k_{\max}$ [min^{-1}]	0.05
k_{abs} [min^{-1}]	0.08	c_1 [·]	0.067	c_2 [·]	1.59
c_3 [·]	0.62	c_4 [·]	1.72	c_5 [·]	2.03
d_1 [·]	1.126	d_2 [·]	0.683	d_3 [·]	0.14
d_4 [·]	0.023	d_5 [·]	1.59	m_{l_0} [U]	6.33
ζ_1 [L pmol^{-1}]	0.0026	ζ_2 [L (pmol min)$^{-1}$]	0.99e^{-4}	K_l [min^{-1}]	0.3621
K_s [min^{-1}]	0.0572	γ [μg min^{-1}]	2.366	α [min^{-1}]	0.615
β [min^{-1}]	0.931	N_1 [min^{-1}]	0.0499	N_2 [min^{-1}]	0.00015
V^Ψ [dL]	11.31	K_{out} [min^{-1}]	68.3041	Cf_2 [min^{-1}nmol^{-1}]	21.1512
τ_ψ [min^{-1}]	35.1	R_{maxC} [nmol]	5.0	ζ [·]	8.248
f_v [·]	0.772	k_{a1} [min^{-1}]	0.021	k_{a2} [min^{-1}]	0.0175
CL [L min^{-1}]	0.6067	CL_{ic} [L min^{-1}]	0.6683	V_p [L]	97.3
k_{off} [min^{-1}]	0.0102	R_{maxP} [nmol]	13	k_{deg} [min^{-1}]	0.0018
V_c [L]	22.2	K_{vd} [nmol L^{-1}]	71.9	k_{v2} [min^{-1}]	0.39
k_{go} [min^{-1}]	1.88e−4	k_{gg} [min^{-1}]	1.85e−4	k_{pg} [min^{-1}]	4.13
k_{gl} [min^{-1}]	0.46	k_{pl} [min^{-1}]	0.00101	k_{lp} [min^{-1}]	0.91
k_{po} [min^{-1}]	0.51	$\nu_{GW,\max}$ [·]	0.9720	$\nu_{L,\max}$ [·]	0.7560
$\nu_{P,\max}$ [·]	0.2960	n_{GW} [·]	2.0	n_L [·]	2.0
n_P [·]	5.0	$\phi_{GW,50}$ [·]	431.0	$\phi_{L,50}$ [·]	521.0
$\phi_{P,50}$ [·]	1024.0	ρ_α [min^{-1}]	54	ρ_β [min^{-1}]	54
α_M [min^{-1}]	0.06	β_M [min^{-1}]	0.1	p_{la} [min^{-1}]	0.5
r_{la} [·]	0.2143	q_{la} [dL^2 mU^{-2}]	3.04e^{-10}	b_{la} [min^{-1}]	0.025
$C_{\max}$ [·]	15.0	k_{la} [min^{-1}]	2.35e−5	p_{fa} [min^{-1}]	0.5
r_{fa} [·]	0.2143	q_{fa} [dL^2 mU^{-2}]	1.3e−11	b_{fa} [min^{-1}]	0.0068
τ_{HR} [min]	5.0	n_e [·]	4.0	a_e [·]	0.8
τ_e [min]	600	α_e [·]	2.974	β_e [bpm^{-1}]	3.39e−4

References

[1] International Diabetes Federation, *IDF Diabetes Atlas*, 9th ed. Brussels, Belgium: International Diabetes Federation, 2019.

[2] R. J. Mahler and M. L. Adler, "Type 2 Diabetes Mellitus: Update on Diagnosis, Pathophysiology, and Treatment," *The Journal of Clinical Endocrinology & Metabolism*, vol. 84, no. 4, pp. 1165–1171, 04 1999.

[3] K. Wong, D. Glovaci, S. Malik, S. S. Franklin, G. Wygant, U. Iloeje, H. Kan, and N. D. Wong, "Comparison of demographic factors and cardiovascular risk factor control among u.s. adults with type 2 diabetes by insulin treatment classification," *Journal of Diabetes and its Complications*, vol. 26, no. 3, pp. 169 – 174, 2012.

[4] C. Cobelli, C. Dalla Man, G. Sparacino, L. Magni, G. De Nicolao, and B. P. Kovatchev, "Diabetes: models, signals, and control," *IEEE reviews in biomedical engineering*, vol. 2, pp. 54–96, 2009.

[5] T. B. Aradóttir, D. Boiroux, H. Bengtsson, J. Kildegaard, B. V. Orden, and J. B. Jørgensen, "Model for simulating fasting glucose in type 2 diabetes and the effect of adherence to treatment," *IFAC-PapersOnLine*, vol. 50, no. 1, pp. 15 086 – 15 091, 2017, 20th IFAC World Congress.

[6] R. M. Røge, S. Klim, N. R. Kristensen, S. H. Ingwersen, and M. C. Kjellsson, "Modeling of 24-hour glucose and insulin profiles in patients with type 2 diabetes mellitus treated with biphasic insulin aspart," *The Journal of Clinical Pharmacology*, vol. 54, no. 7, pp. 809–817, 7 2014.

[7] R. Visentin, C. Cobelli, and C. Dalla Man, "The padova type 2 diabetes simulator from triple-tracer single-meal studies: in silico trials also possible in rare but not-so-rare individuals," *Diabetes technology & therapeutics*, vol. 22, no. 12, pp. 892–903, 2020.

[8] O. Vahidi, K. E. Kwok, R. B. Gopaluni, and F. K. Knop, "A comprehensive compartmental model of blood glucose regulation for healthy and type 2 diabetic subjects," *Medical & Biological Engineering & Computing*, vol. 54, no. 9, pp. 1383–1398, 2016.

[9] R. Visentin, M. Schiavon, and C. Dalla Man, "In silico cloning of target type 2 diabetes population for treatments development and decision support," in *2020 42nd Annual International Conference of the IEEE Engineering in Medicine & Biology Society (EMBC)*. IEEE, 2020, pp. 5111–5114.

[10] J. T. Sorensen, "A physiologic model of glucose metabolism in man and its use to design and assess improved insulin therapies for diabetes," Ph.D. dissertation, Massachusetts Institute of Technology, 1985.

[11] L. Gaohua and H. Kimura, "A mathematical model of brain glucose homeostasis." *Theoretical biology and medical modelling*, vol. 6, no. 26, 2009.

[12] M. D. Breton, "Physical activity—the major unaccounted impediment to closed loop control," *Journal of Diabetes Science and Technology*, vol. 2, no. 1, pp. 169–174, 2008.

[13] M. Rashid, S. Samadi, M. Sevil, I. Hajizadeh, P. Kolodziej, N. Hobbs, Z. Maloney, R. Brandt, J. Feng, M. Park *et al.*, "Simulation software for assessment of nonlinear and

adaptive multivariable control algorithms: Glucose–insulin dynamics in type 1 diabetes," *Computers & Chemical Engineering*, vol. 130, p. 106565, 2019.

[14] C. Dalla Man, M. D. Breton, and C. Cobelli, "Physical activity into the meal glucose—insulin model of type 1 diabetes: In silico studies," pp. 56–67, 2009.

[15] B. Reeder and A. David, "Health at hand: a systematic review of smart watch uses for health and wellness," *Journal of biomedical informatics*, vol. 63, pp. 269–276, 2016.

[16] A. Mishra, V. Podder, S. Modgil, R. Khosla, A. Anand, R. Nagarathna, R. Malhotra, and H. R. Nagendra, "Higher perceived stress and poor glycemic changes in prediabetics and diabetics among indian population," *Journal of Medicine and Life*, vol. 13, no. 2, p. 132, 2020.

[17] A. J. Ahola, C. Forsblom, V. Harjutsalo, and P.-H. Groop, "Perceived stress and adherence to the dietary recommendations and blood glucose levels in type 1 diabetes," *Journal of diabetes research*, vol. 2020, 2020.

[18] MATLAB, *version R2020a*. Natick, Massachusetts: The MathWorks Inc., 2020.

[19] M. Eftekhari and O. Vahidi, "Mechanism based pharmacokinetic pharmacodynamic modeling of vildagliptin as an add-on to metformin for subjects with type 2 diabetes," *Computer Modeling in Engineering & Sciences*, vol. 114, no. 2, pp. 153–171, 2018.

[20] J. Li and J. D. Johnson, "Mathematical models of subcutaneous injection of insulin analogues: a mini-review," *Discrete and continuous dynamical systems. Series B*, vol. 12, no. 2, p. 401, 2009.

[21] C. Dalla Man, R. A. Rizza, and C. Cobelli, "Meal simulation model of the glucose-insulin system," *IEEE Transactions on Biomedical Engineering*, vol. 54, no. 10, pp. 1740–1749, Oct 2007.

[22] L. Sun, E. Kwok, B. Gopaluni, and O. Vahidi, "Pharmacokinetic-pharmacodynamic modeling of metformin for the treatment of type ii diabetes mellitus," *The open biomedical engineering journal*, vol. 5, p. 1, 2011.

[23] C. B. Landersdorfer, Y.-L. He, and W. J. Jusko, "Mechanism-based population modelling of the effects of vildagliptin on glp-1, glucose and insulin in patients with type 2 diabetes," *British journal of clinical pharmacology*, vol. 73, no. 3, pp. 373–390, 2012.

[24] J. Hunt and I. MacDonald, "The influence of volume on gastric emptying," *The Journal of physiology*, vol. 126, no. 3, pp. 459–474, 1954.

[25] H. I. Jacoby, "Gastric emptying," in *Reference Module in Biomedical Sciences*. Elsevier, 2017.

[26] T. Arleth, S. Andreassen, M. Orsini-Federici, A. Timi, and M. Massi-Benedetti, "A model of glucose absorption from mixed meals," *IFAC Proceedings Volumes*, vol. 33, no. 3, pp. 307–312, 2000.

[27] M. J. Munsters and W. H. Saris, "Effects of meal frequency on metabolic profiles and substrate partitioning in lean healthy males," *PloS one*, vol. 7, no. 6, p. e38632, 2012.

[28] D. Jakubowicz, J. Wainstein, B. Ahren, Z. Landau, Y. Bar-Dayan, and O. Froy, "Fasting until noon triggers increased postprandial hyperglycemia and impaired insulin response after lunch and dinner in individuals with type 2 diabetes: a randomized clinical trial," *Diabetes care*, vol. 38, no. 10, pp. 1820–1826, 2015.

[29] F.-S. T. Investigators *et al.*, "Glucose variability in a 26-week randomized comparison of mealtime treatment with rapid-acting insulin versus glp-1 agonist in participants with type 2 diabetes at high cardiovascular risk," *Diabetes Care*, vol. 39, no. 6, pp. 973–981, 2016.

[30] A. Katz, S. S. Nambi, K. Mather, A. D. Baron, D. A. Follmann, G. Sullivan, and M. J. Quon, "Quantitative insulin sensitivity check index: a simple, accurate method for assessing insulin sensitivity in humans," *The Journal of Clinical Endocrinology & Metabolism*, vol. 85, no. 7, pp. 2402–2410, 2000.

[31] D. Šimonienė, A. Platūkiene, E. Prakapienė, L. Radzevičienė, and D. Veličkiene, "Insulin resistance in type 1 diabetes mellitus and its association with patient's micro- and macrovascular complications, sex hormones, and other clinical data," *Diabetes therapy : research, treatment and education of diabetes and related disorders*, vol. 11, no. 1, pp. 161–174, Jan 2020.

[32] T. B. Aradóttir, H. Bengtsson, M. L. Jensen, N. K. Poulsen, D. Boiroux, L. L. Jensen, S. Schmidt, and K. Nørgaard, "Feasibility of a new approach to initiate insulin in type 2 diabetes," *Journal of diabetes science and technology*, vol. 15, no. 2, pp. 339–345, 2021.

[33] S. H. Lee and K.-i. Kwon, "Pharmacokinetic-pharmacodynamic modeling for the relationship between glucose-lowering effect and plasma concentration of metformin in volunteers," *Archives of pharmacal research*, vol. 27, no. 7, pp. 806–810, 2004.

[34] L. Pala, E. Mannucci, I. Dicembrini, and C. Rotella, "A comparison of mealtime insulin aspart and human insulin in combination with metformin in type 2 diabetes patients," *Diabetes research and clinical practice*, vol. 78, no. 1, pp. 132–135, 2007.

[35] R. N. Bergman, Y. Z. Ider, C. R. Bowden, and C. Cobelli, "Quantitative estimation of insulin sensitivity." *American Journal of Physiology-Endocrinology And Metabolism*, vol. 236, no. 6, p. E667, 1979.

[36] S. Woods, D. Porte Jr, E. Bobbioni, E. Ionescu, J. Sauter, F. Rohner-Jeanrenaud, and B. Jeanrenaud, "Insulin: its relationship to the central nervous system and to the control of food intake and body weight," *The American journal of clinical nutrition*, vol. 42, no. 5, pp. 1063–1071, 1985.

[37] B. Zinman, A. Philis-Tsimikas, B. Cariou, Y. Handelsman, H. W. Rodbard, T. Johansen, L. Endahl, C. Mathieu, N.-. B. O. L. T. Investigators *et al.*, "Insulin degludec versus insulin glargine in insulin-naive patients with type 2 diabetes: a 1-year, randomized, treat-to-target trial (begin once long)," *Diabetes care*, vol. 35, no. 12, pp. 2464–2471, 2012.

[38] J. Köhler, M. A. Müller, and F. Allgöwer, "A novel constraint tightening approach for nonlinear robust model predictive control," in *2018 Annual American Control Conference (ACC)*, 2018, pp. 728–734.

[39] E. González, J. Sanchis, S. García-Nieto, and J. Salcedo, "A comparative study of stochastic model predictive controllers," *Electronics*, vol. 9, no. 12, p. 2078, 2020.

[40] A. J. Garber, "Incretin therapy–present and future," *The review of diabetic studies: RDS*, vol. 8, no. 3, p. 307, 2011.

Paper B

Parameter Estimation in Type 2 Diabetes in the Presence of Unannounced Meals and Unmodelled Disturbances

Mohamad Al Ahdab, Henrik Glavind Clausen, Torben Knudsen, Tinna Björk Aradóttir, Signe Schmidt, Kirsten Nørgaard, and John Leth.

The paper has been accepted to be in the
2021 European Control Conference, pp. 1278-1282, 2021.

The layout has been revised.

Abstract

A least squares strategy to estimate states and parameters for type 2 diabetes (T2D) patients based only on continuous glucose measurements and injected insulin in the presence of unannounced meals and disturbances, e.g., physical activity and stress, is presented. The strategy is based on a simple T2D patient model and tested with clinical data in addition to simulated data generated by using jump diffusion models for meals and disturbances. Three parameters are estimated together with the states, meals, and disturbances. The estimated meal states were shown to follow the trend of the unannounced meals. The strategy can be used to obtain a model with the estimated parameters for predictive control design. In addition, the strategy can also be used to test different insulin and meal plans with the estimated disturbances and parameters. Moreover, the paper demonstrates the ability of jump diffusion models to simulate meals and disturbances.

1 Introduction

One of the challenges which faces human health is the arising of the type 2 diabetes (T2D) chronic disorder as a global pandemic. The number of people suffering from diabetes was reported to be 463 million in 2019 and it is expected to increase to 700 million subjects by 2045 [1]. In addition, 90% of the diabetic subjects are type 2 diabetic. subjects with T2D suffer from high blood sugar (blood glucose) concentrations which can lead to various other organ diseases and failures if left untreated. Insulin treatment is initiated for T2D subjects at later stages when lifestyle changes in physical activity and diet together with oral medications have failed. In the insulin treatment process, it is difficult to find the correct insulin doses for each specific patient to regulate glucose to a safe level without risking hypoglycemia (blood glucose levels below 4 mmol/L) [2]. For this reason, the idea of developing an automated insulin dose finder for T2D subjects has been gaining interest recently [3–5]. Developing and fitting a model for the glucose-insulin dynamics is essential for model-based insulin guiders. Moreover, the estimated parameters of a model can be correlated to demographic information of subjects (weight, age, gender, etc.) in order to develop a simulator for the glucose-insulin dynamics of T2D subjects. The amount of parameters that can be estimated depends on the available data. The available data for T2D subjects during treatment are often limited to the amount of injected insulin and measured glucose concentration. A common measurement data for glucose is the self-monitored blood glucose measurement (SMBG) of fasting glucose (glucose concentration before breakfast). The work in [6] estimated three parameters for a T2D model with fasting SMBG using deterministic simulated data and clinical data in which zero order hold is used for insulin instead of impulses. However, the work in [7] managed to estimate only one parameter for a T2D model based on SMBG measurements when stochastically simulated data is used together with modelling insulin inputs as impulses since it is physiologically more realistic. Both of these works did not consider the effect of meals since the estimation is done with fasting measurements. However, the parameters which were estimated during fasting conditions cannot be accurate for glucose predictions during non-fasting conditions. Another type of glucose data can be obtained through continuous glucose monitors (CGMs), which continuously monitor the blood glucose with a typical sampling time of 5 minutes. Due to the

fact that it is monitored with a relatively small sampling time, daily activities and meals of subjects affect estimates of parameters and states based on CGM data. This poses a challenge on parameter and state estimation with CGM data since it is generally difficult for subjects to record meal intake accurately together with their other daily habits. Several works for type 1 diabetes (T1D) handled parameter estimation with known meal times and sizes such as the works in [8, 9]. For the case of unannounced meals, the work in [10] used sliding mode disturbance observers to estimate states and the rate of appearance of glucose in the blood upon the ingestion of meals. Other works used Kalman filter techniques for state estimation such as the one in [11] in which an unscented Kalman filter is employed and [12] in which a variable state dimension Kalman filter is used. The work [13] fitted linear time-varying models using predictor-based subspace identification and an unscented Kalman filter with CGM and exercise data. For the case of T2D, the work in [7] showed that it is possible to use the unscented Kalman filter to estimate three parameters with CGM data of a T2D model when the meal intake is known. None of the mentioned works consider state and parameter estimation for T2D in the presence of unreported meals and uncertainty,

In this work, a least squares based estimation strategy is proposed to estimate states and parameters of a T2D model with unannounced meals and unmodeled disturbances based on CGM data and known insulin injections only. The meals and disturbances are represented by two different optimization variables with distinct penalties chosen based on the nature of the effect of meals on blood glucose. This approach is similar to the work done in [14] for T1D subjects in which a disturbance variable, called the net effect, is introduced and estimated. However in this paper, we distinguish between meals and other disturbances. Additionally, we aim to estimate some parameters of the model together with the states and disturbances. The estimation problem in this paper is applied on clinical data in addition to simulations generated by jump diffusion models for meals and disturbances. The jump diffusion models are also demonstrated to be a good candidate to model meals and disturbances.

2 Model

The model used in this paper is based on a simple model for the glucose-insulin dynamics of T2D patients from [15]. The model is given as follows:

$$\frac{\mathrm{d}x_1(t)}{\mathrm{d}t} = \frac{1}{p_1}\,U(t) - \frac{1}{p_1}\,x_1(t), \tag{B.1a}$$

$$\frac{\mathrm{d}x_2(t)}{\mathrm{d}t} = \frac{1}{p_1}\,x_1(t) - \frac{1}{p_1}\,x_2(t), \tag{B.1b}$$

$$\frac{\mathrm{d}x_3(t)}{\mathrm{d}t} = p_3\,\Big(x_2(t) + p_7\,x_4(t)\Big) - p_3\,x_3(t), \tag{B.1c}$$

$$\frac{\mathrm{d}x_4(t)}{\mathrm{d}t} = -\Big(p_5 + p_4\,x_3(t)\Big)\;x_4(t) + p_6 + \frac{D_2(t)}{p_v\,p_d}, \tag{B.1d}$$

$$\frac{\mathrm{d}D_1(t)}{\mathrm{d}t} = \frac{1000}{M_{\mathrm{wG}}}\,d(t) - \frac{1}{p_d}\,D_1(t), \tag{B.1e}$$

$$\frac{\mathrm{d}D_2(t)}{\mathrm{d}t} = \frac{1}{p_d}\,D_1(t) - \frac{1}{p_d}\,D_2(t). \tag{B.1f}$$

Here, the states x_1 [U/day] and x_2 [U/day] are used to model the infusion of injected insulin $U(t)$ [U] with a time constant p_1 [day]. The endogenous insulin secretion is modeled to be proportional to the blood glucose concentration x_4 [mmol/L] with a constant gain p_7 [U L/mmol/day]. The state x_3 [U/day] represents the delayed effect of infused insulin x_2 and endogenously secreted insulin $p_7\, x_4$ on glucose with an inverse time constant p_3 [1/day]. Equation (B.1d) describes the dynamics of blood glucose concentration x_4 with p_5 [1/day] being an inverse time constant describing the insulin independent lowering effect of glucose, p_4 [1/U] representing the body's sensitivity to insulin for glucose metabolization, and p_6 [mmol/L/day] is a constant for the endogenous glucose production. For ingested carbohydrates, the states D_1 [mmol] and D_2 [mmol] are used to model the ingestion and absorption of glucose as linear second order dynamics with time constant p_d [day] and $d(t)$ [g/day] being the rate of ingested glucose with $M_{wG} = 180.156$ g/mol being the molar weight of glucose. The absorbed glucose appears in the glucose dynamical equation (B.1d) with a term $\frac{D_2(t)}{p_v\, p_d}$ where p_v [L] is the glucose distribution volume. The CGM measurements are moddeled as following:

$$y(k) = x_4(k) + \nu(k), \tag{B.2}$$

where $y(k) = y(kT)$ denotes the k'th meaustement sample with time constant $T = 5$ [min] (similarly for $x_4(k)$ and all the other states in this paper), and $\nu(k)$ are measurement noise.

For the simulations in this paper, the parameter values from [3] presented in Table B.1 are used. When clinical data is used, unestimated parameters are assigned the values in the table.

Table B.1: Parameter values used in the simulation.

Parameter	Value	Unit
p_1	0.5	[day]
p_3	15.8	[1/day]
p_4	1.80	[1/U]
p_5	3.31	[1/day]
p_6	368	[mmol/L/day]
p_7	1.68	[U L/mmol/day]
p_d	0.03	[day]
p_v	22	[L]

3 Estimation Problem

In the estimation problem, we seek to estimate a vector of static parameters $\theta \in \mathbb{R}^\rho$ and the model states such that the sum of squared residuals between measurements and modeled system response is minimized. In addition, we also desire to estimate meal sizes and meal times such that it is possible to use the model with the estimated parameters to simulate the

effect of meals. Additionally, we wish to handle the effect of disturbances and uncertainties in the estimation process. To accomplish this in the presence of unknown meal intake, the rate of ingested carbohydrates $d(t)$ is estimated and constrained to be non-negative. To account for unmodeled disturbances, especially disturbances causing the glucose level to decrease, e.g. exercise, we include the signal $v(t)$ in (C.1d) as

$$\frac{\mathrm{d}x_4(t)}{\mathrm{d}t} = -\left(p_5 + p_4\, x_3(t)\right)\, x_4(t) + p_6 + \frac{D_2(t)}{p_v\, p_d} + v(t). \tag{B.3}$$

As sudden large positive changes to the blood glucose should be assigned to the meal intake and not to $v(t)$, we want to penalize large positive changes in $v(t)$. This is done by letting the change in $v(t)$ be described by

$$\frac{\mathrm{d}v(t)}{\mathrm{d}t} = \xi(t). \tag{B.4}$$

and introducing a slack variable $S(t)$ such that $\xi(t) < S(t)$ and $S(t) \geq 0$ with $S^2(t)$ being part of the cost. This way, large positive changes in $v(t)$ will be penalized (due to S needing to be large), making $d(t)$ the preferred choice when assigning the cause of a large spike in the glucose level. Likewise, sudden negative changes in the glucose level can be assigned to $v(t)$ at no cost. See also (B.8) which describe how the signal $v(t)$ is used in simulation.

Additionally, costs are put on d^2 and v^2 as well to avoid over-fitting to noise in the observations. Note that we do not add a cost to the rate of change in $d(t)$ as $d(t)$ is expected to have an impulse-like behavior.

In the following, let $\tilde{x}(t) = \left[x^{\mathrm{T}}(t)\ v(t)\right]^{\mathrm{T}}$ denote the augmented state vector.

The least squares estimation problem may now be formulated as

$$\begin{aligned} \min_{\substack{x_4(0), x_3(0),\\ \mathcal{D},\mathcal{V},\mathcal{S},\Xi,\theta}} & \sum_{k=0}^{N-1} W_r\, \left(y(k) - x_4(k)\right)^2 \\ & + W_d\, d^2(k) + W_v\, v^2(k) + W_S\, S^2(k) \end{aligned} \tag{B.5a}$$

subject to

$$\tilde{x}(k+1) = F\left(\tilde{x}(k), u(k), d(k), \xi(k), \theta\right), \tag{B.5b}$$

$$d(k) \geq 0, \tag{B.5c}$$

$$\xi(k) < S(k), \tag{B.5d}$$

$$S(k) \geq 0, \tag{B.5e}$$

where $\mathcal{D} = [d(0) \cdots d(N-1)]^{\mathrm{T}}$, $\mathcal{V} = [v(0) \cdots v(N-1)]^{\mathrm{T}}$, $\mathcal{S} = [S(0) \cdots S(N-1)]^{\mathrm{T}}$, $\Xi = [\xi(0) \cdots \xi(N-1)]^{\mathrm{T}}$, and θ is the vector of parameters to be estimated. The weights W_r, W_d, W_v, and W_S may be seen as tuning parameters which influences how much emphasis is put on the different costs.

The initial conditions for glucose $x_4(0)$ and insulin effect $x_3(0)$ are also estimated. The initial conditions for the injected insulin states $x_1(0)$, $x_2(0)$ are set to be zero since the measurements are assumed to be taken at least one day before the initialization of the insulin injection treatment. Similarly, the initial meal states $D_1(0)$ and $D_2(0)$ are also assumed to

be zero (assuming the first measurement to be taken at fasting conditions). Additionally, the initial condition for the disturbance $v(0)$ is assumed to be zero.

The function $F : \mathbb{R}^7 \times \mathbb{R} \times \mathbb{R} \times \mathbb{R} \times \mathbb{R}^\rho \to \mathbb{R}^7$ is the integration of the dynamics in (C.1), (B.3), and (B.4) from k to $k+1$. In our case, we use a simple forward Euler integration scheme to minimize the computation time, as no significant differences were observed in the optimization results when compared to more elaborate integration methods.

Note that the disturbance v and the meals d have some limitations implemented in the optimization problem by including them in the cost and including a slack variable S on the positive changes of v to capture their behaviour. Therefore, the estimated disturbances v and meals are not freely chosen by the optimization problem and are not treated as the fitting error on x_4.

The optimization problem (B.5) corresponds to a multiple shooting transcription of the corresponding continuous-time problem.

In our work, the problem is implemented using `CasADi` [16] in MATLAB with `IPOPT` [17] as a solver.

4 Simulations

It is desired when simulating a patient to account for the uncertainty of eating and other activities of the patient that are difficult to model or measure. Eating times and amounts are generally uncertain for each person and vary from day to day. A Poisson counting process is usually used to model the uncertainty in the time of events. Therefore, it is proposed in this paper to model the meals as a compound Poisson process $J_d(t)$ and replacing the first meal compartment $D_1(t)$ in (C.1e) with the following jump process:

$$\mathrm{d}D_1(t) = \left(-\frac{1}{p_d} D_1(t) \right) \mathrm{d}t + \mathrm{d}J_d(t), \tag{B.6a}$$

$$J_d(t) = \sum_{i=1}^{P_d(t)} \frac{1000}{M_{wG}} m_i, \tag{B.6b}$$

where $P_d(t)$ is a Poisson point process with intensity $\lambda_d(t)$, and m_i is the i^{th} meal size in grams of carbohydrates. Here, $J_d(t)$ represents the accumulation of meals until time t and $dJ_d(t)$ corresponds to the meals $d(t)$ in (C.1e). Of course the eating behaviour for humans can be very complicated in real life and the intensity $\lambda_d(t)$ should depend on the meal sizes. However for simplicity, the intensity rate is chosen to be

$$\lambda_d(t) = \begin{cases} 3, & \text{Between 7:00 and 23:00} \\ 0.5, & \text{Otherwise} \end{cases} \tag{B.7}$$

to take into account that people, on average, eat less frequently at night. Moreover, the meal sizes are chosen to be $m_i \overset{\text{i.i.d.}}{\sim} \text{LogNormal}\left(\ln(60), \ln(1.5)^2\right)$ with i.i.d. meaning that they are independent and identically distributed which is assumed for simplification. In addition, the meal sizes are assumed to be independent from $P_d(t)$. The log-normal distribution is chosen

for the meal sizes since its support is the positive real line and it has a positive skewness that depends on the variance of the logarithm of the random variable. Note that the parameters for m_i are chosen such that the mean and standard deviation of ingested carbohydrates are $\exp(\ln(60) + \ln(1.5)^2/2) \approx 65$ $[g]$ and $(\exp(\ln(1.5)^2) - 1)\exp(2\ln(60) + \ln(1.5)^2) \approx 27$ $[g]$ respectively.

The disturbances and model uncertainty term $v(t)$, is simulated with the following equations:

$$\mathrm{d}v_1(t) = -\frac{1}{\tau_1} v_1(t)\,\mathrm{d}t + \sigma_v\,\mathrm{d}w_v(t), \tag{B.8a}$$

$$\mathrm{d}v_2(t) = \frac{1}{\tau_1}\Big(v_1(t) - v_2(t)\Big)\,\mathrm{d}t, \tag{B.8b}$$

$$\mathrm{d}v_3(t) = -\frac{1}{\tau_2} v_3(t)\,\mathrm{d}t + \mathrm{d}J_v(t), \tag{B.8c}$$

$$\mathrm{d}v_4(t) = \frac{1}{\tau_2}\Big(v_3(t) - v_4(t)\Big)\,\mathrm{d}t, \tag{B.8d}$$

$$J_v(t) = \sum_{i=1}^{P_v(t)} q_i, \tag{B.8e}$$

$$v(t) = v_2(t) - v_4(t). \tag{B.8f}$$

Here, the first two equations (B.8a) and (B.8b) are a second-order low-pass filter for $\mathrm{d}w_v(t)$ with $w_v(t)$ being a Brownian motion. These equations are intended to simulate model uncertainties and the variability observed in clinical CGM data. On the other hand, equations (B.8c) and (B.8d) are included to model the effect of events lowering glucose concentrations such as physical activity. These events are modeled through a filtered compound Poisson process $J_v(t)$ with a Poisson point process $P_v(t)$ having a constant intensity rate λ_v and jump sizes q_i. Empirically, the values for (B.8) are chosen to be $\tau_1 = 0.5$ [day], $\tau_2 = 0.0625$ [day], $\sigma_v = 100$, $\lambda_v = 0.5$ [1/day], and the jump sizes are defined with $q_i \overset{\text{i.i.d.}}{\sim} \text{LogNormal}(\ln(50), \ln(1.5)^2)$ and independent from $P_v(t)$. Note that the events which has a negative impact on glucose are modelled similarly to the meal jump model (B.6) but with a relatively larger time constant $\tau_2 \approx 2p_d$ since they usually have a prolonged effect on the glucose concentration [14].

The simulation model consisting of (C.1) with (C.1d) replaced with (B.3) and (C.1e) replaced with (B.6), together with (B.8). The compound Poisson process (B.6) is simulated with the Euler scheme for jump diffusion models [18]. The CGM observations are assumed to be contaminated with white Gaussian noise $\nu(k) \overset{\text{i.i.d.}}{\sim} \mathcal{N}(0, R)$ with variance $R = 0.1^2$.

The simulation period is assumed to be 14 days in which the patient takes one injection of long-acting insulin every day at 07:00 in the morning, with dose size 0 U for the first five days, 14 U for the next five days, and 18 U for the remaining days.

5 Simulation Results

To verify the proposed method, we first perform a simulation study. As the true states and parameters are known from the simulation, it is possible to quantify how well the method

works.

The weights in the cost function (B.5a) are tuned to be $W_r = 10000$, $W_d = 1/2200$, $W_v = 1/100$ and $W_S = 0.8$. Note that the difference in the order of magnitude between the weights is due to the difference in order of magnitude for the corresponding variables to each weight.

We perform $M = 100$ Monte Carlo simulations using the parameter values from Table C.1. Here M denote the number of simulated patients. The estimation problem was performed for two cases: a case in which only p_4 and p_7 are estimated, and a case in which p_1 is also estimated. The estimation failed when the remaining parameters are considered. Nevertheless, a sensitivity analysis of the model's parameters was performed in [19] and it was shown that the remaining parameters, except for p_6, are not as influential for the glucose state x_4 as the one estimated in this paper. As for p_6, the estimated disturbances can take it into account since they are both additive in (B.3). The fit for the estimated states for each simulated patient is calculated as following:

$$\text{fit} = 1 - \frac{\sqrt{\frac{1}{N}\sum_{k=1}^{N}\left(x(k) - \hat{x}(k)\right)^2}}{\sqrt{\frac{1}{N}\sum_{k=1}^{N}\left(x(k) - \frac{1}{N}\sum_{k=1}^{N} x(k)\right)^2}}. \tag{B.9}$$

And the fit for each parameter p is calculated for the entire Monte Carlo simulation as:

$$\text{fit} = 1 - \sqrt{\frac{1}{M}\sum_{k=1}^{M}\left(\frac{p - \hat{p}_k}{p}\right)^2}, \tag{B.10}$$

In Table B.2 and B.3, the mean and variance for the fit of the estimated states are shown together with the root mean square (RMS) fit of the parameters.

In Figure B.1, a segment of one example from the Monte Carlo simulation with the corresponding state estimates is shown.

As can be seen from the fit values of the states, the fit is generally good. The parameter estimates for p_4 and p_7 are close to the true parameter values. However, for the case of p_1, the estimation accuracy is much lower when compared with p_4 and p_7. Nonetheless, only the insulin states x_1, x_2, and x_3 are noticeably affected when p_1 is estimated. This is expected since p_1 mainly affects the insulin states, and for the case of estimating p_4 and p_7, the parameter p_1 is chosen to be equal to the true value in the simulation. The estimation strategy manages to estimate the time of the meals with good accuracy, as seen from the plot of D_1. Moreover, the estimation strategy manages to capture the trend of the jump process which suggests that this strategy can be used to estimate states driven by jump process. Nevertheless, the size of the meals are always underestimated. This decreases the fit for the states D_1 and D_2 as seen in the tables. Similarly for the estimation of v, the strategy manages to estimate the general trend of v but with an underestimate.

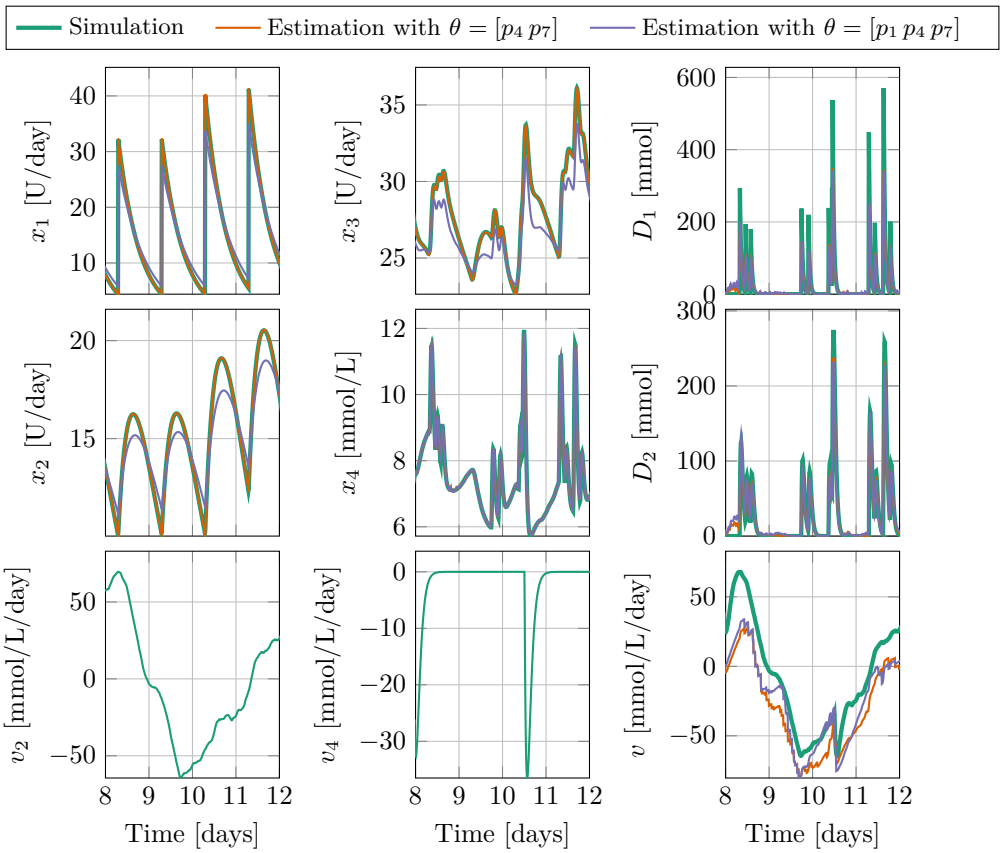

Fig. B.1: Example of Monte Carlo simulation with corresponding state estimates.

6 Clinical Data Results

For this project, data from a clinical study conducted in [20] have been made available. This data consist of CGM and SMBG data recorded for periods of 30–80 days for 8 different insulin-naïve patients initiating insulin treatment with long-acting insulin degludec.

In Figure B.2, a segment of clinical CGM data from one of the patients is shown along with the corresponding state estimates. The parameters were estimated to be $p_1 = 0.53$, $p_4 = 0.79$, and $p_7 = 3.00$. Parameter p_1 is close to the value used in the simulations from Table C.1 which is calculated based on the time profile for ultra long acting insulin. On the other hand, parameters p_4 and p_7 are different and indicate that the patient have low insulin sensitivity p_4 and high gain p_7 which relate to the production of insulin. The marked meals

Table B.2: Simulation results when only p_4 and p_7 are estimated based on 100 Monte Carlo simulations.

State	mean fit	std fit
X_1	100%	0
X_2	100%	0
X_3	81.69%	11.80%
X_4	97.95%	0.05%
D_1	49.78%	0.64%
D_2	68.65%	0.16%
Parameter	fit	
p_4	91.55%	
p_7	92.97%	

in Figure B.2 are meal times reported by the patient. It can be seen that the estimated meal compartment state D_1 follows the trend of the marked meals. Nevertheless, there are small meals estimated between the reported meals. These meals can be the result of model uncertainties, e.g. the effect of different types of ingested carbohydrates, and/or imperfections in the process of recording meal times by the patient. One can use a threshold based on statistical techniques to determine whether an estimated spike is an actual or meal or not. For example, a smart phone application can ask the patient every time a spike is estimated if they had a meal or not until enough data is collected to compute an appropriate threshold for the spikes. However, this can be challenging especially since the meal sizes are underestimated as discussed earlier. For the estimated v, it is seen that it has an average negative value that can be explained by having the actual value of p_6 for the patient being different from the value in Table C.1 which was used in the estimation strategy. Thus, an estimate for p_6 can also be obtained by subtracting the mean of the estimated v from the value of p_6 from Table C.1. In addition, negative jumps on the estimated v can be observed from the figure. These negative jumps can be due to the inaccuracies in the estimated meals and/or unmodeled disturbances such as physical activity. The observed negative jumps supports using a negative jump process in (B.8).

7 Conclusion and Future Work

The estimation strategy presented in this work has been shown to be able to estimate states, two parameters p_4 and p_7 with good accuracy, and one parameter p_1 with lower accuracy from CGM data for T2D patients in the presence of unannounced meals and disturbances. The strategy also manages to estimate meal states and meal times with good accuracy, but with underestimation in the meal sizes. However, it is important to note that the algorithm cannot be used to predict accurately the glucose concentrations since it does not fit the meals and the

Table B.3: Simulation results when p_1, p_4 and p_7 are estimated based on 100 Monte Carlo simulations.

State	mean fit	std fit
X_1	84.27%	5.36%
X_2	87.10%	4.43%
X_3	72.99%	12.72%
X_4	97.94%	0.06%
D_1	49.22%	0.69%
D_2	66.91%	0.03%
Parameter	fit	
p_4	94.83%	
p_7	93.16%	
p_1	66.06%	

disturbances into stochastic models. Nevertheless, the estimated parameters and the states can be used with the model in (C.1) for the design of model-based control strategies for insulin intensification which are robust under the unknown disturbances. In addition, one can use the estimated disturbances with the estimated parameters to reproduce the measured results under different insulin and meal plans. Further work is needed to try to fit the jump diffusion model parameters in equation (C.2) for individual patients. Moreover, fitting a stochastic model for the disturbance term v, e.g. the model used in the simulation (B.8), can help further in the process of simulating and predicting glucose concentrations for subjects with T2D, or for the process of designing a stochastic predictive controller for insulin intensification.

References

[1] International Diabetes Federation, *IDF Diabetes Atlas*, 9th ed. Brussels, Belgium: International Diabetes Federation, 2019.

[2] L. Berard, M. Bonnemaire, M. Mical, and S. Edelman, "Insights into optimal basal insulin titration in type 2 diabetes: Results of a quantitative survey," *Diabetes, Obesity and Metabolism*, vol. 20, no. 2, pp. 301–308, 2018.

[3] T. B. Aradóttir, D. Boiroux, H. Bengtsson, J. Kildegaard, M. L. Jensen, J. B. Jørgensen, and N. K. Poulsen, "Model predictive control for dose guidance in long acting insulin treatment of type 2 diabetes," *IFAC Journal of Systems and Control*, vol. 9, p. 100067, 2019.

[4] D. Eringis, P. A. Munk, B. K. Andersen, R. S. Suresh, and J.-J. Leth, "LPV based control of glucose concentration in type 2 diabetes," *IFAC-PapersOnLine*, vol. 53, no. 2, pp. 16 386–16 393, 2020.

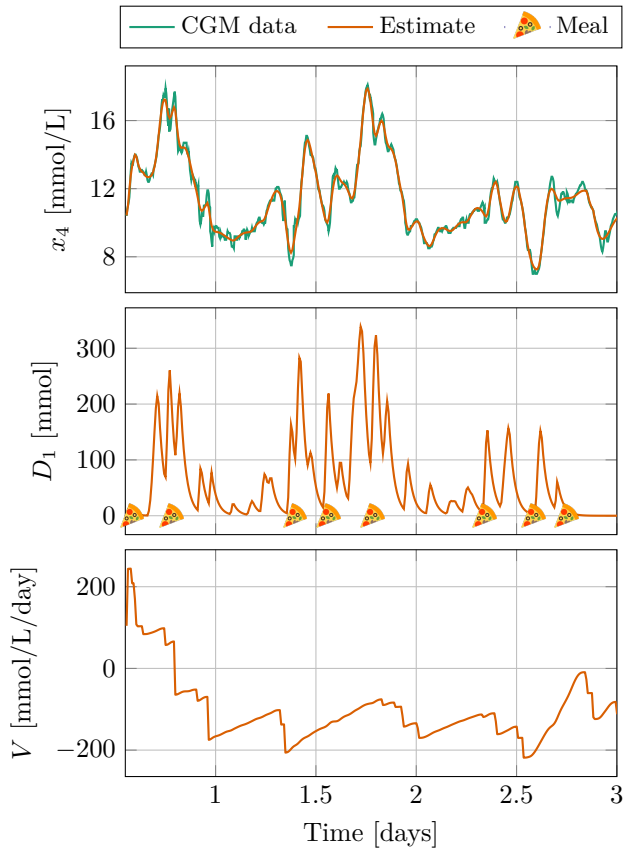

Fig. B.2: Segment of clinical CGM data from one subject with corresponding state estimates. The crosses indicate meal times reported by the patient.

[5] S. Arnolds, T. Heise, F. Flacke, and J. Sieber, "Common standards of basal insulin titration in T2DM," *Journal of Diabetes Science and Technology*, vol. 7, no. 3, pp. 771–788, 2013.

[6] T. B. Aradóttir, D. Boiroux, H. Bengtsson, and N. K. Poulsen, "Modelling of fasting glucose-insulin dynamics from sparse data," in *2018 40th Annual International Conference of the IEEE Engineering in Medicine and Biology Society (EMBC)*. IEEE, 2018, pp. 2354–2357.

[7] H. G. Clausen, J.-J. Leth, T. Knudsen, and H. Schiøler, "State estimation in type 2 diabetes using the continuous-discrete unscented Kalman filter," *IFAC-PapersOnLine*, vol. 53, no. 2, pp. 16 500–16 505, 2020.

[8] D. Boiroux, M. Hagdrup, Z. Mahmoudi, N. K. Poulsen, H. Madsen, and J. B. Jørgensen,

"Model identification using continuous glucose monitoring data for type 1 diabetes," *IFAC-PapersOnLine*, vol. 49, no. 7, pp. 759–764, 2016.

[9] D. Boiroux, Z. Mahmoudi, and J. B. Jørgensen, "Parameter estimation in type 1 diabetes models for model-based control applications," in *2019 American Control Conference (ACC)*, 2019, pp. 4112–4117.

[10] I. Sala-Mira, J.-L. Díez, B. Ricarte, and J. Bondia, "Sliding-mode disturbance observers for an artificial pancreas without meal announcement," *Journal of Process Control*, vol. 78, pp. 68 – 77, 2019.

[11] C. M. Ramkissoon, P. Herrero, J. Bondia, and J. Vehi, "Unannounced meals in the artificial pancreas: Detection using continuous glucose monitoring," *Sensors (Basel, Switzerland)*, vol. 18, no. 3, p. 884, Mar 2018.

[12] J. Xie and Q. Wang, "A variable state dimension approach to meal detection and meal size estimation: In silico evaluation through basal-bolus insulin therapy for type 1 diabetes," *IEEE Transactions on Biomedical Engineering*, vol. 64, no. 6, pp. 1249–1260, 2017.

[13] I. Hajizadeh, M. Rashid, K. Turksoy, S. Samadi, J. Feng, M. Sevil, N. Hobbs, C. Lazaro, Z. Maloney, E. Littlejohn, and A. Cinar, "Incorporating unannounced meals and exercise in adaptive learning of personalized models for multivariable artificial pancreas systems," *Journal of Diabetes Science and Technology*, vol. 12, no. 5, pp. 953–966, 2018.

[14] D. Boiroux, J. B. Jørgensen, S. D. Patek, and M. D. Breton, "The contribution of physical activity in blood glucose concentration for people with type 1 diabetes," *IFAC-PapersOnLine*, vol. 51, no. 27, pp. 270–275, 2018.

[15] T. Aradóttir, D. Boiroux, H. Bengtsson, J. Kildegaard, B. Orden, and J. Jørgensen, "Model for simulating fasting glucose in type 2 diabetes and the effect of adherence to treatment." in *IFAC-PapersOnLine*, vol. 50, no. 1. Elsevier, 2017, pp. 15 086–15 091.

[16] J. A. E. Andersson, J. Gillis, G. Horn, J. B. Rawlings, and M. Diehl, "CasADi – A software framework for nonlinear optimization and optimal control," *Mathematical Programming Computation*, vol. 11, no. 1, pp. 1–36, 2019.

[17] A. Wächter and L. T. Biegler, "On the implementation of an interior-point filter line-search algorithm for large-scale nonlinear programming," *Mathematical Programming*, vol. 106, no. 1, pp. 25–57, Mar 2006.

[18] E. Platen and N. Bruti-Liberati, *Numerical solution of stochastic differential equations with jumps in finance*. Springer Science & Business Media, 2010, vol. 64.

[19] H. G. Clausen, T. Knudsen, T. B. Aradóttir, S. Schmidt, K. Nørgaard, M. A. Ahdab, and J.-J. Leth, "A new stochastic approach for modeling glycemic disturbances in type 2 diabetes," *IEEE Transactions on Biomedical Engineering*, (in press).

[20] T. B. Aradóttir, H. Bengtsson, M. L. Jensen, N. K. Poulsen, D. Boiroux, L. L. Jensen, S. Schmidt, and K. Nørgaard, "Feasibility of a new approach to initiate insulin in type 2 diabetes," *Journal of diabetes science and technology*, vol. 15, no. 2, pp. 339–345, 2021.

Paper C

Parameter Estimation for a Jump Diffusion Model of Type 2 Diabetic Patients in the Presence of Unannounced Meals

Mohamad Al Ahdab, Milan Papež, Torben Knudsen, Tinna Björk Aradóttir, Signe Schmidt, Kirsten Nørgaard, and John Leth.

The paper has been accepted to be in the
2021 IEEE Conference on Control Technology and Applications (CCTA), pp. 176-183, 2021.

The layout has been revised.

Abstract

Type 2 diabetes (T2D) has become one of the most often encountered metabolic disorders threatening the human health. Unannounced meal intake and irregular physical activity cause abrupt changes in the blood glucose concentrations. Therefore, a reliable and accurate algorithms that account for these sudden concentration changes constitute a crucial part of automated insulin pumps and dose guiders. To this end, we develop a stochastic jump diffusion model for T2D patients, reflecting the irregular frequency and uncertain amount of consumed carbohydrates. Moreover, we design a method—combining particle Markov chain Monte Carlo and particle learning—to estimate the unknown parameters of this model, considering only continuous glucose monitoring data and amounts of injected insulin. Our approach is verified on synthetic and clinical data, demonstrating its ability to estimate the unknown parameters with a varying degree of accuracy.

1 Introduction

One of the challenges facing human health is the emergence of the type 2 diabetes (T2D) chronic disorder as a global pandemic. It has been reported in [1] that the number of people suffering from diabetes is expected to increase to 700 million patients by 2045. In addition, 90% of the diabetic patients belong to the T2D category. T2D patients suffer from high blood glucose (sugar) concentrations, which can lead to various organ diseases and failures if left untreated. Insulin treatment is initiated for T2D patients at later stages when changes in physical activity, and oral medications have failed. In the insulin treatment process, it is difficult to calculate suitable insulin doses for individual patients to regulate their glucose concentrations to a safe level without risking hypoglycemia (blood glucose levels below 4 mmol/L) [2]. Therefore, the idea of developing an automated insulin dose guiders for T2D patients has been gaining interest recently [3–5]. Designing accurate models to predict glucose concentrations for T2D patients is crucial for the development of automated insulin guidance algorithms and hypoglycemic alert systems. However, predicting glucose levels for each patient is difficult, since it depends heavily on the patient behavioural and physiological parameters. Therefore, it is important to learn these parameters to each patient individually. For example, one can learn how often a patient eats, and how much they eat on average. Nevertheless, one should also acknowledge the limited types of data which can be obtained from patients following a prescribed treatment plan. The available data for T2D patients during treatment are often limited to the amount of injected insulin and measured glucose concentration. A common measurement data for glucose is the self-monitored blood glucose measurement (SMGB) of fasting glucose (glucose concentration before breakfast). Three physiological parameters for a T2D model with fasting SMBG using clinical and synthetic data, in which the zero order hold is used for insulin instead of the impulses, were estimated in [6]. However, [7] managed to estimate only one parameter for the same T2D model based on the SMBG measurements when synthetic data is used along with modelling insulin inputs as impulses. Both these papers did not consider the effect of meals, since the estimation is done with the fasting measurements. This makes the estimated physiological parameters inaccurate for glucose predictions during non-fasting conditions. Another type of glucose data is gathered from continuous glucose monitors (CGMs), which continuously

measure the blood glucose with a typical sampling time of five minutes. Due to the fact that it is monitored with a relatively small sampling time, daily activities such as eating or exercising affect the estimates of parameters and states based on CGM data. This poses a challenge on parameter and state estimation with CGM data, since it is generally difficult for patients to record meal intake accurately along with their other daily habits. Several papers concerned with type 1 diabetes handled the parameter estimation with known meal times and sizes [8, 9]. For unannounced meals, [10] used sliding mode disturbance observers to estimate states and the rate of appearance of glucose in the blood upon the ingestion of meals. In the same context, the unscented Kalman filter [11] and the Kalman filter with a variable dimension of the state estimate [12] were applied. The linear time-varying models, using the subspace identification and the unscented Kalman filter with CGM and exercise data, were adopted in [13]. Regarding T2D, [14] fitted parameters of a T2D model using data obtained from a triple-tracer meal test including plasma glucose, insulin, and C-peptide concentrations measurements. For the techniques utilizing CGM, [7] showed that it is possible to use the unscented Kalman filter to estimate the three parameters with CGM data of a T2D model when the meal intake is known. However, none of the aforementioned papers considers the state and parameter estimation for T2D in the presence of unannounced meals. Additionally, none of those papers considers a model that can be used to also learn the behavioural parameters.

In this paper, a stochastic jump diffusion model is proposed (Section 2) to characterize the (potentially irregular) eating habits of T2D patients. To estimate the parameters related to the unannounced meals (parameters of the jump process) and the diffusion term representing the uncertainties, including the variance of the CGM error, a particle Markov chain Monte Carlo (PMCMC)-based method, combined with the particle learning, is proposed (Section 3). The estimation method relies only on the CGM measurements and the announced insulin doses, assuming that the physiological parameters are known. The experiments on synthetic and clinical data (Section 4) demonstrate that the proposed method delivers parameter estimates with a varying degree of accuracy.

2 A jump diffusion model of T2D patients

The model used in this paper is based on a simple model for the glucose-insulin dynamics of T2D patients from [15]. To account for glucose variability along the day—in a similar way to [16]—we adopt the meal compartment model from [17]. The model is given as follows:

$$\frac{\mathrm{d}X_1(t)}{\mathrm{d}t} = \frac{1}{p_1}\,u(t) - \frac{1}{p_1}\,X_1(t), \tag{C.1a}$$

$$\frac{\mathrm{d}X_2(t)}{\mathrm{d}t} = \frac{1}{p_1}\,X_1(t) - \frac{1}{p_1}\,X_2(t), \tag{C.1b}$$

$$\frac{\mathrm{d}X_3(t)}{\mathrm{d}t} = p_3\,\big(X_2(t) + p_7\,X_4(t)\big) - p_3\,X_3(t), \tag{C.1c}$$

$$\frac{\mathrm{d}X_4(t)}{\mathrm{d}t} = -\big(p_5 + p_4\,X_3(t)\big)\;X_4(t) + p_6 + \frac{D_2(t)}{p_v\,p_d}, \tag{C.1d}$$

$$\frac{\mathrm{d}D_1(t)}{\mathrm{d}t} = \frac{1000}{M_{\mathrm{wG}}}\,d(t) - \frac{1}{p_d}\,D_1(t), \tag{C.1e}$$

Table C.1: Parameter values adopted in the simulation [16].

Parameter	Value	Unit
p_1	0.5	[day]
p_3	15.8	[1/day]
p_4	1.80	[1/U]
p_5	3.31	[1/day]
p_6	368	[mmol/L/day]
p_7	1.68	[U L/mmol/day]
p_d	0.03	[day]
p_v	22	[L]

$$\frac{\mathrm{d}D_2(t)}{\mathrm{d}t} = \frac{1}{p_d} D_1(t) - \frac{1}{p_d} D_2(t). \tag{C.1f}$$

Here, the states X_1 [U/Day] and X_2 [U/Day] are used to model the infusion process of injected insulin $u(t)$ [U] with a time constant p_1 [Day]. The endogenous insulin secretion is modeled to be proportional to the blood glucose concentration X_4 [mmol/L] with a constant p_7 [U L/mmol/Day]. The state X_3 [U/day] is the delayed effect of infused insulin X_2 and endogenously secreted insulin $p_7 X_4$ on the glucose with an inverse time constant p_3 [1/Day]. (C.1d) describes the dynamics of blood glucose concentration X_4 with p_5 [1/Day] being an inverse time constant describing the insulin independent lowering effect of glucose, p_4 [1/U] representing the patient's sensitivity to insulin for glucose metabolization, and p_6 [mmol/L/Day] is a constant approximation for endogenous glucose production. For ingested carbohydrates, the states D_1 [mmol] and D_2 [mmol] are used to model the ingestion and absorption of glucose as linear, second-order, dynamics with time constant p_d [Day], and $d(t)$ [g/Day] is the rate of ingested glucose, with $M_{wG} = 180.156$ g/mol being the molar weight of glucose. The absorbed glucose appears in the glucose dynamical equation (C.1d) with a term $\frac{D_2(t)}{p_v\, p_d}$, where p_v [L] is the glucose distribution volume. The values of the parameters in (C.1) are assumed known and presented in Table C.1. Note that, in this paper, we focus on T2D patients with basal insulin therapy. Nevertheless, the model (C.1) can be extended to account for fast acting insulin injections by introducing two new states, similar to X_1 and X_2, with appropriate time constants. In this paper, a jump model for the meals is introduced to model the meal in a stochastic fashion by modifying (C.1e) as follows:

$$\mathrm{d}D_1(t) = \left(-\frac{1}{p_d} D_1(t)\right) \mathrm{d}t + \frac{1000}{M_{wG}}\, \mathrm{d}\mathcal{J}(t), \tag{C.2a}$$

$$\mathcal{J}(t) = \sum_{i=1}^{\mathcal{P}(t)} Z(i), \tag{C.2b}$$

where $\mathcal{P}(t)$ is a Poisson process with a constant intensity λ_c, $Z(i)$ is the ith mark (or jump size) characterizing the ith meal amount in grams of carbohydrates, $\mathcal{J}(t)$ is the compound

Poisson process representing the accumulation of meals until time t, and $d\mathcal{J}(t)$ corresponds to the meals $d(t)$ in (C.1e). The jump sizes $Z(i)$ are assumed independent of $\mathcal{P}(t)$, mutually independent and identically distributed with the log-normal distribution,

$$Z(i) \overset{\text{i.i.d.}}{\sim} \text{LogNormal}\left(\mu_z, \sigma_z^2\right).$$

The log-normal distribution is chosen for the meal sizes, since it has a positive support, and its skewness depends on the logarithm of the jump sizes. The independence assumptions above are only approximately true. However, as demonstrated below, we still obtain good results when applied to clinical data, i.e. the dependencies can be neglected, at least for the clinical data considered here. However, it is important to note that one should always be aware of the independence assumptions when applying the methods presented in this paper.

Additionally, (C.1d) is modified to have a diffusion term as follows:

$$\mathrm{d}X_4 = \left(-\left(p_5 + p_4\, X_3(t)\right)\; X_4(t) + p_6 + \frac{D_2(t)}{p_v\, p_d} \right) \mathrm{d}t + \sigma dW, \tag{C.3}$$

where W is the standard Brownian motion. The diffusion term is added to account for uncertainties in the model. The model can now be written in the jump diffusion state-space form,

$$dX = f_m\left(X(t), u(t)\right) dt + g dW + h d\mathcal{J}, \tag{C.4}$$

where

$$\begin{aligned} X(t) &\coloneqq \left[X_1(t), X_2(t), X_3(t), X_4(t), D_1(t), D_2(t)\right]^{\mathsf{T}}, \\ h &\coloneqq \left[0, 0, 0, 0, \frac{1000}{M_{wG}}, 0\right]^{\mathsf{T}}, \\ g &\coloneqq [0, 0, 0, \sigma, 0, 0]^{\mathsf{T}}, \end{aligned}$$

and f_m is the function defined by the right hand side of (C.1) without the firste term in (C.1e).

In the rest of this paper, we work with a discretized version of (C.1). More precisely, the model (C.1) is discretized using the Euler scheme [18, 19], yielding the following discrete approximation:

$$X(k+1) = F\left(X(k), u(k); T_s\right) + g\sqrt{T_s}\xi(k) + hZ(k)J(k), \tag{C.5}$$

where

$$\begin{aligned} F\left(X(k), u(k); T_s\right) &\coloneqq X(k) + T_s f_m\left(X(k), u(k)\right), \\ \xi(k) &\overset{\text{i.i.d.}}{\sim} \mathcal{N}(0, \boldsymbol{I}), \\ J(k) &\sim Ber(\lambda), \end{aligned}$$

with $\lambda = 1 - \exp(-\lambda_c T_s)$ being the probability of having at least one jump within the sample time period T_s. In this paper, the parameter λ will be estimated instead of λ_c. It is remarked

that for all k we have that 1) $X_1(k)$ and $X_2(k)$ are deterministic and 2) $X_3(k)$ and $D_2(k)$ are deterministic given the conditioning, i.e.

$$(X(k-1) = x(k-1), \theta = \vartheta). \tag{C.6}$$

In the sequel, we let $Q(k) \coloneqq \left[J(k), Z(k)\right]^\mathsf{T}$, F_i and $X(1:K) \coloneqq \left[X(1), \ldots, X(K)\right]$ to denote the jump states, the ith row of F and the state trajectory from $k = 1$ to $k = K$, respectively.

2.1 The transition model

Let $f(x(k)|x(k-1), \vartheta)$ denote the conditional probability density of $X(k)$ given (C.6), which we write symbolically as

$$X(k)|(X(k-1) = x(k-1), \theta = \vartheta) \sim f(x(k)|x(k-1), \vartheta).$$

This forms a probabilistic representation of the discrete model (C.5). It holds that

$$f(x(k)|x(k-1), \vartheta) = f(x_4(k), d_1(k)|x(k-1), \vartheta) \tag{C.7}$$

since $X_1(k)$, $X_2(k)$, $X_3(k)$ and $D_2(k)$ are deterministic given (C.6).[1] Note, too, that under (C.6), $X_4(k)$ and $D_1(k)$ are independent, since the first meal compartment $D_1(k)$ at time k cannot effect the glucose state $X_4(k)$. It follows then that

$$f(x(k)|x(k-1), \vartheta) = f(x_4(k)|x(k-1), \vartheta) f(d_1(k)|x(k-1), \vartheta), \tag{C.8}$$

where (using the notation above)

$$X_4(k)|(X(k-1) = x(k-1), \theta = \vartheta) \sim f(x_4(k)|x(k-1), \vartheta), \tag{C.9a}$$
$$D_1(k)|(X(k-1) = x(k-1), \theta = \vartheta) \sim f(d_1(k)|x(k-1), \vartheta). \tag{C.9b}$$

We adopt the normal density for (C.9a), with the mean $\mu_4 = F_4\left(x(k-1), u(k-1), \vartheta\right)$ and the variance $\sqrt{T_s}\vartheta_4$, i.e.

$$f(x_4(k)|x(k-1), \vartheta) = \frac{1}{\sqrt{T_s}\vartheta_4\sqrt{2\pi}} \exp\left(-\frac{1}{2}\left(\frac{x_4(k) - \mu_4}{\sqrt{T_s}\vartheta_4}\right)^2\right). \tag{C.10}$$

(C.9b) is specified as follows:

$$f(d_1(k)|x(k-1), \vartheta) = \begin{cases} p_z\left(\tilde{d}; \vartheta_2, \vartheta_3\right)\vartheta_1 \\ \quad + \delta(\tilde{d})(1 - \vartheta_1), \ \tilde{d} \geq 0, \\ 0, \ \tilde{d} < 0; \end{cases} \tag{C.11}$$

where $\tilde{d} \coloneqq d_1(k) - F_5\left(x(k-1), u(k-1)\right)$, p_z is the probability density function of the jump sizes Z, and δ is the Dirac delta function.

[1] For ease of notation, we have left out the product of Dirac delta functions corresponding to the deterministic states in (C.7).

2.2 The measurement model

The CGM measurements are modeled via

$$Y(k) = X_4(k) + \nu(k),\ \nu(k) \sim \mathcal{N}(0, \sigma_y^2), \tag{C.12a}$$

$$f(y(k)|x(k), \vartheta) = \frac{1}{\vartheta_5\sqrt{2\pi}} \exp\left(-\frac{1}{2}\left(\frac{y(k) - x_4(k)}{\vartheta_5}\right)^2\right), \tag{C.12b}$$

$$Y(k)|(X(k) = x(k), \theta = \vartheta) \sim f(y(k)|x(k), \vartheta). \tag{C.12c}$$

Note that the measurement errors are assumed to be uncorrelated with the glucose concentrations for simplicity. There exist more detailed models, see, e.g. [20].

In summary, the desired parameters to be estimated are $\theta = \left[\lambda, \sigma_z^2, \mu_z, \sigma^2, \sigma_y^2\right]^\mathsf{T}$.

3 The conditional particle filter with ancestor sampling and parameter learning

A practically validated and theoretically sound approach to deal with the state estimation problem in nonlinear and non-Gaussian state-space models is provided by the sequential Monte Carlo (SMC) methods [21], comprising the particle filters as a specific case. The central aim of the SMC methods is to estimate the joint state posterior density, $X(1:K)|(Y(1:K) = y(1:K)) \sim f(x(1:K)|y(1:K))$. The Bayesian way to additionally estimate unknown parameters is to augment the state trajectory, $X(1:K)$, with θ, i.e.

$$X(1:K), \theta|(Y(1:K) = y(1:K)) \sim f(x(1:K), \vartheta|y(1:K)). \tag{C.13}$$

However, this approach can be prone to degeneracy issues, if generating the state trajectories in the single-pass, forward-only, manner, see, e.g. [22] for a recent review on various aspects of this topic. To prevent this problem in our case, we resort to PMCMC methods [23] to approximate the marginal density, $f(x(1:K)|y(1:K))$. A PMCMC method repetitively uses previous trajectories to generate new ones in a Markovian way. We then use these trajectories to compute sufficient statistics representing an analytically tractable posterior density of the unknown parameters, $f(\vartheta|x(1:K), y(1:K))$, as described in more details in the rest of this section.

3.1 Parameter learning

Given a prior density over the unknown parameters, $f(\vartheta)$, which is conjugate to a joint density representing the state-space model, $f(y(k), x(k)|x(k-1), \vartheta)$, the posterior density of the estimated parameters,

$$\theta|(X(1:K) = x(1:k), Y(1:K) = y(1:k)) \sim f\left(\vartheta|x(1:k), y(1:k)\right), \tag{C.14}$$

is fully characterized by a set of finite-dimensional sufficient statistics, $S(k)$, that can be updated recursively via a closed-form updating rule, $S(k) \coloneqq \mathcal{S}\big(S(k-1), X(k),\ Q(k), Y(k)\big)$. For the

specific case of this paper, the updating rule, $\mathcal{S}$, is described in Section 3.4. Combining this idea with particle filters—which (as mentioned before) produce the state trajectories in the forward-only manner—was first introduced in [24], and it was later modified in [25] to what is known as particle learning. Particle learning differs from the approach in [24] by using a resample-propegate framework. Nevertheless, the major issue with particle filters is the particle path degeneracy. This approach is characterized by the loss of trajectory diversity due to the resampling, as particles with high weights are duplicated more than particle with low weights. This problem can be especially significant for jump diffusion systems due to the discontinues nature of the jumps. This becomes even more severe for the jumps in the latent states, as it takes more samples to appropriately reflect the distant jumps. This can be a huge issue for learning the parameters, since their estimates are computed via the sufficient statistics which, in turn, depend on the history of the states trajectories. Smoothing techniques, such as PMCMC methods [23] or backward simulation methods [26], successfully tackle the particle path degeneracy problem, and overcome the difficulties with the jumps occurring in the latent states, since these methods target the distribution for the entire trajectory given the corresponding measurements. In this paper, a PMCMC method which relies on the conditional particle filter with ancestor sampling (CPF-AS) [27] is preferred over the forward-filtering backward-simulation methods. This choice has been made since it has been shown in [28] that the CPF-AS within MCMC might offer better exploration of the state space when compared to a forward-filtering backward-simulation smoother.

3.2 The conditional particle filter with ancestor sampling

The conditional particle filter is similar to a regular particle filter. The main difference is that it conditions on a single, pre-specified, particle trajectory, ${}^{\text{in}}x(1:K)$, to generate N new particle trajectories, $\{x^i(1:K), W^i(K)\}_{i=1}^N$, where $W^i(K)$ is the weight of the ith trajectory $x^i(1:K)$. One of these N trajectories is fixed to a pre-specified trajectory, ${}^{\text{in}}x(1:K)$. The ancestor sampling step is introduced in order to increase the mixing of the Markov chain, to enhance the exploration of the the state space, and to avoid particle path degeneracy. This is accomplished by fragmenting the particle trajectory via sampling the ancestors indices, $a^i(k)$, at each time step. After generating the trajectories, we can sample one of them,

$$ {}^{\text{out}}x(1:K) = x^L(1:K), $$

with $\mathbb{P}(L=i) \propto W^i(K)$ and "$\propto$" denoting "proportional to" where the proportionality constant is equal to the normalizing constant. Therefore, one can view the CPF-AS as a Markov transition kernel from ${}^{\text{in}}x(1:K)$ to ${}^{\text{out}}x(1:K)$. In this paper, we propose to modify the parameter learning methods discussed in Section 3.1 with a variant of the CPF-AS which samples the output trajectory ${}^{\text{out}}\Xi(1:K)$, given the input trajectory ${}^{\text{in}}\Xi(1:K)$, where, specifically, we augment the state trajectory in the following way:

$$ \Xi(1:K) := \big\{x(1:K), q(1:K), s(1:K), \vartheta(1:K)\big\}. \tag{C.15} $$

Note that the time index in the parameters, $\vartheta(k)$, coincides with the one in the sufficient statistics, $s(k)$. We summarize the filter in Algorithm 1. Note, too, that the function $\mathcal{W}$, which

Algorithm 1: The conditional particle filter with ancestor sampling and parameter learning

Input: ${}^{\text{in}}\Xi(1:K), Y(1:K)$

Output: ${}^{\text{out}}\Xi(1:K)$

Draw $x^i(1), q^i(1) \sim f\left(x(1), q(1)\right)$ for $i = 1, \ldots, N-1$.

Set $s^i(1) = {}^{\text{in}}s(1)$ and draw $\vartheta^i(1) | \left(S(1) = s^i(1)\right) \sim f\left(\vartheta | s^i(1)\right)$ for $i = 1, \ldots, N-1$.

Set $\Xi^N(1) = {}^{\text{in}}\Xi(1)$.

Compute $W^i(1) = \mathcal{W}\left(\Xi^i(1)\right)$ for $i = 1, \ldots, N$.

For $k = 2, \ldots, K$ **Do**:

Draw $a^i(k)$ with $\mathbb{P}\left(a^i(k) = l\right) \propto W^l(k-1)$ for $i = 1, \ldots, N-1$.

Sample $x^i(k), q^i(k)$ through the model in (C.5) with $x^{a^i(k)}(k-1)$ and $\vartheta^{a^i(k)}(k-1)$ for $i = 1, \ldots, N-1$.

Update sufficient statistics $s^i(k) = \mathcal{S}\left(s^{a^i(k)}(k-1), x^i(k), q^i(k)\right)$ for $i = 1, \ldots, N-1$.

Draw $\vartheta^i(k) | \left(S(k) = s^i(k)\right) \sim f\left(\vartheta | s^i(k)\right)$ for $i = 1, \ldots, N-1$.

Set $\Xi^N(k) = {}^{\text{in}}\Xi(k)$.

Draw ancestor $a^N(k)$ with $\mathbb{P}(a^N(k) = l) \propto W^l(k-1) f\left(x^N(k) | x^l(k-1), \vartheta^l(k-1)\right)$.

Set $\Xi^i(1:k) = \left\{\Xi^{a^i(k)}(1:k-1), \Xi^i(k)\right\}$.

Compute $W^i(k) = \mathcal{W}\left(\Xi^i(k)\right)$ for $i = 1, \ldots, N$

End for

Draw l with $\mathbb{P}(l = i) \propto W^i(K)$ and set ${}^{\text{out}}\Xi(1:K) = \Xi^l(1:K)$.

is used to assign the weights to the particles, is $\mathcal{W}\left(\Xi^i(k)\right) = W^i(k-1)f\left(y(k)|x(k),\vartheta\right)$. The density of the initial particles, $f\left(x(1),q(1)\right)$, is specified in Section 4.1.

In this CPF-AS, we sample the parameters—which is not necessary, since the sufficient statistics are enough to provide their estimates—in order to further enhance the exploration of the parameter space.

3.3 Markov chain Monte Carlo

To sample from a complicated probability density, π, on a space Z, MCMC proposes to instead sample a Markov chain from a transition kernel, $\mathcal{K}$, which leaves π as its unique stationary density. For an arbitrary initial state, ${}^0\zeta \in \mathsf{Z}$, $\pi\left({}^0\zeta\right) > 0$, it has been shown that—by the ergodicity property of the Markov kernel, $\mathcal{K}$—the successive samples ${}^m\zeta \sim \mathcal{K}\left(\,\cdot\,|\,{}^{m-1}\zeta\right)$ will be, for a sufficiently large m, approximate samples from the target density, π, [29]. Moreover, as demonstrated in [23], the CPF-AS is an ergodic kernel with the stationary density being the smoothing density. Therefore, one can construct an MCMC strategy with the CPF-AS to obtain samples from the smoothing density, as shown in Algorithm 2.

Algorithm 2: MCMC smoother

Input: Arbitrary ${}^1\Xi(1:K)$

Output: A sequence of samples ${}^1\Xi(1:K),\ldots,{}^M\Xi(1:K)$

1 **For** $m = 2,\ldots,M$ **Do**

2 Run the CPF-AS (Algorithm 1) with ${}^{m-1}\Xi(1:K) = {}^{\text{in}}\Xi(1:K)$ to obtain ${}^m\Xi(1:K) = {}^{\text{out}}\Xi(1:K)$.

3 **End For**

The samples from the transition phase of the chain are usually a bad approximation of the smoothing distribution, depending on $\mathcal{K}$ and the choice of ${}^1\Xi(1:K)$. Therefore, only the samples after $M/3$ are considered as a rule of thumb.

3.4 The sufficient statistics

Here, we describe the updating rule $\mathcal{S}$ (Section 3.1) in the specific context of the model designed in Section 2.

For the conjugate system with the beta prior density, $\lambda \sim f(\vartheta_1) \coloneqq Beta(\alpha(1),\beta(1))$, and the Bernoulli likelihood density, $J(2)|(\lambda = \vartheta_1) \sim f(j(2)|\vartheta_1)$, we obtain the beta posterior density, $\lambda|(J(2) = j(2)) \sim f\left(\vartheta_1|j(2)\right)$, i.e.

$$f\left(\vartheta_1|j(2)\right) \propto f(j(2)|\vartheta_1)f(\vartheta_1) \tag{C.16}$$

$$\propto \vartheta_1^{j(2)}(1-\vartheta_1)^{1-j(2)}\vartheta_1^{\alpha(1)}(1-\vartheta_1)^{\beta(1)-1} \tag{C.17}$$

$$= \vartheta_1^{j(2)+\alpha(1)}(1-\vartheta_1)^{\beta(1)-j(2)}, \tag{C.18}$$

where $\alpha(2) \coloneqq \alpha(1)+j(2)$ and $\beta(2) \coloneqq \beta(1)+1-j(2)$ are the shaping parameters. Consequently, we obtain a recursive expression for $\alpha(k)$ and $\beta(k)$ as follows:

$$\alpha(k) = \alpha(k-1) + j(k), \tag{C.19a}$$
$$\beta(k) = \beta(k-1) + 1 - j(k). \tag{C.19b}$$

Here, the parameters $\alpha(k)$ and $\beta(k)$ are the sufficient statistics for λ given the trajectory $j(1:k)$.

For the jump size parameters, we assume a normal-inverse-gamma prior density,

$$\mu_z \sim \mathcal{N}(a_z(1), \sigma_z^2/b_z(1)),$$
$$\sigma_z^2 \sim \mathrm{IG}(c_z(1), d_z(1)),$$

and that $Z(2)|(\mu_z = \vartheta_2, \sigma_z^2 = \vartheta_3) \sim f\left(z(2)|\vartheta_2, \vartheta_3\right)$ is normally distributed. With a similar derivation for the recursive update of the sufficient statistics of λ, see, e.g. [30], one obtains the following recursive formulae:

$$a_z(k) = \frac{b_z(k-1), a_z(k-1) + j(k)\log(z(k))}{b_z(k-1) + j(k)}, \tag{C.20a}$$
$$b_z(k) = b_z(k-1) + j(k), \tag{C.20b}$$
$$c_z(k) = c_z(k-1) + \frac{j(k)}{2}, \tag{C.20c}$$
$$d_z(k) = d_z(k-1) + \frac{j(k)b_z(k-1)}{b_z(k-1)+j(k)} \frac{\left(j(k)\log(z(k)) - a_z(k-1)\right)^2}{2}. \tag{C.20d}$$

The parameters $a_z(k)$, $b_z(k)$, $c_z(k)$ and $d_z(k)$ are the sufficient statistics for μ_z and σ_z, given the trajectories $j(1:k)$ and $z(1:k)$. Note that $z(k)$ is used to account only for samples when the jumps occur.

As for the the diffusion parameter σ, the inverse gamma prior, $\sigma^2 \sim \mathrm{IG}\left(c_d(1), \frac{d_d(1)}{T_s}\right)$, is adopted, since $f(x_4(k)|x(k-1), \vartheta_4)$ is the normal density, (C.10). Therefore, the sufficient statistics are updated recursively as follows:

$$c_d(k) = c_d(k-1) + \frac{x_4(k)}{2}, \tag{C.21a}$$
$$d_d(k) = c_d(k-1) + \frac{\left(x_4(k) - \mu_4\right)^2}{2}. \tag{C.21b}$$

Similarly to σ, an inverse gamma prior is chosen for $\sigma_y \sim \mathrm{IG}\left(c_y(1), d_y(1)\right)$, since $f(y(k)|x_4(k), \vartheta_5)$ is, again, the normal density, (C.12). The sufficient statistics are then updated via

$$c_y(k) = c_y(k-1) + \frac{y(k)}{2}, \tag{C.22a}$$
$$d_y(k) = c_y(k-1) + \frac{\left(y(k) - x_4(k)\right)^2}{2}. \tag{C.22b}$$

In summary, the kth sufficient statistics are

$$s(k) = (\alpha(k), \beta(k), a_z(k), b_z(k), c_z(k), d_z(k), c_d(k), d_d(k), c_y(k), d_y(k)) \tag{C.23}$$

and the update rule, $\mathcal{S}$, is given by (C.19)–(C.22).

3.5 Numerical considerations

If most of the particles are far enough from a measurement due to jumps or a small choice of σ_y, then the evaluation of the weights using the observation model will give very small numbers that are usually rounded to zero automatically in many programming languages (e.g. Matlab). This numerical issue has been avoided by calculating the weights and resampling in the log domain, as it was suggested in [31].

4 Results

4.1 Synthetic data

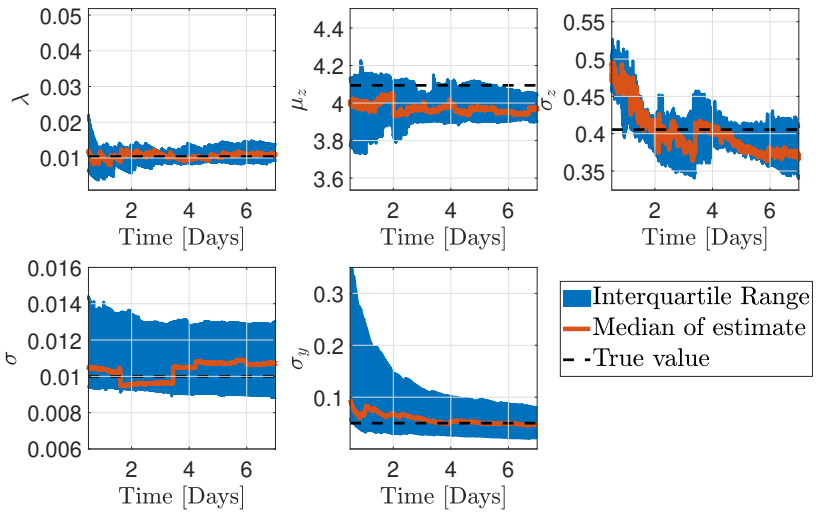

Fig. C.1: The estimated parameters for 8 different simulations. The trajectory of each parameter (from each simulation) is obtained by computing the mean of the last $3M/4$ samples of the Markov chain. The time axis starts from 0.5 days after most of the parameters have nearly converged.

The synthetic data were generated with $\lambda = 0.01$ corresponding to $\lambda_c = 3$ [Days^{-1}], $\mu_z = \log(60)$, $\sigma_z = \log(1.5)$, $\sigma = 0.01$ and $\sigma_y = 0.05$. The sampling time is fixed to $T_s = 5$ [mins]. The initial conditions for the simulation are chosen arbitrary as $x_s(1) = [0, 0, 10.5, 12, 0, 0]^\mathsf{T}$

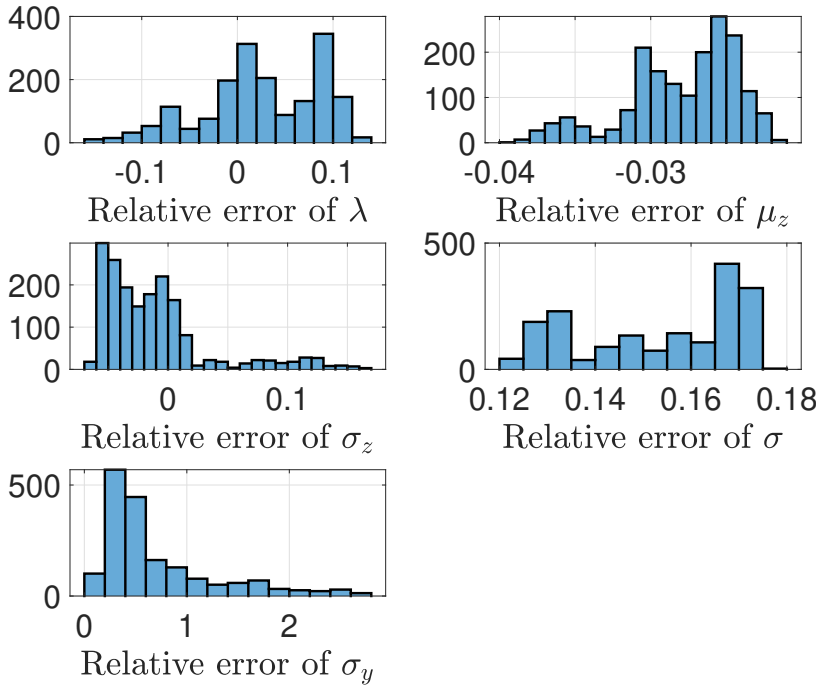

Fig. C.2: The histogram of the relative errors (REs) for the average values of each parameter through time RE($k : K$) computed over the 8 simulations. Here, k is chosen to correspond to the samples starting from 0.5 days.

with x_s being the simulated states. The experiments were carried out for $K = 7$ [Days] and insulin doses administered once per day, starting with a dose of 5 [U] on the first day and increasing it by 5 [U] each day afterwards. The initial distribution for the state particles is taken to be uniform $X(1) \sim \mathcal{U}\left(0.5x_s(1), 1.5x_s(1)\right)$, whereas the initial jumps states, $Q(1)$, are chosen to be zeros. The algorithm is iterated for $M = 5000$ with $N = 20$ particles (it has been shown that the algorithm converges even for just $N = 2$ particles [26]). The initial sufficient statistics, $s(1)$, were set to $\alpha(1) = 0.1,\ \beta(1) = 6,\ a_z(1) = 4,\ b_z(1) = 1,\ c_z(1) = 2,\ d_z(1) = 0.25,\ c_d(1) = 2,\ d_d(1) = 0.005/T_s,\ c_y(1) = 2$, and $d_y(1) = 0.025$. The initial parameters are then drawn from their priors with the initial sufficient statistics and the simulation is done with these parameters and the model in (C.5) and (C.12) to generate the initial trajectory ${}^1\Xi(1 : K)$.

Fig. C.1 shows the trajectory of the estimated parameters with time for eight different simulations while Fig. C.2 shows a histogram for the relative error (RE) computed as

$$\mathrm{RE}(k) = \frac{\frac{1}{N_s}\sum_{n=1}^{N_s}\theta_i^n(k) - \theta_i^r}{\theta_i^r}, \tag{C.24}$$

where N_s is the number of simulations, and θ_i^r is real value of the parameter θ_i. The estimates of the parameters converge. Moreover, the estimates of the jump parameters, λ, μ_z and σ_z, have a narrower interquartile range than the other parameters. The wider interquartile range of the estimates of σ and σ_y may be caused by an improper initialization of their corresponding sufficient statistics. It is also noted that the estimates of μ_z, σ_z and σ are biased. Moreover, the trajectories of the estimated parameters are not smooth, especially for σ_z. Note, too, that the trajectory of σ-estimates experiences abrupt changes when it is close to the true value. These issues may be due to that the probability transition function in (C.8) is nearly degenerate. In other words, it can have zero values. This means the CPF-AS will sometimes fail to perform the ancestor sampling step, as the zero probabilities prevent the mixing of the chain. Solutions to this problem are suggested in [32] and we consider them in more detail in future work. The RE histograms show that, for most of the parameters, a good amount of the samples have the REs close to zero. We also observe the apparent bias in the parameter estimates, especially for σ and μ_z. While the biases are rather small, they can result in either over or under estimation of meals. Considering a larger window of time will help with reducing the biases, since more meal jumps will be present. This will help us to obtain more precise estimation of the meal size parameters. Note, too, that the samples with a relatively large error in σ_y, even though they are few. This can be observed in the wider interquartile range for estimates of σ_y. In general, for all the parameters, samples with larger REs can be explained by the transient phase of the trajectories of the estimated parameters, and the none-smoothness issue.

4.2 Clinical data

In this paper, data from a clinical study conducted in [33] have been made available. The data consist of the CGM and SMBG measurements recorded for periods of 30–80 days for 8 different insulin-naïve patients, initiating insulin treatment with long-acting insulin degludec. Fig. C.3 shows the estimated parameters using the clinical data for one of the patients. The estimated parameters converge. Nevertheless, one should keep in mind the aforementioned biases. In addition, the estimates of λ and σ_r have smaller interquartile range compared to the other parameters. These values were chosen based on [34]. As for the estimated glucose, the results show a good fit to the measurement, except for the cases when there is a negative drop in glucose. This suggests that there is a possibility to add a negative jump model to account for activities that cause the glucose to decrease in short periods of time, such as physical exercise. In addition, we did not fit the drift parameters in this paper. Fitting the drift parameters together along with the stochastic parameters might improve the estimate of glucose.

5 Conclusion and future work

The proposed jump diffusion model for diabetic patients facilitates learning of the behavioural parameters specific for each individual patient, taking into account the amount and frequency of consumed carbohydrates. The models of this type have a great potential to be applied in insulin guidance algorithms and hypoglycemic alert systems. The proposed algorithm has been shown to deliver estimates of such parameters, including the other stochastic parameters, based solely on injected insulin amounts and CGM measurements. The algorithm can be further improved

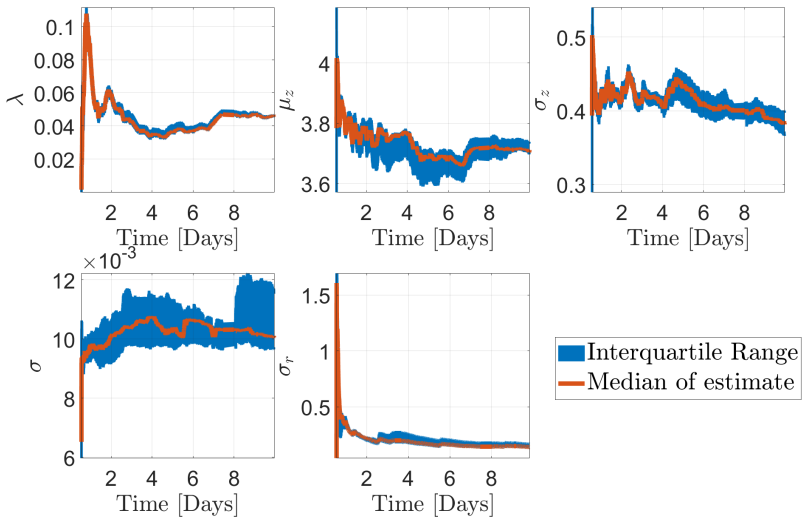

Fig. C.3: The estimated parameters for the clinical data using 10 runs of the algorithm. The trajectory of each estimated parameter (from each simulation) is obtained by computing the mean of the last $3M/4$ samples of the Markov chain.

by estimating the drift parameters or by adopting alternative, particle-based, methods, such as the Liu and West filter [35]. We assume that incorporating the drift parameters will help in achieving a better fit of the model, which will, subsequently, lead to better estimates of the glucose concentrations. Additionally, the disturbances and uncertainty on the glucose were assumed to be the standard Wiener process, which is a rather restrictive assumption.

References

[1] International Diabetes Federation, *IDF Diabetes Atlas*, 9th ed. Brussels, Belgium: International Diabetes Federation, 2019.

[2] L. Berard, M. Bonnemaire, M. Mical, and S. Edelman, "Insights into optimal basal insulin titration in type 2 diabetes: Results of a quantitative survey," *Diabetes, Obesity and Metabolism*, vol. 20, no. 2, pp. 301–308, 2018.

[3] T. B. Aradóttir, D. Boiroux, H. Bengtsson, J. Kildegaard, M. L. Jensen, J. B. Jørgensen, and N. K. Poulsen, "Model predictive control for dose guidance in long acting insulin treatment of type 2 diabetes," *IFAC Journal of Systems and Control*, vol. 9, p. 100067, 2019.

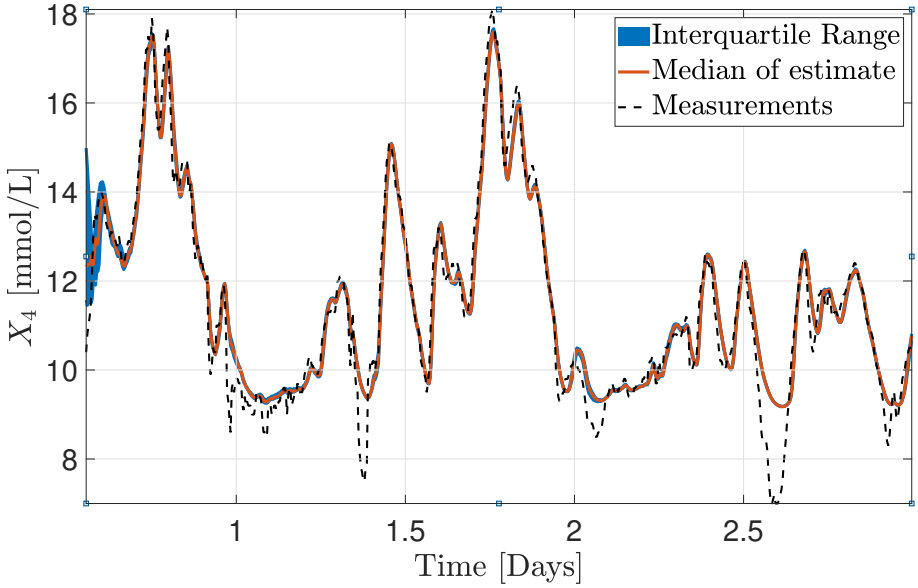

Fig. C.4: The estimated glucose concentrations with the CGM. Each trajectory of the estimated glucose (from each run) is computed by calculating the mean of the last $3M/4$ samples of the Markov chain.

[4] D. Eringis, P. A. Munk, B. K. Andersen, R. S. Suresh, and J.-J. Leth, "LPV based control of glucose concentration in type 2 diabetes," *IFAC-PapersOnLine*, vol. 53, no. 2, pp. 16 386–16 393, 2020.

[5] S. Arnolds, T. Heise, F. Flacke, and J. Sieber, "Common standards of basal insulin titration in T2DM," *Journal of Diabetes Science and Technology*, vol. 7, no. 3, pp. 771–788, 2013.

[6] T. B. Aradóttir, D. Boiroux, H. Bengtsson, and N. K. Poulsen, "Modelling of fasting glucose-insulin dynamics from sparse data," in *2018 40th Annual International Conference of the IEEE Engineering in Medicine and Biology Society (EMBC)*. IEEE, 2018, pp. 2354–2357.

[7] H. G. Clausen, J.-J. Leth, T. Knudsen, and H. Schiøler, "State estimation in type 2 diabetes using the continuous-discrete unscented Kalman filter," *IFAC-PapersOnLine*, vol. 53, no. 2, pp. 16 500–16 505, 2020.

[8] D. Boiroux, M. Hagdrup, Z. Mahmoudi, N. K. Poulsen, H. Madsen, and J. B. Jørgensen, "Model identification using continuous glucose monitoring data for type 1 diabetes," *IFAC-PapersOnLine*, vol. 49, no. 7, pp. 759–764, 2016.

[9] D. Boiroux, Z. Mahmoudi, and J. B. Jørgensen, "Parameter estimation in type 1 diabetes models for model-based control applications," in *2019 American Control Conference (ACC)*, 2019, pp. 4112–4117.

[10] I. Sala-Mira, J.-L. Díez, B. Ricarte, and J. Bondia, "Sliding-mode disturbance observers for an artificial pancreas without meal announcement," *Journal of Process Control*, vol. 78, pp. 68 – 77, 2019.

[11] C. M. Ramkissoon, P. Herrero, J. Bondia, and J. Vehi, "Unannounced meals in the artificial pancreas: Detection using continuous glucose monitoring," *Sensors (Basel, Switzerland)*, vol. 18, no. 3, p. 884, Mar 2018.

[12] J. Xie and Q. Wang, "A variable state dimension approach to meal detection and meal size estimation: In silico evaluation through basal-bolus insulin therapy for type 1 diabetes," *IEEE Transactions on Biomedical Engineering*, vol. 64, no. 6, pp. 1249–1260, 2017.

[13] I. Hajizadeh, M. Rashid, K. Turksoy, S. Samadi, J. Feng, M. Sevil, N. Hobbs, C. Lazaro, Z. Maloney, E. Littlejohn, and A. Cinar, "Incorporating unannounced meals and exercise in adaptive learning of personalized models for multivariable artificial pancreas systems," *Journal of Diabetes Science and Technology*, vol. 12, no. 5, pp. 953–966, 2018.

[14] R. Visentin, C. Cobelli, and C. Dalla Man, "The padova type 2 diabetes simulator from triple-tracer single-meal studies: In silico trials also possible in rare but not-so-rare individuals," *Diabetes technology & therapeutics*, vol. 22, no. 12, pp. 892–903, 2020.

[15] T. Aradóttir, D. Boiroux, H. Bengtsson, J. Kildegaard, B. Orden, and J. Jørgensen, "Model for simulating fasting glucose in type 2 diabetes and the effect of adherence to treatment." in *IFAC-PapersOnLine*, vol. 50, no. 1. Elsevier, 2017, pp. 15 086–15 091.

[16] H. G. Clausen, T. Knudsen, M. Al Ahdab, T. B. Aradottir, S. Schmidt, K. Nrgaard, and J.-J. Leth, "A new stochastic approach for modeling glycemic disturbances in type 2 diabetes," *IEEE Transactions on Biomedical Engineering*, 2021.

[17] R. Hovorka, V. Canonico, L. J. Chassin, U. Haueter, M. Massi-Benedetti, M. O. Federici, T. R. Pieber, H. C. Schaller, L. Schaupp, T. Vering, and M. E. Wilinska, "Nonlinear model predictive control of glucose concentration in subjects with type 1 diabetes," *Physiological Measurement*, vol. 25, no. 4, pp. 905–920, jul 2004.

[18] M. Pollock, A. M. Johansen, and G. O. Roberts, "On the exact and ε-strong simulation of (jump) diffusions," *Bernoulli*, vol. 22, no. 2, pp. 794 – 856, 2016.

[19] E. Platen and N. Bruti-Liberati, *Numerical solution of stochastic differential equations with jumps in finance*. Springer Science & Business Media, 2010, vol. 64.

[20] M. Vettoretti, S. Del Favero, G. Sparacino, and A. Facchinetti, "Modeling the error of factory-calibrated continuous glucose monitoring sensors: Application to dexcom G6 sensor data," in *2019 41st Annual International Conference of the IEEE Engineering in Medicine and Biology Society (EMBC)*. IEEE, 2019, pp. 750–753.

[21] A. Doucet and A. M. Johansen, "A tutorial on particle filtering and smoothing: Fifteen years later," *Handbook of nonlinear filtering*, vol. 12, no. 656-704, p. 3, 2009.

[22] N. Kantas, A. Doucet, S. S. Singh, J. Maciejowski, and N. Chopin, "On particle methods for parameter estimation in state-space models," *Statistical Science*, vol. 30, no. 3, pp. 328–351, Aug. 2015, arXiv: 1412.8695.

[23] C. Andrieu, A. Doucet, and R. Holenstein, "Particle Markov chain Monte Carlo methods," *Journal of the Royal Statistical Society: Series B (Statistical Methodology)*, vol. 72, no. 3,

pp. 269–342, 2010, _eprint: https://rss.onlinelibrary.wiley.com/doi/pdf/10.1111/j.1467-9868.2009.00736.x.

[24] G. Storvik, "Particle filters for state-space models with the presence of unknown static parameters," *IEEE Transactions on Signal Processing*, vol. 50, no. 2, pp. 281–289, 2002.

[25] C. M. Carvalho, M. S. Johannes, H. F. Lopes, and N. G. Polson, "Particle learning and smoothing," *Statistical Science*, vol. 25, no. 1, pp. 88–106, Feb. 2010, publisher: Institute of Mathematical Statistics.

[26] F. Lindsten and T. B. Schön, "Backward simulation methods for Monte Carlo statistical inference," *Foundations and Trends® in Machine Learning*, vol. 6, no. 1, pp. 1–143, Aug. 2013.

[27] F. Lindsten, M. I. Jordan, and T. B. Schön, "Particle Gibbs with ancestor sampling," *The Journal of Machine Learning Research*, vol. 15, no. 1, pp. 2145–2184, Jan. 2014.

[28] A. Svensson, T. B. Schön, and M. Kok, "Nonlinear state space smoothing using the conditional particle filter," *IFAC-PapersOnLine*, vol. 48, no. 28, pp. 975–980, Jan. 2015.

[29] C. Robert and G. Casella, *Monte Carlo statistical methods*. Springer Science & Business Media, 2013.

[30] D. J. Olive, *Statistical Theory and Inference*. Springer International Publishing, 2014.

[31] C. Gentner, S. Zhang, and T. Jost, "Log-PF: Particle Filtering in Logarithm Domain," Mar. 2018.

[32] F. Lindsten, P. Bunch, S. S. Singh, and T. B. Schön, "Particle ancestor sampling for near-degenerate or intractable state transition models," *arXiv:1505.06356*, May 2015.

[33] T. B. Aradóttir, H. Bengtsson, M. L. Jensen, N. K. Poulsen, D. Boiroux, L. L. Jensen, S. Schmidt, and K. Nørgaard, "Feasibility of a new approach to initiate insulin in type 2 diabetes," *Journal of diabetes science and technology*, vol. 15, no. 2, pp. 339–345, 2021.

[34] A. Gray and R. J. Threlkeld, "Nutritional recommendations for individuals with diabetes," 2015.

[35] J. Liu and M. West, "Combined parameter and state estimation in simulation-based filtering," in *Sequential Monte Carlo methods in practice*. Springer, 2001, pp. 197–223.

Paper D

Stochastic Modeling and Inference for Type 2 Diabetes

Mohamad Al Ahdab, Milan Papež, Torben Knudsen, Tinna Björk Aradóttir, Signe Schmidt, Kirsten Nørgaard, and John Leth

The paper has been submitted to be in the
IEEE Transaction on Biomedical Engineering, 2023.

The layout has been revised.

Abstract

Type 2 diabetes (T2D) is a common metabolic disorder that poses threat to human health. Blood glucose (BG) concentrations in T2D subjects can be influenced by various factors, such as stress, physical activity, and meal consumption. Obtaining personalized mathematical models for people with T2D can be beneficial for developing effective T2D management strategies, such as insulin dosing algorithms. However, fitting these models for T2D subjects can be challenging due to the limited data typically available during treatment, consisting of only Continuous Glucose Monitoring (CGM) readings and injected insulin amounts. To address this issue, we propose a stochastic jump diffusion model that incorporates the uncertainties from meal consumption behavior together with other disturbances. Additionally, we provide an inference strategy that enables us to estimate both physiological (e.g., insulin sensitivity) and behavioral (e.g., average number of meals per day) parameters using only CGM data and injected insulin amounts. We validate the proposed stochastic model and inference strategy with synthetic and clinical data, assessing their ability to estimate various parameters of the model and fit CGM data. The results demonstrate that our proposed method, along with the model, manages to estimates parameters with different interquartile range (IQR) values. Moreover, the model, in combination with the method, provide a good fit for CGM data, and demonstrates the ability to obtain estimates of unannounced meal times.

1 Introduction

Diabetes is a chronic disease affecting millions of people worldwide, and its prevalence is increasing at an alarming rate with T2D being the most common type, accounting for 90-95% of diabetic cases [1]. The body of individuals with T2D becomes resistant to the hormone insulin, which is responsible for the regulation of BG levels. Disrupting this mechanism leads to high BG concentrations that can cause complications, such as cardiovascular disease, nerve damage, and kidney damage, over time. In later stages, the production of insulin in the body becomes inefficient too. Insulin treatment is initiated for T2D subjects at later stages, when changes in the lifestyle of the subjects and oral medications are insufficient. It is difficult to calculate a suitable amount of insulin for each individual subject during their treatment, such that their BG concentrations remain within the safe range without risking hypoglycemia (BG levels below 3.9 [mmol/L]) or hyperglycemia (BG levels above 7 [mmol/L]) [2]. Hypoglycemia events are dangerous to humans, since they can cause a range of symptoms, including confusion, dizziness, and even unconsciousness in sever cases. To address these difficulties, various automated solutions have been developed to aid the management of T2D, such as calculating insulin doses, alerting the subjects for a potential case of hypoglycemia, or encouraging T2D individuals to adhere to medications and improve their lifestyle via graphical interfaces. Personalized mathematical models for people with T2D can be used to help with developing the automatic solutions. They can be used for the design of feedback-based insulin dosing strategies [3], hypoglycemia alert systems [4], testing dosing strategies and medications [5], and in graphical interfaces aimed at promoting a healthier lifestyle to T2D subjects [6]. Fitting and personalizing these mathematical models to specific T2D subjects can be a challenging process due to the limited type and number of data T2D subjects usually provide. The available data

for people with T2D during the insulin-based treatment is often limited to the amount of injected insulin and measured glucose concentration, which is typically obtained by Continuous Glucose Monitors (CGMs) devices [7]. CGM devices use a small sensor placed under the skin to continuously measure glucose levels in the interstitial fluid with a few-minute period, providing a real-time view of the glucose levels and trends over time. It is difficult and burdensome for T2D subjects to provide data related to their meal times and amounts accurately, data related to their physical activity, and data related to other factors influencing their BG levels. Therefore, fitting models and estimating physiological (e.g., insulin sensitivity) and behavioral (e.g., average number of meals per day) can be a challenging process with the typical data provided by T2D subjects.

Regarding Type 1 Diabetes (T1D), Several papers handled the parameter estimation with known meal times and sizes [8, 9]. For unannounced meals, [10] used a sliding mode disturbance observer to estimate the states of a deterministic T2D model together with the rate of appearance of BG during the consumption of meals. In the same context, different Kalman filtering techniques were applied to the problem of state estimation in [11, 12]. Regarding T2D, [13] fitted parameters of a T2D model using data obtained from a triple-tracer meal test, including BG, insulin, and C-peptide concentrations. For the techniques utilizing CGM in T2D, [14] showed that it is possible to use the unscented Kalman filter to estimate three physiological parameters with CGM data of a T2D model when the meal intake is known. Additionally, [15] proposed a stochastic model to account for unannounced meals and other disturbance in which only the states were estimated. However, none of the aforementioned papers considers simultaneous state and parameter estimation for T2D in the presence of unannounced meals. Additionally, none of those papers provides a model that can be used to also estimate behavioral parameters in addition to physiological ones. In [16], we proposed to use a simple stochastic jump diffusion model and managed to estimate the states but only the parameters related to stochastic disturbances and unannounced meals. The model and the estimation strategy did not perform well for low BG levels and the possibility of missing samples in the glucose measurement data was not considered.

In this paper, we propose a new jump diffusion model for T2D to better capture the variability in glucose-insulin dynamics of T2D subjects. Jump diffusion models are a type of stochastic models that incorporate random jumps. We use this feature to account for sudden changes in glucose levels. Additionally, we use continuous diffusion to account for gradual changes over time. The proposed jump diffusion model considers the dependence between the meal sizes and does not assume that the disturbances on BG concentrations are uncorrelated, unlike the model in [16]. We use only CGM data and injected insulin to estimate both behavioral and physiological parameters of the model. The main contributions of this paper are summarized as follows.

- We propose a new jump diffusion model with parameters accounting for meal uncertainties, parameters for the uncertainty in the model and other disturbances, and physiological parameters (Section 3). The proposed model and the method extends the results in [15, 16].
- We show how to perform inference on jump diffusion models with sparse data from a Bayesian point of view (Section 4).
- We test the model and the inference strategy on both simulated data and clinical data

(Section 4).

2 Notation

The symbol ":=" is used to denote "defined by". For a random variable X, we write $X \sim \mu$ to denote either that X is distributed according to μ or sampled from μ. We also write $X \sim p_X(x)$ if $p_X(x)$ is the density of the random variable X. For random variables X and Y, we use the notation $p_{Y|X}(Y = y \mid X = x)$ or simply $p_{Y|X}(y \,|\, x)$ to denote the (conditional) density of the conditional distribution of Y given $X = x$. Additionally, for ease of notations, we will drop the subscripts X, $Y \,|\, X$ and write $p(x), p(y \,|\, x)$ in cases when it is clear from the context. Let two successive time instants t_k and t_{k+j} be such that $t_{k+j} - t_k = jT,\ j \in \mathbb{Z}$ with $T \in \mathbb{R}$; then the variables $x(t_k), x(t_{k+j})$ will be denoted as $x(k), x(k+j)$. Moreover, for the sequence of integers $k_1, \ldots, k_N$, we use $\boldsymbol{x}\left(k_1 : k_N\right) \coloneqq \begin{bmatrix} x(k_1) & \ldots & x(k_N) \end{bmatrix}^{\mathrm{T}}$. For integers $k_\ell < k_u$, we use $\boldsymbol{x}\left[k_\ell : k_u\right] \coloneqq \begin{bmatrix} x(k_1) & \ldots & x(k_N) \end{bmatrix}^{\mathrm{T}}$ such that $k_i \in [k_\ell, k_u]$ for all $i \in \{1, \ldots, N\}$. We use $\mathcal{U}[a, b]$, $\mathrm{Exp}(\mu_e)$, $\mathcal{N}\left(\boldsymbol{\mu}_n, \boldsymbol{\Sigma}\right)$, $Ber(p_b)$, $Beta(\alpha, \beta)$, and $G(0, 1)$ for the uniform probability distribution on an interval $[a, b]$, the exponential distribution with the mean μ_e, the normal distribution with the mean $\boldsymbol{\mu}_n$ and the variance $\boldsymbol{\Sigma}$, the Bernolli distribution with the probability p_b, the Beta distribution with the parameters α, β, and the standard Gumbel distribution, respectively. We use $p \propto q$ to denote that p is proportional to q, with the proportionality constant equal to the normalization constant. Given a vector $\boldsymbol{x}$, we use $\mathrm{diag}\left(\boldsymbol{x}\right)$ to denote the diagonal matrix, with its diagonal elements being the elements of $\boldsymbol{x}$.

3 Jump Diffusion Models for T2D subjects

We propose the following general form jump diffusion model for T2D subjects[1]:

$$d\boldsymbol{X} = \boldsymbol{f}\left(\boldsymbol{X}(t), \boldsymbol{u}(t), t\right) dt + \boldsymbol{g}(\boldsymbol{X}(t), t) dW(t) + \boldsymbol{h}(\boldsymbol{X}(t), t) d\mathcal{J}(\boldsymbol{X}(t), t), \tag{D.1}$$

where

- $\boldsymbol{X} \in \mathbb{R}^{n_X}$ is a random state vector, containing variables related to BG concentration, insulin concentration, and others to handle meals and disturbances, see Table D.1.
- $\boldsymbol{u}(t) \in \mathbb{R}^{n_u}_{\geq 0}$ is a vector of inputs, such as long-acting insulin and fast-acting insulin.
- $W(t) \in \mathbb{R}$ is a Wiener process, representing uncertainties resulting from unmodelled inputs and dynamics, such as the effect of physical activity.
- $\mathcal{J}(t) \in \mathbb{R}$ is a compound Poisson process, representing uncertain events that causes sudden changes in BG, such as eating.
- $\boldsymbol{f} : \mathbb{R}^{n_X} \times \mathbb{R}^{n_u} \times \mathbb{R}_{\geq 0} \to \mathbb{R}^{n_X}$ is the drift function, containing injected insulin kinetics, insulin-glucose dynamics, and dynamics related to CGM measurements and disturbances.
- $\boldsymbol{g} : \mathbb{R}^{n_X} \times \mathbb{R}_{\geq 0} \to \mathbb{R}^{n_X}$ is the diffusion vector, relating the Wiener process to the overall dynamics.

[1] The stochastic differential equations in this paper are to be understood in the Ito sense.

- $\boldsymbol{h} : \mathbb{R}^{n_X} \times \mathbb{R}_{\geq 0} \to \mathbb{R}^{n_X}$ is the jump vector, accounting for the effect of uncertain events on BG concentration.

In this paper, we choose a model based on a combination of (and a modification between) the diffusion model in [15] and the jump diffusion model in [16]. Additionally, we consider our inputs to be only the long-acting insulin, $u(t) \in \mathbb{R}_{\geq 0}$[2]. The functions $\boldsymbol{f}$, $\boldsymbol{g}$, and $\boldsymbol{h}$ of our model are as following:

$$\boldsymbol{f}(\boldsymbol{X}(t), u(t), t) = \begin{bmatrix} p_I \left(u(t) - X_1(t)\right) \\ p_I \left(X_1(t) - X_2(t)\right) \\ p_3 \left(X_2(t) + p_7 X_4(t)\right) - p_3 X_3(t) \\ -\left(p_5 + p_4 X_3(t)\right) X_4(t) + p_6 + \frac{p_d X_6(t)}{p_v} + X_7(t) X_4(t) \\ -p_d X_5(t) \\ p_d X_5(t) - p_d X_6(t) \\ -p_8 X_7(t) \\ p_c X_4(t) - p_c X_8(t) \end{bmatrix}, \tag{D.2}$$

$$\boldsymbol{g}\left(\boldsymbol{X}(t), t\right) = \begin{bmatrix} \mathbf{0}_6^{\mathrm{T}} & \sigma & 0 \end{bmatrix}^{\mathrm{T}}, \tag{D.3}$$

$$\boldsymbol{h}(\boldsymbol{X}(t), t) = \begin{bmatrix} \mathbf{0}_4^{\mathrm{T}} & c_u \exp\left(-\alpha_z X_5(t)\right) & \mathbf{0}_3^{\mathrm{T}} \end{bmatrix}^{\mathrm{T}}. \tag{D.4}$$

Table D.1 provides a summary for the different variables and parameters of the model in (D.1).

The random variables X_1 [U/day] and X_2 [U/day] are used to model the infusion process of injected long-acting insulin $u(t)$ [U] with a rate p_I [1/day]. The endogenous insulin secretion is modeled to be proportional to the BG concentration X_4 [mmol/L] with a constant p_7 [U L/mmol/day]. The random variable X_3 [U/day] is the effect of infused insulin X_2, and the endogenously secreted insulin $p_7 X_4$ on the glucose with a rate p_3 [1/day]. The fourth element of (D.2) describes the dynamics of BG concentration where p_5 [1/day] is a rate constant describing the insulin independent lowering effect of glucose, p_4 [1/U] is the subject's sensitivity to insulin for glucose metabolization, and p_6 [mmol/L/day] is a constant approximation for endogenous glucose production. The absorbed glucose is reflected in the dynamics of BG concentration (fourth element of f) with a term $\frac{X_6}{p_v\, p_d}$, where p_v [L] is the glucose distribution volume, and p_d [1/day] is a rate constant. The state X_7 is related to the stochastic uncertainties in the diffusion part with a diffusion term σ, and it effects the dynamics of BG, X_4, at the fourth element of f with the term $X_4 X_7$. In other words, the random variable X_7 is the solution to the Ornstein–Uhlenbeck (OU) model [17]. The variable X_8 is the glucose concentration in the interstitial compartment to account for the fact that CGM devices measure the glucose in the interstitial tissues (IG), which is delayed from the BG concentration. The first-order model with parameter p_c [1/day] is used to address the lag between BG concentration and IG concentration, as done in [18]. For ingested carbohydrates, the random variables X_5 [mmol] and X_6 [mmol] are used to model the ingestion and absorption of glucose as linear, second-order, dynamics with rate constant p_d [1/day]. The constant $c_u = \frac{1000}{M_{\mathrm{wG}}}$ with M_{wG} being the molar weight of glucose is used for unit conversion. The random variable X_5 is driven by the

[2]This choice was made for simplicity and due to the fact that the clinical data we have is for T2D subjects administering long-acting insulin only.

Variable	Description	Units
X_1	First compartment for injected insulin	[U/day]
X_2	Second compartment for injected insulin	[U/day]
X_3	Effect of the endogenous and the exogenous insulin	[U/day]
X_4	BG concentration	[mmol/L]
X_5	First compartment for ingested carbohydrates	[mmol]
X_6	Second compartment for ingested carbohydrates	[mmol]
X_7	Stochastic uncertainties (Solution of the OU equations)	[1/day]
X_8	IG concentration	[mmol/L]

Parameter	Description	Units
p_I	Insulin injection rate	[1/day]
p_7	Glucose sensitivity for secreted insulin	[U L/mmol/day]
p_3	Effect of insulin rate	[1/day]
p_4	Insulin sensitivity for glucose metabolization	[1/U]
p_5	Rate constant for the insulin independent lowering effect of glucose	[1/day]
p_6	Endogenous glucose production	[mmol/L/day]
p_8	Drift constant for the OU process	[1/day]
σ	Diffusion constant for the OU process	-
p_c	Rate for the IG compartment	[1/day]
p_d	Rate constant for the ingested carbohydrates compartments	[1/day]
p_v	Glucose distribution Volume	[L]
M_{wG}	Molar weight of glucose (180.1559 [g/mol])	[g/mol]
λ_c	Average number of meals per day	[1/day]
μ_z	Mean jump sizes for meals	[g]
α_z	Constant for the dependence between meal sizes	[1/day]

Table D.1: Summary for the variables in the random state vector $\boldsymbol{X}$ of the model in (D.2).

compound Poisson process, $\mathcal{J}(t)$ in (D.1), representing the accumulation of meals until the time t, given by

$$\mathcal{J}(t) = \sum_{i=1}^{\mathcal{P}(t)} Z(i), \tag{D.5}$$

where $\mathcal{P}(t)$ is a Poisson process with a constant intensity, λ_c, and $Z(i)$ is the ith mark (or jump size). The jump sizes, $Z(i)$ [g], are assumed independent of $\mathcal{P}(t)$, mutually independent, and identically exponential distributed, i.e.,

$$Z(i) \overset{\text{i.i.d.}}{\sim} \text{Exp}\left(\mu_z\right).$$

The term $\exp\left(-\alpha_z X_5(t)\right)$ is used to introduce the dependence in meal sizes. Modeling the jumps with the exponential distribution was chosen because it has a positive support and can be defined by one parameter, making it a convenient choice for this application.

Remark 3.1. *The use of the OU model for the unmodelled disturbances X_7 is introduced in [15]. The difference here is that we introduce it into the glucose equation with the bi-linear term X_4X_7 instead of a linear term. This modification is done to reduce the fluctuations in BG when it is low, which is more realistic [19]. The jump model is similar to the one in [16]. The difference is the inclusion of the term $\exp\left(-\alpha_z X_5(t)\right)$, with jump sizes distributed according to an exponential distribution.*

Remark 3.2. *Different types and classes of meals can be considered by compounding more Poisson processes. For example, we can use three processes $\mathcal{J}_1, \mathcal{J}_2$, and $\mathcal{J}_3$ (with three different rates λ_{c_1}, and λ_{c_2}, and λ_{c_3}) representing breakfast, lunch, and dinner meals, respectively. In this case, $\boldsymbol{h}(\boldsymbol{X}(t),t) = \left[\boldsymbol{h}_1(\boldsymbol{X}(t),t)\ \boldsymbol{h}_2(\boldsymbol{X}(t),t)\ \boldsymbol{h}_3(\boldsymbol{X}(t),t)\right] \in \mathbb{R}^{n_x\times 3}$. The matrix $\boldsymbol{h}$ can be switching in time to select the appropriate compound Poisson process with $\boldsymbol{h}_i(\boldsymbol{X}(t),t) = \boldsymbol{0}$ if $\operatorname{mod}(t,1) \in \left[t_i^\ell, t_u^u\right]$, with $t_i^\ell < t_i^u \in (0,1],\ i \in \{1,2,3\}$.*

For the CGM measurements, we consider the following model [18]:

$$Y(k) = X_8(k) + X_8(k)\sigma_y E_y(k), \quad k \in \mathbb{Z} \tag{D.6a}$$

$$E_y(k) \sim \mathcal{N}(0,1), \tag{D.6b}$$

$$Y(1) \sim p_{Y(1)|X_8(1)}\left(y(1) \mid x_8(1)\right), \tag{D.6c}$$

$$\tag{D.6d}$$

where, for ease of notations, we write $Y(k)$ and $X_8(k)$ for $Y(kT_s)$ and $X_8(kT_s)$, respectively, and $p_{Y(1)|X_8(1)}\left(y(1) \mid x_8(1)\right)$ is the density of the initial measurement. Here, the constant T_s [min] is a sampling time, and $\sigma_y = 0.42$ in accordance to a Mean Absolute Relative Difference (MARD) of 10% [20] (as done in [18]). Note that more complex models exists for CGM devices, such as the ones presented in [21–23]. However, due to the limited available data we consider, along with the assumption that the CGM data has already been calibrated, we resort to a simplified model (as done in [18]), which is a more detailed model than the one considered in [15] and [16]. For the rest of this paper, we work with a discretized version of (D.1) detailed in (D.2),(D.3), and (D.4). More precisely, the model (D.1) is discretized using the Euler scheme [24, 25], yielding the following discrete approximation:

$$\boldsymbol{X}(k+1) = \boldsymbol{F}\left(\boldsymbol{X}(k), u(k); T_s\right) + \boldsymbol{g}\sqrt{T_s}E(k) + \mu_z \boldsymbol{h}\left(\boldsymbol{X}(k)\right)\bar{Z}(k)J(k), \tag{D.7a}$$

$$\boldsymbol{X}(1) \sim p_{\boldsymbol{X}(1)}\left(x(1)\right), \tag{D.7b}$$

where

$$\boldsymbol{F}\left(\boldsymbol{X}(k), u(k); T_s\right) \coloneqq \boldsymbol{X}(k) + T_s \boldsymbol{f}\left(\boldsymbol{X}(k), u(k)\right),$$

$$E(k) \overset{\text{i.i.d.}}{\sim} \mathcal{N}(0,1), J(k) \overset{\text{i.i.d.}}{\sim} Ber(\lambda), \bar{Z}(k) \overset{\text{i.i.d.}}{\sim} \operatorname{Exp}(\mu_z),$$

with $\lambda = 1 - \exp(-\lambda_c T_s)$ being the probability of having at least one jump within the sample time period T_s, and $p_{\boldsymbol{X}(1)}\left(\boldsymbol{X}(1)\right)$ representing the uncertainty in our knowledge for the initial conditions. For the rest of the paper, we will deal with the case where we have missing measurements, which is more realistic since CGM readings are not always consistent and the

devices need calibrations and changes from time to time. We will denote the vector of available CGM readings up until time K by $\boldsymbol{y}[1\!:\!K] := \left[y(k_1), \ldots, y(k_n)\right]^{\mathrm{T}} \in \mathbb{R}^{N_y}$ where $k_1 \geq 1$ and $k_n \leq K$[3].

4 Inference Strategy

This section contains detailed technical information for the algorithms used for inference in this paper. It can be skipped on a first reading.

Estimating the parameters and the states of the model in (D.7) or (D.8) is a challenging process due to the nonlinear and partially non-Gaussian nature of the models. Additionally, the impact of the jump noise $Z(k)J(k)$ on the measured state $X_8(k)$ can only be observed with later measurements. Therefore, state filtering approaches (targeting $p\left(\boldsymbol{x}(k) \,|\, \boldsymbol{y}[1\!:\!k], \boldsymbol{\theta}\right)$) are inefficient, as they rely on *previous* and *current* measurements to estimate the current state. To address these issues, we aim at obtaining samples from the joint posterior density $p\left(\boldsymbol{x}(1\!:\!K), \boldsymbol{\theta} \,|\, \boldsymbol{y}[1\!:\!K]\right)$ given that we have a prior density for the parameters we want to estimate $p_{\boldsymbol{\Theta}}(\boldsymbol{\theta})$. To obtain the samples, we adopt a Markov Chain Monte Carlo (MCMC) approach. MCMC methods are a class of algorithms used for sampling from probability distributions which are difficult or impossible to evaluate in a closed-form. They involve constructing an ergodic Markov chain which has a target distribution as its stationary distribution. After the chain passes its transition (burn-in) phase and thus reaches its stationary regime, the samples of this chain are approximately i.i.d. and can be used to estimate quantities of interests [26].

Targeting $p\left(\boldsymbol{x}(1\!:\!K), \boldsymbol{\theta} \,|\, \boldsymbol{y}[1\!:\!K]\right)$ takes into account all the available measurements to estimate the states and the parameters, which is suitable for the delayed effect of the jump noises.

However, it is important to note that the state-space model in (D.7), with the measurement model in (D.6), is degenerate, i.e., the process noise does not enter (D.7) for all of the states (only on X_7 and X_5). This fact makes the transition density function, $p\left(\boldsymbol{X}(k+1) \mid \boldsymbol{X}(k)\right)$ degenerate. Therefore, it is inefficient to use with strategies targeting $p\left(\boldsymbol{x}(1\!:\!K), \boldsymbol{\theta} \,|\, \boldsymbol{y}[1\!:\!K]\right)$ that relies on backward simulation or the ancestor sampling [27, 28]. To address this and to have a non-degenerate transition density as suggested in [27, 28], it is possible to transfer the model in (D.7) and (D.6) to the innovation form.

In Section 4.1, the innovation form of the model will be described. Afterwards, sections 4.2, 4.3 and 4.4 describes the inference strategy in details for the transformed model.

[3]For measurements $y(t_1), \ldots, y(t_N)$, we choose $y(k_i T_s) \approx y(t_i)$ for $i \in \{1, \ldots, N\}$ with $k_i = \operatorname{argmin}_{k \in \{1,2,\ldots,K\}} |t_i - kT_s|$.

4.1 Innovation Form

To represent the model in (D.7) and (D.6) in the innovation form, we let $\boldsymbol{Q}(k) \coloneqq \begin{bmatrix} J(k) & \bar{Z}(k) & E(k) \end{bmatrix}^{\mathsf{T}}$ to denote the driving (innovation) noise and rewrite (D.7) and (D.6) as

$$J(k) \overset{\text{i.i.d.}}{\sim} Ber(\lambda), \bar{Z}(k) \overset{\text{i.i.d.}}{\sim} \operatorname{Exp}(1), E(k) \overset{\text{i.i.d.}}{\sim} \mathcal{N}(0,1), \tag{D.8a}$$

$$Y(k) = \big(1 + \sigma_y E_y(k)\big)\, r_{\boldsymbol{\theta}}\big(\boldsymbol{Q}(1\!:\!k-1), \boldsymbol{X}(1)\big), \tag{D.8b}$$

$$E_y(k) \overset{\text{i.i.d.}}{\sim} \mathcal{N}(0,1), \tag{D.8c}$$

where $r_{\boldsymbol{\theta}}\left(\boldsymbol{Q}(1\!:\!k), \boldsymbol{X}(1)\right) \coloneqq X_8(k{+}1)$ is defined through the model (D.7) for a specific choice of model parameters $\boldsymbol{\theta}$. The reason for defining $r_{\boldsymbol{\theta}}\left(\boldsymbol{Q}(1\!:\!k), \boldsymbol{X}(1)\right)$, instead of just using $X_8(k{+}1)$ is to emphasize the dependence on the innovation noise $\boldsymbol{Q}$. Observe that the model (D.8) is non-Markovian, since the output $Y(k)$ depends on the all the previous innovation variables $\boldsymbol{Q}(1\!:\!k-1)$. This reformulation will be used in Section 4.3. Note that for a given $\boldsymbol{\theta}$, the density of $\boldsymbol{Q}$ is

$$p(\boldsymbol{q}\,|\,\boldsymbol{\theta}) = \varphi_b(j;\lambda)\varphi_e(\bar{z})\varphi_n(e;0,1), \tag{D.9}$$

where $\varphi_b(\cdot;\lambda), \varphi_e(\cdot)$, and $\varphi(\cdot;0,1)$ are the probability density functions for the Bernoulli distribution with probability λ, the exponential distribution with mean 1, and the normal distribution with mean 0 and variance 1, respectively. Note that for $k \geq 1$, we have

$$p\left(y(k+1)\,|\,\boldsymbol{q}(1\!:\!k), \boldsymbol{x}(1), \boldsymbol{\theta}\right) = \varphi_n\left(y(k+1); r_{\boldsymbol{\theta}}\left(\boldsymbol{q}(1\!:\!k), \boldsymbol{x}(1)\right), \sigma_y^2 r_{\boldsymbol{\theta}}^2\left(\boldsymbol{q}(1\!:\!k), \boldsymbol{x}(1)\right)\right). \tag{D.10}$$

4.2 Gibbs Sampling

We will adopt a Gibbs sampling approach, a type of MCMC strategies, to obtain samples from the joint distribution $p\left(\boldsymbol{q}(1\!:\!K), \boldsymbol{\theta}\,|\,\boldsymbol{y}[1\!:\!K]\right)$ by altering between the sampling from $p\left(\boldsymbol{q}(1\!:\!K)\,|\,\boldsymbol{\theta}, \boldsymbol{y}[1\!:\!K]\right)$ and $p\left(\boldsymbol{\theta}\,|\,\boldsymbol{q}(1\!:\!K), \boldsymbol{y}[1\!:\!K]\right)$. Algorithm 3 summarizes the Gibbs sampling method in which the procedure for obtaining approximate samples from $p\left(\boldsymbol{q}(1\!:\!K)\,|\,\boldsymbol{\theta}, \boldsymbol{y}[1\!:\!K]\right)$ is described in Section 4.3, and the procedure for obtaining samples from $p\left(\boldsymbol{\theta}\,|\,\boldsymbol{q}(1\!:\!K), \boldsymbol{y}[1\!:\!K]\right)$ is described in Section 4.4.

4.3 Sampling Trajectories

We use a Particle MCMC (PMCMC) [29] method to sample from the distribution $p\left(\boldsymbol{q}(1\!:\!K)\,|\,\boldsymbol{\theta}, \boldsymbol{y}[1\!:\!K]\right)$. PMCMC methods use Sequential Monte Carol (SMC) [30] strategies to construct efficient, high-dimensional, ergodic Markov kernels. Particle Gibbs (PG) [29], is a PMCMC method in which the Markov kernel is constructed by the conditional particle filter [31]. In the conditional particle filter, one of the particle trajectories is fixed to a reference trajectory and an output trajectory is sampled according to the importance weights of this filter. However, if the underlying filter suffers from path degeneracy (loss of the diversity in the sampled trajectories (particle paths) due to the resampling), then the mixing of the PG as

Algorithm 3: Gibbs Sampling for Inference

Input: Arbitrary ${}^{0}\boldsymbol{q}(1{:}K)$, a prior density for the parameters $p_{\boldsymbol{\Theta}}(\boldsymbol{\theta})$, and $\boldsymbol{y}[1{:}K]$.

Output: Sequences ${}^{1}\boldsymbol{q}(1{:}K), \ldots, {}^{M}\boldsymbol{q}(1{:}K)$ and ${}^{1}\boldsymbol{\theta}, \ldots, {}^{M}\boldsymbol{\theta}$.

for $m = 0$, **do**

  ${}^{0}\boldsymbol{\theta} \sim p_{\boldsymbol{\Theta}}(\boldsymbol{\theta})$.

for $m = 1$ **to** M, **do**

  Generate ${}^{m}\boldsymbol{q}(1{:}K)$ using Algorithm 4 with ${}^{m-1}\boldsymbol{q}(1{:}K)$,${}^{m-1}\boldsymbol{\theta}$, and $\boldsymbol{y}[1{:}K]$ (sample from $p\left(\boldsymbol{q}(1{:}K)\,|\,{}^{m-1}\boldsymbol{\theta}, \boldsymbol{y}[1{:}K]\right)$).

  Generate ${}^{m}\boldsymbol{\theta}$ with ${}^{m}\boldsymbol{q}(1{:}K)$, and $\boldsymbol{y}[1{:}K]$ according to Section 4.4 (sample from $p\left(\boldsymbol{\theta}\,|\,{}^{m}\boldsymbol{q}(1{:}K), \boldsymbol{y}[1{:}K]\right)$).

a Markov kernel will be poor [27, 29]. To deal with this problem, PG with Ancestor Sampling (PGAS) was introduced in [27]. The ancestor sampling fragments the fixed particle trajectory via the sampling of new ancestor indices at different time steps. Nevertheless, if we consider to apply the ancestor sampling step to the model (D.7), in which it has a degenerate transition density, then the ancestor sampling step will be inefficient [27, 28]. Therefore, the authors in [27, 28] proposed to represent degenerate state-space models in terms of their innovation noise in order to obtain a non-Markovian model, such as the one we have in (D.8). Hence, we rely on the innovation representation in (D.8) instead of (D.7).

To obtain samples from $p\left(\boldsymbol{q}(1{:}K)\,|\,\boldsymbol{\theta}, \boldsymbol{y}[1{:}K]\right)$, we propose a modified version of the PGAS for the non-Markovian model in (D.8). Our version computes the particle weights, performs resampling, and samples ancestor indices only when the measurements are available. Furthermore, the method tackles the issue of the particles being too distant from the measurements, resulting in negligible weight values which many programming languages (e.g., Matlab) set to zero. This issue is particularly prominent in our case due to the jump noise $Z(K)J(k)$, which can make the distance between the particles and the measurement bigger. To overcome this challenge, we calculate the weights via the Gumble-Max trick, see Appendix A. This allows us to sample efficiently from the unnormalized logarithmic weights. In Algorithm 4, $\boldsymbol{w}(k)$ is the vector of importance weights at time step k. The truncation parameter $\tilde{L}$ reflects the assumption that the influence of the past innovation noise on the present measurements (D.8) decays with time. The value of $\tilde{L}$ depends on the rate at which this influence decreases and it is determined via trial and error.

Algorithm 4: PGAS with sparse data

parameter: Number of particles N, and truncation parameter $\tilde{L}$.
Input: ${}^{\text{in}}\boldsymbol{q}(1{:}K)$,$\boldsymbol{y}[1{:}K]$, and $\boldsymbol{\theta}$.
Output: ${}^{\text{out}}\boldsymbol{q}(1{:}K)$

Draw $\boldsymbol{q}^i(1) \sim p_{\boldsymbol{Q}|\boldsymbol{\Theta}}\left(\boldsymbol{q}\,|\,\boldsymbol{\theta}\right)$ for $i = 1, \ldots, N-1$.
Draw $\boldsymbol{x}(1) \sim p_{\boldsymbol{X}(1)}(\boldsymbol{x})$.
Set $\boldsymbol{q}^N(1) = {}^{\text{in}}\boldsymbol{q}(1)$.
Compute $\boldsymbol{w}^i(1) = p_{\boldsymbol{Q}|\boldsymbol{\Theta}}(\boldsymbol{q}^i(1)\,|\,\boldsymbol{\theta})$ for $i = 1, \ldots, N$.
for $k = 2$ **to** K, **do**
  if $y(k)$ *is available* **then**
    Draw a^i using (D.12) with $\ln_e \boldsymbol{w}(k)$ and set $\bar{\boldsymbol{q}}^i(1{:}k-1) = \boldsymbol{q}^{a^i}(1{:}k-1)$ for $i = 1, \ldots, N-1$.
    $L = \min\left(\tilde{L}, K-k-1\right)$.
    if $y(k), \ldots, y(k+L-1)$ *are available* **then**
      Set $\tilde{\boldsymbol{q}}^i = \left[\bar{\boldsymbol{q}}^i\,(1{:}k-1)\;\; {}^{in}\boldsymbol{q}\,(k{:}k+L-1)\right]$ for $i = 1, \ldots, N-1$.
      Compute $\ln w_a^i = \ln w^i(k-1) + \sum_{i=1}^{L} \ln p(y(k+i-1)\,|\,\tilde{\boldsymbol{q}}^i\,(1{:}k-2+i)\,, \boldsymbol{x}(1), \boldsymbol{\theta})$ for $i = 1, \ldots, N$.
      Sample an ancestor b using (D.12) with $\ln_e \boldsymbol{w}_a$.
    else
      Set $b = N$.
    Set $\boldsymbol{q}^N(1{:}k) = \left[\boldsymbol{q}^b(1{:}k-1)\;\; {}^{in}\boldsymbol{q}(k)\right]$.
    Sample $\boldsymbol{q}^i(k) \sim p_{\boldsymbol{Q}|\boldsymbol{\Theta}}\left(\boldsymbol{q}\,|\,\boldsymbol{\theta}\right)$ for $i \in \{1, \ldots, N-1\}$.
    Set $\boldsymbol{q}^i(1{:}k) = \left[\bar{\boldsymbol{q}}^i(1{:}k-1)\;\boldsymbol{q}^i(k)\right]$, for $i \in \{1, \ldots, N-1\}$.
    Compute weights $\ln w^i(k) = \ln p\left(y(k)\,|\,\boldsymbol{q}^i(1{:}k-1), \boldsymbol{x}(1), \boldsymbol{\theta}\right)$, for $i \in \{1, \ldots, N\}$.
  else
    Sample $\boldsymbol{q}^i(k) \sim p_{\boldsymbol{Q}|\boldsymbol{\theta}}\left(\boldsymbol{q}\,|\,\boldsymbol{\theta}\right)$ and set $\boldsymbol{q}^i(1{:}k) = \left[\boldsymbol{q}^i(1{:}k-1)\;\boldsymbol{q}^i(k)\right]$ for $i \in \{1, \ldots, N-1\}$ and $\boldsymbol{q}^N(1{:}k) = \left[\boldsymbol{q}^N(1{:}k-1)\;\; {}^{in}\boldsymbol{q}(k)\right]$.
    Compute weights $\ln w^i(k) = \ln p_{\boldsymbol{Q}|\boldsymbol{\Theta}}(\boldsymbol{q}^i(k)\,|\,\boldsymbol{\theta})$, for $i \in \{1, \ldots, N\}$.
Draw l using (D.12) with $\ln_e \boldsymbol{w}(K)$ and set ${}^{\text{out}}\boldsymbol{q}(1{:}K) = \boldsymbol{q}^l(1{:}K)$.

4.4 Sampling Parameters

For the model in (D.8), if the jump probability λ is among the parameters to be estimated, then we consider $[\lambda, \tilde{\boldsymbol{\theta}}]^{\mathrm{T}} \coloneqq \boldsymbol{\theta}$ and $p_{\boldsymbol{\Theta}}(\boldsymbol{\theta}) \coloneqq p_{\Lambda}(\lambda) p_{\tilde{\boldsymbol{\Theta}}}(\tilde{\boldsymbol{\theta}})$.

If the prior distribution $p_\Lambda(\lambda)$ is the Beta distribution $Beta\,(\alpha, \beta)$ with the likelihood being $p(j(1:K) \mid \lambda) = \prod_{k=1}^{K} \varphi_b(j(k); \lambda)$, then the posterior $p(\lambda \mid \boldsymbol{q}(1:K)) = p(\lambda \mid j(1:K))$ has the same functional form $Beta\left(\alpha + \sum_{i=1}^{K} j(i), \beta + K - \sum_{i=1}^{K} j(i)\right)$ [32].

As for the rest of the parameters $\tilde{\boldsymbol{\theta}}$, given the prior $p_{\tilde{\boldsymbol{\Theta}}}\left(\tilde{\boldsymbol{\theta}}\right)$, and the likelihood

$$\mathcal{L}\left(\boldsymbol{q}(1{:}K), \boldsymbol{y}\,[1{:}K]\,, \boldsymbol{x}(1)\right) \coloneqq \prod_{i=1}^{N_y-1} p\left(y(i+1) \,|\, \boldsymbol{q}\,(1{:}i)\,, \boldsymbol{x}(1), \tilde{\boldsymbol{\theta}}\right) p\left(y(1) \,|\, x_8(1)\right),$$

it is possible to write the posterior $p\left(\tilde{\boldsymbol{\theta}} \,|\, \boldsymbol{q}(1{:}K), \boldsymbol{y}\,[1{:}K]\right)$ up to a proportionality constant

$$p\left(\tilde{\boldsymbol{\theta}} \,|\, \boldsymbol{q}(1{:}K), \boldsymbol{y}\,[1{:}K]\right) \propto \mathcal{L}\left(\boldsymbol{q}(1{:}K), \boldsymbol{y}\,[1{:}K]\,, \boldsymbol{x}(1)\right) p_{\tilde{\boldsymbol{\Theta}}}\left(\tilde{\boldsymbol{\theta}}\right). \tag{D.11}$$

We use the Metropolis Hasting (MH) MCMC strategy [33] to sample from the posterior in (D.11). We run it for M_{MH} iterations and take the last iteration as an approximate sample from the posterior (D.11). The proposal density of the MH algorithm is chosen to be a random walk driven by a Gaussian white noise $\mathcal{N}\left(\mathbf{0}, \mathrm{diag}^2\left(\boldsymbol{\sigma}_{MH}\right)\right)$ for all the parameters $\tilde{\boldsymbol{\theta}}$.

4.5 Hyper-Parameters for the Inference Strategy

In this subsection, we list and briefly discuss the hyper-parameters for the strategy. For the number of particles N in the PGAS Algorithm 4, we choose a low number $N = 10$ since the PGAS algorithm in [34] was shown to converge for $N \geq 1$. Additionally, it was shown that the PGAS algorithm has a good performance for a low number of particles, with minor improvement on the performance when the number of particles is significantly increased [34]. After some tuning, we found that $N = 10$ gave us a sufficiently good performance. For the truncation parameter, we choose $\tilde{L} = 10$. The value was found after some tuning and observing that increasing $\tilde{L}$ further does not yield any significant improvement on the results. We select the uniform prior for the parameters $\tilde{\boldsymbol{\Theta}}$ and the Beta distribution prior for Λ. For the number of MH iterations, we choose $M_{MH} = 800$. The vector $\boldsymbol{\sigma}_{MH}$ of the driving Gaussian white noise is set to $\boldsymbol{\sigma}_{MH} = 0.01\,{}^0\tilde{\boldsymbol{\theta}}$ with ${}^0\tilde{\boldsymbol{\theta}} \sim p_{\tilde{\boldsymbol{\Theta}}}\left(\tilde{\boldsymbol{\theta}}\right)$. Finally, the value of the number of iterations in the Gibbs sampling strategy Algorithm 3 is $M = 10000$. To ensure that the results reported in this paper are representative of the desired stationary distribution of the Markov kernel Algorithm 4, we perform burn-in for $3M/4$ iterations, i.e., we discard the first three quarters.

Recall that the purpose of burn-in is to discard an initial portion of the generated samples in order to allow the Markov chain to converge to its stationary distribution. This means that we do not consider these initial samples when analyzing the results. Instead, we focus solely on the last quarter of the samples, which are expected to be more representative of the desired stationary distribution. This approach help us to ensure that the reported results are based on a reliable sample representation of the desired target distribution.

5 Results

In this section, we analyze the proposed jump diffusion model and the inference strategy based on simulated data in Section 5.1 and clinical data in Section 5.2. The results with the simulated

data evaluate the performance of the inference strategy in estimating the parameters of (D.7). The results with the clinical data aim at validate the inference method and the model in fitting and predicting CGM measurements from real T2D subjects.

5.1 Simulated data

We simulate CGM data from a T2D subject using the model in (D.7) with the parameters specified in Table D.2. Note that the value of $\lambda = 0.01$ in Table D.2 gives $\lambda_c = \frac{\ln(1-\lambda)}{T_s} = 3$ [meals/day]. with $T_s = 5$ [min]. The selection of the parameters p_4, p_7 and p_I to be estimated from the drift part in (D.2) is based on the sensitivity analysis carried out in [15]. The estimation of the diffusion constant σ in (D.3) was not successful (the histogram of the posterior samples is close to a uniform distribution). The value of σ was determined through an iterative process using clinical data, by testing various values ranging from 1 to the value chosen in [15], which is 300. We found that a value of $\sigma = 30$ resulted in the lowest average Mean Square Error (MSE) when the model is fitted to different CGM data for 8 different T2D subjects. Using the parameters in Table D.2, and with an initial condition for the states of $\boldsymbol{x} = [0, 0, 10.5, 12, 0, 0, 0, 12]^{\mathrm{T}}$ which matches the one used in [15, 16], we simulate the model (D.7) for $T = 10$ [day]. During the simulation, we assume that the subject is administering a long-acting insulin dose starting at 5 [U] on the first day and gradually increasing it by the same amount each day, until it reaches 20 [U] by the last day. Additionally, we assume that the CGM measurements will be missing for three arbitrary time intervals of the simulation. These intervals are $[3.3, 3.5]$ [day] (corresponding to 290 minutes), $[5, 5.035]$ [day] (corresponding to 15 minutes), and $[9.9306, 9.9583]$ [day] (corresponding to 40 minutes). For the inference strategy, we choose the prior $p_\Lambda(\lambda)$ to be the Beta distribution with the parameters $\alpha = 0.5$ and $\beta = 0.45$. As for the prior of the remaining parameters $p_{\tilde{\Theta}}(\tilde{\boldsymbol{\theta}})$, we assume a uniform prior of $\mathcal{U}\left(0.5\tilde{\boldsymbol{\theta}}_s, 1.5\tilde{\boldsymbol{\theta}}_s\right)$, where $\tilde{\boldsymbol{\theta}}_s$ is the value of the parameters from Table D.2 used for generating the simulated data. Fig. D.1 shows the histogram of the samples from the posterior of the parameters. We can see that the median of the relative error for the parameters' samples is relatively low. However, we see that the histograms for μ_z, α_z and p_8 are more disperse than the other histograms with a higher IQR for the relative error. In other words, accuracy for the estimated parameters μ_z, α_z and p_8 is lower when compared to the other estimated parameters. Increasing the amount of measurements can possibly help with obtaining less disperse histograms for the parameters.

Table D.2: Table of Parameters for Model (D.1). Parameters in Blue are to be estimated. The values of these parameters are selected according to [15].

λ	0.01	μ_z	70	α_z	0.05
σ	30	σ_y	0.42	p_I	2
p_3	15.8	p_4	1.8	p_5	3.31
p_6	300	p_7	1.68	p_8	10
p_d	1/0.03	p_v	1/22	p_c	$7/(24 \times 60)$

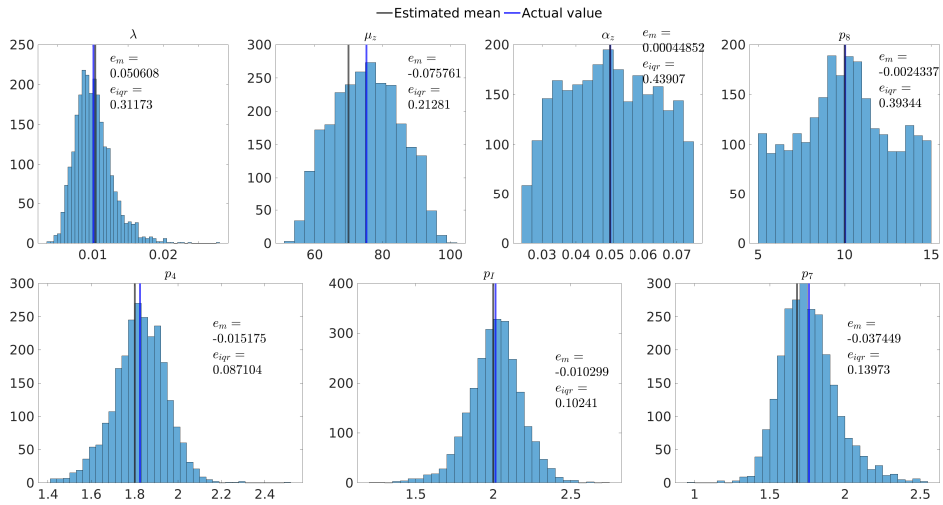

Fig. D.1: Histogram of the parameters sample from the posterior using the simulated data and Algorithm 3. Here, e_m is the median of the relative error and e_{iqr} is the interquartile range (IQR) of the relative error.

5.2 Clinical data

The data from a clinical study conducted in [35] have been made available. The data consist of the CGM and SMBG measurements recorded for periods of 30–80 days by 8 different insulin-naïve patients, initiating insulin treatment with long-acting insulin Degludec. The recorded CGM sequences range from 30 to 80 days. One of the subjects has provided reliable meal announcement times for the first three days of treatment. We apply our inference strategy to the model in (D.7) for all of the 8 subjects. Fig. D.2 presents the CGM data with the estimated X_8 (IG concentration) for one of the subjects. Fig. D.3 shows the state X_5 (first meal compartment) for the subject who provided reliable meal announcement times. Fig. D.4 demonstrate the prediction for the CGM data for all of the 8 subjects. Finally, Table D.3 shows some statistical results for all the 8 subjects together with Table D.4 showing the estimated parameters for each subject.

From Table D.3 and Fig. D.2, we observe that the proposed method achieves good fits with the CGM data from each subject. This demonstrates the effectiveness of the method in capturing the glucose dynamics. Notably, unlike our previous work in [16], the proposed model with the method shows improved capability in handling drops in the glucose concentration. Fig. D.2 provides insights into the behavior of the method during periods when CGM readings are missing. The uncertainty in the predictions substantially increases during these periods, which is evident from the larger $10_{th} - 90_{th}$ range. Additionally, we observe that the estimated glucose during the missing CGM readings period has two peaks. Indicating that the method assumes the subject to have two meals during the period of missing CGM measurements. Noticeably,

these meals align with the peaks observed in the other days when the CGM readings are available. This suggests that the method incorporates a sensible strategy for handling missing data and inferring meal events.

Analyzing the meal detection results depicted in Fig. D.3, we can see that the estimated trend of X_5 closely resembles the reported times of meals. Furthermore, there are relatively large peaks in the proximity to the reported meal announcements by the subject. However, other meals are also estimated between the reported meals. These additional meals could be due to model uncertainties, such as the effect of different types of ingested carbohydrates, or imperfections in the subject's meal time recording process, such as unreported small snacks.

As for the estimated parameters presented in Table D.4, we observe that the average number of meals per day λ_c and the mean size of meals μ_z are consistently close across all subjects. These values align with the recommended meal consumption statistics for individuals with T2D [36]. Furthermore, we note that the parameter α_z, which indicates the degree of association between subsequent meals, exhibits variability among the subjects. This suggests individual differences in meal patterns and highlights the personalized nature of the proposed model. In addition, we find that a lower estimate of the insulin sensitivity parameter p_4 corresponds to a lower estimate of the insulin secretion parameter p_7, which aligns with the pathophysiology of T2D. This observation reinforces the physiological validity of the estimated parameters. Regarding the insulin injection parameter p_I in Table D.3, we find that they are consistent with the expected value for the type of injected insulin (Degludec) for each subject [15]. This observation further validates the accuracy of the parameter estimation process. Lastly, we notice from Table D.3 that the accuracy of the fitted model for the prediction diminishes within 40 minutes which is consistent with the prediction results reported in [37] for different CGM prediction approaches for T1D subjects. This outcome is not surprising, as the model faces inherent limitations in accounting for all the uncertainties associated with a human subject over periods longer than 40 minutes. However, it is worth highlighting that the fitted model still exhibits the capability to predict potential meals within minutes from the point of prediction, as can be seen in Fig. D.4 for some of the subjects. Furthermore, it is worth noting that in Fig. D.4, the majority of the CGM readings fall within the $10_{th} - 90_{th}$ range for a duration exceeding 200 minutes of prediction.

Table D.3: Average Root Mean Square Error (RMSE) in [mmol/L], median of error in [mmol/L], and the IQR of error in [mmol/L] for fitting model (D.7) with Algorithm 3 with clinical data of 8 subjects, and the prediction of the fitted model for different time horizons.

	Fitting	Pred.10 [min]	Pred.30 [min]	Pred.40 [min]
RMSE	0.114	0.412	1.058	1.418
Median	0.1	0.49	0.89	1.04
IQR	0.03	0.23	1.52	2

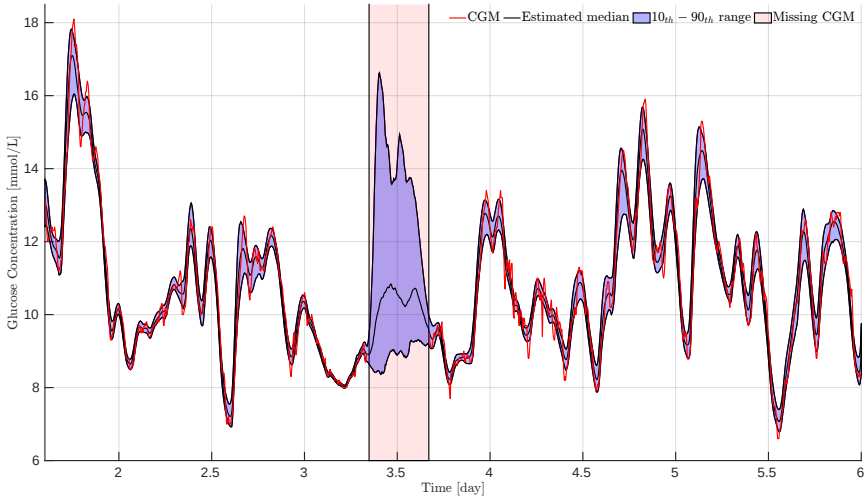

Fig. D.2: The median and the $10_{th} - 90_{th}$ range for the glucose concentration state X_8 with the CGM readings.

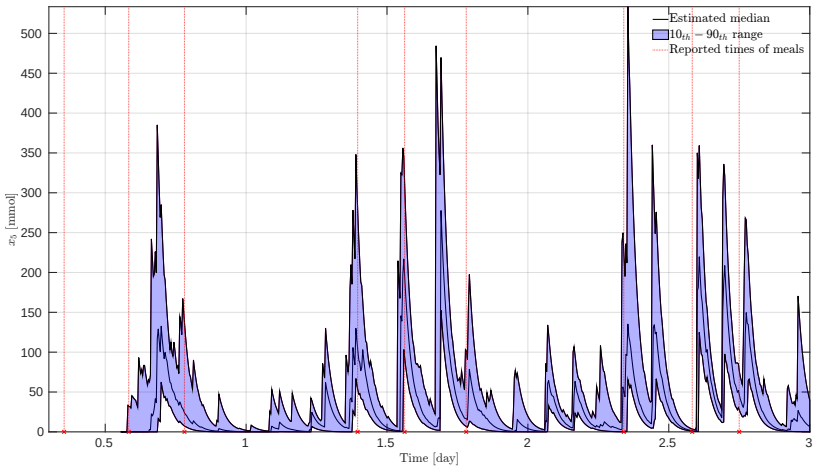

Fig. D.3: Meal times with estimated median and $10_{th} - 90_{th}$ range of the state X_5.

6 Conclusion and future work

The proposed jump diffusion model, in conjunction with the inference method, provides a framework for learning personalized behavioral and physiological parameters in subjects with T2D. This model type holds potential for practical applications, including insulin guidance

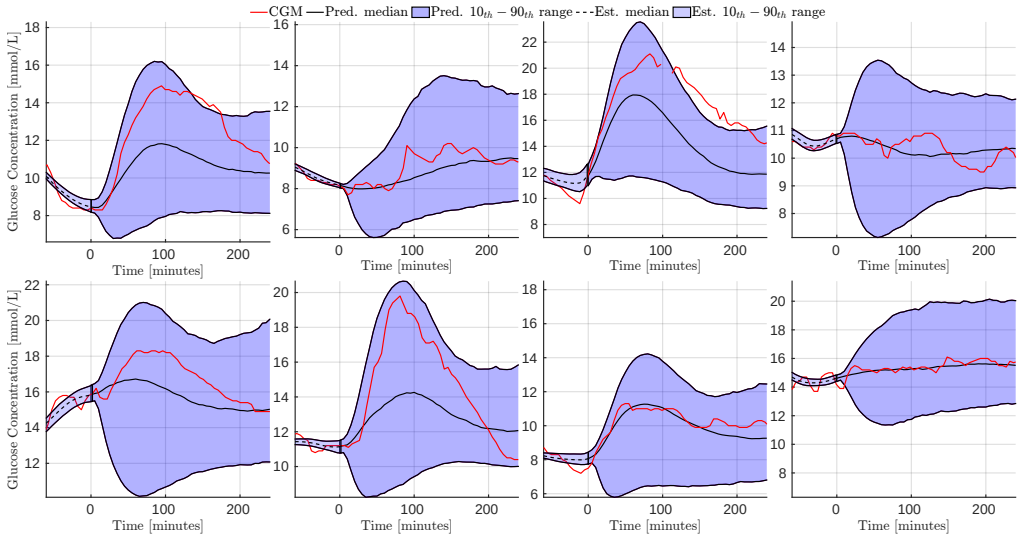

Fig. D.4: Estimated (Est.) and predicted (Pred.) glucose state X_8 with the CGM readings for all of the 8 subjects.

Table D.4: Median and IQR values for the estimated posterior of the parameters using the clinical data from the different 8 subjects.

Subject	λ_c		μ_z		α_z		p_8		p_4		p_7		p_1	
	Median	IQR	Median	IQR	Median	IQR	Median	IQR	Median	IQR	Median	IQR	Median	IQR
1	3.7	1.38	65.4	13.21	0.05	0.022	8.91	3.2	0.8	0.54	1.2	0.42	1.92	0.24
2	4.3	0.3	60	8.59	0.038	0.021	9.8	0.91	1.65	0.6	1.34	0.3	1.9	0.1
3	2.98	0.9	58.61	9.19	0.05	0.013	7.6	2	0.63	0.65	0.8	0.32	2.05	0.3
4	3	0.4	71	5.12	0.06	0.04	8.1	0.27	0.91	0.43	1.04	1.2	1.81	0.45
5	3.2	1.24	65.2	13.81	0.05	0.023	8.67	3.1	1.03	0.92	0.9	1.6	1.83	0.12
6	4.5	0.98	63.1	5.2	0.07	0.004	9.2	1.2	1.7	0.1	1.4	0.1	2.01	0.32
7	2.5	1.65	68.4	11.12	0.06	0.06	8.88	3.1	1.6	0.31	1.48	0.21	1.94	0.26
8	3.02	0.98	70.4	8.17	0.045	0.011	10.1	2.02	1.9	0.56	1.71	0.98	1.82	0.32

algorithms, hypoglycemic alert systems, and interfaces aimed at assisting T2D subjects and medical professionals in reflecting on the diabetes management process. The effectiveness of the proposed inference method has been demonstrated in providing parameter estimates solely based on injected insulin doses and CGM measurements. Additionally, the method, together with the model, shows potential for estimating meal times and predicting future meal occurrences within minutes. These findings highlight the promising utility of the proposed approach in enhancing meal detection and prediction strategies. To further enhance the model and the estimation method, several directions of improvement can be pursued. Firstly, incorporating different types of meals can improve the model's accuracy in estimating meals. Additionally, including different types of meals would enable us to estimate additional behavioral parameters, expanding the understanding of a subject's eating pattern. Moreover, integrating additional

data sources, such as heart rate measurements, could yield further insights into the interplay between physiological variables and provide better prediction results. Exploring alternative models for general disturbances beyond the OU model may also enhance the model's accuracy and flexibility. Furthermore, to ensure the robustness and generalizability of the proposed strategy, further investigation with a larger and more diverse dataset of T2D subjects is needed. Expanding the data used for the validation will provide a more comprehensive evaluation of the model's performance and applicability across different populations.

A Gumble-Max Trick

Consider we have $w^1, \dots, w^N$ being non-negative and $\sum_{i=1}^N w^i > 0$. Let $g^1, \dots, g^N$ be independent samples from the standard Gumbel distribution $\mathrm{G}(0,1)$, then we have

$$\mathbb{P}\left(a = \mathrm{argmax}_{i\in\{1,\dots,N\}}(\ln w^i + g^i)\right) = \frac{w^a}{\sum_{i=1}^n w^i}. \tag{D.12}$$

References

[1] International Diabetes Federation, *IDF Diabetes Atlas*, 9th ed. Brussels, Belgium: International Diabetes Federation, 2019.

[2] L. Berard, M. Bonnemaire, M. Mical, and S. Edelman, "Insights into optimal basal insulin titration in type 2 diabetes: Results of a quantitative survey," *Diabetes, Obesity and Metabolism*, vol. 20, no. 2, pp. 301–308, 2018.

[3] S. Patek, C. Hughes, M. Breton, and B. Kovatchev, "Anticipating meals with behavioral profiles: Towards stochastic model predictive control of T1DM," *IFAC Proceedings Volumes*, vol. 42, no. 12, pp. 37 – 42, 2009, 7th IFAC Symposium on Modelling and Control in Biomedical Systems.

[4] K. Turksoy, E. S. Bayrak, L. Quinn, E. Littlejohn, D. Rollins, and A. Cinar, "Hypoglycemia early alarm systems based on multivariable models," *Industrial & engineering chemistry research*, vol. 52, no. 35, pp. 12 329–12 336, 2013.

[5] M. Al Ahdab, T. Knudsen, J. Stoustrup, and J.-J. Leth, "An online stochastic optimization approach for insulin intensification in type 2 diabetes with attention to pseudo-hypoglycemia," in *2022 IEEE 61st Conference on Decision and Control (CDC)*, 2022, pp. 2572–2579.

[6] P. Colmegna, A. Bisio, R. McFadden, C. Wakeman, M. C. Oliveri, R. Nass, and M. Breton, "Evaluation of a web-based simulation tool for self-management support in type 1 diabetes: A pilot study," *IEEE Journal of Biomedical and Health Informatics*, 2022.

[7] M. A. Jackson, A. Ahmann, and V. N. Shah, "Type 2 diabetes and the use of real-time continuous glucose monitoring," *Diabetes technology & therapeutics*, vol. 23, no. S1, pp. S–27, 2021.

[8] D. Boiroux, M. Hagdrup, Z. Mahmoudi, N. K. Poulsen, H. Madsen, and J. B. Jørgensen, "Model identification using continuous glucose monitoring data for type 1 diabetes," *IFAC-PapersOnLine*, vol. 49, no. 7, pp. 759–764, 2016.

[9] D. Boiroux, Z. Mahmoudi, and J. B. Jørgensen, "Parameter estimation in type 1 diabetes models for model-based control applications," in *2019 American Control Conference (ACC)*, 2019, pp. 4112–4117.

[10] I. Sala-Mira, J.-L. Díez, B. Ricarte, and J. Bondia, "Sliding-mode disturbance observers for an artificial pancreas without meal announcement," *Journal of Process Control*, vol. 78, pp. 68 – 77, 2019.

[11] C. M. Ramkissoon, P. Herrero, J. Bondia, and J. Vehi, "Unannounced meals in the artificial pancreas: Detection using continuous glucose monitoring," *Sensors (Basel, Switzerland)*, vol. 18, no. 3, p. 884, Mar 2018.

[12] J. Xie and Q. Wang, "A variable state dimension approach to meal detection and meal size estimation: In silico evaluation through basal-bolus insulin therapy for type 1 diabetes," *IEEE Transactions on Biomedical Engineering*, vol. 64, no. 6, pp. 1249–1260, 2017.

[13] R. Visentin, C. Cobelli, and C. Dalla Man, "The padova type 2 diabetes simulator from triple-tracer single-meal studies: In silico trials also possible in rare but not-so-rare individuals," *Diabetes technology & therapeutics*, vol. 22, no. 12, pp. 892–903, 2020.

[14] H. G. Clausen, J.-J. Leth, T. Knudsen, and H. Schiøler, "State estimation in type 2 diabetes using the continuous-discrete unscented Kalman filter," *IFAC-PapersOnLine*, vol. 53, no. 2, pp. 16 500–16 505, 2020.

[15] H. G. Clausen, T. Knudsen, M. Al Ahdab, T. B. Aradottir, S. Schmidt, K. Nrgaard, and J.-J. Leth, "A new stochastic approach for modeling glycemic disturbances in type 2 diabetes," *IEEE Transactions on Biomedical Engineering*, 2021.

[16] M. A. Ahdab, M. Papež, T. Knudsen, T. B. Aradóttir, S. Schmidt, K. Nørgaard, and J.-J. Leth, "Parameter estimation for a jump diffusion model of type 2 diabetic patients in the presence of unannounced meals," in *2021 IEEE Conference on Control Technology and Applications (CCTA)*, 2021, pp. 176–183.

[17] I. Karatzas and S. Shreve, *Brownian motion and stochastic calculus*. Springer Science & Business Media, 1991, vol. 113.

[18] P. Colmegna, K. Wang, J. Garcia-Tirado, and M. D. Breton, "Mapping data to virtual patients in type 1 diabetes," *Control Engineering Practice*, vol. 103, p. 104605, 2020.

[19] T. Aradóttir, D. Boiroux, H. Bengtsson, J. Kildegaard, B. Orden, and J. Jørgensen, "Model for simulating fasting glucose in type 2 diabetes and the effect of adherence to treatment." in *IFAC-PapersOnLine*, vol. 50, no. 1. Elsevier, 2017, pp. 15 086–15 091.

[20] D. Rodbard, "Characterizing accuracy and precision of glucose sensors and meters," *Journal of diabetes science and technology*, vol. 8, no. 5, pp. 980–985, 2014.

[21] A. Facchinetti, S. Del Favero, G. Sparacino, and C. Cobelli, "Model of glucose sensor error components: identification and assessment for new dexcom g4 generation devices," *Medical & biological engineering & computing*, vol. 53, no. 12, pp. 1259–1269, 2015.

[22] M. Vettoretti, A. Facchinetti, G. Sparacino, and C. Cobelli, "Type-1 diabetes patient decision simulator for in silico testing safety and effectiveness of insulin treatments," *IEEE Transactions on Biomedical Engineering*, vol. 65, no. 6, pp. 1281–1290, 2017.

[23] M. Vettoretti, C. Battocchio, G. Sparacino, and A. Facchinetti, "Development of an error model for a factory-calibrated continuous glucose monitoring sensor with 10-day lifetime," *Sensors*, vol. 19, no. 23, p. 5320, 2019.

[24] M. Pollock, A. M. Johansen, and G. O. Roberts, "On the exact and ε-strong simulation of (jump) diffusions," *Bernoulli*, vol. 22, no. 2, pp. 794 – 856, 2016.

[25] E. Platen and N. Bruti-Liberati, *Numerical solution of stochastic differential equations with jumps in finance*. Springer Science & Business Media, 2010, vol. 64.

[26] C. Robert and G. Casella, *Monte Carlo statistical methods*. Springer Science & Business Media, 2013.

[27] F. Lindsten, M. I. Jordan, and T. B. Schon, "Particle gibbs with ancestor sampling," *Journal of Machine Learning Research*, vol. 15, pp. 2145–2184, 2014.

[28] F. Lindsten, T. B. Schön *et al.*, "Backward simulation methods for monte carlo statistical inference," *Foundations and Trends® in Machine Learning*, vol. 6, no. 1, pp. 1–143, 2013.

[29] C. Andrieu, A. Doucet, and R. Holenstein, "Particle markov chain monte carlo methods," *Journal of the Royal Statistical Society: Series B (Statistical Methodology)*, vol. 72, no. 3, pp. 269–342, 2010.

[30] A. Doucet, N. De Freitas, N. J. Gordon *et al.*, *Sequential Monte Carlo methods in practice*. Springer, 2001, vol. 1, no. 2.

[31] A. Svensson, T. B. Schön, and M. Kok, "Nonlinear state space smoothing using the conditional particle filter," *IFAC-PapersOnLine*, vol. 48, no. 28, pp. 975–980, Jan. 2015.

[32] D. Fink, "A compendium of conjugate priors," *See http://www. people. cornell. edu/pages/df36/CONJINTRnew% 20TEX. pdf*, vol. 46, 1997.

[33] S. Chib and E. Greenberg, "Understanding the metropolis-hastings algorithm," *The american statistician*, vol. 49, no. 4, pp. 327–335, 1995.

[34] F. Lindsten, M. I. Jordan, and T. B. Schön, "Particle Gibbs with ancestor sampling," *The Journal of Machine Learning Research*, vol. 15, no. 1, pp. 2145–2184, Jan. 2014.

[35] T. B. Aradóttir, H. Bengtsson, M. L. Jensen, N. K. Poulsen, D. Boiroux, L. L. Jensen, S. Schmidt, and K. Nørgaard, "Feasibility of a new approach to initiate insulin in type 2 diabetes," *Journal of diabetes science and technology*, vol. 15, no. 2, pp. 339–345, 2021.

[36] A. Gray and R. J. Threlkeld, "Nutritional recommendations for individuals with diabetes," 2015.

[37] F. Prendin, S. Del Favero, M. Vettoretti, G. Sparacino, and A. Facchinetti, "Forecasting of glucose levels and hypoglycemic events: head-to-head comparison of linear and nonlinear data-driven algorithms based on continuous glucose monitoring data only," *Sensors*, vol. 21, no. 5, p. 1647, 2021.

Paper E

State Space Temporal Gaussian Processes for Glucose Measurements

Mohamad Al Ahdab, Torben Knudsen, and John Leth.

The paper has been published in the
2022 European Control Conference (ECC), pp. 284-290, 2022.

Abstract

Measuring the blood glucose (BG) concentrations for people with diabetes is essential to achieve a better glycemic control either by medical professionals or by using feedback control algorithms. Continuous Glucose Monitoring (CGM) devices provide indirect measurements of the BG each 1–5 minutes. However, CGM devices suffer from correlated measurement errors and calibration errors. Detailed models for the errors of CGM devices already exist in the literature. Nonetheless, the identification of these models requires data from multiple CGM devices at once and accurate reference blood glucose measurements obtained clinically. This fact makes these models difficult to be subject-specific during typical treatment since diabetic subjects only use one CGM device with 3–4 finger pricking blood glucose measurements per day. In this paper, a methodology to obtain subject-specific CGM error models using Temporal Gaussian Processes (TGP) in their state space form is introduced. Three different TGPs are proposed and a strategy based on a particle Markov Chain Monte Carlo (MCMC) is used to perform regression and fit parameters for the models. The strategy is tested against data generated from virtual subject using detailed CGM error measurement models which were fitted with more than one CGM device and detailed clinical data from the literature. The results demonstrated the ability for TGP models with the proposed particle MCMC strategy to obtain subject-specific CGM error models using data available during the typical life of diabetic subjects.

1 Introduction

Subjects with diabetes employ different methods to monitor their BG concentration during their treatment to manage it and to determine appropriate insulin doses. One common method is to use Self-Monitored Glucose Measurement (SMBG) devices which measure glucose concentration in blood drops obtained with a finger prick [1]. Measurements acquired from such devices are sparse and do not provide enough information about the variability of glucose concentration. On the other hand, CGM devices provide measurement samples each 1-5 minuts allowing for a better description of glucose variability. Obtaining a better description about glucose variability with CGM devices has been shown to provide improvement in glycemic control and detection of low BG concentrations [2]. Nevertheless, CGM devices do not provide direct measurement of BG. Instead, CGM devices measure the interstitium glucose (IG) concentration, and therefore, there is a time lag between CGM measurements and BG concentrations which depends on the diffusion process of BG to IG. Additionally, CGM devices have been shown to be affected by systematic and random errors [3]. Therefore, patients usually use SMBG measurement to calibrate CGM devices during the day [4]. Obtaining and fitting subject-specific models for the errors of CGM devices is important for more accurate automated insulin dose calculators and fitting personalised insulin-glucose dynamical models for patients [5, 6].

In the literature, several models exist for the error of CGM measurements with various degrees of complexity. In [7], a posteriori recalibration of CGM is performed first using BG references with a sample time of 15 minutes for around 40 hours. After that, a first order model between BG and IG is used with a fixed time constant of 17 minuts to estimate IG based on interpolated reference BG data. Finally, the residual between CGM and the estimated IG, taken as the measurement noise of the sensor, is fitted with a first order autoregressive (AR)

model. The work in [8] then refined the work in [7] by considering forcing functions. Values for the time constant for the BG to IG kinetics were also estimated for each individual subject with the help of BG reference values collected every 15 minutes through BG a venous cannula. The work in [9–12] considered a more detailed model with reference BG sampled more frequently and multiple CGM devices. The models consider polynomials in time for both the gain and the drift on the CGM measurements in addition to modeling the additive random error as the sum of two different second order AR processes AR(2). Lastly, AR(2) models for both the drift and the additive noise are used to model continuous intravascular glucose monitoring sensor. Each of the mentioned methods above relied on reference BG values taken more frequently than the usual case of SMBG measurements. This make these models difficult to be used in subject-specific settings. The works in [13–15] intended to improve CGM measurements with the help of Kalman filters using the typical SMBG data patients provide. In [13], an extended Kalman filter (EKF) is used to estimate BG concentrations from SMBG and CGM measurements. The model for the EKF consists of a first order model with a time constant assumed between IG and BG, a random walk model for BG and other constant parameters to be estimated, and an additive Gaussian noise for the measurements of SMBG and CGM with the latter having a scale parameter on IG that was estimated. The variance of the additive noise on SMBG was assumed to be proportional to percentage of the SMBG value while the variance for CGM measurememnts was fixed to constant value and was not estimated. In [14], a dual rate Kalmanfilter is used on a similar model to the one in [13] but now the rate of change for BG and the scale parameters evolve to two independent random walks. Additionally, no model for IG to BG concentrations is assumed. Moreover, the variance on SMBG was also assumed to be constant and known. Finally in [15], an EKF is used similarly to the one in [13] but with the assumption that the scale parameters evolves according to a triply integrated white noise while the BG evolves according to a doubly integrated white noise. Additionally, the time constant parameter was not estimated between IG and BG due to the difficulties in estimating it with sparse SMBG measurements. Nevertheless, the proposed EKF strategy was shown to be robust to the different values of the time constant. As for the variances, only the variance of the white noise associated with the scale parameters was estimated. The rest of the variances were fixed to be the same variances used in simulation. All the mentioned methods did not attempt to estimate variances for measurement noises. Moreover, they all assumed an additive gaussian noise for CGM measurements. Additionally, all the of these methods assumed integrated white noise models for the evolution of BG. Their main intention was to improve the CGM measurements rather than obtaining a subject-specific CGM model.

As for SMBG models, several models have been concerned through the literature with various degrees of complexity. Some works, such as [16, 17], assumed that the relative error of the SMBG measurement to be an identically and independently distributed (iid) Gaussian process with a bias term. Others, as in [18], modelled the error on SMBG measurement to be gaussinally distributed with zero mean and variances depending on the BG concentration. More specifically, the variance of the error was assumed constant for BG below 4.2 [mmol/L] and linearly dependent on BG for BG above 4.2 [mmol/L]. This assumption was done to simulate the International Organization for Standardization (ISO) standard for SMBG devices [19]. The ISO standard states that 95 percent of glucose measurement should lie within ± 0.83 [mmol/L] when BG concentration is below 4.2 [mmol/L] and within 20% of BG values when BG concentration is above 4.2 [mmol/L]. Recently, [11] considered two different skew normal distributions

for the SMBG relative error when BG concentrations are above 4.2 [mmol/L] and the SMBG error when BG concentrations are below 4.2 [mmol/L]. Parameters for the two different distribution were estimated in addition to parameters for exponential distributions accounting for outliear measurements. To be able to estimate the parameters of the error distributions, highly accurate reference BG data obtained by a laboratory equipment each 15 minutes in parallel to SMBG measurements were used. The main contribution of this paper is as follows. We propose a new strategy based on TGP to obtain subject-specific CGM error models using SMBG and CGM measurements. Additionally, we propose to model the CGM errors with only one CGM device and SMBG measurements unlike the other strategies which uses multiple CGM devices and/or reference BG samples obtained with a relatively higher sampling rate than SMBG measurements. The structure of the paper is as follows. Section 3 presents an introduction to TGP regression. After that, we present the proposed models for the CGM and SMBG errors in section 4. The regression strategy is then presented in section 5. Subsequently, we present simulation models in section 6 to generate data and compare with our proposed strategy to later be followed with results in section 7 and a conclusion in section 8.

2 notations

All probabilistic considerations in this paper will be with respect to an underlying probability space $(\Omega, \mathcal{F}, \mathbb{P})$. For a random variable x we write $\mathsf{x} = x(\omega)$ for the value of the random variable, and $x \sim p(\mathsf{x})$ for the corresponding density. We use $\mathcal{N}(\mu, \sigma)$ to denote the normal distribution with mean μ and variance σ. If the difference between two consecutive time instants t_k and t_{k+j} is such that $t_{k+j} - t_k = jT,\ j \in \mathbb{Z}$ with $T \in \mathbb{R}$ being a constant, then variables that are indexed with time $x(t_k), x(t_{k+j})$ will be denoted by $x(k), x(k+j)$ for ease of notations. For a collection of $n \in \mathbb{Z}$ variables $\{x(i)\}_{i=1}^n$ or $\{x(t_i)\}_{i=1}^n$, the notation $x^{1:n}$ is used for both of them. Moreover, if each of $\{x(i)\}_{i=1}^n$ is a scalar, then $x^{1:n} = \big[x(1), \ldots, x(n)\big]^{\mathrm{T}}$. In addition, for a diagonal matrix $A_{n\times n}$ with diagonal elements $a_1, \ldots, a_n$, the notation $A = \operatorname{diag}(a_1, \ldots, a_n)$ is used. Moreover, the symbol I_n is used to denote an n dimensional identity matrix and the symbol $\mathbf{1}_n$ is used to denote an n dimensional column vector of 1s.

3 Gaussian Process Regression

A TGP is a stochastic process $f(t)$ indexed by time inputs $t \in \mathbb{R}_{\geq 0}$ such that any finite collection of the random variables $\{f(t_1), \ldots, f(t_n)\}$ has an n-dimensional Gaussian distribution [20]. The TGP regression address the estimation of the statistics of $f(t^*)$ with t^* being an arbitrary point in time given a set of data $\{t_i, \mathsf{y}(t_i)\}_{i=1}^n$ with output $\mathsf{y}(t_i)$ being the value $\mathsf{f}(t_i)$ corrupted with noise e.g.,

$$y(t_i) = f(t_i) + \varepsilon_i \tag{E.1}$$

with $\varepsilon_i \sim \mathcal{N}(\mu_{\epsilon_i}, \sigma_{\epsilon_i})$.

The TGP regression uses the fact that the joint distribution of any finite collection of its random variable is Guassian, and therefore completely determined by its mean and co-variance

functions. A TGP process is commonly denoted as

$$f(t) \sim \mathcal{GP}\left(\mu(t), \mathrm{c}\left(t, t^{'}, \theta_{\mathrm{c}}\right)\right) \tag{E.2}$$

with $\mu(t)$ the mean function and $\mathrm{c}\left(t, t^{'}, \theta_{\mathrm{c}}\right)$ the covariance function between time points t and $t^{'}$ with hyperparameters θ_{c}. The the mean and the covariance functions represent part of the prior information regarding the process. For this paper, we assume that $\mu(t) = 0$ and restrict the prior information in the choice of the TGP model to be provided by $\mathrm{c}\left(t, t^{'}, \theta_{\mathrm{c}}\right)$ as a first approach towards using TGP for CGM error models. Given the collection $\{t_i\}_{i=1}^{n}$, one can write as a prior $f(t_1), \ldots, f(t_n) \sim \mathcal{N}(0, \mathrm{C})$ where the ijth entry of the covariance matrix C is $\mathrm{C}_{ij} = \mathrm{c}(t_i, t_j, \theta_{\mathrm{c}})$.

The computational complexity for TGP can scale up to $\mathcal{O}(n^3)$ for all kinds of output processes, even in the Gaussian case (E.1), see [20]. This can be a problem for large data sets. Especially when time is the input and the sampling frequency is high as it is the case for CGM measurements. One way to deal with this is to use state space representation for TGPs. In [21, 22], exact or approximate methods to obtain state space representations for TGPs with stationary covariance function $(\mathrm{c}(t, t^{'}, \theta_{\mathrm{c}}) = \mathrm{c}(\tau, \theta_{\mathrm{c}}),\ \tau = t - t^{'})$ have been presented and discussed. In addition, the regression problem for TGPs in (E.2) with a general likelihood can be seen as a smoothing problem for the likelihood together with the following linear system

$$\mathrm{d}x_{gp}(t) = A_{gp}x_{gp}(t)\mathrm{d}t + L_{gp}\mathrm{d}B \tag{E.3a}$$

$$f(t) = H_{gp}x_{gp}(t) \tag{E.3b}$$

with B denoting standard Brownian motion. The stationary covariance functions determines the matrices A_{gp}, L_{gp}, and H_{gp} together with the state dimension. For some covariance functions, exact state representation can be found in closed form as shown in [21, 22]. For example, the TGP with an exponential covariance function is represented by an Ornstein–Uhlenbeck (OU) process.[1]Other example which have closed form state space representation are TGPs with half integers Matérn covariance functions. For other stationary covariance functions such as the squared exponential function, they can be approximated using Taylor series or Padé approximation for their spectral density to obtain an approximate linear state representation as done in [21, 23].

4 Regression Model

4.1 CGM model

To consider that CGM devices measure IG instead of BG, a first order model is considered between the two concentration with time constant τ_c [min^{-1}] as done in [9, 15]

$$\mathrm{d}x_c(t) = \frac{1}{\tau_c}\left(x_g(t) - x_c(t)\right)\mathrm{d}t \tag{E.4}$$

[1]For a scalar OU TGP with $c(t, t^{'}) = \frac{\sigma^2}{2\gamma}\mathrm{e}^{-\gamma|t-t^{'}|}$, $A_{gp} = -\gamma$, $L_{gp} = \sigma^2$, $H_{gp} = 1$

with x_g [mmol/L] the BG concentration, and x_c [mmol/L] is the IG concentration. The time constant τ_c is taken to be the median from [9] which is 7 [min^{-1}]. For the CGM measurement, the model is assumed in this paper to be on the form

$$y_c(k) = \big(1 + g(k)\big)\, x_c(k) + v(k) + \varepsilon_c(k),\ \varepsilon_c(k) \sim \mathcal{N}(0, \sigma_c^2), \tag{E.5}$$

where $t_{k+j} - t_k = jT_s, j \in \mathbb{Z}$ with T_s being the sampling time of the CGM device. The process $g(k)$ represents the time dependent gain error of the sensor due to calibration. As for $v(k)$ and $\varepsilon_c(k)$, they represent the additive calibration and measurement errors of the sensor. In this paper, three different models are assumed for $g(k)$ and $v(k)$ summarized in Table E.1. For the first model, the additive noise is assumed to be an AR(2) process, inspired by [9]. As for the gain error, the exponential covariance function (OU) is chosen inspired by the work in [14] since their model for the gain error can assumed to be a discritized version of an OU process. Additionally, the induced OU model is simple since it becomes one dimensional. Nevertheless, the solutions for the OU process are continuous but not differentiable which is not an ideal property for the gain error. For the second model, a TGP with a squared exponential covariance function is considered instead of an AR(2) process. The squared exponential covariance function gives solutions which are infinitely differentiable. Moreover, it is a common choice for covariance functions in TGPs when no information about the underlying true process is known [20]. However, the squared exponential kernel cannot be exactly represented by a finite linear system in the form of (E.3). Instead, a 6th order Taylor series approximation for the spectral density of the covariance function is used in this paper to obtain a 6th order state space representation [22, 23]. Finally, the third model considers two different TGPs with a Matérn 5/2 covariance functions. The Matérn 5/2 covariance functions can be written as the product of a second degree polynomial and an exponential covariance function. This choice was made here since the works in [9–12, 24] all considered polynomials in time for the sensor's calibration error with a maximum degree of two. Additionally, TGPs with the Matérn 5/2 covariance function have an exact third order state space representation [21, 22].

Model Number	$g(k)$	$v(k)$
Model 1	Exponential (OU)	AR(2)
Model 2	Exponential (OU)	Squared Exponential
Model 3	Matérn 5/2	Matérn 5/2

Table E.1: Different models of CGM considered in the paper

The aim of this paper is to provide a methodology for the use of TGPs with CGM and SMBG measurements, and to demonstrate the ability of TGPs to model CGM measurements with only one CGM device and SMBG measurements.

To avoid a model for the BG concentration x_g, the dynamics in (E.4) is discretized using forward Euler discritization with the sampling time T_s to obtain

$$x_c(k+1) = (1 - \frac{T_s}{\tau_c})x_c(k) + \frac{T_s}{\tau_c}x_g(k). \tag{E.6}$$

Now, $x_g(k)$ can be written in terms of $y_c(k+1)$ and $y_c(k)$ by isolating $x_g(k)$ in (E.6) and using

(E.5) to obtain

$$x_g(k) = \frac{\tau_c}{T_s}\frac{y_c(k+1) - v(k+1) - \varepsilon_c(k+1)}{1+g(k+1)} - \left(\frac{\tau_c}{T_s} - 1\right)\frac{y_c(k) - v(k) - \varepsilon_c(k)}{1+g(k)}. \tag{E.7}$$

4.2 SMBG

The SMBG measurements are modelled as

$$y_s(t_s) = x_g(t_s) + \sigma_s\left(x_g(t_s)\right)\varepsilon_s(t_s), \tag{E.8a}$$

$$\sigma_s\left(x_g\right) = \frac{1}{\kappa}\sigma_2 \log\left(1 + \mathrm{e}^{\kappa\left(x_g - 4.2\right)}\right) + \sigma_1, \tag{E.8b}$$

where t_s is the time instant of the measurement. The model for the standard deviation (E.8b) is chosen such that it provides a smooth transition between the two zones (mentioned in the introduction) which simulates the ISO standard for SMBG devices [19]. The value of κ determines how smooth the transition is. For this paper, a value of $\kappa = 5$ is chosen to produce the function in Figure E.1.

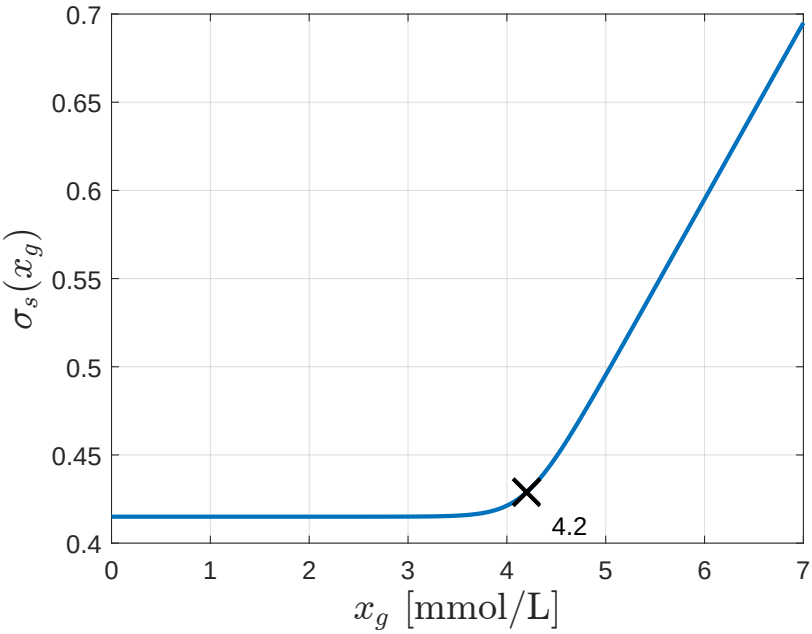

Fig. E.1: A plot of $\sigma_s\left(x_g\right)$ for $\kappa = 5$. The values of σ_1 and σ_2 are chosen in accordance to the ISO [19] to be $\sigma_1 = 0.415$ [mmol/L] and $\sigma_2 = 0.1$.

Note that it is now possible to write the measurement models here in a state space representation where the dynamics are given by the state space representation of $g(k)$ and $v(k)$ (dis-

crtized in case of a TGP using Euler–Maruyama), and the output equation is (E.8) with $x_g(k)$ given by (E.7). This can be done by matching SMBG measurements at time t_s with the nearest CGM measurement t_k. For the following sections, $x_g(k) \in \mathbb{R}^{n_g}, x_v(k) \in \mathbb{R}^{n_v}$ are denoted for the states corresponding to the model of $g(k), v(k)$ respectively, and $x(k) = [x_g^{\mathrm{T}}(k), x_v^{\mathrm{T}}(k)]^{\mathrm{T}}$. The overall state space model can then be written in the following form

$$x(k+1) = Ax(k) + L\zeta(k),\ \zeta(k) \sim \mathcal{N}(0, \sqrt{T_s}\mathrm{I}_{n_g+n_v}), \tag{E.9a}$$

$$\begin{bmatrix} g(k) \\ v(k) \end{bmatrix} = Hx(k). \tag{E.9b}$$

with the output equation given by (E.7) and (E.8), and

$$A = \begin{bmatrix} (\mathrm{I}_{n_g} + T_s A_g) & 0 \\ 0 & (\mathrm{I}_{n_v} + T_s A_v) \end{bmatrix}, \tag{E.10a}$$

$$L = \begin{bmatrix} L_g & 0 \\ 0 & L_v \end{bmatrix}, \tag{E.10b}$$

$$H = \begin{bmatrix} H_g & 0 \\ 0 & H_v \end{bmatrix}, \tag{E.10c}$$

with A_g, L_g, H_g and A_v, L_v, H_v the corresponding state space matrices for $g(k)$ and $v(k)$ respectively.

5 Regression Strategy

As discussed in [22], regression of TGPs can be done using smoothing techniques when they are represented as a state space model. The two TGPs considered in this paper come together in a nonlinear fashion as in (E.7). Additionally, the noise for the likelihood in (G.10) is clearly not additive Gaussian noise. Moreover, the SMBG measuremens which are the outputs of the modeling strategy proposed in section 4 happens only 3-4 times per day. Due to these reasons, a particle smoother is considered for the regression of the model. In addition to the smoothing, it is desired that the strategy should also estimate the hyper parameters of the TGP covariance functions (or the AR(2) process) θ_g and θ_v of $g(k)$ and $v(k)$ respectively. In addition, the strategy is also desired to estimate σ_1 and σ_2 in (G.10b), and σ_c in (E.5) to have $\theta = \begin{bmatrix} \theta_g^{\mathrm{T}} & \theta_v^{\mathrm{T}} & \sigma_c & \sigma_1 & \sigma_2 \end{bmatrix}^{\mathrm{T}}$ as the overall parameters desired to be estimated. For these reasons, Particle Gibbs with Ancestor Sampling (PGAS) [25] together with Metropolis Hasting (MH) [26] are chosen as a smoothing (regression) and a parameter estimation strategy. PGAS is a particle MCMC algorithm which combines Sequential Monte Carlo methods with MCMC. MCMC strategies are concerned with obtaining samples from a desired density by means of sampling a Markov chain from a transition kernel which has the desired density as its unique stationary density. Thus, from an arbitrary initial state of the Markov chain, successive samples (by the ergodicity property of the Markov kernel) from the transition kernel will approximate samples from the target density, provided that the Markov chain has reached its stationary distribution. The PGAS is constructed as an ergodic kernel with the stationary density being

the smoothing density $p(\mathsf{x}^{1:N}|\mathsf{y}_s^{1:N_s}, \theta)$, where N is the number of CGM samples and N_s is the number of SMBG measurements matched with the CGM measurements. Thus, one can use the PGAS to obtain M subsequent samples $\mathsf{x}^{1:N}[1], \ldots, \mathsf{x}^{1:N}[m], \ldots, \mathsf{x}^{1:N}[M]$ approximately from the smoothing distribution by running the kernel with $\mathsf{x}^{1:N}[m-1]$ to obtain $\mathsf{x}^{1:N}[m]$. Additionally, if it is desired to estimate parameters, then one can use the PGAS kernel in another MCMC sampling procedure such as Gibbs sampling [27] in order to sample parameters from their posterior density as shown in Algorithm 5. For the model in this paper, it is possible to know the posterior up to a proportionality constant

$$\log\left(p\left(\theta|\mathsf{x}^{1:N}[m], \mathsf{y}_s^{1:N_s}\right)\right) = -\frac{1}{2}\sum_{i=1}^{N_s}\log\left(2\pi\sigma_s^2\left(\mathsf{x}_g(i)\right)\right)$$
$$-\frac{1}{2}\sum_{i=1}^{N_s}\frac{\mathsf{y}_s(i)-\mathsf{x}_g(i)}{\sigma_s^2\left(\mathsf{x}_g(i)\right)} + \log(p(\theta)) + \text{constant},$$

Note that $\mathsf{x}_g(i)$ depends on the parameters θ and $\mathsf{x}^{1:i+1}[m]$, despite this not being indicated in the notation. To sample from the posterior distribution, another MCMC algorithm can be used. In this paper we used the MH to sample from the posterior $p\left(\theta|\mathsf{x}^{1:N}[m], \mathsf{y}_s^{1:N_s}\right)$. The proposal density of the MH algorithm is chosen to be a random walk driven by white noise for all the parameters. Note that the complexity order of the PGAS in [25] is $\mathcal{O}(NN_p)$ and $\mathcal{O}(NN_pM)$ for smoothing with N_p being the number of particles. For the PGAS, it was shown that it still provides good mixing for low number of particles due to the ancestor sampling step introduced in [25], even for $N_p = 5$ particles.

Algorithm 5: Gibbs sampling with PGAS

Input: Arbitrary $\mathsf{x}^{1:N}[1]$ and $\theta[1]$, a prior distribution for the parameters $\theta \sim p(\theta)$, and N_s measurements $\mathsf{y}_s^{1:N_s}$

Output: A sequence of samples $\mathsf{x}^{1:N}[1], \ldots, \mathsf{x}^{1:N}[M]$ and $\theta[1], \ldots, \theta[M]$

1 **For** $m = 2, \ldots, M$ **Do**

2 Run the PGAS kernel with $\mathsf{x}^{1:N}[m-1]$ to obtain $\mathsf{x}^{1:N}[m]$ given $\theta[m-1]$ see [25].

3 Sample $\theta[m]$ from the posterior $p\left(\theta|\mathsf{x}^{1:N}[m], \mathsf{y}_s^{1:N_s}\right)$. **End For**

6 Simulation Model

6.1 Generating Virtual Diabetic subjects Data

The model from [28] is used to generate IG and BG data of 100 type 2 diabetic subjects for 10 days. The BG concentration is taken to be the glucose concentration in the heart and lung compartment, while the IG concentration is taken to be the glucose concentration in the periphery interstitial fluid compartment. To simulate different subjects, specific parameters

from the model are changed randomly from subject to subject according to [29]. Moreover, the time constant to the periphery interstitial fluid compartment is changed uniformly for each subject within an interval of 40% of its nominal value to simulate the effect of different time lags between IG and BG. Additionally, subjects consume three different meals per day denoted as breakfast, lunch, and dinner. The meals are allocated randomly within the following time intervals: 6:00-8:00 [h] for breakfast, 12:00-14:00 [h] for lunch, and 19:00-21:00 [h] for dinner. The Carbohydrate intake for each meals is also drawn randomly from a normal distribution with mean$\pm$ SD given by 45$\pm$10 [g] for breakfast, 75$\pm$10 [g] for lunch, and 85$\pm$10 [g] for dinner. The simulated subjects took 4 SMBG measurements. One measurement time drawn uniformly 10–30 [min] before breakfast, one drawn uniformly 30–90 [min] after breakfast, another drawn uniformly between 10–30 [min] before dinner, and one drawn uniformly 30-90 [min] after dinner. This scheduling is usually done by subjects since they likely measure their BG concentration before a meal to determine how much they can eat and later after the meal to check their BG after meal consumption. In addition to the 4 SMBG measurements, a measurement is taken by the subject whenever BG goes below 4 [mmol/L]. This is also usually done since subject can feel low BG episodes and would likely take an SMBG measurement to check it. Finally, all subjects are assumed to take constant long acting insulin doses each day starting from 30 units of insulin and increasing by 10 units for each three days. This choice was done to insure that some of the subject will have low BG episodes.

6.2 Generating CGM and SMBG Measurements

To generate CGM data for the generated IG data, the polynomial and AR(2) models discussed in [9–12, 24] are used. Each of the references used polynomials for the calibration gain error and for the calibration additive error with different degrees and piece-wise constant coefficient between calibration points. The degrees of these polynomial differed from article to article depending on the device used in the study, the data set used, and the day in which the identification is carried out ([10] identified polynomials with different degrees for Day 1, Day 4, and Day 7 of the CGM device). Additionally, two additive random errors are modeled with two separate AR(2) process. The first random error represent random calibration error, and the second one represent other random measurement errors. In order to simulate these models with polynomials of different degrees, a count for how many times an n_{pg}th and an n_{pv}th degree polynomial is used for the calibration gain error and the calibration additive error respectively has been done. Afterwards, for each subject, the degrees of the polynomials associated with their CGM measurements is drawn randomly according to the following categorical (multinoulli) distribution obtained by the counts of the polynomials For the coefficients of

	$n_{pg}=0$	$n_{pg}=1$	$n_{pg}=2$
$n_{pv}=0$	4/15	2/15	×
$n_{pv}=1$	2/15	5/15	1/15
$n_{pv}=2$	×	1/15	×

Table E.2: Probabilities for the polynomial degree used to simulate CGM devices. The × is used for cases which were not reported in the literature and thus has no probability

the calibration gain error polynomial $\alpha = [\alpha_0\ \alpha_1\ \alpha_2]^{\mathrm{T}}$ and the coefficients of calibration additive error polynomial $\beta = [\beta_0\ \beta_1\ \beta_2]^{\mathrm{T}}$, a normal distribution is fitted for the coefficients $\alpha \sim \mathcal{N}(\mu_\alpha \Sigma_\alpha)$, and $\beta \sim \mathcal{N}(\mu_\beta, \Sigma_\beta)$ based on a collection of the coefficient's statistics provided in the references [9–12, 24] with

$$\mu_\alpha = \begin{bmatrix} 1.001 & 2.066 \times 10^{-5} & 0 \end{bmatrix}^{\mathrm{T}}, \tag{E.11a}$$

$$\Sigma_\alpha = \operatorname{diag}\begin{pmatrix} 0.0625 & 7.225 \times 10^{-5} & 1.936 \times 10^{-5} \end{pmatrix}, \tag{E.11b}$$

$$\mu_\beta = \begin{bmatrix} -0.0175 & 0.002 & 4.480 \times 10^{-5} \end{bmatrix}^{\mathrm{T}}, \tag{E.11c}$$

$$\Sigma_\beta = \operatorname{diag}\begin{pmatrix} 4.297 & 5.138 \times 10^{-7} & 2.009 \times 10^{-9} \end{pmatrix}. \tag{E.11d}$$

Moreover, a negative cross correlation term of -0.95 between the coefficients for the calibration gain error polynomials and the coefficients for the calibration additive error polynomials is added according to the reported results by [9]. Finally, the coefficient for the two AR(2) process are taken from the population reported in [10]. Simulating CGM errors with this approach produces a wide variety of cases to test against due to the way the parameters are sampled. This is in line with the aim of this paper which is to test the validity of using GP models as CGM error models derived with one CGM device and SMBG measurements. Note that this simulation approach can generate improbable cases. However it does not invalidate the method used in this paper, quite the contrary, it demonstrates the robustness of the method. For the SMBG measurements, the two zones skew normal distributions for One Touch Ultra 2 (OTU2) device is used [11].

7 Results and Discussion

Each of the 100 patients' CGM and SMBG, generated as described in section 6, were used in Algorithm 5 with the three proposed different models in Table E.1. The prior for each parameter was chosen to be uniform between 0 and 10 since all of them are positives. The algorithm was used to generate $M = 10000$ Markov chain samples of $x^{1:N}$ and θ. For sample $\mathsf{x}^{1:N}[m]$ of the Markov chain, 300 samples of parameters are drawn using the MH strategy and only the last sample is taken to be $\theta[m]$. This is done to try to ensure that the Markov chain sample of the MH strategy is an approximate sample from the posterior in (5). For the PGAS, the number of particles is chosen to be 20. To ensure that the samples of trajectory and parameters are from the smoothing and posterior distribution respectively, the last 1000 of the Markov chain sample are considered.

To asses the smoothing and modeling strategy in this paper, the last 1000 smoothed samples $\{\mathsf{x}^{1:N}[m]\}_{m=M-1000}^{M}$ are used to generate estimates of $\{\hat{\mathsf{x}}_g^{1:N}[m]\}_{m=M-1000}^{M}$ using (E.7). Figure E.2 shows the results for one subject using the three different models. As seen from the figure, the first model performs poorly with the CGM errors and cannot be used to obtain an estimate of the actual blood glucose concentration when compared to the second and third model. The second and third model perform similarly. The chosen covariance functions for the second and third models give the possibility to produce highly correlated time series which are suitable for biases and drifts. It is also seen from the figure that the third model performs slightly better

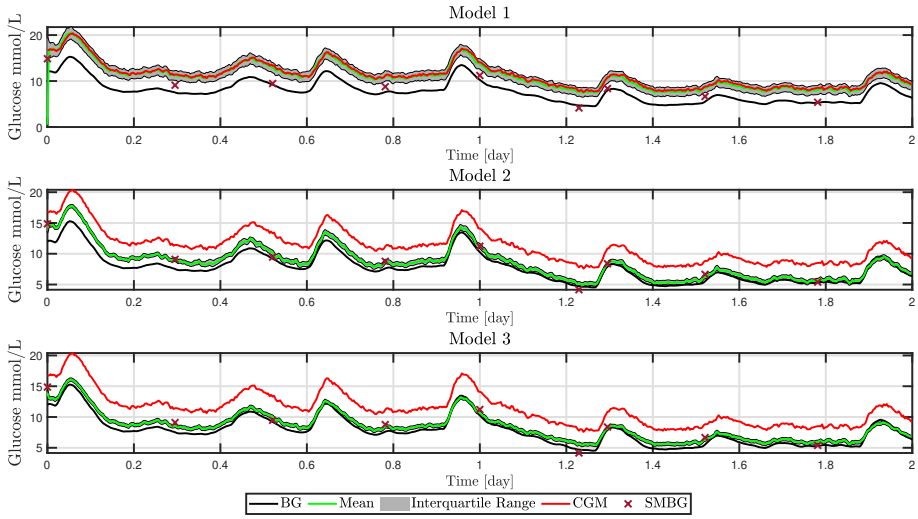

Fig. E.2: Results of the smoothing strategy for one subject using the last 1000 samples with the three different Models from Table E.1

on the first day than the second model while the second model perform slightly better on the second day than the third model.

Additionally, a fit is computed between each sample from $\{\hat{\mathsf{x}}_g^{1:N}[m]\}_{m=M-1000}^{M}$ and the true BG concentration $\mathsf{x}_g^{1:N}$ as following

$$\text{fit}[m] = 1 - \frac{\sqrt{\left(\mathsf{x}_g^{1:N} - \hat{\mathsf{x}}_g^{1:N}[m]\right)^{\mathrm{T}} \left(\mathsf{x}_g^{1:N} - \hat{\mathsf{x}}_g^{1:N}[m]\right)}}{\sqrt{\left(\mathsf{x}_g^{1:N} - \frac{1}{N}\mathbf{1}^{\mathrm{T}}\mathsf{x}_g^{1:N}\right)^{\mathrm{T}} \left(\mathsf{x}_g^{1:N} - \frac{1}{N}\mathbf{1}^{\mathrm{T}}\mathsf{x}_g^{1:N}\right)}}. \tag{E.12}$$

The mean and standard deviation for the fits over all $m \in \{M-1000, \ldots, M\}$ are then computed in Table E.3 and reported as a percentage for each model from Table E.1. It is seen from Table E.3 that the first model performs poorly in general when compared with the other models. It also exhibits a higher uncertainty in the fits (std fits) when compared with the second and the third model. This can also be seen from the subject in Figure E.2. The second and third model appear to perform relatively similar. It is seen also that the uncertainty of the fits for the second and third model is much lower than the first model. To asses the precision of the fitted parameters, the dispersion of the posterior is measured by the Quartile Coefficient of Dispersion (QCD) $QCD = \frac{Q_3 - Q_1}{Q_3 + Q_1}$ with Q_1 and Q_3 being the first and the third quantile respectively. The QCD is computed for the posterior of each parameter using the last 1000 samples and the results are reported in Table E.4. The reported numbers shows that the parameters $\theta_g, \theta_v, \sigma_c$ were estimated to a better precision when compared to σ_1 and σ_2. This is because for subjects who almost never experienced low BG levels in the simulation, σ_2 was estimated much better than σ_1 since most the time their BG levels were far from 4.2 [mmol/l]

Model	mean fit	std fit
Model 1	72%	14.3%
Model 2	92.5%	5.03%
Model 3	94.2%	1.61%

Table E.3: Mean and standard deviation of fits

Model	θ_g	θ_v	σ_c	σ_1	σ_2
Model 1	0.21, 0.18	0.18, 0.184, 0.23	0.094	0.42	0.31
Model 2	0.11, 0.16	0.112, 0.06	0.064	0.412	0.29
Model 3	0.13, 0.21	0.162, 0.08	0.044	0.425	0.33

Table E.4: QCD values for the posterior of the parameters. Note that the number of reported QCD values for θ_g and θ_v is based on their dimension.

which is the threshold in (G.10). On the other hand, σ_1 was estimated better for subjects who has lower BG levels for most of the time. Moreover, since more subjects have higher BG levels, the reported QCD values for σ_2 are better than σ_1.

8 Conclusion and Future Work

The suggestion of using TGP in this paper with the presented smoothing strategy has been shown to be able to model correlated and time dependent CGM errors with only one CGM device and SMBG measurements. The TGP models can handle varying parameters for both multiplicative and additive measurement errors on CGM devices. Moreover, the fact that the models and the strategy can be applied with one CGM device and SMBG measurements only make them suitable for subject-specific modeling. For future work, one can investigate different model choices. Additionally, one can use the proposed strategy with the suggested models with real CGM patient data accompanied with detailed BG concentration data sampled at a rate similar to the real CGM device for conformation. Finally, an investigation for improving the smoothing strategy or proposing an alternative one can be carried out.

References

[1] S. Clarke and J. Foster, "A history of blood glucose meters and their role in self-monitoring of diabetes mellitus," *British journal of biomedical science*, vol. 69, no. 2, pp. 83–93, 2012.

[2] B. Kovatchev and C. Cobelli, "Glucose variability: timing, risk analysis, and relationship to hypoglycemia in diabetes," *Diabetes Care*, vol. 39, no. 4, pp. 502–510, 2016.

[3] B. P. Kovatchev, S. D. Patek, E. A. Ortiz, and M. D. Breton, "Assessing sensor accuracy for non-adjunct use of continuous glucose monitoring," *Diabetes technology & therapeutics*, vol. 17, no. 3, pp. 177–186, 2015.

[4] G. Acciaroli, M. Vettoretti, A. Facchinetti, and G. Sparacino, "Chapter 9 - calibration of cgm systems," in *Glucose Monitoring Devices*, C. Fabris and B. Kovatchev, Eds. Academic Press, 2020, pp. 173–201.

[5] L. Biagi, A. Hirata Bertachi, I. Conget, C. Quirós, M. Giménez, F. J. Ampudia-Blasco, P. Rossetti, J. Bondia, and J. Vehí, "Extensive assessment of blood glucose monitoring during postprandial period and its impact on closed-loop performance," *Journal of diabetes science and technology*, vol. 11, no. 6, pp. 1089–1095, 2017.

[6] C. Boettcher *et al.*, "Accuracy of blood glucose meters for self-monitoring affects glucose control and hypoglycemia rate in children and adolescents with type 1 diabetes," *Diabetes technology & therapeutics*, vol. 17, no. 4, pp. 275–282, 2015.

[7] M. Breton and B. Kovatchev, "Analysis, modeling, and simulation of the accuracy of continuous glucose sensors," *Journal of diabetes science and technology*, vol. 2, no. 5, pp. 853–862, 2008.

[8] D. Lunn, C. Wei, and R. Hovorka, "Fitting dynamic models with forcing functions: application to continuous glucose monitoring in insulin therapy," *Statistics in medicine*, vol. 30, no. 18, pp. 2234–2250, 2011.

[9] A. Facchinetti, S. Del Favero, G. Sparacino, J. R. Castle, W. K. Ward, and C. Cobelli, "Modeling the glucose sensor error," *IEEE Transactions on Biomedical Engineering*, vol. 61, no. 3, pp. 620–629, 2013.

[10] A. Facchinetti, S. Del Favero, G. Sparacino, and C. Cobelli, "Model of glucose sensor error components: identification and assessment for new dexcom g4 generation devices," *Medical & biological engineering & computing*, vol. 53, no. 12, pp. 1259–1269, 2015.

[11] M. Vettoretti, A. Facchinetti, G. Sparacino, and C. Cobelli, "A model of self-monitoring blood glucose measurement error," *Journal of diabetes science and technology*, vol. 11, no. 4, pp. 724–735, 2017.

[12] M. Vettoretti, C. Battocchio, G. Sparacino, and A. Facchinetti, "Development of an error model for a factory-calibrated continuous glucose monitoring sensor with 10-day lifetime," *Sensors*, vol. 19, no. 23, p. 5320, 2019.

[13] E. J. Knobbe and B. Buckingham, "The extended kalman filter for continuous glucose monitoring," *Diabetes technology & therapeutics*, vol. 7, no. 1, pp. 15–27, 2005.

[14] M. Kuure-Kinsey, C. C. Palerm, and B. W. Bequette, "A dual-rate kalman filter for continuous glucose monitoring," in *2006 International Conference of the IEEE Engineering in Medicine and Biology Society*. IEEE, 2006, pp. 63–66.

[15] A. Facchinetti, G. Sparacino, and C. Cobelli, "Enhanced accuracy of continuous glucose monitoring by online extended kalman filtering," *Diabetes technology & therapeutics*, vol. 12, no. 5, pp. 353–363, 2010.

[16] J. C. Boyd and D. E. Bruns, "Quality specifications for glucose meters: assessment by simulation modeling of errors in insulin dose," *Clinical Chemistry*, vol. 47, no. 2, pp. 209–214, 2001.

[17] N. S. Virdi and J. J. Mahoney, "Importance of blood glucose meter and carbohydrate estimation accuracy," *Journal of diabetes science and technology*, vol. 6, no. 4, pp. 921–926, 2012.

[18] M. D. Breton and B. P. Kovatchev, "Impact of blood glucose self-monitoring errors on glucose variability, risk for hypoglycemia, and average glucose control in type 1 diabetes: an in silico study," *Journal of Diabetes Science and Technology*, vol. 4, no. 3, pp. 562–570, 2010.

[19] *In vitro diagnostic test systems: requirements for blood-glucose monitoring systems for self-testing in managing diabetes mellitus.* International Organization for Standardization, 2003.

[20] C. E. Rasmussen, "Gaussian processes in machine learning," in *Summer school on machine learning.* Springer, 2003, pp. 63–71.

[21] J. Hartikainen and S. Särkkä, "Kalman filtering and smoothing solutions to temporal gaussian process regression models," in *2010 IEEE international workshop on machine learning for signal processing.* IEEE, 2010, pp. 379–384.

[22] S. Sarkka, A. Solin, and J. Hartikainen, "Spatiotemporal learning via infinite-dimensional bayesian filtering and smoothing: A look at gaussian process regression through kalman filtering," *IEEE Signal Processing Magazine*, vol. 30, no. 4, pp. 51–61, 2013.

[23] S. Särkkä and R. Piché, "On convergence and accuracy of state-space approximations of squared exponential covariance functions," in *2014 IEEE International Workshop on Machine Learning for Signal Processing (MLSP).* IEEE, 2014, pp. 1–6.

[24] L. Biagi, C. M. Ramkissoon, A. Facchinetti, Y. Leal, and J. Vehi, "Modeling the error of the medtronic paradigm veo enlite glucose sensor," *Sensors*, vol. 17, no. 6, p. 1361, 2017.

[25] F. Lindsten, M. I. Jordan, and T. B. Schon, "Particle gibbs with ancestor sampling," *Journal of Machine Learning Research*, vol. 15, pp. 2145–2184, 2014.

[26] S. Chib and E. Greenberg, "Understanding the metropolis-hastings algorithm," *The american statistician*, vol. 49, no. 4, pp. 327–335, 1995.

[27] D. Spiegelhalter, A. Thomas, N. Best, and W. Gilks, "Bugs 0.5: Bayesian inference using gibbs sampling manual (version ii)," *MRC Biostatistics Unit, Institute of Public Health, Cambridge, UK*, pp. 1–59, 1996.

[28] M. Al Ahdab, J.-J. Leth, T. Knudsen, P. Vestergaard, and H. G. Clausen, "Glucose-insulin mathematical model for the combined effect of medications and life style of type 2 diabetic patients," *Biochemical Engineering Journal*, vol. 176, p. 108170, 2021.

[29] R. S. Parker, F. J. Doyle III, J. H. Ward, and N. A. Peppas, "Robust $\mathcal{H}_\infty$ glucose control in diabetes using a physiological model," *AIChE Journal*, vol. 46, no. 12, pp. 2537–2549, 2000.

Paper F

Sensor Fusion for Glucose Monitoring Systems

Mohamad Al Ahdab, Karim Davari Benam, Hasti Khoshamadi, and Anders Lyngvi Fougner, and Sebastien Gros

The paper has been accepted/in press in the
2023 IFAC World Congress, 2023.

The layout has been revised.

Abstract

A fully automated artificial pancreas (AP) requires accurate blood glucose (BG) readings. However, many factors can affect the accuracy of commercially available sensors. These factors include sensor artifacts due to the pressure on surrounding tissues, connection loss, and poor calibration. The AP may administer an incorrect insulin bolus due to inaccurate sensor data when the patient is not supervising the system. The situation can be even worse in animal experiments because animals are eager to play with the sensor and apply pressure. In this study, we propose and derive a Multi-Model Kalman Filter with Forgetting Factor (MMKFF) for the problem of fusing information from redundant subcutaneous glucose sensors. The performance of the developed MMKFF was assessed by comparing it against other Kalman Filter (KF) strategies on experimental data obtained in two different animals. The developed MMKFF was shown to provide a reliable fused glucose reading. Additionally, compared to the other KF approaches, the MMKFF was shown to be better able to adjust to changes in the accuracy of the glucose sensors.

1 Introduction

Monitoring blood glucose (BG) level in subjects with diabetes is important for managing their treatment. Over the last two decades, continuous glucose monitoring (CGM) systems have become more and more common in patients with diabetes mellitus type 1. Most commercially available CGMs provide measurement samples each 5 minutes allowing for a better description of the subject's glucose variability.

The artificial pancreas (AP) automates BG control by reading levels from a CGM, calculating the insulin bolus dose using a control algorithm, and infusing the insulin with a pump. A reliable system for measuring BG level with minimal supervision is essential to achieve the ultimate goal of reducing supervision. However, real-life situations can cause CGMs to provide inaccurate information or disconnect from APs, posing a risk to BG control in a single-sensor APs.

For simplicity and to reduce the wiring, the common off-the-shelf CGMs have a transmitter to connect wirelessly with the AP. The communication methods are Bluetooth or ANT+, which will lose connection if the CGM and the receiver/pump are on opposite sides of the body, e.g. during sleep. Furthermore, compression artifacts caused by external pressure on the CGM can rapidly decrease the measured BG level and cause failure of the APs. Many other circumstances make single-sensor APs unreliable, making the supervision of the CGM necessary for patients. These circumstances have been summarised by [1].

The glucose sensors have a warm-up period, which means that each new sensor attached will not provide accurate data for a while. Warm-up times vary between brands and range from 2 hours to 2 days. In other words, if the CGM fails unexpectedly in single-sensor APs, patients must manually control the BG during the warm-up period of the new sensor. The issue gets aggravated in awake animal experiments since it is challenging to take frequent blood samples to measure the BG. Additionally, since animals are eager to play with the sensors attached to their bodies or exert pressure on them, the circumstances above are more likely to occur

in animal experiments. Notably, the warm-up period in the animal experiment is not ideal because it lengthens the experiment and raises the cost of the experiment. In this setting, the animal experiments are used to test controllers.

Redundant sensors are advised in the literature to address the issues above. For example, [2] used two sensors in their AP where one sensor would replace the active one in the event of a sensor failure. In the present study, instead of using the other sensor(s) only for backup, we developed a method based on a Multi-Model Kalman Filter (MMKF) approach to combine the data from all the glucose sensors attached on the subject to increase the reliability. The proposed method was evaluated using experimental data from anesthetized and awake pigs.

The works in [3–5] used data batches from multiple CGMs devices together with an accurate reference BG data for the aim of obtaining a detailed parametric model description for the measurement errors in specific CGM devices. Therefore, the methods developed in these works are not suitable for a real time sensor fusion of CGMs for APs.

Kalman Filter (KF) strategies have been used in previously reported studies with CGMs for the purpose of calibrating one CGM device with self monitored blood glucose samples obtained by finger pricking [6–8]. While these solutions primarily focused on sensor calibration, in this paper we aim to fuse information from numerous CGM devices with varying degrees of accuracy considering that one or more sensors can fail and recover over time.

The contributions of this work are as following:

- We show how MMKF can be used for the fusing of CGM devices. In addition, we derive a MMKF with a Forgetting Factor (MMKFF) in Section 4.
- We apply the MMKFF on two sets of experimental data and evaluate its performance in Section 5 comparing it with different types of KFs.

2 Animal Experiments

The example data sets used in this paper are from two different animal experiments. The tests were carried out in two non-diabetic farm pigs (Sus scrofa domesticus) of 36 and 40 kg, respectively.

The first experiment (Exp1) was performed in an anesthetized pig for 24 hours. Three Medtronic Enlite glucose sensors (Northridge, Canada) with custom transmitters from Inreda Diabetic (Goor, the Netherlands) were used (hereafter named Exp1.S1, Exp1.S2, and Exp1.S3) with a 1.2s sampling time. The provided data acquisition system could only receive data from two of the sensors. Therefore, one of the sensors only served as a backup sensor. Blood samples were taken sporadically to calibrate the sensors and compare them. A blood gas analyser (BGA) of ABL800 FLEX (Copenhagen, Denmark) was used to measure the actual BG level throughout the experiment. We compared the performance of the developed MMKFF method with the BGA. Exp1.S1 and Exp1.S2 were attached to each side of the belly as shown in Figure. F.1, and Exp1.S3 was attached to the neck as backup. The protocol for this animal experiment was similar to the protocols used in [9] and [10].

The second experiment (Exp2) was closer to real-life conditions than Exp1 since it was performed in an awake animal where it could move freely. In this experiment, four sensors were used to decrease the chance of losing data or basing decisions on faulty data. Sensors Exp2.S1

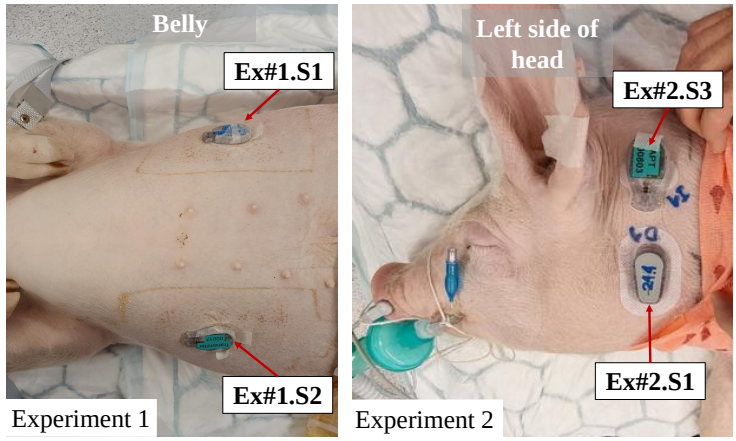

Fig. F.1: Placement of glucose sensors. Left: Experiment 1, both sensors Exp1.S1 and Exp1.S2 placed on the pig's belly. Right: Experiment 2, two sensors on the left side of the neck. Another two sensors were on the pig's right side, with sensor Exp2.S4 attached at the bottom and Exp2.S2 at the top.

and Exp2.S2 were factory-calibrated Dexcom G6 (San Diego, CA) with 5min sampling time. Sensors Exp2.S3 and Exp2.S4 were Medtronic Guardian sensors 3 (Northridge, Canada) with custom-made transmitters from Inreda Diabetic (Goor, the Netherlands) with 1.2s sampling time. To reduce the connection losses during the experiments, the sensors were mounted on both sides of the neck, as shown in Figure F.1. Unlike Exp1, taking frequent blood samples was not possible. However, depending on the sensor connection losses, general behaviours of the sensors compared to others, and position of the pig, the experiment's operators were giving each sensor a reliability indicator between 0 and 1. Then we calculated a weighted average of the sensors using their assigned reliability indicators. With the weighted average value as a benchmark, we evaluated the performance of the proposed sensor fusion technique. Readings at time $5k$ [min], $k \in \mathbb{Z}_{\geq 0}$ from Exp1.S1/ Exp2.S1, Exp1.S2/Exp2.S2, Exp2.S3, and Exp2.S4 will be denoted as $y_k[1]$,$y_k[2]$,$y_k[3]$, and $y_k[4]$, respectively.

3 Notations

For a random variable x, we write x for its realization. We write $\mathcal{N}(\mu, \Sigma)$ for the normal distribution with mean μ and variance Σ. Let two successive time instants t_k and t_{k+j} be such that $t_{k+j} - t_k = jT$, $j \in \mathbb{Z}$ with $T \in \mathbb{R}$, then variables $x(t_k), x(t_{k+j})$ will be denoted as x_k, x_{k+j}. The symbol $\mathbb{S}^n_{>0}$ ($\mathbb{S}^n_{\geq 0}$) is used for the set of positive definite (semi-definite) matrices with dimension n. We write $[N] = \{1, \ldots, N\}$, $N \in \mathbb{Z}_{>0}$. We write a diagonal matrix with diagonal elements $v = [v_1, \ldots, v_n]^\top$ as $\mathrm{diag}\,(v)$. We use $\mathbf{I}$ for the identity matrix.

4 Method

In this section, we will first present the models used for the glucose sensors in 4.1. Afterwards, the MMKFF method will be described in 4.2.

4.1 Problem Setup

We consider a setup in which we have $N \in \mathbb{Z}_{>0}$ CGM sensors. At each sample time k, a portion of the sensors $0 \leq n_k \leq N$ will provide readings $y_k \in \mathbb{R}^{n_k}$. This setup considers cases when the sensors can fail for some periods of time. For the modeling, we consider in this paper N linear Gaussian dynamic models $\mathcal{M}^i$ with $i \in [N]$ as the following

$$x^i_{k+1} = A^i x^i_k + E^i w^i_k,\ w^i_k \sim \mathcal{N}(0, Q^i), \tag{F.1a}$$

$$y_k = C^i_k x^i_k + v^i_k,\ v^i_k \sim \mathcal{N}(0, R^i_k), \tag{F.1b}$$

with $x^i \in \mathbb{R}^{n_x}, n_x \in \mathbb{Z}_{>0},\ A^i \in \mathbb{R}^{n_x \times n_x},\ E^i \in \mathbb{R}^{n_x \times n_q},\ n_q \in \mathbb{Z}_{>0},\ Q_i \in \mathbb{S}^{n_q}_{>0},\ w^i_k$ is an independent and identically distributed (IID) process, $C^i_k \in \mathbb{R}^{n_k \times n_x}$, $R^i_k \in \mathbb{S}^{n_k}_{\geq 0}$, and $v^i_k \in \mathbb{R}^{n_k}$ is a IID process. Similar to the previous works in [6, 8] in which integrators of white noise with different orders are chosen to represent a description for the dynamics of BG concentrations, we choose matrices $A^i = A,\ E^i = E,\ Q^i = Q$ and $C^i_k = C_k$ for all the models $i \in [N]$ such that A, E, Q, and C represent the discrete output of a triple integrated white noise w as following

$$A = \begin{bmatrix} 1 & 0 & 0 \\ T & 1 & 0 \\ T^2/2 & T^3/6 & 1 \end{bmatrix}, E = \begin{bmatrix} T \\ T^2/2 \\ T^3/6 \end{bmatrix}, C_k = \begin{bmatrix} 0 & 0 & 1 \\ & \vdots & \\ 0 & 0 & 1 \end{bmatrix} \in \mathbb{R}^{n_k \times 3},$$

with T [min] being the sampling time[1]. The integrated white noise model serves as a prior assumption regarding the stationarity and the power spectrum density of the BG concentration. Additionally, if the model in (F.1a) is viewed as a discretized version of a continuous time dynamical glucose model, then it captures our knowledge that BG concentration is differentiable with respect to time. This choice is common in time series estimation of physiological processes (see [11] for e.g.). The higher the order of the integrator, the smoother the continuous time BG concentration is assumed to be. The variance Q of the driving white noise can be understood as a representation of how confident we are in the assumed model (see Section 5.1 for more details). Note that the model does not reflect the ground truth of the time evolution for BG concentration and different models with different accuracy and inputs (e.g. insulin, physical activity, meals, etc...) can also be considered and used. For the simplicity in this paper, we considered a simple white noise integrator which can work in a general setting in which data regarding more specific inputs is not available. As for the covariance matrix R^i_k for the measurement noise, it will be chosen differently for each model $i \in [N]$. To define R^i_k, let $r^i \in \mathbb{R}^N$ such that the i_{th} element of r^i is σ^2_l while the rest of the elements in r^i are σ^2_u with $\sigma_u > \sigma_l$. Let $s_k \in \mathbb{R}^N$ such that the i_{th} element of s_k is 1 if the i_{th} sensor is providing a reading at sample k and zero otherwise. Then the covariance matrix R^i_k is chosen as $R^i_k = \operatorname{diag}\left(s_k^\top r^i\right)$. This basically means that for each

[1] If the sensors are operating at different sampling rates then T can be chosen to be the minimum of the different sampling times.

sensor i, we have a model $\mathcal{M}^i$ that assumes a lower variance for the i_{th} sensor (σ_l^2) than the variance for the other sensors (σ_u^2). In other words, each model is more confident with respect to one sensor than the others. Note that it is possible with this structure to have a continuum of models weighting the sensors differently. However, we chose to have a finite number of models for simplicity and tractability. Finally, we define for each model $\mathcal{M}^i$ a random variable $m_k^i \in \{0,1\}$ such that $p(\mathrm{m}_k^i) = \mathbb{P}(\mathrm{m}_k^i = 1) := \mathbb{P}\left(\mathcal{M}^i \text{ is the best model at step } k\right)$. Note that the time dependence for m_k^i is included to account for the fact that some sensors will become better than others for a period of time. To relate m_{k+1}^i with m_k^i, we use the following

$$p(\mathrm{m}_{k+1}^i) = p(\mathrm{m}_{k+1}^i|\mathrm{m}_k^i)p(\mathrm{m}_k^i) := (1-\alpha)p(\mathrm{m}_k^i) + \alpha\bar{\beta}^i, \tag{F.2}$$

with $0 \leq \alpha \leq 1$ a constant which we call the *forgetting factor*, and $0 \leq \bar{\beta}^i \leq 1$ with $\sum_{i=1}^N \bar{\beta}^i = 1$ are predefined probabilities for the models. The dynamic model in (F.2) is to be understood as a prior model in the absence of measurement updates (similar to (F.1a)). A measurement correction step will be introduced in section 4.2. To understand more what "forgetting" is meant with (F.2), assume we start from probabilities $p(\mathrm{m}_k^i) > 0,\ \forall i \in [N]$ representing our knowledge at step k regarding the models. If we only follow the update in equation (F.2), then the $l-step$ prediction is $p(\mathrm{m}_{k+l}^i) = (1-\alpha)^l p(\mathrm{m}_k^i) + \left(1-(1-\alpha)^l\right)\bar{\beta}^i$. If $0 < \alpha \leq 1$, we can see that $\lim_{l\to\infty} p(\mathrm{m}_{k+l}^i) = \bar{\beta}^i$. This means that $\forall i \in [N]$, our knowledge regarding the models $p(\mathrm{m}_k^i)$ with equation (F.2) only is "forgotten" exponentially with a rate $1-\alpha$ to converge to a predefined knowledge captured in $\bar{\beta}^i$. The predefined probabilities $\bar{\beta}^i$ can be uniform ($\bar{\beta}^i = \frac{1}{N},\ \forall i \in [N]$) or prior probabilities regarding the models.

4.2 Multiple Models Kalman Filter with Forgetting Factor

The idea of the MMKF, which was first introduced in [12], is to run a KF for each model $\mathcal{M}^i$ in parallel and combine the estimated results to obtain a better new estimate. In this section, we will extend the MMKF with the forgetting factor equation (F.2) and provide a description for the MMKFF strategy. Note that the MMKFF can be thought of as a specific case for dynamic MMKF where the probabilities of the true models evolve with time and it is different from the one in [13, chapter 11] since (F.7) is not a homogeneous Markov chain. For ease of notation, we will use $\beta_{k_1|k_2}^i := p\left(\mathrm{m}_{k_1}^i|\mathcal{Y}_{k_2}\right)$ with $k_1, k_2 \in \mathbb{Z}_{\geq 0}$, and $\mathcal{Y}_{k_2} = (y_1, \ldots, y_{k_2})$ being a tuple of all the available measurement up until sample k_2. Assume now at iteration k we have an estimate $\hat{x}_{k|k} \sim \mathcal{N}\left(\mu_{k|k}, P_{k|k}\right)$ for the states and probabilities $\beta_{k|k}^i$. If there is an available measurement reading y_{k+1}, then we run a KF for each model $\mathcal{M}^i$ as following

Time update:

$$\mu_{k+1|k} = A\mu_{k|k}, P_{k+1|k} = AP_{k|k}A^\top + EQE^\top \tag{F.3a}$$

Measurement Correction:

$$\tilde{y}_{k+1|k} = y_{k+1} - C_k\mu_{k+1|k},\ S_{k+1|k}^i = C_k P_{k+1|k}^i C_k^\top + R_k^i \tag{F.4a}$$

$$\mu_{k+1|k+1}^i = \mu_{k+1|k} + P_{k+1|k}C_k^\top (S_{k+1|k}^i)^{-1}\tilde{y}_{k+1|k} \tag{F.4b}$$

$$P_{k+1|k+1}^i = \left(\mathbf{I} - P_{k+1|k}C_k^\top (S_{k+1|k}^i)^{-1}C_k\right)P_{k+1|k} \tag{F.4c}$$

To derive a time update step and a measurement correction step for the probabilities $\beta^i_{k+1|k+1}$, we use Baye's rule to write

$$\begin{aligned}
\beta^i_{k+1|k+1} &= p(\mathrm{m}^i_{k+1}|\mathcal{Y}_{k+1}) = \frac{p(\mathrm{m}^i_{k+1}, \mathcal{Y}_{k+1})}{p(\mathcal{Y}_{k+1})} \\
&= \frac{p(\mathrm{m}^i_{k+1}, \mathcal{Y}_k, \mathrm{y}_{k+1})}{p(\mathcal{Y}_{k+1})} = \frac{p(\mathrm{m}^i_{k+1}, \mathcal{Y}_k, \tilde{\mathrm{y}}_{k+1|k})}{p(\mathcal{Y}_{k+1})} \\
&= \frac{p(\tilde{\mathrm{y}}_{k+1|k}|\mathrm{m}^i_{k+1}, \mathcal{Y}_k)p(\mathrm{m}^i_{k+1}, \mathcal{Y}_k)}{p(\mathcal{Y}_{k+1})} \\
&= \frac{p(\tilde{\mathrm{y}}_{k+1|k}|\mathrm{m}^i_{k+1})p(\mathrm{m}^i_{k+1}|\mathcal{Y}_k)p(\mathcal{Y}_k)}{p(\mathcal{Y}_{k+1})} \\
&= \frac{p(\tilde{\mathrm{y}}_{k+1|k}|\mathrm{m}^i_{k+1})p(\mathrm{m}^i_{k+1}|\mathcal{Y}_k)}{p(\tilde{\mathrm{y}})} \\
&= \frac{p(\tilde{\mathrm{y}}_{k+1|k}|\mathrm{m}^i_{k+1})}{\sum_{i=1}^N p(\tilde{\mathrm{y}}_{k+1|k}|\mathrm{m}^i_{k+1})p(\mathrm{m}^i_{k+1}|\mathcal{Y}_k)} p(\mathrm{m}^i_{k+1}|\mathcal{Y}_k)
\end{aligned} \tag{F.5}$$

with

$$\begin{aligned}
p(\mathrm{m}^i_{k+1}|\mathcal{Y}_k) &= p(\mathrm{m}^i_{k+1}|\mathrm{m}^i_k)p(\mathrm{m}^i_k|\mathcal{Y}_k) \\
&= (1-\alpha)p(\mathrm{m}^i_k|\mathcal{Y}_k) + \alpha\bar{\beta}^i
\end{aligned} \tag{F.6}$$

To summarize, (F.5) and (F.6) are written as a time update step and a measurement correction step with the notation $\beta^i_{k_1|k_2}$ as following

Time update (using (F.6)):

$$\beta^i_{k+1|k} = (1-\alpha)\beta^i_{k|k} + \alpha\bar{\beta}^i \tag{F.7}$$

Measurement Correction (using (F.5)):

$$\beta^i_{k+1|k+1} = \frac{p\left(\tilde{y}_{k+1|k} \mid \mathrm{m}^i_{k+1}\right)}{\sum_{i=1}^N \beta^i_{k+1|k} p\left(\tilde{y}_{k+1|k} \mid \mathrm{m}^{\mathrm{i}}_{\mathrm{k+1}}\right)} \beta^i_{k+1|k}. \tag{F.8}$$

with $p\left(\tilde{y}_{k+1|k} \mid \mathrm{m}^i_{k+1}\right)$ being the multi-normal probability density function with zero mean and covariance matrix $S^i_{k+1|k}$. Finally, let $\Delta\mu^i_{k+1} := \mu^i_{k+1|k+1} - \mu_{k+1|k+1}$, then the estimated mean and covariance matrix of the states are computed as following

$$\mu_{k+1|k+1} = \sum_{i=1}^N \beta^i_{k+1|k+1}\mu^i_{k+1|k+1} \tag{F.9a}$$

$$P_{k+1|k+1} = \sum_{i=1}^N \beta^i_{k+1|k+1}\left(P^i_{k+1|k+1} + \Delta\mu^i_{k+1}\left(\Delta\mu^i_{k+1}\right)^\top\right). \tag{F.9b}$$

Note that the values $\beta^i_{k+1|k+1}$ in (F.9a) are acting as weights for the estimates obtained from the different KFs. The values $\beta^i_{k+1|k+1}$ will be referred to as "trust values for sensor i" in the next section.

5 Results

We compare the MMKFF presented in this paper with the following KFs:

- Linear KF.
- The Distributionally Robust KF (DRKF) from [14] with a moment based ambiguity set and an $\epsilon-$contamination set for outliers.
- The Adaptive Fading KF (AFKF) based on [15] but with the fading applied to the covariance matrix $R(k)$ adapting to sensor changes.
- The MMKF.

5.1 Choice of the Kalman Filters' Parameters

All the KFs share the same value of Q. For a higher value of Q, the KFs will rely on the measurements more for their estimates which will make them faster to respond to changes in BG but more prone to noise. On the other hand, a smaller value of Q will make the KFs rely more on the model predictions but will hinder their ability to respond quickly to changes in BG. The value of Q in this paper was chosen to be $Q = 1$. For the distributionally robust KF, we tuned the parameters denoted in the paper [14] as $\theta_{2,x}, \theta_{2,v}, \epsilon$ to be $\theta_{2,x} = \theta_{2,v} = 1.02$ and $\epsilon = 0.005$. For Exp1, we only compared MMKF and MMKFF due to limited space. For Exp2, the one model KFs share one covariance matrix $R_k = \text{diag}\left(s_k^\top r\right)$ with $r = [1\ 1\ 100\ 100]^\top$ since our prior knowledge is such that Exp2.S1 and Exp2.S2 perform better than Exp2.S3 and Exp2.S4. For the multi-model KFs, we chose $\sigma_l^2 = 1$ and $\sigma_u^2 = 100$ for the both experiments. The forgetting factor was chosen to be $\alpha = 0.05$. The KFs for both Exp1 and Exp2 were initialized with $\mu_{0|0} = \left[0\ 0\ 0.5y_0[1] - 0.5y_0[2]\right]^\top$ and $P_{0|0} = \mathbf{I}$ where $y_0[1]$ and $y_0[2]$ are the measurements of the first and second sensors of both experiments, respectively. For Exp1, we chose $\beta_{0|0} = \bar{\beta} = [0.5\ 0.5]^\top$ based on our prior knowledge (no prior preference over the sensors). As for Exp2, $\beta_{0|0} = \bar{\beta} = [0.3\ 0.3\ 0.2\ 0.2]^\top$ based on our prior knowledge.

5.2 Results from Exp1

In Figure F.2, MMKFF and MMKF were tested on data from Exp1.S1 and Exp2.S2 and the result compared to BGA. The MMKF and MMKFF performed similarly, with their fused CGM being close to the accurate BG readings. The fused CGM managed to overcome the drifting in Exp1.S2 and stayed close to the reading from the Blood Gas Analyser (BGA). However, we can see that the trust values $\beta_{k|k}^1$ and $\beta_{k|k}^2$ evolved differently with the CGM readings. The trust values from the MMKF converged faster towards Exp1.S1 ($\beta_{k|k}^1 \approx 1,\ \beta_{k|k}^2 \approx 0$) during the case when Exp1.S2 was being calibrated than the trust values of MMKFF (see Figure F.3). In this particular excerpt for Exp1, favoring Exp1.S1 quickly from the beginning as done by MMKF is better since the performance of Exp1.S2 continued to degrade during the period of data collection. However, events like Exp2.S2 improving beyond the calibration point without drifting or Exp1.S1 deteriorating during the trial, for instance, due to connection loss, can still occur. In these events, the MMKFF will perform better than MMKF since it does not immediately converge to trusting one sensor over the others. Additionally, it is able to "forget"

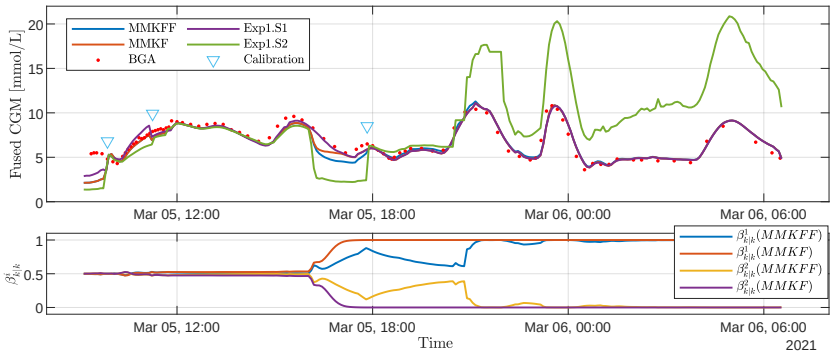

Fig. F.2: Results from Exp1. BGA represents the values from the blood gas analyser, and 'Calibration' represents points where sensors S1 and S2 were calibrated using the BGA values. The Upper plot shows a comparison between MMKFF and MMKF using the readings from Exp1.S1 and Exp1.S2, while the lower plot shows the trust values β^i in (F.8) for each of the sensors $i \in \{1, 2\}$.

past experiences which will enable it to adapt to new changes. This is shown in the findings for Exp2, where the MMKFF outperformed the MMKF in a more realistic case where the quality of the sensors varied over time. It is important to note that even though forgetting can offer better adaptivity to changes in the quality of sensors, it comes with the cost of slower reaction towards abrupt events as seen in Figure F.3. The lower the forgetting factor, the faster the reaction of MMKFF to abrupt events and vice versa.

5.3 Results from Exp2

Figure F.4 shows the results for three different excerpts of Exp2 compared to a fused CGM signal obtained by manually tuning a weighted average of the four CGMs in an online fashion (labeled Manual in the plots). In the first excerpt (left of the figure), the four sensors were all working as expected and readings were provided each 5 minutes. The MMKFF was the closest to the manually tuned signal. For the second excerpt (middle of the figure), Exp2.S3 was not working properly and stopped providing measurements towards the end. Additionally, Exp2.S2 was performing poorly with missing measurements and reporting readings which were close to 0 [mmol/L] while Exp2.S4 was performing better and close to Exp2.S1. This situation is challenging not only due to the missing and wrong readings of some sensors, but also due to the fact that our prior knowledge prefers Exp2.S1 and Exp2.S2 over Exp2.S3 and Exp2.S4. Despite these challenges, the MMKFF performed the best in the sense of being the closest to the manually tuned reading. Observe how both the MMKF and MMKFF reduced the trust value of Exp2.S4 when it stopped providing readings around 50 [min] of the excerpt. However, the MMKFF increased the trust value of Exp2.S4 when it started providing good readings again, unlike the MMKF. Moreover, the MMKFF started trusting Exp2.S2 more when its readings improved. For the third excerpt (right of the figure), Exp2.S3 was not providing any readings, and Exp2.S4 started providing readings around the time when Exp2.S1 and Exp2.S2

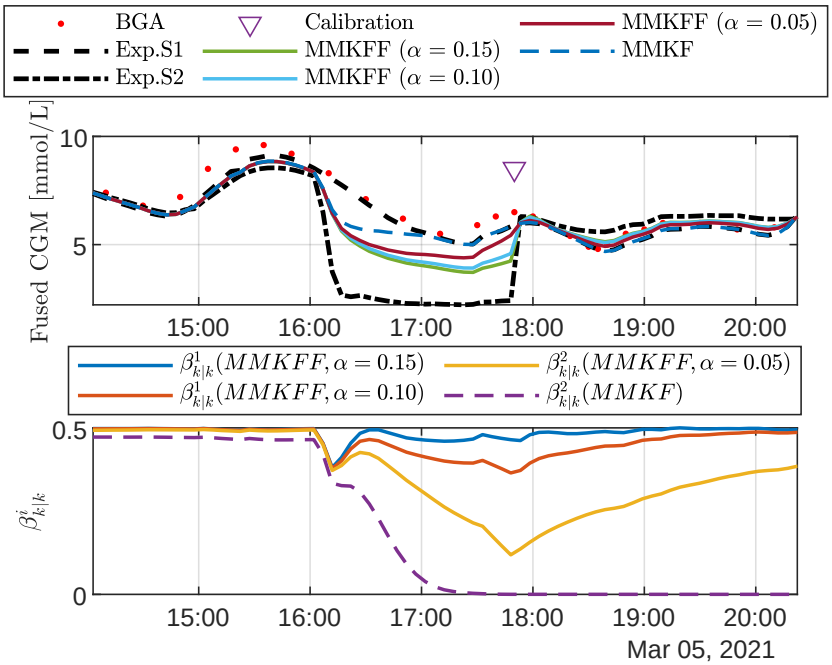

Fig. F.3: The upper plot shows the response of MMKFF and MMKF with different forgetting factors, while the lower plot shows the trust values.

stopped providing readings. Out of the four KFs, the MMKFF was still the closest to the manually tuned reading on average and had the lowest maximum ARE value. Additionally, notice how it was difficult for the MMKF to increase its trust value of EX2.S4 again when it was providing readings. On the other hand, the MMKFF increased the trust value of EX2.S4 when it started providing readings again. These results show how the MMKFF is able to adapt better to changes in the quality of the sensors.

6 Conclusion and Future Work

For CGM devices, the MMKFF fusing approach was introduced. The technique was evaluated using two separate sets of experimental data, and it was shown to be capable of producing a reliable fused CGM signal. It was demonstrated that MMKFF can respond to variations in the quality of the CGM readings more effectively when compared to other KF approaches. However, it was observed that MMKFF's ability for adaptation came at the expense of a slower reaction to sudden changes. Future studies could improve this by taking into account an adaptive forgetting factor for MMKFF. Additionally, the past data and inputs can be used

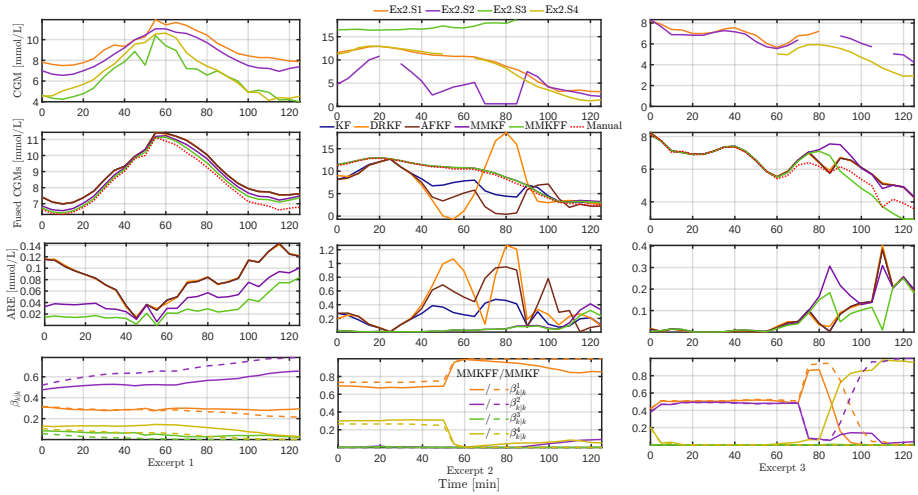

Fig. F.4: Results of fusion using four different glucose sensors in the Exp2, for three different excerpts (left, middle, right column). First row: Original glucose sensor values for sensors S1 to S4. Second row: Comparison of fused glucose sensor values for the various sensor fusion methods. Third row: ARE (absolute relative error with respect to manual sensor fusion). Fourth row: Trust values $\beta^i_{k|k}$ in (F.8), where solid lines are MMKFF and dashed lines are MMKF.

with the high gain observer suggested in [16] and [17] to estimate the BG levels when the sensor connection is lost. Evaluating the proposed fusing approach on additional data from various experiments can provide a better understanding of the strategy's performance and its likelihood of being applied in a human environment.

7 Acknowledgment

The experimental services were provided by the Comparative medicine Core Facility (CoMed), Norwegian University of Science and Technology (NTNU). CoMed is funded by the Faculty of Medicine at NTNU and Central Norway Regional Health Authority. The transmitters (for Exp1 and Exp2) and the hormone infusion systems in Exp1 were provided by Inreda Diabetic BV (Goor, the Netherlands). We want to thank Marte Kierulf Åm, Oddveig Lyng, and Patrick Christian Bösch for their invaluable contribution to the data collection. We also thank Professor Sven Magnus Carlsen for his help in experimental design and discussions.

References

[1] A. Facchinetti, "Continuous glucose monitoring sensors: past, present and future algorithmic challenges," *Sensors*, vol. 16, no. 12, p. 2093, 2016.

[2] P. G. Jacobs, J. El Youssef, J. Castle *et al.*, "Automated control of an adaptive bihormonal, dual-sensor artificial pancreas and evaluation during inpatient studies," *IEEE Trans Biomed Eng*, vol. 61, no. 10, pp. 2569–2581, 2014.

[3] A. Facchinetti, S. Del Favero, G. Sparacino, J. R. Castle, W. K. Ward, and C. Cobelli, "Modeling the glucose sensor error," *IEEE Transactions on Biomedical Engineering*, vol. 61, no. 3, pp. 620–629, 2013.

[4] A. Facchinetti, S. Del Favero, G. Sparacino, and C. Cobelli, "Model of glucose sensor error components: identification and assessment for new dexcom g4 generation devices," *Medical & biological engineering & computing*, vol. 53, no. 12, pp. 1259–1269, 2015.

[5] M. Vettoretti, C. Battocchio, G. Sparacino, and A. Facchinetti, "Development of an error model for a factory-calibrated continuous glucose monitoring sensor with 10-day lifetime," *Sensors*, vol. 19, no. 23, p. 5320, 2019.

[6] E. J. Knobbe and B. Buckingham, "The extended kalman filter for continuous glucose monitoring," *Diabetes technology & therapeutics*, vol. 7, no. 1, pp. 15–27, 2005.

[7] M. Kuure-Kinsey, C. C. Palerm, and B. W. Bequette, "A dual-rate kalman filter for continuous glucose monitoring," in *2006 International Conference of the IEEE Engineering in Medicine and Biology Society*. IEEE, 2006, pp. 63–66.

[8] A. Facchinetti, G. Sparacino, and C. Cobelli, "Enhanced accuracy of continuous glucose monitoring by online extended kalman filtering," *Diabetes technology & therapeutics*, vol. 12, no. 5, pp. 353–363, 2010.

[9] M. Halvorsen, K. D. Benam, H. Khoshamadi, and A. L. Fougner, "Blood glucose level prediction using subcutaneous sensors for in vivo study: Compensation for measurement method slow dynamics using kalman filter approach," in *2022 IEEE 61st Conference on Decision and Control (CDC)*. IEEE, 2022, pp. 6034–6039.

[10] K. D. Benam, H. Khoshamadi, M. K. Åm, Ø. Stavdahl, S. Gros, and A. L. Fougner, "Identifiable prediction animal model for the bi-hormonal intraperitoneal artificial pancreas," *Journal of Process Control*, vol. 121, pp. 13–29, 2023.

[11] G. De Nicolao, G. Sparacino, and C. Cobelli, "Nonparametric input estimation in physiological systems: Problems, methods, and case studies," *Automatica*, vol. 33, no. 5, pp. 851–870, 1997.

[12] D. Magill, "Optimal adaptive estimation of sampled stochastic processes," *IEEE Transactions on Automatic Control*, vol. 10, no. 4, pp. 434–439, 1965.

[13] Y. Bar-Shalom, X. R. Li, and T. Kirubarajan, *Estimation with applications to tracking and navigation: theory algorithms and software*. John Wiley & Sons, 2004.

[14] S. Wang and Z.-S. Ye, "Distributionally robust state estimation for linear systems subject to uncertainty and outlier," *IEEE Transactions on Signal Processing*, vol. 70, pp. 452–467, 2022.

[15] Q. Xia, M. Rao, Y. Ying, and X. Shen, "Adaptive fading kalman filter with an application," *Automatica*, vol. 30, no. 8, pp. 1333–1338, 1994.

[16] K. D. Benam, H. Talebi, and M. A. Khosravi, "Full order high gain observer design for image-guided robotic flexible needle steering," in *2019 27th Iranian Conference on Electrical Engineering (ICEE)*. IEEE, 2019, pp. 1151–1156.

[17] K. D. Benam, H. Khoshamadi, L. Lema-Pérez, S. Gros, and A. L. Fougner, "A nonlinear state observer for the bi-hormonal intraperitoneal artificial pancreas," in *2022 44th Annual International Conference of the IEEE Engineering in Medicine & Biology Society (EMBC)*. IEEE, 2022, pp. 171–176.

Paper G

An Online Stochastic Optimization Approach for Insulin Intensification in Type 2 Diabetes with Attention to Pseudo-Hypoglycemia

Mohamad Al Ahdab, Torben Knudsen, Jakob Stoustrup, and John Leth.

The paper has been published in the
2022 61th IEEE Conference on Decision and Control (CDC),pp. 2572-2579, 2022.

Abstract

In this paper, we present a model free approach to calculate long-acting insulin doses for Type 2 Diabetic (T2D) subjects in order to bring their blood glucose (BG) concentration to be within a safe range. The proposed strategy tunes the parameters of a proposed control law by using a zeroth-order online stochastic optimization approach for a defined cost function. The strategy uses gradient estimates obtained by a Recursive Least Square (RLS) scheme in an adaptive moment estimation based approach named AdaBelief. Additionally, we show how the proposed strategy with a feedback rating measurement can accommodate for a phenomena known as relative hypoglycemia or pseudo-hypoglycemia (PHG) in which subjects experience hypoglycemia symptoms depending on how quick their BG concentration is lowered. The performance of the insulin calculation strategy is demonstrated and compared with current insulin calculation strategies using simulations with three different models.

1 Introduction

Subjects with type 2 diabetes (T2D) experience elevated levels of blood glucose (BG) concentrations known as hyperglycemia due to an imbalance between their insulin secretion rate and the effectiveness of insulin to lower glucose concentration. If high BG concentrations are left untreated, subjects can develop complications such as cardiovascular diseases, eyesight damage, and more. The treatment procedure for T2D initially begins with lifestyle changes and oral medications. However, when these methods are insufficient to lower BG concentrations, T2D subjects can begin to administer long acting insulin, for example once daily using insulin pens, based on self monitored blood glucose measurements (SMGB) of Fasting BG (FBG). The insulin treatment initially aims at finding the optimal insulin (insulin intensification/titration) dose to keep BG concentration within a safe range. This process is clinically challenging since subjects with T2D are different on a behavioural and a physical level. Moreover, administrating too much insulin can lead to low BG levels known as hypoglycemia which can cause blurred vision, fainting, or death in severe cases. On the other hand, not administrating enough insulin will cause the subject to remain in hyperglycemia for extensive periods of time. In addition to these challenges, T2D subjects can experience symptoms of hypoglycemia even when they have a BG level above the clinical level of hypoglycemia. This phenomena is referred to as relative hypoglycemia or Pseudo-HypoGlycemia of Type I (PHG) [1, 2]. PHG happens when T2D patients reduce their FBG aggressively after staying at a fixed level for a period of time. Due to these challenges, several attempts were made to use automated insulin dose calculators for T2D. Standard of care insulin guidance algorithms such as the ones in [3] are based on SMBG measurement to decide on a fixed insulin dose weekly. These titration strategies can take a long time to bring FBG concentrations to a safe level. While this can be beneficial to avoid PHG, it is still conservative since T2D subjects are different from each other and long titration periods can be limiting for subjects which can have their FBG levels lowered more quickly. Other titration algorithms based on control theory exists in the literature such as [4] which is model based and [5] which is model free. The work in [4] relies on a model which can be limiting and challenging to apply for a wide range of T2D subjects. Additionally, the algorithms lower the FBG concentration aggressively which can be problematic for PHG. On

the other hand, the work in [5] proposed to use an Extremum Seeking Control (ESC) strategy to alleviate the need for a detailed model of T2D subjects and demonstrated the effectiveness of such approach. Nevertheless, the strategy was tested against one model only and with limited variation on the parameters without measurement noise. Additionally, the strategy lowers the FBG aggressively for all subjects without consideration for PHG. The contributions in this paper are as follows:

- We propose a model free strategy which handles measurement noise on SMBG. Additionally, we test the strategy for three different models. Namely, the model which was used in [5], an extended version of it from [6], and a model based on the high fidelity model [7]. The strategy was shown in simulation to be more robust to parameter variations than the recently proposed model free approach in [5].
- We investigate the possibility of designing our strategy to handle PHG in insulin titration, which to our knowledge, never has been done before. The idea for handling PHG is inspired by the recent works of including human ratings as feedback in control strategies as done in [8]. We propose to use a score in the calculation of insulin doses, provided by the T2D subjects, and/or their medical professionals on a daily basis reflecting their well-being with respect to PHG symptoms.
- We propose a zeroth-order online optimization approach for a defined cost to tune the parameters of a chosen feedback control law. The method uses the recently proposed adaptive moment estimation algorithm AdaBelief [9] with gradient information provided by a RLS.

The paper is structured as follows. Section 3.1 explains the setup of the problem. Sections 3.2 and 3.3 provide a description on a directional forgetting RLS and the AdaBelief strategy in the context of tuning the control law parameters, respectively. Section 3.4 then defines the cost functions which we aim to minimize in order to tune the control law parameters. After that, we propose a simulation model for PHG in section 4.1 and provide a discussion on the used glucose-insulin models for simulation in section 4.2. Finally, we present the simulation results in section 5 and provide a conclusion in section 6.

2 Notations

The symbol := indicates "defined by". All vectors are considered as column vectors, $\|\cdot\|$ denotes the 2-norm, and $^{\mathrm{T}}$ denotes transpose. All probabilistic considerations in this paper will be with respect to an underlying probability space $(\Omega, \mathcal{F}, \mathbb{P})$ and *every statement will be understood to be valid with probability 1.* We let $L_l^2 = L_l^2(\Omega, \mathcal{F}, \mathbb{P})$ denote the set of l-valued measurable maps $f : \Omega \to \mathbb{R}^l$ with $\mathbb{E}[\|f\|^2] < \infty$. For a random variable x we write $\mathsf{x} = x(\omega)$ for the realization of the random variable. For probability distributions, we use $Beta(\alpha, \beta)$ to denote the beta distribution with parameters α and β, $\mathcal{N}(\mu, \Sigma)$ to denote the normal distribution with mean μ and covariance Σ, $\mathcal{U}(a, b)$ for a continuous uniform distribution with bounds a and b, and $\mathcal{U}\{a, b\}$ for a discrete uniform distribution with bounds a and b. If the difference between two consecutive time instants t_k and t_{k+j} is such that $t_{k+j} - t_k = jT,\ j, k \in \mathbb{N}$ with $T \in \mathbb{R}$ being a constant, then variables that are indexed with time $x(t_k), x(t_{k+j})$ will be denoted by $x(k), x(k+j)$ for ease of notation. We write $\{a : s : b\}$ for a sequence of numbers going from

a to b equally spaced by s. We let $[a, b]$ denote the closed interval from a to b, and $[a\ b]$ denote the row vector with coordinates a and b. For a diagonal matrix A with diagonal entries $a = [a_1 \cdots a_n]^{\mathrm{T}}$, the notation $A = \mathrm{diag}(a)$ is used. The symbol I_n is used to denote the $n \times n$ identity matrix and the symbol $\mathbf{1}$ is used to denote a vector of ones. Finally, a projection operator is defined as $\Pi_{\Theta,\Sigma}(x) := \mathrm{argmin}_{\theta\in\Theta}\|\Sigma^{1/2}(\theta - x)\|$ with Σ a positive definite matrix and Θ a compact set.

3 Control Strategy

3.1 Problem Specification

In this section we present the aim and the proposed strategy for insulin titration. We assume that the insulin-glucose dynamics of a T2D subject can be modeled according to the following general form

$$x(k+1) = f(x(k), \Delta u(k), w(k)), \tag{G.1a}$$

$$\Delta u(k) = \frac{K_p}{1 + K_s e_s(k)} e_g(k), \tag{G.1b}$$

$$y(k) = h(x(k), v(k)), \tag{G.1c}$$

$$z(k) = c(y(k)), \tag{G.1d}$$

where $x(k) \in \mathbb{R}^n$ are internal states, $w(k)$ being a sufficiently regular stochastic process (see Remark 3.1), $\Delta u(k)$ is the change of the insulin dose size $u(k)$ [U] at day k such that $u(k) = \max\big(\Delta u(k) + u(k-1), 0\big)$ with the feedback control law (G.1b) parameterized with $\theta = [K_p\ K_s]^{\mathrm{T}} \in \Theta \subseteq \mathbb{R}^2$, $y(k) = [y_g(k)\ y_s(k)]^{\mathrm{T}} \in \mathbb{R}^2$ represents the SMBG measurement $y_g(k)$ and the PHG score $y_s(k)$ at day k, the measurement noise $v(k)$ is an i.i.d. stochastic process independent of $w(k)$, $e_g(k) := r - y_g(k)$ with r being a reference, $e_s(k) := (H - y_s(k))/H$ with $H \in \mathbb{R}_{>0}$ being the maximum score for a PHG scale used by the subjects as a feedback method for their hypoglycemia symptoms. The maximum score H means no hypoglycemia symptoms were experienced by the subjects. See Section 4.1 for more details. The variable $z(k) \in \mathbb{R}$ is the value of a cost function $c(y(k))$ we desire to minimize. We write $x(k;\theta)$, $y(k;\theta)$ and $z(k;\theta)$ whenever the dependency on the control parameter is relevant.

Remark 3.1. *The structure in (G.1) represents a vast variety of models in the current literature e.g., the ones in [5, 6] where w represents white noise in [5], a jump process in [6], and v represents white noise in [6].*

We assume that the functions f, h, g are sufficiently regular e.g., Lipschitz continuous which is a typical assumptions for biological systems. Now for ease of notation let q denote either x or y. We then assume that there exists[1] $\Theta \subseteq \mathbb{R}^2$ with $0 \in \Theta$ such that for every $\theta \in \Theta$ we have $q(k;\theta) \in L_l^2$, $(l = 2, n)$, $\|q(k;\theta)\| \leq \tilde{q}$ for some $\tilde{q} \in L_1^2$, and $\lim_{k\to\infty} q(k;\theta) = q^*$ with probability 1. Note that q^* depends on θ, and that by dominated convergence we obtain $q^* \in$

[1] In application/simulation Θ can often be obtained by a conservative guess.

L_l^2, $\lim_{k\to\infty}\mathbb{E}[\|q(k)-q^*\|^2]=0$, and $\lim_{k\to\infty}\mathbb{E}[q(k)]=\mathbb{E}[q^*]$. Let $\bar{c}(k,\theta):=c\left(y\left(k;\theta\right)\right)+c_\theta(k,\theta)$ with $c_\theta(k,\theta)$ being a known (in closed form) differentiable cost in θ, we aim to find a sequence of estimates $\{\hat{\theta}(k)\}_{k\in\mathbb{N}}$ in Θ which tracks the sequence $\{\theta^*(k)\}_{k\in\mathbb{N}}$ that solves the following

$$\theta^*(k)=\underset{\theta\in\Theta}{\operatorname{argmin}}\ \bar{c}(k+1,\theta). \tag{G.2}$$

This problem can be thought of as a tracking problem where a pursuer $\hat{\theta}(k)$ tries to track a target $\theta^*(k)$. For each $\hat{\theta}(k)$, an inexact gradient $\hat{g}(k+1)$ will be estimated based on $\bar{c}\left(k+1,\hat{\theta}(k)\right)$. The pursuer will then use $\hat{g}(k+1)$ to obtain an estimate $\hat{\theta}(k+1)$. This problem is known as zeroth-order online optimization in the bandit setting. The term zeroth-order refers to the fact that for every estimate $\hat{\theta}(k)$ we only obtain a cost function value information. Note that by assumption, the sequence $\theta^*(k)$ will converge (with probability 1) to a random variable θ^*. See the works in [10–12] for convergence analysis in a related setting. For the work in this paper, we use an adaptive moment based method named AdaBelief [9] for a gradient based optimization as detailed in section 3.3. For the gradient estimates, we assume a local linear model for the cost $z(k)=c\left(y(k,\hat{\theta}(k-1))\right)$.

$$z(k;\hat{\theta}(k-1))\approx[\hat{\theta}^{\mathrm{T}}(k-1)\ \mathbf{1}^{\mathrm{T}}]\begin{bmatrix}g_z(k)\\ b(k)\end{bmatrix}:=\phi^{\mathrm{T}}(k)\psi(k), \tag{G.3}$$

where $g(k)=g_z(k)+\nabla_\theta c_\theta(k,\hat{\theta}(k-1))$ represents an approximate for the gradient $\nabla_\theta\bar{c}(k,\hat{\theta}(k-1))$, and $b(k)$ is a bias term. A recursive least squares (RLS) strategy can then be used to obtain an estimate $\hat{g}_z(k)$ as described in section 3.2.

3.2 Estimating the gradient with RLS

For the estimation of the gradient, (G.3) is used in an RLS with exponential forgetting setting. Least square estimation with exponential forgetting aims at finding the value $\hat{\psi}$ which minimizes $\sum_{i=0}^{k}\lambda^{k-i}\left(\mathrm{z}(i)-\boldsymbol{\phi}^{\mathrm{T}}(i)\hat{\boldsymbol{\psi}}(i)\right)^{\mathrm{T}}\left(\mathrm{z}(i)-\boldsymbol{\phi}^{\mathrm{T}}(i)\hat{\boldsymbol{\psi}}(i)\right)$ with $\lambda\in(0,1]$ being a forgetting factor. The forgetting factor is used to put more emphasis on recent incoming data when compared to old one. This makes it useful for estimating time varying parameters such as the gradient $g(k)$ which we aim to estimate. Additionally, it is known that without persistent excitation in $\phi(k)$ (see [13] for more details), the covariance $P:=\mathbb{E}\left[(\psi-\hat{\psi})^{\mathrm{T}}(\psi-\hat{\psi})\right]$ can become unbounded. We can ensure persistence by adding a small dither to our control law parameters $\hat{\theta}(k)$. Moreover, to further ensure the boundedness of the covariance matrix regardless of the persistent excitation condition, we apply the directional forgetting RLS algorithm proposed in [14]. The recursive estimation is summarized in Algorithm 6. Note that the algorithm includes an update step for the information matrix $R(k)$ separately from $P(k)$ to avoid computing $P^{-1}(k)$ in the calculation of $\bar{P}(k)$ and $M(k)$.

The matrix M in the RLS strategy applies the forgetting factor λ on a subspace of the column space of the information matrix R, for details see [14].

Algorithm 6: RLS with directional forgetting

Input: Estimates $\hat{\psi}(k-1)$ with covariance matrix $P(k-1)$ and $R(k-1) = P^{-1}(k-1)$, regressor $\boldsymbol{\phi}(k)$ and measurement $\mathrm{z}(k)$, forgetting factor $\lambda \in (0, 1]$, and a threshold ϵ_ϕ (chosen to be in the order of the minimum added dither) to stop forgetting when $\|\boldsymbol{\phi}(k)\| < \epsilon_\phi$.

Output: $\hat{g}(k)$ as a component in $\hat{\psi}(k)$, $P(k)$ and $R(k)$.

if $\|\boldsymbol{\phi}(k)\| \geq \epsilon_\phi$ **then**

$\quad \bar{P}(k) = P(k-1) + \frac{1-\lambda}{\lambda}\left(\boldsymbol{\phi}(k)R(k-1)\boldsymbol{\phi}^{\mathrm{T}}(k)\right)^{-1}\boldsymbol{\phi}^{\mathrm{T}}(k)\boldsymbol{\phi}(k)$

$\quad M(k) = (1-\lambda)\frac{R(k-1)\boldsymbol{\phi}(k)\boldsymbol{\phi}^{\mathrm{T}}(k)}{\boldsymbol{\phi}^{\mathrm{T}}(k)R(k-1)\boldsymbol{\phi}(k)}$

else

$\quad \bar{P}(k) = P(k-1)$

$\quad M(k) = 0$

$K_f(k) = \bar{P}(k)\boldsymbol{\phi}(k)\left(1 + \boldsymbol{\phi}^{\mathrm{T}}(k)\bar{P}(k)\boldsymbol{\phi}(k)\right)^{-1}$

$\hat{\psi}(k) = \hat{\psi}(k-1) + K_f(k)\left(\mathrm{z}(k) - \boldsymbol{\phi}^{\mathrm{T}}(k)\hat{\psi}(k-1)\right)$

$P(k) = \bar{P}(k) - \bar{P}(k)\boldsymbol{\phi}(k)\left(1 + \boldsymbol{\phi}^{\mathrm{T}}(k)\bar{P}(k)\boldsymbol{\phi}(k)\right)^{-1}\boldsymbol{\phi}^{\mathrm{T}}(k)\bar{P}(k)$

$R(k) = (\mathrm{I} - M(k))R(k-1) + \boldsymbol{\phi}(k)\boldsymbol{\phi}^{\mathrm{T}}(k)$

3.3 Gradient Decent Strategy

Due to the stochastic nature of the problem and the fact that our gradient estimates are noisy, we propose to use a stochastic optimization method with an adaptive step size. Adaptive moment based strategies such as Adam and its variants [15] have gained wide interest in the field of deep learning as methods to perform stochastic optimization. Additionally, the work in [16] proposed to use the original Adam in an ESC scheme to adapt the step size based on the estimated gradient. However, the original Adam can diverge even for a convex optimization problem [15]. In this work, we propose to use AdaBelief, a variant of Adam [9]. In [9], AdaBelief was shown to combine the fast convergence of Adam based strategies with the good generalization of stochastic gradient decent strategies. The online stochastic optimization based AdaBelief strategy (AdaOS) is presented in Algorithm 7. To get an intuition of how AdaOS works, we note that $m(k)$ is an exponential moving average (the output of a first order low pass filter) for the gradient estimate $\hat{\mathrm{g}}(k)$. Thus, the algorithm produces a smoother version $\hat{m}(k)$ of the estimated gradient $\hat{g}(k)$. As for $s(k)$, it reflects the difference between the gradient estimate $\hat{\mathrm{g}}(k)$ and our "belief" $m(k)$ such that, for an increased difference, the stepping size $\alpha/\left(\sqrt{\hat{s}(k)} + \epsilon\right)$ will decrease and vice versa. In this paper, the parameters for the algorithm are chosen to be $\alpha = 10^{-3}$, $\beta_1 = 0.99$, $\beta_2 = 0.999$ and $\epsilon = 10^{-8}\mathbf{1}$ which are the typical parameters used in [9] for AdaBelief and Adam based strategies in practice [15]. Additionally,

Algorithm 7: AdaOS algorithm

parameter: Parameter $\alpha > 0$, smoothing parameters $0 \leq \beta_1 \leq 1$ and $0 \leq \beta_2 \leq 1$, vector of small numbers ϵ, and projection $\Pi_{\Theta,\Sigma}(x) = \text{argmin}_\theta \|\Sigma^{1/2}(\theta - x)\|$. Note that all the operations in the algorithm are element-wise.

Input: initial moments $m(0) = 0$ and $s(0) = 0$.

Output: $\hat{\theta}(k)$

1 k=0

2 **while** *Ongoing Titration* **do**

3 $k \leftarrow k + 1$

4 Run RLS to obtain $\hat{\text{g}}_z(k)$.

5 $\hat{\text{g}}(k) = \hat{\text{g}}_z(k) + \nabla_\theta c_\theta(\hat{\theta}(k-1))$.

6 $m(k) = \beta_1 m(k-1) + (1-\beta_1)\hat{\text{g}}(k)$

7 $s(k) = \beta_2 s(k-1) + (1-\beta_2)(m(k) - \hat{\text{g}}(k))^2 + \epsilon$,

8 $\hat{m}(k) = \frac{m(k)}{1-\beta_1^k}, \hat{s}(k) = \frac{s(k)}{1-\beta_2^k}$, (Bias-Correction.)

9 $\hat{\theta}(k) = \Pi_{\Theta,\text{diag}(\hat{s}(k))}\left(\hat{\theta}(k-1) - \alpha\frac{\hat{m}(k)}{\sqrt{\hat{s}(k)}+\epsilon}\right)$

we choose $\Theta = [0\ 2]^2$ for the control law parameters.[2] The step in line 7 of the algorithm is used to correct for the initialization bias.

3.4 Cost function definition

The main aim of the control strategy is to bring the glucose concentration $y_g(k)$ to a safe level. For this objective, we propose the following cost function

$$c_g(k) = \left(e_g(k)/r\right)^2, \tag{G.4}$$

Note that the division by r was made to scale $c_g(k)$ to be of order 1. The safe range of FBG is chosen to be between 4 [mmol/L] and 6 [mmol/L] according to the standard of care for insulin titration strategies [3]. Therefore, we choose the reference $r = 5.5$ [mmol/L]. Note that the reference is chosen to be larger than the middle of the range [4 6] [mmol/L] since hypoglycemia (FBG concentrations below 4 [mmol/L]) are more dangerous than hyperglycemia. Additionally, we use the following cost to penalize FBG concentrations which are within the hypoglycemic range

$$c_h(k) = \text{softmin}\left(e_g(k), 0\right)^2, \tag{G.5}$$

[2]Simulation results show that all parameters in Θ give rise to a stable behaviour.

where softmin is the soft minimum function.[3] Moreover, to keep the PHG score y_s as high as possible, the following is used

$$c_s(k) = \left(e_s(k)\right)^2. \tag{G.6}$$

The cost in measurements is then chosen as $c(y(k)) = c_g(k) + 10c_h(k) + 10c_s(k)$. In addition to the cost in measurement, we include a cost which is more related to our setup of the optimization scheme. Namely, we consider the cost $c_\theta(k,\theta) = 0.5\left\|\theta - \hat{\theta}(k-2)\right\|^2$ in order to ensure a smooth change in the decision variables between iterations and to ensure that $\hat{\theta}(k) = \hat{\theta}(k-1)$ when $e_s(k) = 0$ and $e_g(k) = 0$. Finally, the total cost is $\bar{c}(k,\theta) = c\left(y(k)\right) + c_\theta(k,\theta)$.

4 Simulation Models

In this paper, we use simulations in order to test and validate the developed titration strategy. In this section, we first describe the development of a model to simulate the PHG scores provided by T2D subjects during their treatment in Section 4.1. Afterwards, we describe three different models used to simulate the glucose-insulin dynamics in Section 4.2.

4.1 PHG score model

For the PHG scores, we assume that at each day k the T2D subjects will provide a score $y_s(k) \in [0, H]$ if a continuous scale is used or $y_s(k) \in \{0, \ldots, H\}$ if a discrete scale is used. If the subjects were experiencing no hypoglycemia symptoms then they would provide the maximum score H. On the other hand, if the subjects were experiencing severe hypoglycemia symptoms then they would provide the minimum score 0. The determination of the range of symptoms and what they correspond to on the scale can be assigned by the medical professionals. See the study in [17] for an example. We intend in this section to develop a general simulation model for PHG scores which can then be used together with simulated T2D subjects. This model is used to test if the strategy can work with a feedback score which correlates with how rapid the BG concentration is lowered. The PHG simulation model should also take into account that subjects may react differently to how rapid their BG is being lowered. Following the observations that patients who have been staying at a high BG concentration level for a period of time can develop hypoglycemia like symptoms when BG are decreased aggressively, we first define the BG decrease ratio $x_r(k)$ as following

$$x_r(m) := \max\left(\frac{x_g(m)}{\mu(m)}, 1\right), \quad \mu(m) = \frac{1}{h'}\sum_{i=m-h'}^{m} x_g(i), \tag{G.7}$$

where $x_g(m)$ [mmol/L] is the BG concentration at minute mT_m with T_m being a sampling time in the order of minutes, and $h' = \frac{24\times 60}{T_m}h$ with h [Day] being a time window for the moving average $\mu(m)$ which captures the history of the BG concentration for the T2D subjects. If the BG levels do not change significantly when compared to the moving average $\mu(m)$ then the value

[3] $\text{softmin}(x_1, x_2) = -\frac{1}{a}\log(\exp(-ax_1) + \exp(-ax_2))$, with a being a constant chosen as 50 in this paper.

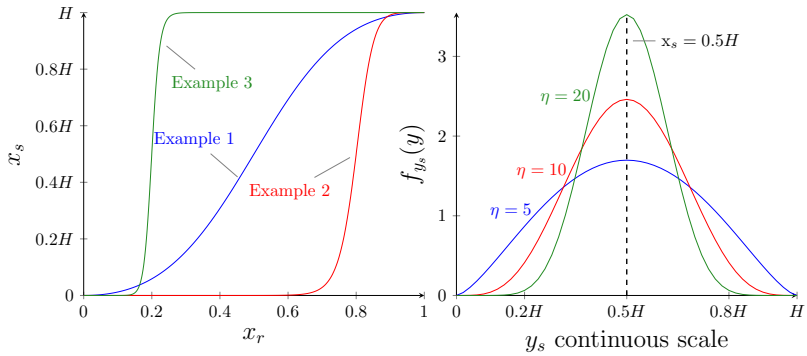

Fig. G.1: Left: Three different examples of the noise-free PHG score x_s. Example 1: $\rho = 2$ and $d = 0.5$. Example 2: $\rho = 5$ and $d = 0.8$. Example 3: $\rho = 20$ and $d = 0.2$. **Right**: The density function of y_s with a continuous scale given $\mathrm{x}_s = 0.5H$ for different values of η.

of $x_r(m)$ is close to 1. However, when the BG level drops significantly compared to the previous history of BG levels (captured in the moving average $\mu(m)$), the value of $x_r(m)$ will be closer to 0. The BG decrease ratio $x_r(m)$ models the aggressiveness of lowering BG concentration. Now, in order to also take into account that subjects with T2D react differently to the drop of their BG concentration, we define the function $\mathrm{sig}_{\rho,d} : [0,1] \to [0,1];\ x \mapsto \mathrm{sig}_{\rho,d}(x)$ as

$$\mathrm{sig}_{\rho,d}(x) := \begin{cases} \frac{1}{1+\left(\frac{x^{-\log(2)/\log(d)}}{1-x^{-\log(2)/\log(d)}}\right)^{-\rho}}, & x \in [0,1) \\ 1, & x = 1 \end{cases} \tag{G.8}$$

with ρ being a constant representing the sensitivity for different $x_r(k)$, and d is the value such that $\mathrm{sig}_{\rho,d}(d) = 0.5$. Finally, the noise-free PHG score is defined as

$$x_s(k) := H\mathrm{sig}_{\rho,d}(x_r(k)) \tag{G.9}$$

Figure G.1 shows three different examples of noise-free x_s versus BG decrease ratios x_r for three different subjects. In Example 1, the range of BG decrease ratio x_r in which the subject reacts to with different scores is the widest ($\rho = 2$), While in Example 3, the subject has the narrowest range ($\rho = 20$). In Example 2, the subject has the lowest tolerance for BG decrease ratio ($d = 0.8$), while the subject in Example 3 has the highest tolerance ($d = 0.2$). With the shape parameters d and ρ, one can construct a wide variety of sigmoidal curves which enables us to model different possibilities of subjects reacting to their BG decrease ratio. To model noises and disturbances on the PHG score, let $\zeta(k) \sim Beta\left((x_s(k)/H)\eta, (1 - x_s(k)/H)\eta\right)$, then the PHG score measurements are $y_s(k) = H\zeta(k)$ if continuous scales are used, or $y_s(k) = \mathrm{round}\left(H\zeta(k)\right)$ if discrete scales are used. Note that given the realization $x_s(k) = \mathrm{x}_s$, then $\mathbb{E}[H\zeta(k)] = \mathrm{x}_s$ and $\mathrm{Var}(H\zeta(k)) = \frac{\mathrm{x}_s(H-\mathrm{x}_s)}{1+\eta}$, this means that the parameter η can be viewed as a precision parameter in the sense that for a fixed $x_s(k)$, the larger η is the smaller is the variance and

vice versa. Figure G.1 shows the probability density function of a continuous scale y_s given $\mathrm{x}_s = 0.5H$.

Additionally in simulation, if T2D subjects report a lower score when their BG is actually in the hypoglycemia region, then the PHG score is ignored since it is clearly not a case of PHG.

4.2 Glucose-Insulin Simulation Models

For the glucose-insulin dynamic simulations in this paper, we consider three different simulation models. The first model, denoted "Model 1", is the same model used in [5]. Model 1 considers FBG only and it will be used in Section 5.2 for a detailed comparison with the insulin titration strategy presented in [5]. As for the second model, denoted "Model 2", we use an extension of Model 1 in order to consider BG concentrations by using a jump diffusion model for meals and disturbances [6]. The average meal rate in the jump part is chosen to be 3 [Meals/Day] between the hours 7:00 and 23:00 and 0.1 [Meals/Day] otherwise to consider that subjects eat less frequently at night. As for the diffusion part, a constant diffusion is added to the BG concentration state. The third model denoted as "Model 3" is the high fidelity model [7]. The meal times for Model 3 are drawn from uniform distributions as following: $\mathcal{U}(6,8)$ [h] for breakfast meals, $\mathcal{U}(12,14)$ [h] for lunch meals, and $\mathcal{U}(19,20)$ [h] for dinner meals. The carbohydrate intake for each meals is also drawn uniformly according to $\mathcal{U}(10,25)$ for breakfast, $\mathcal{U}(20,30)$ for lunch, and $\mathcal{U}(25,45)$ for dinner. We choose to simulate meals differently for Model 3 to test the strategies against a different type of stochastic disturbances. Moreover, we consider an SMBG measurement error model [18] for "Model 2" and "Model 3" as following

$$y_s(k) = x_g(k) + \sigma_s\left(x_g(k)\right)\varepsilon_s(k), \tag{G.10a}$$

$$\sigma_s\left(x_g\right) = \frac{1}{\kappa}\sigma_2 \log\left(1 + \mathrm{e}^{\kappa\left(x_g - 4.2\right)}\right) + \sigma_1, \tag{G.10b}$$

with σ_1 and σ_2 chosen in accordance to the ISO standard [19] to be $\sigma_1 = 0.415$ [mmol/L] and $\sigma_2 = 0.1$, and $\kappa = 5$. We did not add measurement noises to "Model 1" since the model is intended for a detailed comparison with the strategy in [5] and we want to have the same model used in [5] which did not consider measurement noises. Table G.1 summarizes the models used for simulations in this paper.

Table G.1: Glucose-insulin simulation models used in the paper

Model 1	Based on [5]. Does not include a measurement noise model. Simulates FBG concentrations only. Includes process noise. Intended to be used for a detailed comparison with [5] in Section 5.2
Model 2	Based on [6]. Includes a measurement error model.
Model 3	Based on the model from [7]. Meals times and their sizes are drawn from uniform distributions. Includes a measurement error model. A diffusion term matching the one in [6] is added to the state corresponding to BG concentration.

5 Results and Discussion

In this section, we simulate our proposed strategy with different scenarios and compare it with three different strategies. The first strategy is the extremum seeking control strategy proposed in [5] denoted as ESC[4]. As for the second (denoted as 202) and third (denoted as Step) strategies, we use the standard of care titration strategies from [3] shown in Table G.2. The 202 strategy adjusts the dose weekly based on the last day SMBG measurement while the Step strategy adjusts the dose weekly based on an average of the last three days SMBG measurements. For our strategy, we simulate it with five different scenarios as following

Table G.2: Standard of care titration strategies.

Strategy	SMBG [mmol/L]	Dose adjustment Δu[U]
202	> 6	$+2$
	$4 - 6$	No change
	< 3.9	-2
Step	> 9	$+8$
	$8 - 8.9$	$+6$
	$7 - 7.9$	$+4$
	$5 - 6.9$	$+2$
	$3.9 - 4.9$	No change
	$3.1 - 3.8$	-2
	< 3.1	-4

- **AdaOS**: Default strategy. Initial conditions $\hat{K}_p(0) = 0.3$, $\hat{K}_s(0) = 1$. A continuous score scale $y_s \in [0, H]$ is used with $H = 10$.
- **AdaOS-H5**: Same as AdaOS but with a discrete score scale $y_s \in \{0, 1, \ldots, H\}$ with $H = 5$.
- **AdaOS-F**: same as AdaOS but $\hat{K}_s = 0$ (No PHG feedback) and $\hat{K}_p(0) = 0.8$.
- **AdaOS-pf**: Same as AdaOS but subjects do not provide a PHG score on day k with a probability p_f. If the subjects do not provide a score on day k, then $y_s(k) = y_s(k-1)$.
- **AdaOS-C**: Same as AdaOS-F and it is intended to be compared mainly with ESC (similar settings to ESC) in section 5.2. The reference is adjusted to be $r = 5$ [mmol/L] to match the one in ESC. The parameter $\hat{K}_p(0)$ is chosen to match the initial insulin dose for ESC in [5].

For all the scenarios, we let $\hat{\psi}(0) = [0\ 0]^{\mathrm{T}}$, $P = \mathrm{I}$, $\lambda = 0.9$, $\epsilon_\phi = 10^{-3}$, and additive dithers on $\hat{K}_p(k)$ and $\hat{K}_s(k)$ chosen as $0.01\,\mathrm{square}(10k)$, with $\mathrm{square}(x) = \mathrm{sign}(\sin(x))$. Note that the choice of $\hat{K}_p(0)$ is important for the performance of the strategy. If it is chosen to be high, then

[4]The sign of the gradient step was written to be positive in equation 6 in [5] in a gradient *decent* setup. Therefore, we used a negative sign instead since it is clearly a typo. Especially since the algorithm performed poorly when a positive sign is used.

the initial insulin doses would be high which can lower glucose concentrations too fast for the the estimation of $\hat{K}_s$ to catch up. This is especially due to the fact that K_s has its main effect during the beginning of the titration phase. For our strategy, a value of $\hat{K}_p(0) = 0.3$ gave us good results for all the simulations with the different models. For the case of AdaOS-F, there was no need to estimate K_s. Therefore, we chose $\hat{K}_p(0) = 1$.[5]

5.1 Results with PHG

In this section, we perform a one year simulation for 400 subjects with T2D. The first 200 subjects of the 400 were generated with Model 2, and the second 200 were generated with Model 3. For each subject, initial glucose and insulin concentrations were drawn uniformly together with parameters affecting insulin resistivity, insulin secretion, and the time constant for injected long-acting insulin. Table G.3 summarizes the parameters drawn for each T2D model in addition to the parameters drawn for the PHG score model. To compare the scenarios

Table G.3: Parameters for generating subjects from Model 2 and Model 3. The state x_g denotes the BG concentration while x_I denotes the blood insulin concentration.

Model 2	$x_g(0) \sim \mathcal{U}(13, 20)$ [mmol/L], $p_4 \sim \mathcal{U}(0.5, 2.5)$, $p_7 \sim \mathcal{U}(0.5, 2.5)$, $p_1 \sim \mathcal{U}(1.5, 2.5)$, p_6 and the initial conditions of the remaining states are calculated such that $x_g(0)$ is stationary. Diffusion $\sigma_g \sim \mathcal{U}(0.1, 2)$.
Model 3	$x_g(0) \sim \mathcal{U}(13, 20)$ [mmol/L], $x_I(0) \sim \mathcal{U}(0.5, 1)$ [mU/L], $c_1 \sim \mathcal{U}(0.01, 0.03)$, $c_2 \sim \mathcal{U}(1, 2)$, $c_4 \sim \mathcal{U}(1, 2)$, and the initial conditions of the remaining states are calculated such that $x_g(0)$ and $I_g(0)$ are stationary. Diffusion $\sigma_g \sim \mathcal{U}(0.1, 2)$.
PHG	$\rho \sim \mathcal{U}(2, 20)$, $\bar{d} \sim \mathcal{U}(0.35, 0.85)$, $h \sim \mathcal{U}14, 30$, $\eta_1 \sim \mathcal{U}(5, 20)$. For AdaOS-pf, $p_f \sim \mathcal{U}(0.1, 0.4)$.

and the algorithms used in the simulations, we use the performance measures and their targets described in [20] for glucose managements. The measures are shown in Table G.4.

In addition to the measures in Table G.4, we compute the mean long acting insulin dose, percentage of time for the PHG score x_s being above 0.8 ($PHG_{>0.8}$), percentage of time for the PHG score x_s being below 0.5 ($PHG_{<0.5}$), and the percentage of time for the PHG score x_s being below 0.2. Note that we use x_s here instead of y_s since x_s in (G.9) represents the true score of how the subjects will rate their PHG symptoms and not the noisy (and possibly discrete) score y_s. Table G.5 shows computed mean and Inter-Quartile Range (IQR) over the 400 simulations for each strategy or scenario. Additionally, Figure G.2 shows the results for AdaOS, AdaOS-F, and ESC. From the results in Table G.5, it can be seen that all the AdaOS variations have a mean satisfying the targets of the glucose management measures. AdaOS, AdaOS-H5 and AdaOS-pf have the best mean/IQR values for TIR, TBR1, TBR2, and for the

[5]The code used for the simulations can be found on `https://gitlab.com/aau-adapt-t2d/T2D-AdaOS.git`.

Table G.4: Glucose management measures from [20]. The unit for the ranges and glucose values is [mmol/L].

Measure	% of time for BG in	Target
Time in Range (TIR)	$[3.9, 10)$	$> 70\%$
Time Above Range 1 (TAR1)	$[10, 13.9)$	$< 25\%$
Time Above Range 2 (TAR2)	$[13.9, \infty)$	$< 5\%$
Time Below Range 1 (TBR1)	$[3, 3.9)$	$< 4\%$
Time Below Range 2 (TBR2)	$[0, 3)$	$< 1\%$
Average Glucose (AG)		< 8.6
Glucose Variability (GV)		$< 36\%$
Glucose Managment Index (GMI)		$< 7\%$

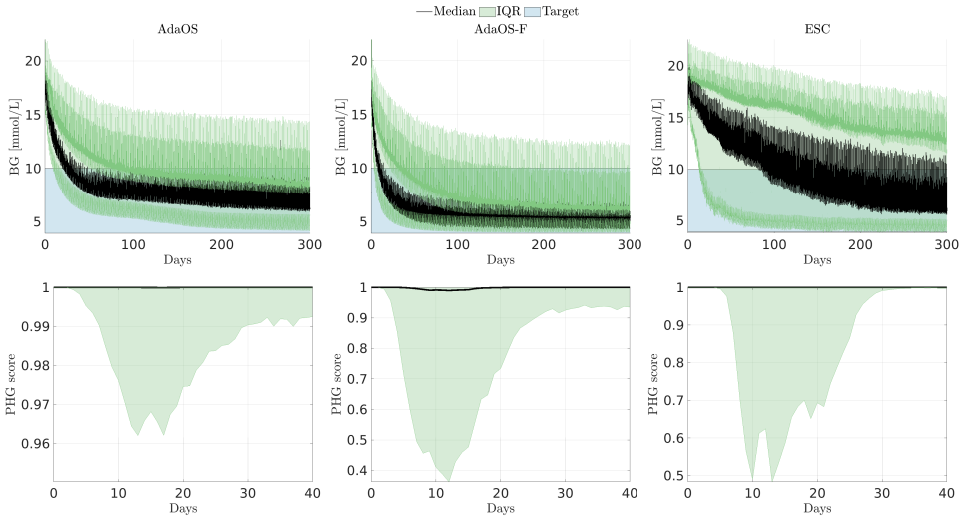

Fig. G.2: Simulation results for AdaOS, AdaOS-F, and ESC with Model 2 and Model 3. The time axis for PHG is only for 40 days since PHG is relevant during the initial titration phase.

Table G.5: Statistics for different scenarios and algorithms (red numbers indicate values outside the target range).

	Mean TIR	IQR TIR	Mean TBR1	IQR TBR1	Mean TBR2	IQR TBR2	Mean AG	IQR AG
Target [20]	> 70%		< 4%		< 1%		< 8.6 [mmol/L]	
AdaOS	95.35%	2.8%	1.2%	2%	0%	0%	8.43	4.77
AdaOS-F	96.77%	2.56%	2.11%	3.14%	0%	0%	6.77	3.24
AdaOS-H5	95.5%	3.06%	1.12%	1.76%	0%	0%	8.38	4.75
AdaOS-pf	94.61%	3.03%	1.01%	1.5%	0%	0%	8.46	4.87
Step	91.08%	0.489%	2.3%	3.1%	0%	0%	8.9	5.57
202	77.96%	14.06%	3.39%	0.43%	0%	0%	11.89	9.32
ESC	66.4%	16.45%	17.12%	11.9%	0.83%	0.69%	10.46	9.85

	Mean TAR1	IQR TAR1	Mean TAR2	IQR TAR2	Mean Insulin	Mean GV	IQR GV	Mean GMI	IQR GMI
Target [20]	< 25%		< 5%			< 36%		< 7%	
AdaOS	2.59%	1.81%	0.77%	0.97%	92.14 [U]	25.5%	8.22%	6.98%	2.1%
AdaOS-F	0.85%	0.53%	0.27%	0.4%	162.96 [U]	28.26%	11.38%	6.25%	1.41%
AdaOS-H5	2.58%	1.84%	0.79%	1.04%	93.76 [U]	25.92%	7.65%	6.96%	2.06%
AdaOS-pf	3.59%	1.82%	0.8%	3.02%	92.64 [U]	25.48%	8.05%	6.99%	2.11%
Step	4.8%	3.14%	1.78%	2.51%	125.55 [U]	33.71%	7.29%	7.18%	2.42%
202	14.99%	15.76%	3.66%	5.31%	57 [U]	22.64%	21.91%	8.48%	4.05%
ESC	4.6%	2.53%	11.87%	4.19%	69.61 [U]	31.92%	25.86%	7.86%	4.28%

	Mean $PHG_{>0.8}$	IQR $PHG_{>0.8}$	Mean $PHG_{<0.5}$	IQR $PHG_{<0.5}$	Mean $PHG_{<0.2}$	IQR $PHG_{<0.2}$
AdaOS	98.51%	0%	0.85%	0%	0.33%	0%
AdaOS-F	89.26%	22.75%	6.06%	2.5%	3.1%	0%
AdaOS-H5	98.4%	0%	0.89%	0%	0.49%	0%
AdaOS-pf	98.38%	0%	0.88%	0%	0.54%	0%
Step	98.79%	0%	0.53%	0%	0.13%	0%
202	99.93%	0%	0%	0%	0%	0%
ESC	87.7%	25%	8.86%	15%	5.86%	5%

PHG measures when compared to the other strategies. However, the mean GMI of AdaOS, AdaOS-H5, and AdaOS-pf is very close to the limit of its target range. AdaOS-F has better TIR statistics and mean/IQR values for AG, GMI, and GV when compared to the other strategies. However, AdaOS-F has a higher mean/IQR values for TBR1 when compared to the other AdaOS variation. Additionally, AdaOS-F preforms poorly for the PHG score when compared to the other AdaOS variations. This is expected since AdaOS-F is the version which does not use PHG scores as a feedback from the subjects. The Step strategy also performs as good as the AdaOS, AdaOS-H5, and AdaOS-pf in terms of PHG. However, the Step strategy does not perform as good as the AdaOS variations in terms of the glucose management measures and has mean AG and GMI violating their target. The 202 strategy has mean AG and GMI violating their target with poor performance for TIR, TBR1 and GV. Finally, ESC has mean TIR, TBR1, AG, TAR2, and GMI violating their targets. We provide a more detailed comparison with ESC in Section 5.2.

5.2 Comparison with ESC

We compare ESC from [5] with AdaOS-C using Model 1 without the PHG score since ESC does not account for it. We use simulation Model 1 with the same parameters used for the simulations in [5] but with subjects having the parameter labeled $p_{EGP} \in \{110 : 5 : 410\}$ for

each one of them. Thus, allowing p_{EGP} to take larger values than the range in which [5] tested their strategy against which was $p_{EGP} \in [350, 380]$. The initial insulin dose for the simulated subjects in [21] was chosen to be 5 [U] with a fixed initial BG concentration of 12 [mmol/L]. Therefore, we choose $\hat{K}(0)_p = (12 - 5)/5 = 1.4$ such that the initial insulin dose for AdaOS-C is also 5 U. The results are shown in Figure G.3. In addition, we report in Table G.6 percentages of samples of FBG being within different ranges as done in [5] with $[4, 6]$ [mmol/L] being the desired range, $[0, 4)$ [mmol/L] being the hypoglycemic range, and the $[0, 3)$ [mmol/L] being the severe hypoglycemic range. It can be seen from the results that the proposed strategy

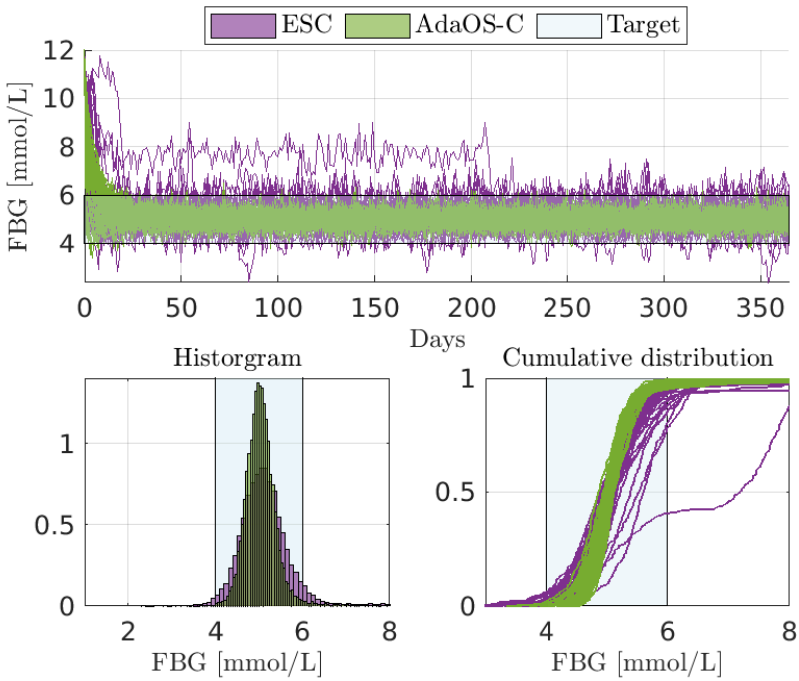

Fig. G.3: Simulating 61 T2D subjects using Model 1 with $p_{EGP} \in \{110 : 5 : 410\}$ for ESC and AdaOS-C

in this paper outperforms the ESC strategy and it is more robust to inter-subject variations. Note that the values which were chosen for p_{EGP} in this simulation are realistic (see e.g. [22]). In addition, we point out that the maximum conditioning number for the covariance matrix of the RLS in ESC was 1.5×10^{10} while the maximum condition number for the covariance matrix in AdaOS-C was 99.2. The relatively high condition number in ESC when compared to AdaOS-C can be one of the reasons why AdaOS-C performs better. AdaOS-C ensures that the covariance matrix is well conditioned by using directional forgetting (the forgetting factors are not constant in the RLS) as discussed in Section 3.2.

Table G.6: Average and worst case percentages of FBG samples within different ranges for each simulated subject with ESC and AdaOS-C using Model 1. Unit for the ranges is [mmol/L].

Average FBG	$4-6$	<4	<3
ESC	92.61%	0.87%	0.03%
AdaOS-C	97.67%	0.085%	0%
Worst case FBG	$4-6$	<4	<3
ESC	40.44%	4.92%	0.55%
AdaOS-C	95.36%	1.37%	0%

6 Conclusion and Future Work

A model free approach based on an online stochastic optimization is proposed for insulin titration in T2D subjects. The proposed strategy combines the stochastic optimization algorithm AdaBelief with a RLS scheme to tune a feedback control law with SMBG measurements and personal feedback ratings from the subjects with respect to their PHG symptoms. Using simulations with different T2D models, the strategy was compared to different titration strategies from the literature with respect to the glucose management measures in [20] and preventing PHG symptoms. The proposed strategy was shown to outperform the other titration strategies under different scenarios. As two of the titration strategies were standard of care titration strategies, this indicates that the proposed strategy can be further developed to be implemented in a clinical setting. Furthermore, it shows the potential of including subjects' personal rating as feedback for automatic dosing strategies. Future work involves deriving theoretical guarantees for the proposed strategy, validating the strategy against other high fidelity T2D simulation models, testing different scenarios for PHG ratings, and to test it against a more accurate model for PHG when such a model become available.

References

[1] M. T. McDermott, "Pseudopheochromocytoma," *Management of Patients with Pseudo-Endocrine Disorders: A Case-Based Pocket Guide*, p. 193, 2019.

[2] E. R. Seaquist, J. Anderson, B. Childs, P. Cryer, S. Dagogo-Jack, L. Fish, S. R. Heller, H. Rodriguez, J. Rosenzweig, and R. Vigersky, "Hypoglycemia and diabetes: a report of a workgroup of the american diabetes association and the endocrine society," *The Journal of Clinical Endocrinology & Metabolism*, vol. 98, no. 5, pp. 1845–1859, 2013.

[3] T. Kadowaki, H. Jinnouchi, K. Kaku, M. L. Hersløv, J. Hyllested-Winge, and S. Nakamura, "Insulin degludec in a simple or stepwise titration algorithm in a japanese population of patients with type 2 diabetes: a randomized, 26-week, treat-to-target trial," *Diabetology international*, vol. 8, no. 1, pp. 87–94, 2017.

[4] T. B. Aradóttir, D. Boiroux, H. Bengtsson, J. Kildegaard, M. L. Jensen, J. B. Jørgensen, and N. K. Poulsen, "Model predictive control for dose guidance in long acting insulin

treatment of type 2 diabetes," *IFAC Journal of Systems and Control*, vol. 9, p. 100067, 2019.

[5] D. Krishnamoorthy, D. Boiroux, T. B. Aradóttir, S. E. Engell, and J. B. Jørgensen, "A model-free approach to automatic dose guidance in long acting insulin treatment of type 2 diabetes," *IEEE Control Systems Letters*, vol. 5, no. 6, pp. 2030–2035, 2020.

[6] M. A. Ahdab, M. Papež, T. Knudsen, T. B. Aradóttir, S. Schmidt, K. Nørgaard, and J.-J. Leth, "Parameter estimation for a jump diffusion model of type 2 diabetic patients in the presence of unannounced meals," in *2021 IEEE Conference on Control Technology and Applications (CCTA)*, 2021, pp. 176–183.

[7] M. Al Ahdab, J.-J. Leth, T. Knudsen, P. Vestergaard, and H. G. Clausen, "Glucose-insulin mathematical model for the combined effect of medications and life style of type 2 diabetic patients," *Biochemical Engineering Journal*, vol. 176, p. 108170, 2021.

[8] M. Menner, L. Neuner, L. Lünenburger, and M. N. Zeilinger, "Using human ratings for feedback control: A supervised learning approach with application to rehabilitation robotics," *IEEE Transactions on Robotics*, vol. 36, no. 3, pp. 789–801, 2020.

[9] J. Zhuang, T. Tang, Y. Ding, S. C. Tatikonda, N. Dvornek, X. Papademetris, and J. Duncan, "Adabelief optimizer: Adapting stepsizes by the belief in observed gradients," *Advances in neural information processing systems*, vol. 33, pp. 18 795–18 806, 2020.

[10] A. D. Flaxman, A. T. Kalai, and H. B. McMahan, "Online convex optimization in the bandit setting: gradient descent without a gradient," *arXiv preprint cs/0408007*, 2004.

[11] S. Vlaski, E. Rizk, and A. H. Sayed, "Tracking performance of online stochastic learners," *IEEE Signal Processing Letters*, vol. 27, pp. 1385–1389, 2020.

[12] A. S. Bedi, P. Sarma, and K. Rajawat, "Tracking moving agents via inexact online gradient descent algorithm," *IEEE Journal of Selected Topics in Signal Processing*, vol. 12, no. 1, pp. 202–217, 2018.

[13] A. Goel, A. L. Bruce, and D. S. Bernstein, "Recursive least squares with variable-direction forgetting: Compensating for the loss of persistency [lecture notes]," *IEEE Control Systems Magazine*, vol. 40, no. 4, pp. 80–102, 2020.

[14] L. Cao and H. Schwartz, "A directional forgetting algorithm based on the decomposition of the information matrix," *Automatica*, vol. 36, no. 11, pp. 1725–1731, 2000.

[15] A. Alacaoglu, Y. Malitsky, P. Mertikopoulos, and V. Cevher, "A new regret analysis for adam-type algorithms," in *International Conference on Machine Learning*. PMLR, 2020, pp. 202–210.

[16] X. Wu and M. W. Mueller, "In-flight range optimization of multicopters using multivariable extremum seeking with adaptive step size," in *2020 IEEE/RSJ International Conference on Intelligent Robots and Systems (IROS)*. IEEE, 2020, pp. 1545–1550.

[17] P. Divilly *et al.*, "Hypo-metrics: Hypoglycaemia–measurement, thresholds and impacts–a multi-country clinical study to define the optimal threshold and duration of sensor-detected hypoglycaemia that impact the experience of hypoglycaemia, quality of life and health economic outcomes: the study protocol," *Diabetic Medicine*, p. e14892, 2022.

[18] M. Ahdab, T. Knudsen, and J.-J. Leth, "State space temporal gaussian processes for glucose measurements," in *2022 European Control Conference (ECC)*. United States: IEEE, 2021, pp. 1277–1282.

[19] *In vitro diagnostic test systems: requirements for blood-glucose monitoring systems for self-testing in managing diabetes mellitus.* International Organization for Standardization, 2003.

[20] R. I. Holt, J. H. DeVries, A. Hess-Fischl, I. B. Hirsch, M. S. Kirkman, T. Klupa, B. Ludwig, K. Nørgaard, J. Pettus, E. Renard *et al.*, "The management of type 1 diabetes in adults. a consensus report by the american diabetes association (ada) and the european association for the study of diabetes (easd)," *Diabetes Care*, vol. 44, no. 11, pp. 2589–2625, 2021.

[21] N. R. Kristensen, H. Madsen, and S. B. Jørgensen, "Parameter estimation in stochastic grey-box models," *Automatica*, vol. 40, no. 2, pp. 225 – 237, 2004.

[22] H. G. Clausen, T. Knudsen, M. Al Ahdab, T. B. Aradottir, S. Schmidt, K. Nrgaard, and J.-J. Leth, "A new stochastic approach for modeling glycemic disturbances in type 2 diabetes," *IEEE Transactions on Biomedical Engineering*, 2021.

Paper H

Blood Glucose Reference Personalization for Subjects with Type 2 Diabetes

Mohamad Al Ahdab, Torben Knudsen, Jakob Stoustrup, and John Leth.

The paper has been accepted/in press in the
2023 IEEE Conference on Control Technology and Applications (CCTA), 2023.

Abstract

In this paper, we present two simple and novel methods for automatic personalization of target blood glucose concentration values for individuals with Type 2 Diabetes (T2D). The methods can be integrated with any insulin dosing algorithm, or used to provide an individualized reference BG concentration value for medical professionals to consider when determining long-acting insulin doses and other oral medications. The proposed methods were tested in three different simulation models, with different long-acting insulin dosing strategies, and were found to reduce instances of hypoglycemia.

1 Introduction

Type 2 diabetes (T2D) is characterized by high blood glucose (BG) concentrations, or hyperglycemia, caused by an imbalance between insulin secretion and the ability of insulin to lower BG concentrations. If left untreated, high BG concentrations can lead to complications such as cardiovascular diseases and damage to eyesight. The first steps in the treatment of T2D typically involve lifestyle adjustments and the use of oral medications. However, if these methods are insufficient in lowering BG concentrations, individuals with T2D may need to use long-acting insulin, such as once-daily insulin pens, based on self-monitored blood glucose (SMBG) measurements or continuous glucose monitoring (CGM) devices. Strategies for automatically computing insulin doses for T2D subjects range from simple table-based strategies, as described in [1], to physiological model-based strategies, such as the one in [2], as well as model-free strategies, like the ones discussed in [3, 4]. The glucose target for these titration algorithms is fixed. However, for individuals with high variations in blood glucose concentrations, this fixed target may not be ideal as it can lead to increased instances of low BG concentrations (hypoglycemia) which can cause symptoms such as nausea, fainting, and in severe cases, death. To address this issue, we propose adapting the glucose target in real-time to reduce the occurrence of hypoglycemic events. The idea of adapting has been shown to be effective in closed-loop artificial pancreas systems for individuals with type 1 diabetes in combination with a model predictive controller [5]. In this paper, we propose new methods for automatic penalization of target BG for individuals with T2D utilizing CGM readings. The developed strategies can generally be connected with any insulin dosing algorithm or they can be directly recommending an individualized reference BG to the medical professionals who are deciding on the long-acing insulin dose and other medications. The contribution of this paper are as follows

- We propose a simple integral-derivative (ID) controller with a nonlinear error function to adapt a personalized target BG concentration for T2D subjects.
- We propose a different method which calculates a personalized BG target by taking a weighted average of the outputs from multiple ID controllers. The weights are adapted in an online fashion for each subject.
- We test the method with three different simulation models augmented with three different insulin dosing strategies: two standard of care dosing strategies, and a newly proposed modified version of one of them.

2 notations

The symbol $:=$ indicates *defined by*. All vectors are considered as column vectors, $\|\cdot\|_p$ denotes the p-norm, and $^{\mathrm{T}}$ denotes transpose. We use $\mathcal{N}(\mu, \Sigma)$ to denote the normal distribution with mean μ and covariance Σ, and $\mathcal{U}(a, b)$ for a continuous uniform distribution with bounds a and b. If the difference between two time instants t_k and t_{k+j} is such that $t_{k+j} - t_k = jT,\ j, k \in \mathbb{N}$ with $T \in \mathbb{R}$ being a constant, then variables that are indexed with time $x(t_k), x(t_{k+j})$ will be denoted by $x(k), x(k+j)$ for ease of notation. We let $[a, b]$ denote the closed interval from a to b, and $[a\ b]$ denote the row vector with coordinates a and b. For a diagonal matrix A with diagonal entries $a = [a^1 \cdots a^n]^{\mathrm{T}}$, the notation $A = \mathrm{diag}(a)$ is used. The symbol I_n is used to denote the $n \times n$ identity matrix and the symbol $\mathbf{1}_n$ is used to denote the n_{th} dimensional column vector of 1s. For an interval $\Theta = [x_\ell, x_u]$, we define the saturation function $\Pi_\Theta : \mathbb{R} \to \Theta$, $\Pi_\Theta(x) := \max\left(\min\left(x, x_u\right), x_\ell\right)$. For $w, v \in \triangle_n := \left\{w \in \mathbb{R}^n_{\geq 0} \mid \|w\|_1 = 1\right\}$, we write the Kullback–Leibler (KL) divergence (relative entropy) as $D_{KL}(w \mid\mid v) = \sum_{i=1}^n w^i \ln\left(w^i / v^i\right)$. For a vector $x = [x_1, \ldots, x_N]^{\mathrm{T}} \in \mathbb{R}^N$, we define a vector of moving averages with a window $H \leq N$ as $\mu_H(x) := 1/H \left[\sum_{i=1}^H x_i, \ldots, \sum_{i=N-H+1}^N x_i\right]^{\mathrm{T}}$.

3 Description of the method

As discussed in the introduction, the adaptive BG target methods in this paper are designed to be used in connection with an insulin dosing strategy or as a recommendation to medical professionals, see figure H.1. We will first describe a nonlinear error function in 3.1. Afterwards, we describe the simple ID method for BG target adaptation in 3.2 and an adaptive weighted average version of it in 3.2.

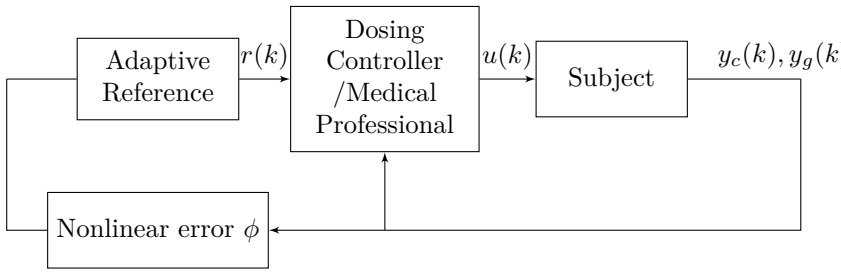

Fig. H.1: Block diagram of the setup. The command $r(k)$ is a personalized average/fasting glucose target, $u(k)$ is a long-acting insulin dose, $y_c(k)$ is a vector of the available CGM measurements between the days $(k-1)T$ and kT, and $y_g(k)$ is an average/fasting BG measurement.

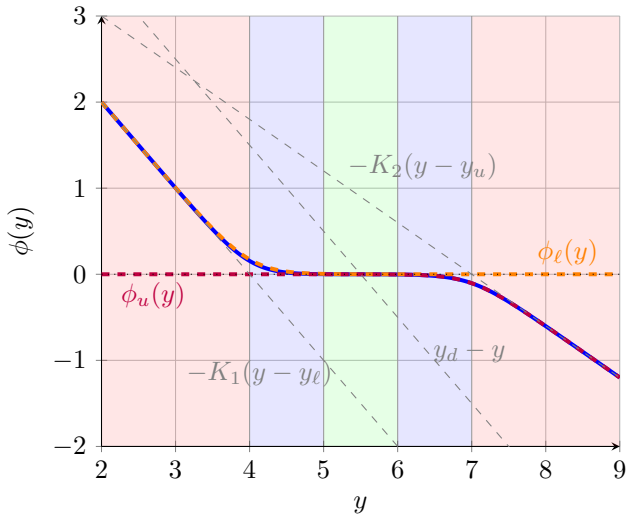

Fig. H.2: A plot of $\phi(y)$ defined in (H.1c) with $K_1 = 1, K_2 = 0.6, a = b = 2, y_\ell = 4, y_u = 7$. The figure demonstrates the approximately linear error zones, the zero zone, and the transitioning zones. Note that $y > 0$ since it represents a BG concentration value

3.1 Nonlinear Error Functions

Let $k \in \mathbb{Z}_{\geq 0}$ represent the current iteration of our strategy at time $t_k := kT$ [day]. Similarly, let $m \in \mathbb{Z}_{\geq 0}$ represent the CGM sample at time $t_m := mT_m$ [day] with $T_m < T$. We define the vector $y_c(k) \in \mathbb{R}^q$ as the vector of the available q CGM measurements y from time t_{k-1} until t_k. In other words, $y_c(k) = \begin{bmatrix} y(m_{k_1}) & \dots & y(m_{k_q}) \end{bmatrix}^{\mathrm{T}}$ such that $T_m m_{k_i} \in \big[(k-1)T, kT\big]$ for $i \in \{1, \dots, q\}$. Before proceeding to the description of the strategies, we first define the functions $\phi_\ell, \phi_u, \phi : \mathbb{R} \to \mathbb{R}$

$$\phi_\ell(y) := K_1 s_a(-(y - y_\ell)) \tag{H.1a}$$
$$\phi_u(y) := -K_2 s_b(y - y_u) \tag{H.1b}$$
$$\phi(y) := \phi_u(y) + \phi_\ell(y) \tag{H.1c}$$

where $s_\alpha(x) := \frac{1}{\alpha}\log(1+\mathrm{e}^{\alpha x})$, $K_1, K_2 \in \mathbb{R}_{>0}$ are gain constants, $a, b \in \mathbb{R}$ are shape parameters, and $y_\ell, y_u \in \mathbb{R}$ are lower and upper bounds respectively. Figure H.2 shows an example of $\phi(y)$. The function $\phi(y)$ can be viewed as a modified version of the linear error $e(y) := y_d - y$ where y_d is taken as a "desired value". Unlike $e(y)$, the function $\phi(y)$ asymptotically converges to a linear error $-K_1(y - y_\ell)$ when $y \to -\infty$ and to another linear error $-K_2(y - y_u)$ when $y \to \infty$. In between, the function will be approximately zero. Additionally, observe that for $y_\ell = y_u = y_d$, and $K_1 = K_2 = 1$, we have $\phi(y)$ asymptotically converging to $e(y)$ when $a, b \to \infty$. Loosely put, the function $\phi(y)$ divides its domain "smoothly" into five different zones (see Figure H.2): two zones with two different approximately linear error functions, one zone where the function

is approximately zero, and two zones to transition from approximately zero to approximately linear error functions. On the other hand, the linear error function $e(y)$ is linear with the same gain for all $y \in \mathbb{R}$. The smoothing for the error function $\phi(y)$ between the approximately linear error zones and the zero zone helps with damping chattering effects when $\phi(y)$ is used as a feedback. The smooth transition is controlled by the parameters a and b. The parameters for ϕ for the rest of the paper are chosen as $K_1 = 1, K_2 = 0.6, a = b = 2, y_\ell = 4$, and $y_u = 7$. For the following subsections, we will present the two reference adapting approaches with the use of the function ϕ.

3.2 Reference Adaptation

We propose two approaches for adapting an average/fasting BG reference for each specific T2D individual based on $\phi(y)$ in (H.1c) and CGM measurements. The first approach is a single Integral-Derivative (ID) based controller and the second approach is an Adaptive Weighted Average method of multiple ID based controllers (AWAID).

Single ID Method

Consider an initial average/fasting BG reference $r(0) \geq 4$ [mmol/L]. At iteration k at time kT [day], we use the available CGM measurements $y_c(k)$ to compute a quantity related to the average error as

$$\bar{\phi}(y_c(k)) := \frac{1}{q} \sum_{i=1}^{q} \gamma_{y_\ell, y_u}(y(m_{k_i}))\phi(y(m_{k_i})), \tag{H.2}$$

where the cutoff function [1]γ_{y_ℓ, y_u} is defined as

$$\gamma(y)_{y_\ell, y_u} := \begin{cases} 0, & y \in [y_\ell + 1, y_u - 1] \\ 1, & \text{Otherwise.} \end{cases} \tag{H.3}$$

Afterwards, the suggested single point average/fasting BG reference is updated according to an ID type controller

$$\begin{aligned} r(k) = \Pi_\Omega \Big(& r(k-1) + TK_I \bar{\phi}\left(y_c(k)\right) \\ & + K_D \left(\bar{\phi}\left(y_c(k)\right) - d_r(k-1) \right) \Big), \end{aligned} \tag{H.4a}$$

$$d_r(k) = (1-\beta) d_r(k-1) + \beta \bar{\phi}\left(y_c(k)\right), \; d_r(0) = 0. \tag{H.4b}$$

[1]The cutoff function is added to ensure that the error function ϕ is zero for $y \in [y_\ell + 1, y_u - 1]$ to avoid drift in the ID controller since $s(x)$ only asymptotically converges to zero for $x \to -\infty$. Although including the cutoff function affects the smoothness of the average error, the impact on chattering is negligible. This is because the cutoff function is applied within a region where the error is close to zero.

where $K_I > 0$ is the integral gain, $K_D \geq 0$ is the derivative gain, $0 < \beta \leq 1$, and $\Omega = [r_\ell, r_u]$ [2] The bounds r_ℓ and r_u are chosen to ensure that at any point, the reference $r(k)$ will always be safe. In this paper, we choose $r_\ell = 5$ [mmol/L] and $r_u = 10$ [mmol/L].

Adaptive Weighted Average ID (AWAID)

For this method, we consider multiple ID based controllers of the form (H.4) and take the weighted average of their individual outputs as the suggested average/fasting BG reference. The method is made adaptive by updating the weights using an online multiplicative weight approach. Let $\theta := [K_I \ K_D \ \beta]^{\mathrm{T}}$ and consider $N \in \mathbb{Z}_{>0}$ different ID based controllers such that each individual controller is characterized by the parameters $\theta^i \in \Theta = \left\{\theta^1, \ldots, \theta^N\right\}$. To compute a reference $r(k)$ at time kT [day], we first compute the output of the N different ID controllers

$$\begin{aligned} r^i(k) &= r(k-1) + TK_I^i \bar{\phi}\left(y_c(k)\right) \\ &\quad + K_D^i \left(\bar{\phi}\left(y_c(k)\right) - d_r(k-1)\right), \end{aligned} \tag{H.5a}$$

$$d_r^i(k) = (1-\beta^i) d_r^i(k-1) + \beta^i \bar{\phi}\left(y_c(k)\right), \ d_r(0) = 0. \tag{H.5b}$$

The output recommended reference is then computed as a weighted average with weights

$$w(k) = \left[w^1(k) \ \ldots \ w^N(k)\right]^{\mathrm{T}} \in \triangle_N,$$

as following

$$r_a(k) = \sum_{i=1}^{N} w^i(k) r^i(k), \tag{H.6a}$$

$$r(k) = \Pi_\Omega\left(r_a(k)\right). \tag{H.6b}$$

The weights $w(k)$ at step k are chosen such that $\phi(r_a(k))$ is close to zero to promote references on the interior of Ω which makes it safer for the subject. We achieve this with the following update step

$$\tilde{w}^i(k) = \frac{e^{-\eta(k)\phi^2\left(r^i(k)\right)}}{\sum_{i=1}^{N} e^{-\eta(k)\phi^2(r^i(k))} w^i(k-1)} w^i(k-1), \tag{H.7a}$$

$$w^i(k) = \zeta(k)\tilde{w}^i(k) + (1-\zeta(k))\frac{1}{N}\mathbf{1}_N, \tag{H.7b}$$

with $\eta(k) = \sqrt{\frac{\ln(N)}{50k}}$ (see Remark 3.2) and $\zeta(k) = \frac{\eta(k+1)}{\eta(k)} \in (0, 1]$. The update rule (H.7a) scales the weight for each individual reference output $r^i(k)$ based on how small the value of $\phi^2(r^i(k))$

[2] r_ℓ can be made time dependent with $r_\ell(k) = r_\ell(k-1) + T\alpha\left(\tilde{r}_\ell - r_\ell(k-1)\right)$ to give the option of the medical professionals to restrict how fast the BG reference should drop to minimum value of $\tilde{r}$ with a rate α $[day^{-1}]$ to prevent complications and pseudo-hypoglycemia symptoms [6].

is, meaning that reference outputs which are closer to the zero safe zone of the function ϕ will be scaled higher than other reference outputs. The update rule in (H.7) is the solution of the following optimization problem

$$\tilde{w}(k) = \underset{w \in \triangle_N}{\operatorname{argmin}} \sum_{i=1}^{N} \eta(k) \phi^2 \left(r^i(k) \right) w^i + D_{KL}(w \mid\mid w(k-1)), \tag{H.8}$$

and

$$\phi^2(r_a(k)) \leq \sum_{i=1}^{N} \phi^2 \left(r^i(k) \right) w^i(k)$$

using Jensen's inequality since ϕ^2 is convex. In other words, minimizing $\sum_{i=1}^{N} \phi^2 \left(r^i(k) \right) w^i(k)$ will minimize an upper bound on $\phi^2(r_a(k))$ to promote for a safer output reference $r_a(k)$. The regularization term $D_{KL}(w \mid\mid w(k-1))$ is to ensure that the weights do not change arbitrary between different iterations in order to avoid sharp changes in $r(k)$. Additionally, the inclusion of the term $D_{KL}(w \mid\mid w(k-1))$ pushes w away from the boundary of $\triangle_N$, and towards where $\sum_{i=1}^{N} \phi^2 \left(r^i(k) \right) w^i(k)$ is minimized [7].

Remark 3.1. *The step in equation (H.7b) performs interpolation between uniform weights ($\frac{1}{N}\mathbf{1}_N$) and the updated weights $\tilde{w}(k)$ at each iteration to account for the time-varying nature of the problem ($r^i(k)$ varies with k) by preventing the weights from quickly converging to one of the vertices of the simplex $\triangle_N$ and becoming fixed there.*

Remark 3.2. *Let $J_k(w) = \phi^2 \left(\sum_{i=1}^{N} r^i(k) w^i \right)$, and define the average regret Ψ_K up until time step K between the weights computed according to (H.7) and the fixed weights $v = \underset{w \in \triangle_N}{argmin} \sum_{k=1}^{K} J_k(w)$ as*

$$\Psi_K := \frac{1}{K} \left(\sum_{k=1}^{K} J_k(w(k)) - \sum_{k=1}^{K} J_k(v) \right), \tag{H.9}$$

then using Corollary 10 in [8] and applying Jensen's inequality, we can bound the average regret with the update in (H.7) and $\zeta(k) = \frac{\eta(k+1)}{\eta(k)}$ with $w(1) = \frac{1}{N}\mathbf{1}_N$ as following

$$\Psi_K \leq \frac{1}{K} \sum_{k=1}^{K} \frac{\eta(k) \left\| g(k) \right\|_\infty^2}{2} + \frac{1}{K} \frac{\ln(N)}{\eta(K+1)}, \tag{H.10}$$

where $g(k) = \left[\phi^2 \left(r^1(k) \right) \dots \phi^2 \left(r^N(k) \right) \right]^{\mathrm{T}}$.

Furthermore, due to the fact that the blood glucose concentration must have limits, and with parameters $\theta^i \in \Theta$, $i \in \{1, \dots, N\}$ that ensures bounded input bounded output stability of the corresponding controllers, we can bound $\left\| g(k) \right\|_\infty^2 \leq G_\infty^2$. With this bound, if we choose

$\eta(k) = \sqrt{\frac{2\ln(N)}{kG_\infty^2}}$, *then the average regret becomes*

$$\Psi_K \leq \frac{\sqrt{2\ln(N)}G_\infty}{K}\left(\frac{1}{2}\sum_{k=1}^{K}\frac{1}{\sqrt{k}} + \sqrt{K+1}\right) \leq \frac{2G_\infty\sqrt{2\ln(N)}}{\sqrt{K}}, \tag{H.11}$$

where we used $\sum_{k=1}^{K}\frac{1}{\sqrt{k}} \leq 2\sqrt{K} - 1$ *(using the integral test) and* $\sqrt{K+1} \leq \sqrt{K} + \frac{1}{2}$ *for* $K \geq 1$ *(using the concavity and differentiability of the square root function). With* $v = \underset{w\in\triangle_N}{argmin}\sum_{k=1}^{K} J_k(w)$ *being the best weights choice up until* K*, it means that the performance of the weights computed according to* (H.7) *compared to the case when we take the best fixed weights* v *over the horizon* K *is bounded by a function in the order of* $\frac{1}{\sqrt{K}}$*. For the choice of* G_∞*, we used simulation results with the three different models in 4.2 to obtain an estimate bound* $\hat{G}_\infty^2 = 100$ *for* G_∞^2 *such that* $G_\infty^2 \leq \hat{G}_\infty^2$*. Therefore, our choice for* $\eta(k)$ *is* $\eta(k) = \sqrt{\frac{\ln(N)}{50k}}$.

4 Simulation Setup

In this section, we intend to simulate and compare between insulin dosing strategies on T2D subjects with and without the adaptive reference scheme in (H.4). To do so, we first present our choice of insulin dosing strategies in 4.1. Afterwards, we present 3 different insulin-glucose simulation models in 4.2, Finally, we present and discuss the results of the simulations in 5.

4.1 Simulated Dosing Strategies

In this section, we list the long-acing insulin dosing strategies which we will use for the simulations of individual with T2D. The first two strategies are the standard of care methods

$$202 \quad \Delta u(k) = \begin{cases} 2, & y_g(k) > r(k) + 1 \\ 0, & y_g(k) \in [r(k) - 1, r(k) + 1] \\ -2, & y_g(k) < r(k) - 1 \end{cases} \tag{H.12a}$$

$$\text{Step} \quad \Delta u(k) = \begin{cases} 8, & \bar{y}_g(k) \geq r(k) + 4 \\ 6, & \bar{y}_g(k) \in [r(k) + 3, r(k) + 4) \\ 4, & \bar{y}_g(k) \in [r(k) + 2, r(k) + 3) \\ 2, & \bar{y}_g(k) \in [r(k) + 1, r(k) + 2) \\ 0, & \bar{y}_g(k) \in [r(k) - 1, r(k) + 1) \\ -2, & \bar{y}_g(k) \in [r(k) - 2, r(k) - 1) \\ -4, & \bar{y}_g(k) < r(k) - 2 \end{cases} \tag{H.12b}$$

$$u(k) = u(k-1) + \Delta u(k) \tag{H.12c}$$

where $u(k)$ is the prescribed insulin dose at $t = kT$ [day], $y_g(k)$ is a glucose value that can either be a glucose measurement obtained by finger pricking devices (SMBG) before breakfast, or a value calculated from CGM readings as $y_g(k) = \min\left(\mu_H\left(y_c(k)\right)\right)$ similar to [9], and $\bar{y}_g(k) := \frac{1}{3}\sum_{i=0}^{2} y_g(k-i)$ is an average value of $y_g(k)$ over the last three days. For the default standard of care strategies, $r(k)$ is constant and it is chosen to be 5 mmol/L. In addition to the standard of care strategies in (H.12), we consider a linear smooth (LS) version of Step defined as

$$\Delta u(k) = 2s_2(\bar{y}_g(k) - r(k) - 1) - 2s_2(r(k) - 1 - \bar{y}_g(k)) \tag{H.13a}$$

$$u(k) = u(k-1) + \Delta u(k) \tag{H.13b}$$

Note that the right-hand side of (H.13a) is $\phi(\bar{y}_g(k))$ in (H.1c) with $K_1 = K_2 = -2, a = b = 2, y_\ell = r(k) - 1$, and $y_u = r(k) + 1$. Figure H.3 shows $\Delta u(k)$ versus $\bar{y}_g$ for both the Step and LS schemes. The parameters for the methods with AWAID are

$$\Theta = \{0.2, 0.3, 0.4, 0.5, 0.6, 0.7, 0.8\} \times \{0.8, 1, 1.2\} \times \{1, 0.8, 0.2\} \tag{H.14}$$

where $\theta^i = \begin{bmatrix} K_I^i & K_D^i & \beta^i \end{bmatrix}^{\mathrm{T}}$ are the parameters for the i_{th} controller. For the methods with single ID, we choose after some simple tuning $\theta = [0.5\ 1\ 0.8]^{\mathrm{T}}$ (the median ID controller in Θ). The time constant T is chosen to be 7 days. Meaning that the reference and the insulin dose are updated every week.

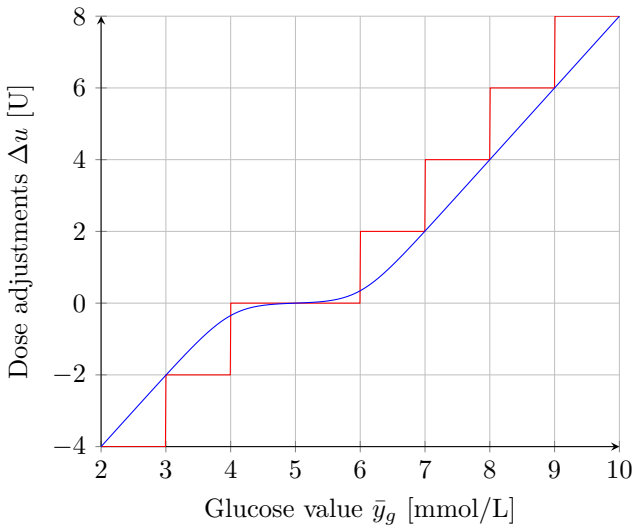

Fig. H.3: The Step strategy (red) and its LS (blue) approximation with $r = 5$ mmol/L.

4.2 Glucose-Insulin Simulation Models

For the glucose-insulin dynamic simulations, we consider three different simulation models. For the first model, denoted "Model 1", we consider the jump diffusion model in [10]. The average meal rate in the jump part is chosen to be 3 meals/day between the hours 7:00 and 23:00 and 0.1 meals/day otherwise to take into account that individuals do not eat as frequently at night. As for the diffusion part, a constant diffusion is added to the BG concentration state. For the second model, denoted "Model 2", we consider the model presented in [11] augmented with a jump diffusion model for meals and disturbances matching "Model 1". Finally, the third model, denoted "Model 3", is the high fidelity model [12]. The meal times for Model 3 are drawn from uniform distributions as following: $\mathcal{U}(6,8)$ [h] for breakfast meals, $\mathcal{U}(12,14)$ [h] for lunch meals, and $\mathcal{U}(19,20)$ [h] for dinner meals. The carbohydrate intake for each meal is also drawn uniformly according to $\mathcal{U}(10,25)$ [g] for breakfast, $\mathcal{U}(20,30)$ [g] for lunch, and $\mathcal{U}(25,45)$ [g] for dinner. The choice of simulating the meals differently for Model 3 was to evaluate the insulin dosing strategies against a distinct type of stochastic disturbances. For the measurement errors, we consider an SMBG measurement error model [13] as the following

$$y_g(k) = x_g(k) + \sigma_s\left(x_g(t_s)\right)\varepsilon_s(k), \tag{H.15a}$$

$$\sigma_s\left(x_g\right) = \frac{1}{\kappa}\sigma_2 \log\left(1 + \mathrm{e}^{\kappa\left(x_g - 4.2\right)}\right) + \sigma_1, \tag{H.15b}$$

with σ_1 and σ_2 chosen in accordance to the ISO standard [14] to be $\sigma_1 = 0.415$ [mmol/L] and $\sigma_2 = 0.1$, and $\kappa = 5$. Additionally, we consider a CGM measurement error model according to

$$y(m) = x_c(m) + \sigma_c x_c(m)\varepsilon_c(m), \tag{H.16}$$

with $\sigma_c = 0.42$ in accordance to a MARD of 10% [15] as done in [16]. The state x_c represents the glucose concentration in the blood for the models. Table H.1 summarizes the models used for simulations in this paper.

Table H.1: Glucose-insulin simulation models used in the paper

Model 1	Based on [10]. Includes a measurement error model.
Model 2	Based on the model from [11]. Augmented with a jump diffusion model matching the one in [10] for meals. Includes measurement error models.
Model 3	Based on the model from [12]. The timing and size of meals are drawn from uniform distributions. Includes a measurement error model. A diffusion term matching the one in [10] is added to the state corresponding to BG concentration.

5 Results and Discussion

This section describes a simulation involving 1500 individuals with T2D over the course of one year. The first 500 subjects were generated using Model 1, the next 500 using Model 2, and the final 500 using Model 3. Initial glucose and insulin concentrations, as well as parameters affecting insulin resistance and insulin secretion, and the time constant for injected long-acting insulin, were randomly chosen for each individual. Table H.3 provides a summary of the parameters used for each T2D model.
We simulate the Step and LS strategies with different scenarios according to table H.2.
To compare the scenarios and the algorithms used in the simulations, we use the performance

Table H.2: Summary of the Different Setups Considered for Simulations. If CGM is used for y_g, then $H = 3$ [hour].

Name	y_g Value Based On	Adaptive Target	Insulin Dosing
Step	SMBG	none	Method (H.12b)
StepR	SMBG	Single ID (H.4)	Method (H.12b)
StepAR	SMBG	AWAID (H.6)	Method (H.12b)
202	SMBG	none	Method (H.12a)
202R	SMBG	Single ID (H.4)	Method (H.12a)
202AR	SMBG	AWAID (H.6)	Method (H.12a)
LS	SMBG	none	Method (H.13)
AvgLS	CGM	none	Method (H.13)
LSR	SMBG	Single ID (H.13)	Method (H.12b)
AvgLSR	CGM	Single ID (H.13)	Method (H.12b)
LSAR	SMBG	AWAID (H.6)	Method (H.13)
AvgLSAR	CGM	AWAID (H.6)	Method (H.13)

measures and their targets described in [17] for glucose managements. The measures are shown in table H.4. In addition to the measures in table H.4, we compute the mean long acting insulin dose. Table H.5 shows computed mean and Standard deviation (Std) over the 1500 simulations for each strategy or scenario.
Figure H.4 illustrates the outcomes of various methods: LS, LSAR, AvgLS, AvgLSAR, Step, StepAR, 202, and 202AR. Additionally, table H.5 presents statistical data for all the methods discussed in table H.2. Among these methods, LSAR, AvgLSAR, and StepAR, which employ an adaptive BG reference, exhibit higher mean BG concentrations compared to LS, AvgLS, and Step. Consequently, there are lower BG values within the hypoglycemic range, as indicated by the BG histograms across all subjects.

This observation aligns with the table's results, demonstrating how adapting the reference can reduce instances of hypoglycemia. The table also reveals that the average glucose, TAR1, and TAR2 are higher when BG reference adaptation is utilized, which concurs with the findings in the figure. In summary, the adaptive BG reference strategies for Step and LS effectively

Table H.3: Parameters for generating subjects from Model 1, Model 2, and Model 3. The state x_G denotes the BG concentration state while x_I denote the blood insulin concentration state.

Model 1	$x_G(0) \sim \mathcal{U}(15, 25)$ [mmol/L], $p_4 \sim \mathcal{U}(0.5, 2.5)$, $p_7 \sim \mathcal{U}(0.5, 2.5)$, $p_1 \sim \mathcal{U}(1.5, 2.5)$, p_6 and the initial conditions of the remaining states are calculated such that $x_G(0)$ is stationary. Diffusion term $\sigma_G \sim \mathcal{U}(0.1, 2)$.
Model 2	$x_G(0) \sim \mathcal{U}(15, 25)$, $x_I(0) \sim \mathcal{U}(20, 30)$ [pmol/L], $CL_{GI} \sim \mathcal{U}(0.71 \times 10^{-4}, 0.11 \times 10^{-2})$, $I_{PRG} \sim \mathcal{U}(0.05, 2)$, and the initial conditions of the remaining states are calculated such that $x_G(0)$ and $I_G(0)$ are stationary. Diffusion term $\sigma_G \sim \mathcal{U}(0.1, 2)$.
Model 3	$x_G(0) \sim \mathcal{U}(15, 25)$ [mmol/L], $x_I(0) \sim \mathcal{U}(0.5, 2)$ [mU/L], $c_1 \sim \mathcal{U}(0.04, 0.09)$, $c_2 \sim \mathcal{U}(2.3, 0.95)$, $c_4 \sim \mathcal{U}(1, 2.4)$, and the initial conditions of the remaining states are calculated such that $x_G(0)$ and $I_G(0)$ are stationary. Diffusion term $\sigma_G \sim \mathcal{U}(0.1, 2)$.

Table H.4: Glucose management measures from [17]. The unit for the ranges and glucose values is [mmol/L].

Measure	% of time for BG in	Target
Time in Range (TIR)	$[3.9, 10)$	$> 70\%$
Time Above Range 1 (TAR1)	$[10, 13.9)$	$< 25\%$
Time Above Range 2 (TAR2)	$[13.9, \infty)$	$< 5\%$
Time Below Range 1 (TBR1)	$[3, 3.9)$	$< 4\%$
Time Below Range 2 (TBR2)	$[0, 3)$	$< 1\%$
Average Glucose (AG)		< 8.6
Glucose Variability (GV)		36%
Glucose Management Index (GMI)		7%

elevate the BG reference, thus preventing hypoglycemic episodes in susceptible subjects. It is worth noting that methods employing an adaptive moving average of multiple ID controllers exhibit better performance in reducing incidents of hypoglycemia with slightly lower average BG concentration compared to those using a single ID controller. Although it may be possible to fine-tune the parameters of a single ID controller for improved results, this process can be challenging, particularly when dealing with different groups of T2D subjects. On the other hand, the AWAID strategy offers a more flexible approach, as it only requires specifying the

parameters of multiple ID controllers. The method then adapts the weights in an online manner to enhance performance. However, in the case of the 202 strategies, the results shown in the figure do not demonstrate good performance, which is consistent with the TIR, TAR1, and TAR2 statistics presented in table H.5. Even when an adaptive BG reference is employed, these statistics do not change significantly. In fact, the adaptive reference strategies worsen TIR, TAR1, and TAR2 in exchange for a slightly lower TBR1.

This occurs because the 202 strategy is slow in bringing BG levels within the safe range (indicated by the mean insulin dose being lower than other methods). The adaptive references cannot decrease the BG reference below $r_\ell = 5$ [mmol/L] to ensure a safe range according to (H.12a). Consequently, they are unable to expedite the titration process more than the default strategy with $r = 5$ [mmol/L]. As a result, the adaptive reference methods can solely increase the reference r to reduce instances of hypoglycemia. Moreover, due to the strategy's slowness, it takes a relatively long time for BG concentration to reach the elevated glucose reference.

This suggests that when the default strategy is not fast enough, employing the adaptive reference strategy does not offer significant improvements.

Table H.5: Statistics for different scenarios and algorithms. Std. is short for standard deviation.

	Mean TIR	Std. TIR	Mean TBR1	Std. TBR1	Mean TBR2	Std. TBR2	Mean AG	Std. AG
Target [17]	> 70%		< 4%		< 1%		< 8.6 [mmol/L]	
LS	93%	5.55%	1.8%	0.5%	0%	0%	6.26	1.08
LSR	93.4%	5.52%	0.9%	0.5%	0%	0%	6.4	1.1
LSAR	94.2%	5.02%	0%	0.03%	0%	0%	6.52	1.2
AvgLS	92.7%	0.5%	0.1%	0%	0%	0%	7.3	0.8
AvgLSR	92.7%	0.5%	0.1%	0%	0%	0%	7.3	0.8
AvgLSAR	94.4%	0.48%	0%	0%	0%	0%	7.38	2.12
Step	91.27%	5.3%	1.2%	2.92%	0%	0%	6.46	1.05
StepR	92%	5%	0.9%	2.9%	0%	0%	6.61	0.92
StepAR	93.1%	5%	0.01%	0.06%	0%	0%	6.8	0.74
202	77.67%	14%	0.9%	3%	0%	0%	7.8	1.6
202R	76.5%	13.4%	0.87%	2.4%	0%	0%	7.9	1.63
202AR	76.5%	13.4%	0.87%	2.4%	0%	0%	7.9	1.63

	Mean TAR1	Std. TAR1	Mean TAR2	Std. TAR2	Mean Insulin	Mean GV	Std. GV	Mean GMI	Std. GMI
Target [17]	< 25%		< 5%			< 36%		< 7%	
LS	4.02%	4.24%	1.18%	0.8%	75.8 [U]	27.7%	6.7%	6.04%	0.45%
LSR	5.2%	4%	1.3%	0.73%	80.1 [U]	25%	5.4%	6.81%	1.2%
LSAR	5.5%	1.23%	1.02%	0.4%	109.67 [U]	28%	5.88%	6.98%	1.5%
AvgLS	6.35%	5%	0.9%	0.9%	58.9 [U]	19.77%	3.44%	6.46%	0.38%
AvgLSR	6.4%	5.1%	0.87%	0.9%	61 [U]	20.02%	3.53%	6.5%	0.5%
AvgLSAR	6.38%	5%	0.87%	0.9%	64.9 [U]	19.85%	3.45%	6.48%	0.38%
Step	5.91%	4.81%	1.63%	1.64%	74.7 [U]	29.47%	7.8%	6.12%	0.46%
StepR	5.7%	4.5%	1.6%	1.6%	72.04 [U]	28.2%	7.8%	6.2%	0.4%
StepAR	5.71%	4.5%	1.6%	1.6%	68.04 [U]	26.01%	6%	6.27%	0.32%
202	17.3%	11.5%	4.1%	5.2%	47.77 [U]	30.6%	8%	6.7%	0.7%
202R	18%	11%	4.3%	5%	47.8 [U]	30.65%	8%	6.7%	0.71%
202AR	18%	11%	4.3%	5%	47.8 [U]	30.65%	8%	6.7%	0.71%

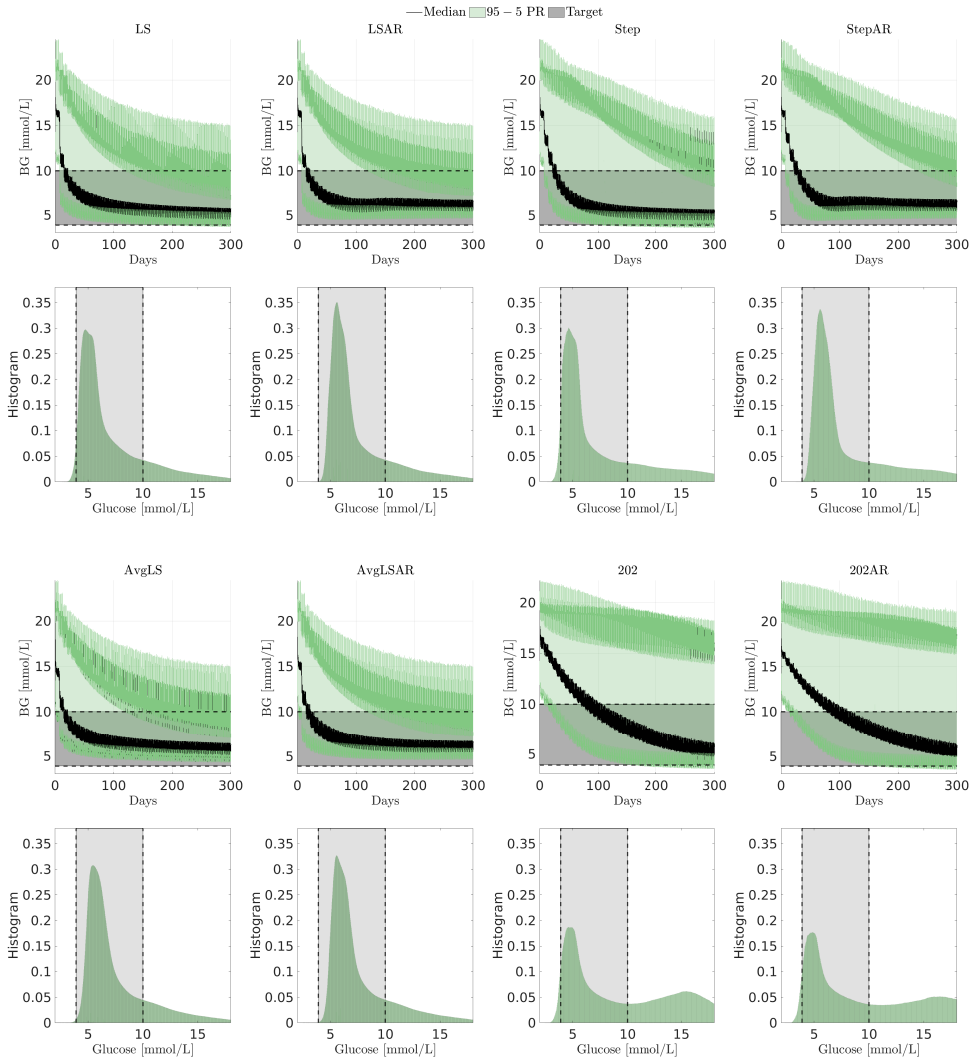

Fig. H.4: Simulation results for LS, LSAR, AvgLS, AvgLSAR, Step, StepAR, 202, 202AR with Model 1, Model 2, and Model 3. The plots on the second row are normalized histograms for all the glucose readings with $T_m = 5$ [min] among the 1500 simulated subjects.

6 Conclusion and Future Work

In this paper, we presented two simple methods for adapting the BG target for subjects with T2D based on CGM measurements. Simulation results with three different models showed that these methods, when combined with insulin titration strategies, managed to reduce instances of hypoglycemia when compared to using the insulin titration methods alone. Future research will involve conducting a more thorough analysis of the proposed methods under various simulation scenarios and in combination with different insulin titration strategies, as well as testing them in different models of T2D.

References

[1] T. Kadowaki, H. Jinnouchi, K. Kaku, M. L. Hersløv, J. Hyllested-Winge, and S. Nakamura, "Insulin degludec in a simple or stepwise titration algorithm in a japanese population of patients with type 2 diabetes: a randomized, 26-week, treat-to-target trial," *Diabetology international*, vol. 8, no. 1, pp. 87–94, 2017.

[2] T. B. Aradóttir, D. Boiroux, H. Bengtsson, J. Kildegaard, M. L. Jensen, J. B. Jørgensen, and N. K. Poulsen, "Model predictive control for dose guidance in long acting insulin treatment of type 2 diabetes," *IFAC Journal of Systems and Control*, vol. 9, p. 100067, 2019.

[3] D. Krishnamoorthy, D. Boiroux, T. B. Aradóttir, S. E. Engell, and J. B. Jørgensen, "A model-free approach to automatic dose guidance in long acting insulin treatment of type 2 diabetes," *IEEE Control Systems Letters*, vol. 5, no. 6, pp. 2030–2035, 2020.

[4] M. Al Ahdab, T. Knudsen, J. Stoustrup, and J.-J. Leth, "An online stochastic optimization approach for insulin intensification in type 2 diabetes with attention to pseudo-hypoglycemia (in press)," in *2022 IEEE 61th Conference on Decision and Control (CDC)*, 2022.

[5] D. Shi, E. Dassau, and F. J. Doyle, "Adaptive zone model predictive control of artificial pancreas based on glucose- and velocity-dependent control penalties," *IEEE Transactions on Biomedical Engineering*, vol. 66, no. 4, pp. 1045–1054, 2019.

[6] M. T. McDermott, "Pseudopheochromocytoma," *Management of Patients with Pseudo-Endocrine Disorders: A Case-Based Pocket Guide*, p. 193, 2019.

[7] E. Hazan *et al.*, "Introduction to online convex optimization," *Foundations and Trends® in Optimization*, vol. 2, no. 3-4, pp. 157–325, 2016.

[8] H. Fang, N. Harvey, V. Portella *et al.*, "Online mirror descent and dual averaging: keeping pace in the dynamic case," in *International conference on machine learning*. PMLR, 2020, pp. 3008–3017.

[9] T. B. Aradóttir, H. Bengtsson, M. L. Jensen, N. K. Poulsen, D. Boiroux, L. L. Jensen, S. Schmidt, and K. Nørgaard, "Feasibility of a new approach to initiate insulin in type 2 diabetes," *Journal of diabetes science and technology*, vol. 15, no. 2, pp. 339–345, 2021.

[10] M. A. Ahdab, M. Papež, T. Knudsen, T. B. Aradóttir, S. Schmidt, K. Nørgaard, and J.-J. Leth, "Parameter estimation for a jump diffusion model of type 2 diabetic patients in the presence of unannounced meals," in *2021 IEEE Conference on Control Technology and Applications (CCTA)*, 2021, pp. 176–183.

[11] S. E. Engell, T. B. Aradóttir, H. Bengtsson, M. Ekelund, and J. B. Jørgensen, "Glucose response to fast-and long-acting insulin in people with type 2 diabetes," *IFAC-PapersOnLine*, vol. 54, no. 15, pp. 496–501, 2021.

[12] M. Al Ahdab, J.-J. Leth, T. Knudsen, P. Vestergaard, and H. G. Clausen, "Glucose-insulin mathematical model for the combined effect of medications and life style of type 2 diabetic patients," *Biochemical Engineering Journal*, vol. 176, p. 108170, 2021.

[13] M. Ahdab, T. Knudsen, and J.-J. Leth, "State space temporal gaussian processes for glucose measurements," in *2022 European Control Conference (ECC)*. United States: IEEE, 2021, pp. 1277–1282.

[14] *In vitro diagnostic test systems: requirements for blood-glucose monitoring systems for self-testing in managing diabetes mellitus*. International Organization for Standardization, 2003.

[15] D. Rodbard, "Characterizing accuracy and precision of glucose sensors and meters," *Journal of diabetes science and technology*, vol. 8, no. 5, pp. 980–985, 2014.

[16] P. Colmegna, K. Wang, J. Garcia-Tirado, and M. D. Breton, "Mapping data to virtual patients in type 1 diabetes," *Control Engineering Practice*, vol. 103, p. 104605, 2020.

[17] R. I. Holt, J. H. DeVries, A. Hess-Fischl, I. B. Hirsch, M. S. Kirkman, T. Klupa, B. Ludwig, K. Nørgaard, J. Pettus, E. Renard *et al.*, "The management of type 1 diabetes in adults. a consensus report by the american diabetes association (ada) and the european association for the study of diabetes (easd)," *Diabetes Care*, vol. 44, no. 11, pp. 2589–2625, 2021.

Paper I

Online Optimization Approach for Calculating Insulin Doses for Individuals with Type 2 Diabetes

Mohamad Al Ahdab, Torben Knudsen, Jakob Stoustrup, and John Leth.

The paper has been submitted to be in the
IEEE Transaction on Control Systems Technology, 2023.

The layout has been revised.

Abstract

This paper presents a novel and computationally efficient approach for determining long-acting insulin doses in subjects with type 2 diabetes (T2D) without relying on a specific physiological model. The main objective is to maintain safe blood glucose levels within a targeted range. The proposed strategy utilizes continuous glucose monitoring (CGM) readings to personalize glucose reference levels, thereby enhancing the safety of T2D patients. To achieve this, the strategy optimizes the parameters of a designated control law through an online optimization method combined with a gradient estimation technique that relies on noisy evaluations of an objective function. Two different control laws are employed and compared, along with two distinct gradient estimation methods: Recursive Least Squares (RLS) and a one-point residual feedback method. Through comprehensive simulations with three different models, the performance of the proposed insulin calculation framework is demonstrated to surpass existing strategies from the literature.

1 Introduction

Because of an imbalance between their insulin secretion rate and the ability of insulin to lower glucose concentration, subjects with type 2 diabetes (T2D) suffer increased levels of blood glucose (BG) concentrations known as hyperglycemia. Untreated high BG concentrations can cause complications in individuals such as cardiovascular disease, damage to the eyesight, and more. Adjusting one's lifestyle and using oral drugs are the first steps in the T2D treatment process. However, if these techniques are ineffective at lowering BG concentrations, T2D subjects can start using long-acting insulin, for example once daily using insulin pens, based on Self Monitored Blood Glucose (SMGB) measurements of Fasting BG (FBG), or based on Continuous Glucose Monitoring (CGM) devices. Insulin titration is the process of determining a patient's ideal long-acting insulin dosage. This procedure is critical because if the insulin dose is insufficient, BG levels will remain high which can result in hyperglycemia. Contrarily, a too high insulin dosage can lower the BG concentration to an unsafe level (hypoglycemia), which can result in fainting, brain damage, or even death. Due to these challenges, several attempts were made to use automated insulin dose calculators for T2D. Standard of care insulin guidance algorithms such as the ones in [1] are based on SMBG measurements each week to decide on a fixed insulin dose. These titration strategies can take a long time to bring FBG concentrations to a safe level. Other titration algorithms based on control theory have been proposed in the literature such as [2], which is a physiological model based strategy using SMBG measurements, and [3], which is a "model-free" approach (in the sense that it does not use a physiological model) with SMBG measurements. The work in [2] relies on a physiological model which can be limiting and challenging to apply for a wide range of T2D subjects. On the other hand, the work in [3] proposed to use an Extremum Seeking Control (ESC) strategy and demonstrated the effectiveness of such approach. The strategy was tested against one model only with limited variation on the parameters and without measurement noise. In [4], we proposed an online optimization strategy based on SMBG measurements and we tested it

with two different model structures[1]. All the previously mentioned strategies target FBG only, by using SMBG measurements. Targeting FBG only is not ideal as the subjects can still have either high BG or low BG during the day. With the development of CGM devices, it is now possible to use CGM measurements and define new BG requirements [5] based on the CGM measurements as done for type 1 diabetes subjects in [6]. The contributions in this paper are as follows:

- We propose a new online optimization strategy (OPS) to tune the parameters of a chosen feedback control law. The OPS technique is derived from the first order Karush–Kuhn–Tucker (KKT) conditions [7] with inequality constraints coupled with gradient estimates computed only using noisy objective function evaluations in a bandit setting.
- We employ and compare between two distinct methods—the recursive least squares (RLS) approach and the one-point residual feedback method—to obtain the gradient estimates that OPS uses.
- We test the strategy with three different simulation models with different structures detailed in Table G.1. The proposed method is also shown in simulation to be more robust to inter-subject variations of T2D subjects than the standard of care strategies in [1] and the proposed "model free" approach in [3]. Additionally, the performance of the developed technique against intra-subject variations and non-adherence to medications was also assessed with simulations. Evaluating insulin dosing strategies with simulations is common practice for both T1D and T2D dosing strategies (see for example [2, 3, 6, 8–11]). The difference in this paper is we test them with three different simulation models with different types of disturbances. A version of one of those models can be accessed online on `www.t2d.aau.dk` and is being tested and used currently by the medical staff at Aalborg University Hospital for teaching purposes.
- We adapt and personalize a target BG value for each T2D individual based on CGM data using an online optimization scheme.

The paper is structured as follows. Section 3.1 explains the setup of the problem with section 3.2 providing descriptions for gradient estimation methods. Section 3.3 discusses the optimization strategy used to tune the control law parameters. In Section 3.4 the cost functions which we aim to minimize to tune the control law parameters are defined. After that, we provide a discussion on the glucose-insulin simulation models used to perform the simulations in section 4. Finally, we present the simulation results in section 5 and provide a conclusion in section 6.

2 Notations

The symbol := indicates "defined by". All vectors are considered as column vectors, $\|\cdot\|$ denotes the 2-norm, and $^{\mathrm{T}}$ denotes transpose. All probabilistic considerations in this paper will be with

[1] We tested with three models but two of them had the same model structure in which one of them was with a measurement noise model and the other was without a measurement noise model.

respect to an underlying probability space $(\Omega, \mathcal{F}, \mathbb{P})$ and *every statement involving stochastic variables will be understood to be valid with probability 1.*

For a random variable x we write $\mathsf{x} = x(\omega)$ for the value of the random variable. We use $\mathcal{N}(\mu, \Sigma)$ to denote the normal distribution with mean μ and covariance Σ, $\ln\mathcal{N}(\mu_m, \sigma_m^2)$ for the log-Normal distribution with parameters μ_m and σ_m^2, $\mathcal{U}(a, b)$ for a continuous uniform distribution with bounds a and b, and $\mathcal{U}_d(a, b)$ for a discrete uniform distribution with bounds a and b. The symbols $\geq_e, >_e, \leq_e, <_e$ denote element-wise inequalities for vectors. If the difference between two consecutive time instants t_k and t_{k+j} is such that $t_{k+j} - t_k = jT,\ j, k \in \mathbb{N}$ with $T \in \mathbb{R}$ being a constant, then variables that are indexed with time $x(t_k), x(t_{k+j})$ will be denoted by $x(k), x(k+j)$ for ease of notation. We let $[a, b]$ denote the closed interval from a to b, and $[a\ b]$ denote the row vector with coordinates a and b. For a diagonal matrix A with diagonal entries $a = [a_1 \cdots a_n]^{\mathrm{T}}$, the notation $A = \mathrm{diag}(a)$ is used. The symbol I_n is used to denote the $n \times n$ identity matrix and the symbol $\mathbf{1}$ is used to denote a column vector of ones. Finally, a projection operator is defined as $\Pi_{\Theta,\Sigma}(x) := \mathrm{argmin}_{\theta\in\Theta}\|\Sigma^{1/2}(\theta - x)\|^2$ with Σ a positive definite matrix and Θ a compact set. Let $\mathbb{B}^d := \left\{x \in \mathbb{R}^d : \|x\|_2 \leq 1\right\}$ denote the closed unit ball in $\mathbb{R}^d$ with $\mathcal{U}\left(\mathbb{B}^d\right)$ the uniform distribution over $\mathbb{B}^d$, and let $\mathbb{S}^{d-1} := \left\{x \in \mathbb{R}^d : \|x\|_2 = 1\right\}$ denote the unit sphere in $\mathbb{R}^d$ with $\mathcal{U}\left(\mathbb{S}^{d-1}\right)$ the uniform distribution on $\mathbb{S}^{d-1}$. For a vector $x = [x_1, \ldots, x_N]^{\mathrm{T}}$, we define a vector of moving averages with a window $H \leq N$ as $\mu_H(x) := 1/H \left[\sum_{i=1}^{H} x_i, \ldots, \sum_{i=N-H+1}^{N} x_i\right]^{\mathrm{T}}$. For $x \in \mathbb{R}$, we denote the softplus function with parameter $\alpha > 0$ as $\mathrm{s}_\alpha(x) := 1/\alpha \log\left(1 + \exp(\alpha x)\right)$. Additionally, if x is a vector, then $\mathrm{s}_\alpha(x)$ is to be understood element-wise.

3 Dosing Strategy

3.1 Problem Specification

In this section we describe the problem setup and the dosing strategy. We consider that at each time instant $kT_K,\ k \in \mathbb{Z}_{\geq 0}$ with T_K being in the order of days (e.g. $T_K = 1$ [day] or $T_K = 7$ [day]) a subject with T2D will provide BG related measurements which will be used to calculate a new long-acting insulin dose recommendation for the subject to administer once everyday until the $(k+1)T_K$ day. See figure I.1 for an overview of the setup. We consider to adjust the insulin doses according to a control law π

$$\Delta u(k) = \pi\left(y_g(k), \theta(j(k))\right), j(k) = \left\lfloor T_K k / T_J \right\rfloor, \tag{I.1}$$

$$u(k) = \max\left(0, u(k-1) + \Delta u(k)\right) \tag{I.2}$$

where $u(k)$ [U] is the long-acting insulin dose recommended at day kT_K to be administered once daily until day $(k+1)\,T_K$, $\theta(j(k))$, or $\theta(j)$ referring to $\theta(jT_J)$ for ease of notations, are parameters for the control law π which are updated every $T_J \geq T_K$ days with $T_J \in \mathbb{Z}_{>0}$. For example, if $T_K = 1$ [day] and $T_J = 7$ [day], then $\Delta u(0) = \pi\left(y_g(0), \theta(0)\right), \Delta u(1) = \pi\left(y_g(1), \theta(0)\right), \ldots, \Delta u(7) = \pi\left(y_g(7), \theta(1)\right)$, and so on. The value $y_g(k)$ is a glucose value calculated based on the available glucose measurements. If SMBG measurements of fasting

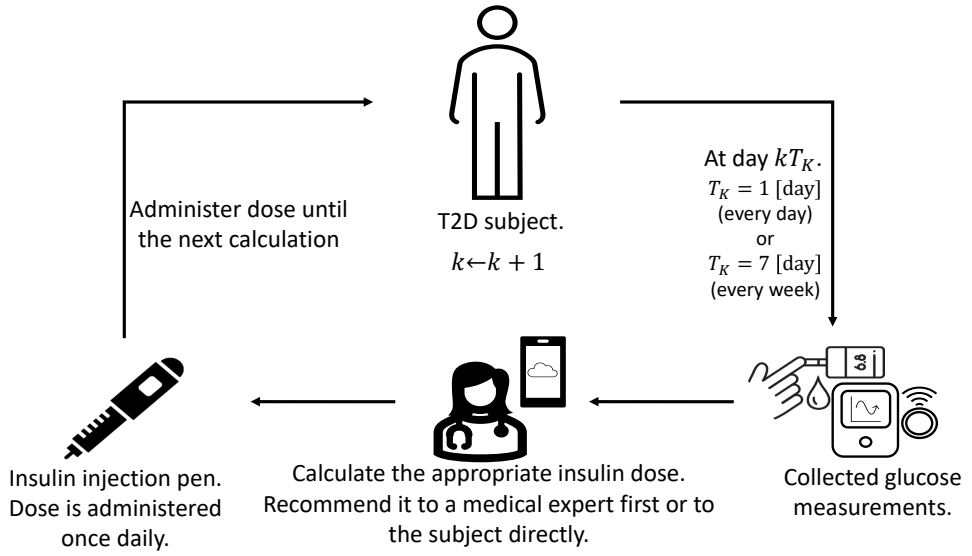

Fig. I.1: Overview of the setup. Each kT_K days, the subject provides collected glucose measurements for the insulin dosing strategy. The dosing strategy calculates a new dose and recommended it either to a medical expert first, or to the subject directly. The subject then administer the recommended dose every day until the next calculation.

BG (FBG) are available, then $y_g(k)$ is the SMBG measurement of FBG. Alternatively, if CGM measurements are available, then $y_g(k) = \min\left(\mu_H\left(\mathcal{Y}_c(k)\right)\right)$ with $\mathcal{Y}_c$ being a vector of the available CGM measurements from day $(k-1)\,T_K$ until day kT_K, and $H = 3$ [hour][2]. In this paper, we will consider two different control laws parameterized with a gain parameter K_p and a desired glucose reference r for y_g such that $\theta = [K_p\ r]^{\mathrm{T}}$. The first control law is

$$\pi\left(y_g(k), \theta(j)\right) = \pi_p\left(y_g(k), \theta(j)\right) := K_p(j)\left(y_g(k) - r(j)\right) \tag{I.3}$$

and the second one is

$$\pi\left(y_g(k), \theta(j)\right) = \pi_s\left(y_g(k), \theta(j)\right) := K_p(j)\left(s_2(\bar{y}_g(k) - r(j) - 1) - s_2(r(j) - 1 - \bar{y}_g(k))\right) \tag{I.4}$$

Figure I.2 showcases the two control laws π_p and π_s for a fixed K_p and r together with a standard of care strategy (Step) [1] (see Table G.2). The control law π_s damps the changes of insulin doses for values close to the reference r when compared to π_p, and thus, is less sensitive to noise and disturbances when the glucose value y_g is close to the target r.

[2]Taking the minimum of a moving average gives an estimate of the lowest BG concentration during the day. This has been introduced in a clinical trial [12].

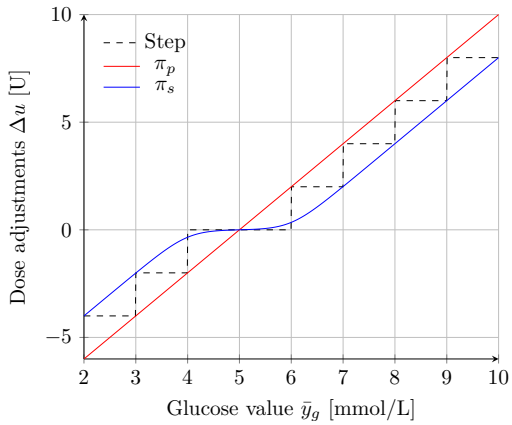

Fig. I.2: The standard of care Step strategy together with the two control laws π_p and π_s for $r = 5$ [mmol/l] and $K_p = 2$.

The goal of the strategy is to tune the values of $K_p(j)$ and $r(j)$ based on $y_g(k)$ or $\mathcal{Y}_c(k)$ to calculate a new insulin dose $u(k)$. The tuning of $\theta(j) := \begin{bmatrix} K_p(j) & r(j) \end{bmatrix}^{\mathrm{T}}$ is made by an online optimization scheme which finds estimates $\hat{\theta} = \begin{bmatrix} \hat{K}_p(j) & \hat{r}(j) \end{bmatrix}^{\mathrm{T}}$ that tracks

$$\theta^*(j) = \underset{\theta \in \Theta}{\operatorname{argmin}} \ \eta(j)\bar{c}(j,\theta) + \alpha \frac{\|\theta - \theta^*(j-1)\|^2}{2}, \tag{I.5}$$

where $\bar{c}\,(j,\theta) := c\left(y_g(j;\theta), \mathcal{Y}_c(j;\theta)\right)$ is an objective function chosen by the designer with $y_g(j;\theta), \mathcal{Y}_c(j;\theta)$ being the glucose measurements obtained with using parameters θ from day $(j-1)\,T_J$ until day jT_J, $\eta(j) > 0$, and $\alpha > 0$. This problem can be thought of as a tracking problem where a pursuer $\hat{\theta}(j)$ tries to track a target $\theta^*(j)$. For each $\hat{\theta}(j)$, an inexact gradient $\hat{g}(j+1) \approx \nabla \bar{c}(j+1, \hat{\theta}(j)))$ will be estimated. The pursuer will then use $\hat{g}(j+1)$ to obtain an estimate $\hat{\theta}(j+1)$. The term $\alpha \frac{\|\theta - \theta^*(j-1)\|^2}{2}$ is added to ensure that the parameters θ^* do not change abruptly between iterations. Additionally, the parameters $\eta(j)$ and α are included to help balance between the cost $\bar{c}(j,\theta)$ and $\frac{\|\theta - \theta^*(j-1)\|^2}{2}$.

The objective function $\bar{c}(j,\theta)$ is chosen with the following assumption

Assumption 3.1. *The function $\bar{c}$ is uniformly bounded over the set Θ, i.e. there exists a constant $\bar{C}$ such that $\bar{c}(j,\theta) \geq \bar{C}$ for all $\theta \in \Theta$ and $j \geq 0$.*

This assumption ensures that there exists a finite minimizer to $\bar{c}(j,\theta)$. See the work in [13, 14] for convergence analysis in a related setting. For the work in this paper, we introduce a time varying optimization scheme as detailed in section 3.3. For the gradient estimates, we employ and compare between two different methods in 3.2, namely a recursive least squares method and a randomization method based on the residual feedback method first introduced in [15].

3.2 Methods for Gradient Estimates

In this section, we describe two different methods to obtain a gradient estimate that can be used for the online optimization scheme in 3.3.

Recursive Least Squares

We assume a local linear model for the cost

$$\bar{c}(j;\hat{\theta}(j-1)) \approx [\hat{\theta}^{\mathrm{T}}(j-1)\ \mathbf{1}^{\mathrm{T}}] \begin{bmatrix} \mathrm{g}(j) \\ \mathrm{b}(j) \end{bmatrix} := \boldsymbol{\phi}^{\mathrm{T}}(j)\boldsymbol{\psi}(j), \tag{I.6}$$

where $\mathrm{g}(j)$ represent the gradient $\nabla\bar{c}(j,\theta)$, and $\mathrm{b}(j)$ is a bias term. We utilize the first order approximation in (I.6) in an RLS context with exponential directional forgetting for a gradient estimate $\mathrm{g}(j)$. See appendix A for a description of the RLS algorithm.

Residual Feedback

Unlike the RLS strategy for gradient estimation, this method does not require a local linear approximation model for the cost. The residual between two successive feedback (cost function) values is the foundation of the one-point residual feedback gradient estimate proposed by [15] for zeroth-order optimization. Let $\Delta\bar{c}(j,\hat{\theta}(j-1),\hat{\theta}(j-2)) := \bar{c}\left(j,\hat{\theta}(j-1)+\gamma\nu(j-1)\right) - \bar{c}\left(j-1,\hat{\theta}(j-2)+\gamma\nu(j-2)\right)$, the one-point residual feedback estimate is computed as

$$\hat{g}(j) = n_\theta \Delta\bar{c}(j,\hat{\theta}(j-1),\hat{\theta}(j-2))\gamma^{-1}\nu(j-1), \tag{I.7}$$

where $\nu(j) \sim \mathcal{U}\left(\mathbb{S}^{n_\theta-1}\right)$, n_θ is the dimension of θ, and $\gamma \in \mathbb{R}^{n_\theta}_{>0}$ is called an exploration parameter. Note that all the operations on the vectors ν and γ in (I.7) are element-wise operations. The gradient estimate (I.7) satisfies the following [16]

$$\mathbb{E}\left[\hat{g}(j) \mid \nu(j-2)=v,\hat{\theta}(j-2)\right] = \nabla\bar{c}_\gamma(j,\hat{\theta}(j-1)),$$

where $\bar{c}_\gamma(j,\theta) := \mathbb{E}[\bar{c}_\gamma(j,\theta+\gamma\zeta)]$ with $\zeta \sim \mathcal{U}\left(\mathbb{B}^{n_\theta}\right)$ is a smoothed version of $\bar{c}(j,\theta)$ obtained by averaging over the ball $\mathbb{B}^{n_\theta}$. In other words, $\hat{g}(j)$ in (I.7) is an unbiased estimator for the gradient of a smoothed version $\bar{c}_\gamma(j,\theta)$ of $\bar{c}(j,\theta)$.

3.3 Tracking Strategy

Due to the time varying nature of the optimization problem, we propose a strategy inspired by time varying optimization algorithms [17, 18]. Let the set Θ be defined by inequality constraints $\Theta = \left\{\theta \in \mathbb{R}^2 | h(\theta) \in \mathbb{R}^2, h(\theta) \leq_e 0\right\}$ such that the Jacobian $\nabla h(\theta)$ is full rank. We can then

write the first order KKT conditions of (I.5) as following

$$\theta^*(j) = \bar{\theta}(j) + \frac{1}{\alpha}\nabla h\left(\theta^*(j)\right)^{\mathrm{T}}\mu(j) \tag{I.8a}$$

$$h\left(\theta^*(j)\right) \leq_e 0, \tag{I.8b}$$

$$h\left(\theta^*(j)\right)^{\mathrm{T}}\mu(j) = 0, \tag{I.8c}$$

$$\mu(j) \geq_e 0, \tag{I.8d}$$

where $\bar{\theta}(j) := \theta^*(j-1) - \frac{\eta(j)}{\alpha}\nabla\bar{c}\left(j, \theta^*(j)\right)$, and $\mu(j)$ are the Lagrange multipliers. Note that the KKT conditions (I.8) are the same KKT conditions for the problem

$$\theta^*(j) = \underset{\theta\in\Theta}{\operatorname{argmin}} \frac{\alpha}{2}\|\theta - \bar{\theta}(j)\|^2, \tag{I.9}$$

In other words, the solution $\theta^*(j)$ for (I.8) is equivalent to the following

$$\theta^*(j) = \Pi_{\Theta,\alpha\mathrm{I}}\left(\theta^*(j-1) - \frac{\eta(j)}{\alpha}\nabla\bar{c}\left(j, \theta^*(j)\right)\right), \tag{I.10}$$

Observe that (I.10) is an implicit equation since both $\nabla\bar{c}(j, \theta^*(j))$ and $h(\theta^*(j))$ depend on $\theta^*(j)$. For some cases of $h\left(\theta^*(j)\right)$, the solution to the projection problem (I.9) can be found in closed form and without an implicit dependence on $\theta^*(j)$. In this paper we choose $h(\theta^*(j))$ to be affine (box constraints). This choice provides an explicit closed form solution to (I.9). With the choice of affine constraints, equation (I.10) is still an implicit equation but now it is implicit only due to the term $\nabla\bar{c}(j, \theta^*(j))$. One way to approximately solve (I.10) is to assume that $\nabla\bar{c}(j, \theta^*(j)) \approx \nabla\bar{c}(j, \theta^*(j-1))$. This can be a reasonable assumption if the difference between $\theta^*(j)$ and $\theta^*(j-1)$ is assumed to be small, which is reasonable assumption given the cost on the change between $\theta^*(j)$ and $\theta^*(j-1)$. A more accurate approximation for the solution is to use a quasi-Newton method [19] by using the first order Taylor approximation $\nabla\bar{c}(j, \theta^*(j)) \approx \nabla\bar{c}(j, \theta^*(j-1)) + Q_{j-1}\left(\theta^*(j) - \theta^*(j-1)\right)$ where the matrix Q_{j-1} is an approximate for the hessian matrix $\nabla^2_\theta\bar{c}(j, \theta^*(j-1))$. If a quasi-Newton method is used then (I.8a) in the KKT condition (I.8) is approximately

$$\theta^*(j) \approx \theta^*(j-1) - \eta(j)\tilde{Q}^{-1}_{j-1}\nabla\bar{c}\left(j, \theta^*(j-1)\right) + \tilde{Q}^{-1}_{j-1}\nabla h\left(\theta^*(j)\right)^{\mathrm{T}}\mu(j), \tag{I.11}$$

which is equivalent to

$$\theta^*(j) \approx \Pi_{\Theta,\tilde{Q}_{j-1}}\left(\theta^*(j-1) - \eta(j)\tilde{Q}^{-1}_{j-1}\nabla\bar{c}\left(j, \theta^*(j-1)\right)\right), \tag{I.12}$$

where $\tilde{Q}_{j-1} = \alpha\mathrm{I} + \eta(j)Q_{j-1}$. Since for our problem we only have noisy estimates of the gradient $\hat{\mathrm{g}}(j) = \nabla\bar{c}(j, \theta^*(j-1))$, we need to use a stochastic Quasi-Newton method. In our previous work [4], the AdaBelief strategy [20] was demonstrated to have a good performance for our application. Therefore, we will continue to use it in this work. The AdaBelief Strategy calculates a simple diagonal approximation matrix Q_{j-1} which was shown to be related to the curvature of the cost function. In this paper, we use the AdaBelief strategy to obtain Q_{j-1} and the summary of our Online optimization strategy (OPS) is presented in Algorithm 8. Note

Algorithm 8: OPS algorithm

parameter: Parameters $\eta(j) > 0,\ \alpha > 0$, smoothing parameters $0 \leq \beta_1 \leq 1$ and $0 \leq \beta_2 \leq 1$, and a vector of small numbers ϵ. Note that all the operations in the algorithm are element-wise.

Input: Initial $m(0) = 0$, $s(0) = 0$, and $\hat{\theta}(0) \in \Theta$.

Output: $\hat{\theta}(j)$

1 $j = 0$

2 **while** *Ongoing Titration* **do**

3 $\quad j \leftarrow j + 1$

4 $\quad$ Run algorithm 9 or use equation (I.7) to obtain $\hat{\mathrm{g}}(j)$.

5 $\quad m(j) = \beta_1 m(j-1) + (1-\beta_1)\hat{\mathrm{g}}(j)$

6 $\quad s(j) = \beta_2 s(j-1) + (1-\beta_2)(m(j) - \hat{\mathrm{g}}(j))^2 + \epsilon,$

7 $\quad \hat{m}(j) = \frac{m(j)}{1-\beta_1^j}, \hat{s}(j) = \frac{s(j)}{1-\beta_2^j},$ (Bias-Correction.)

8 $\quad \hat{\theta}(j) = \Pi_{\Theta, \mathrm{diag}\left(\eta(j)\sqrt{s(j)}\right)+\alpha \mathrm{I}} \left(\hat{\theta}(j-1) - \eta(j) \frac{m(j)}{\eta(j)\sqrt{s(j)}+\alpha+\epsilon} \right)$

that $m(j)$ is an exponential moving average (the output of a first order low pass filter with a gain of 1) for the gradient estimate $\hat{\mathrm{g}}(j)$. As a result, the algorithm uses a smoother version of the gradient. As for $s(j)$, it reflects the difference between the gradient estimate $\hat{\mathrm{g}}(j)$ and $m(j)$ such that, for an increased difference, the stepping size will decrease and vice versa. The matrix Q_{j-1} in the algorithm is diag $\big(s(j)\big)$.

In this paper, the parameters for the algorithm 8 are chosen to be $\eta(j) = 1, \alpha = 1,\ \beta_1 = 0.99,\ \beta_2 = 0.999$ and $\epsilon = 10^{-8}\mathbf{1}$. Additionally, we choose $\Theta = [0, 5] \times [5, 6.9]$ for the control law parameters. Note that with this choice of Θ, the projection in line 8 of the OPS algorithm 8 is an element-wise saturation function on the bounds of the set Θ [3]. Note that the lower and upper limits for $\hat{r}(j)$ are design parameters. If it is acceptable for specific subjects to have a reference FBG/ABG above 6.9 [mmol/L] or below 5 [mmol/L] then the user can set different bounds.

3.4 Cost function definition

The main aim of the control strategy is to bring the glucose concentration to a safe zone. For this objective, we define two different objective functions based on the glucose measurement used and whether or not we want to adapt the glucose reference r. If only y_g is to be used (for example if only SMBG measurements are available), then we define an objective function intended to optimize for K_p only as following:

$$c_{g_1}(y_g(j)) = (y_g - 5.5)^2 + 4s_2\,(5.5 - y_g)^2\,, \tag{I.13}$$

The decision to use 5.5 [mmol/L] was based on the fact that the FBG should be between

[3] Simulation results demonstrate that parameters in Θ leads to a stable response

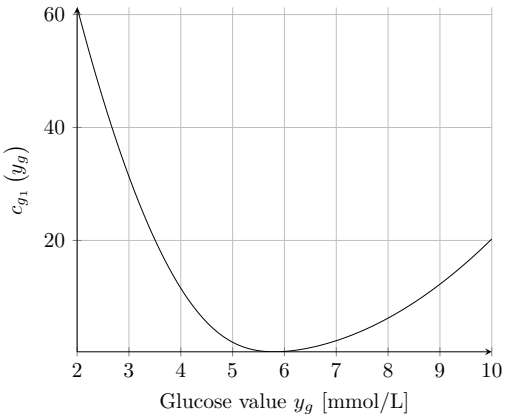

Fig. I.3: The function c_{g_1} against y_g.

4 [mmol/L] and 6 [mmol/L] according to the standard of care for insulin titration schemes [1]. Because hypoglycemia (BG concentrations from 3.9 [mmol/L] and below) is more harmful than hyperglycemia, we chose 5.5 [mmol/L] rather than the middle of the range $[4, 6]$ [mmol/L]. Additionally, the softplus function s_2 is included to assign more weights to regions close to the hypoglycemia region as shown in Figure I.3.

IF CGM measurements are used, then we can use information regarding the BG during the day to also adjust for the reference r of y_g. Therefore, we define the following objective function

$$c_{g_2}(\mathcal{Y}(j)) = 8s_2\left(5.5 - \mathcal{Y}(j)\right)^{\mathrm{T}} s_2\left(5.5 - \mathcal{Y}(j)\right) + 4s_2\left(\mathcal{Y}(j) - 10\right)^{\mathrm{T}} s_2\left(\mathcal{Y}(j) - 10\right) \tag{I.14}$$

The objective function (I.14), see Figure I.4, is based on the range defined for safe CGM readings in [5]. With the CGM dependent cost in (I.14), it is possible to penalize BG concentrations, in contrast to only FBG concentrations, which are not safe. This can be useful to reduce hypoglycemic events happening during the day. For example, the strategy can increase the y_g tracking reference r in (I.1) or (I.2) if a subject is having hypoglycemic events during the day more frequently. In conclusion, if only y_g is to be used, then the the objective function is $\bar{c}(j, \theta) = c_{g_1}\left(y_g(j)\right)$ defined in (I.13). If $\mathcal{Y}_c$ is available, then the objective function is $\bar{c}(j, \theta) = c_{g_2}\left(\mathcal{Y}(j)\right)$ defined in (I.14).

4 Glucose-Insulin Simulation Models

For the glucose-insulin dynamic simulations in this paper, we consider three different simulation models. For the first model, denoted "Model 1", we consider an extension of [3] to consider BG concentrations and not only FBG concentration by using a jump diffusion model for meals and disturbances [21]. In the jump diffusion models, the times for the meal events

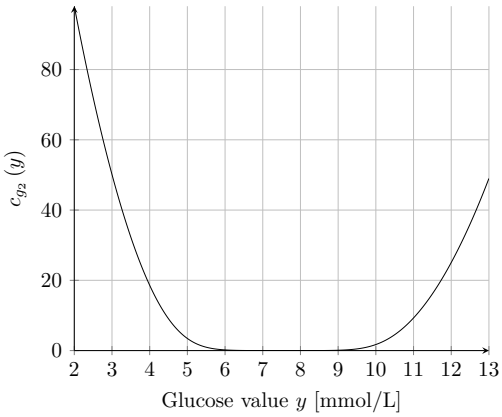

Fig. I.4: The function c_{g_2} against a glucose value y.

are drawn according to a Poisson process and the size of the meals is drawn according to a log-Normal distribution $\ln\mathcal{N}(\mu_m, \sigma_m^2)$ with parameters $\mu_m = \ln(60)$ and $\sigma_m = \ln(1.5)$ (a mean of 65.14 and a variance of 50.9). The average meal rate for the Poisson process is chosen to be 3 [meals/day] between the hours 7:00 and 23:00 and 0.1 [meals/day] during other hours to take into account that individuals do not eat as frequently at night. As for the diffusion part, a constant diffusion is added to the BG concentration state. For the second model, denoted "Model 2", we consider the model presented in [22] augmented with a jump diffusion model for meals and disturbances matching "Model 1". Finally, the third model, denoted "Model 3", is the high fidelity model [23]. The meal times for Model 3 are drawn from uniform distributions as following: $\mathcal{U}(6, 8)$ [h] for breakfast meals, $\mathcal{U}(12, 14)$ [h] for lunch meals, and $\mathcal{U}(19, 20)$ [h] for dinner meals. The carbohydrate intake for each meal is also drawn uniformly according to $\mathcal{U}(10, 40)$ [g] for breakfast, $\mathcal{U}(20, 50)$ [g] for lunch, and $\mathcal{U}(30, 100)$ [g] for dinner. The choice of simulating the meals differently for Model 3 was to evaluate the insulin dosing strategies against a distinct type of stochastic disturbances. Additionally, we conduct simulations with two distinct cases to model changes in the physiological state of the subjects. The first case involves a decrease in insulin sensitivity and insulin secretion rate over time. The evolution of these parameters is described by the following equations:

$$I_{sen} = \bar{I}_{sen}\left(1 - \Delta I_{sen}\left(1 - \mathrm{e}^{-t/\tau_v}\right)\right), \tag{I.15}$$

$$I_{sec} = \bar{I}_{sec}\left(1 - \Delta I_{sec}\left(1 - \mathrm{e}^{-t/\tau_v}\right)\right), \tag{I.16}$$

where I_{sen} and I_{sec} represent the insulin sensitivity and insulin secretion parameters for each simulation model, respectively. The values $\bar{I}_{sen}, \bar{I}_{sec}$ are the nominal values for I_{sen} and I_{sec}, respectively. The values ΔI_{sen} and ΔI_{sec} are the changes on the nominal values for I_{sen} and I_{sec}, respectively. The rate parameter τ_v [Day^{-1}] is a time constant to set how fast the nominal

values $\bar{I}_{sen}, \bar{I}_{sec}$ will converge to $\bar{I}_{sen}(1-\Delta I_{sen}), \bar{I}_{sec}(1-\Delta I_{sec})$, respectively. The second case involves an improvement in insulin sensitivity during treatment as following

$$I_{sen} = \bar{I}_{sen}\left(1+\Delta I_{sen}\left(1-\mathrm{e}^{-t/\tau_v}\right)\right). \tag{I.17}$$

For each subject, we randomly select between the two cases in (I.15) and (I.17) with equal probability of 0.5. For the measurement errors, we consider an SMBG measurement error model [24] as the following

$$y_s(k) = x_g(k) + \sigma_s\left(x_g(t_s)\right)\varepsilon_s(k), \tag{I.18a}$$

$$\sigma_s\left(x_g\right) = \frac{1}{\kappa}\sigma_2 \log\left(1+\mathrm{e}^{\kappa\left(x_g-4.2\right)}\right)+\sigma_1, \tag{I.18b}$$

with σ_1 and σ_2 chosen in accordance to the ISO standard [25] to be $\sigma_1 = 0.415$ [mmol/L] and $\sigma_2 = 0.1$, $\kappa = 5$, and $x_g(k)$ is the state corresponding to the BG concentration. Additionally, we consider a CGM measurement error model according to

$$y_c(k) = x_c(k) + \sigma_c x_c(k)\varepsilon_c(k), \tag{I.19}$$

with $\sigma_c = 0.42$ in accordance to a MARD of 10% [26] as done in [27]. Here, the state x_c represents the glucose concentration in the interstitial compartment of the models 2 and 3 and the BG concentration for model 1 since it does not have an interstitial compartment. Table I.2 summarizes the models used for simulations in this paper. For the results in this paper, we simulate 1500 T2D individuals for a year. The first 500 of the 1500 subjects were produced using Model 1, the following 500 were produced using Model 2, and the final 500 were produced using Model 3. The initial glucose and insulin concentrations for each individual were drawn uniformly together with parameters effecting insulin resistivity and insulin secretion, and the time constant for injected long-acting insulin. Table I.1 summarizes the parameters drawn for each T2D model.

Remark 4.1. *It is important to note that drawing the parameters independently, as done in prior studies such as [2, 3, 11, 22], will provide a larger set of subjects to simulate than the case if the parameters were drawn from a joint probability distribution. The larger set of subjects might contain extreme or unrealistic cases. However, if a dosing strategy perform well on the larger set of simulated subjects then it is likely to be more robust to extreme or rare cases which is safer. Moreover, obtaining a joint probability distribution which covers all the possible cases is generally difficult and would require a large set of data covering different cases and extremes of T2D subjects.*

5 Results and Discussion

In this section, we compare our suggested strategy to three other strategies by simulating it in various scenarios. The code for the simulations can be found on the repository `https://gitlab.com/aau-adapt-t2d/cgm-based-online-optimisation-for-t2d`. The simulations

Table I.1: Parameters for generating subjects from Model 1, Model 2, and Model 3. The state x_g denotes the BG concentration state while x_I denote the blood insulin concentration state.

Model 1	$x_g(0) \sim \mathcal{U}(15, 25)$ [mmol/L], $p_4 \sim \mathcal{U}(0.5, 2.5)$, $p_7 \sim \mathcal{U}(0.5, 2.5)$, $p_1 \sim \mathcal{U}(1.5, 2.5)$, p_6 and the initial conditions of the remaining states are calculated such that $x_g(0)$ is stationary. Parameters p_4, p_7 are I_{sec}, I_{sen} respectively with $\Delta I_{sec}, \Delta I_{sen} \sim \mathcal{U}(0.05, 0.25)$ and $\tau_v \sim \mathcal{U}(40, 80)$. Diffusion term $\sigma_g \sim \mathcal{U}(0.1, 2)$.
Model 2	$x_g(0) \sim \mathcal{U}(15, 25)$, $x_I(0) \sim \mathcal{U}(20, 30)$ [pmol/L], $CL_{GI} \sim \mathcal{U}(0.71 \times 10^{-4}, 0.11 \times 10^{-2})$, $I_{PRG} \sim \mathcal{U}(0.05, 2)$, and the initial conditions of the remaining states are calculated such that $x_g(0)$ and $x_I(0)$ are stationary. Parameters CL_I, CL_{GI} are I_{sec}, I_{sen} respectively with $\Delta I_{sec} \sim \mathcal{U}(0.05, 0.25), \Delta I_{sen} \sim \mathcal{U}(0.05, 0.1)$ and $\tau_v \sim \mathcal{U}(40, 80)$. Diffusion term $\sigma_g \sim \mathcal{U}(0.1, 2)$.
Model 3	$x_g(0) \sim \mathcal{U}(15, 25)$ [mmol/L], $x_I(0) \sim \mathcal{U}(0.5, 2)$ [mU/L], $c_1 \sim \mathcal{U}(0.04, 0.09)$, $c_2 \sim \mathcal{U}(2.3, 0.95)$, $c_4 \sim \mathcal{U}(1, 2.4)$, and the initial conditions of the remaining states are calculated such that $x_g(0)$ and $x_I(0)$ are stationary. Scales S_{sec}, S_{sen} are I_{sec}, I_{sen} scaling insulin secretion ration rate and hepatic glucose uptake respectively with $\Delta I_{sec}, \Delta I_{sen} \sim \mathcal{U}(0.05, 0.25)$ and $\tau_v \sim \mathcal{U}(40, 80)$. The nominal values of the sacles are assumed to be 1. Diffusion term $\sigma_g \sim \mathcal{U}(0.1, 2)$.

were performed in Matlab [28] on a Linux machine with an Intel Xeon W-2145 processor running at 4.5 [GH_z] and a memory of 32 [GB]. The first strategy we compare with is the Extremum Seeking Control technique (ESC) suggested in [3]. For ESC, we implement the code which was provided in a repository[4] by the authors which includes a correction and a modification to the algorithm discussed in their paper [3]. We adopt the standard of care titration procedures from [1] given in Table I.3 for the second (denoted as 202) and third (denoted as Step) strategies. The Step method changes the dose weekly based on an average of the prior three days' SMBG data, whereas the 202 strategy modifies the dose weekly depending on the SMBG measurement from the previous day. For our strategy, we simulate with different scenarios as following

- **OPS-RLS**: The strategy is based on π_s with CGM measurements. The RLS is used for

[4] https://github.com/dinesh-krishnamoorthy/Diabetes-Model-free-Titration

Table I.2: Glucose-insulin simulation models used in the paper

Model 1	Based on [21]. Includes a measurement error model.
Model 2	Based on the model from [22]. Augmented with a jump diffusion model matching the one in [21] for meals. Includes measurement error models.
Model 3	Based on the model from [23]. The timing and size of meals are drawn from uniform distributions. Includes a measurement error model. A diffusion term matching the one in [21] is added to the state corresponding to BG concentration.

the gradient estimate. Initial conditions $\hat{K}_p(0) = 0.25$, $\hat{r}(0) = 5.5$. Sampling times are $T_K = 1$ [day] and $T_J = 7$ [day] with a sampling time of 5 minutes for CGM readings.

- **OPS-S**: The strategy is based on π_s with CGM measurements. The one-point residual feedback is used for the gradient estimate. Initial conditions $\hat{K}_p(0) = 0.25$, $\hat{r}(0) = 5.5$. Sampling times are $T_K = 1$ [day] and $T_J = 7$ [day] with a sampling time of 5 minutes for CGM readings.
- **OPS-P**: The strategy is based on π_p with CGM measurements. The one-point residual feedback is used for the gradient estimate. Initial conditions $\hat{K}_p(0) = 0.25$, $\hat{r}(0) = 5.5$. Sampling times are $T_K = 1$ [day] and $T_J = 7$ [day] with a sampling time of 5 minutes for CGM readings.
- **OPS-NA**: Similar to OPS-S, but with the individuals failing to take the recommended insulin dose at time k with probability $p_{na} \sim \mathcal{U}(0.01, 0.05)$ (non-adherence).
- **OPS-SMBG**: OPS-OPRS but with SMBG measurements only. $\hat{K}_p(0) = 0.25$ and the reference is constant $r = \hat{r}(0) = 5.5$ [mmol/L]. Sampling times are $T_K = 1$ [day] and $T_J = 7$ [day] with a sampling time of 5 minutes for CGM readings.

If the one-point residual feedback is used, we choose $\gamma(j) = \frac{1}{1+j^{0.5}}[\gamma_K \ \gamma_r]^{\mathrm{T}}$ with $\gamma_K = 1$ and $\gamma_r = 1.1$. Note that the random perturbation size γ_r for $\hat{r}_d(j)$ is higher than γ_K for $\hat{K}_p(j)$. This is done to make $\hat{r}_d(j)$ converge faster than the proportional gain $\hat{K}_p(j)$. Having $\hat{r}_d(j)$ converge faster will improve the performance of the proportional controller. If the RLS is used, we let $\hat{\psi}(0) = [0\ 0\ 0]^{\mathrm{T}}$, $P = \mathrm{I}$, $\lambda = 0.55$, $\epsilon_\phi = 10^{-3}$. Additionally, we use the same random perturbations $\gamma(j)\nu(j)$ from the one-point residual feedback on $\hat{K}_p(j)$ and $\hat{r}_d(j)$ to improve convergence speed. Note that since RLS is used with directional forgetting, we can decay the size of the dither with time to reduce the oscillations in the estimates on the long run while ensuring the boundedness on $P(j)$. Moreover, we choose $\eta(j) = \frac{0.2}{1+j^{0.5}}$. Note that the choice of $K_p(0)$ is important for the performance of the strategy. If it is chosen to be high, then the initial insulin doses would be high which can lower glucose concentrations too fast for the estimation of $\hat{r}_d$ to catch up. For our strategy, a value of $\hat{K}_p(0) = 0.5$ gave good results for all the simulations with the different models. To compare the scenarios and the algorithms used in the simulations, we use the performance measures and their targets described in [5] for glucose

Table I.3: Standard of care titration strategies.

Strategy	SMBG [mmol/L]	Dose adjustment Δu[U]
202	> 6	$+2$
	$4 - 6$	No change
	< 3.9	-2
Step	> 9	$+8$
	$8 - 8.9$	$+6$
	$7 - 7.9$	$+4$
	$5 - 6.9$	$+2$
	$3.9 - 4.9$	No change
	$3.1 - 3.8$	-2
	< 3.1	-4

Table I.4: Glucose management measures from [5]. The unit for the ranges and glucose values is [mmol/L].

Measure	% of time for BG in	Target
Time in Range (TIR)	$[3.9, 10)$	$> 70\%$
Time Above Range 1 (TAR1)	$[10, 13.9)$	$< 25\%$
Time Above Range 2 (TAR2)	$[13.9, \infty)$	$< 5\%$
Time Below Range 1 (TBR1)	$[3, 3.9)$	$< 4\%$
Time Below Range 2 (TBR2)	$[0, 3)$	$< 1\%$
Average Glucose (AG)		< 8.6
Glucose Variability (GV)		36%
Glucose Management Index (GMI)		7%

managements. The measures are shown in Table I.4. In addition to the measures in Table I.4, we compute the mean long acting insulin dose. Table I.5 shows computed mean and standard deviations (Std) over the 1500 simulations for each strategy or scenario.

Additionally, Figure I.5 shows the results for OPS-S, OPS-P, Step, and ESC. Moreover, Figure I.6 shows violin plots for TIR, TB1, and TA1 with the different strategies and scenarios.

From the results presented in Table I.5, we can observe that all OPS variations, except for OPS-RLS with TA1, achieve a mean which meets the targets for the glucose management measures. Among the OPS variations, OPS-S exhibits the highest mean for TB1, while OPS-SMBG demonstrates the best mean and standard deviation for TIR and AG. However, it is worth noting that incorporating CGM measurements leads to a decrease in the mean and standard deviation for TB1 and TB2 for OPS-S, OPS-P, and OPS-NA. This improvement comes at the expense of a slight reduction in TIR and an increase in TAR1, TAR2, AG, and GMI. Furthermore, the violin plot in Figure I.6 provides additional insights. It illustrates that the fitted kernel density for TB1 values with OPS-SMBG crosses the threshold line of 4%, which indicates a higher risk of hypoglycemia. In contrast, the fitted kernel densities for TIR and TA1

with OPS-SMBG are more distant from the threshold lines when compared to OPS-S, OPS-P, and OPS-NA. It is important to note that reducing TB1 and TB2 is particularly desirable since hypoglycemia poses a greater danger than hyperglycemia. when comparing the results obtained using the RLS method for gradient estimation with OPS-RLS to those achieved with one-point residual-feedback, it becomes clear that OPS-RLS does not perform as effectively. This observation is supported by both Figure I.6 and Table I.5. The violin plot for OPS-RLS shows the presence of strong heavy-tailed fitted kernel distributions for the metrics, indicating a significant number of outlier samples that crosses from the target threshold. Nevertheless, it is worth noting that using RLS with OPS-RLS could potentially yield results similar to OPS-S or even better than them. This could be achieved by exploring different parameter values for RLS that were not considered in our study.

When comparing the utilization of π_p as a control law in OPS-P instead of π_s in OPS-S, it becomes evident, based on the results depicted in Figure I.5, that the blood glucose (BG) levels exhibit greater variability over time and have samples falling below the target range when employing OPS-P compared to OPS-S. The statistics in Table I.5 further supports this observation, indicating that OPS-P demonstrates higher mean and standard deviation values for TB1 in contrast to OPS-S. Conversely, OPS-P exhibits slightly better mean and standard deviation values for TIR, TA1, AG, and GMI compared to OPS-S. These findings are consistent with the results observed in the violin plots presented in Figure I.6. The limited dose adjustments in π_s when the BG values are in proximity to the target range makes the BG response less susceptible to noise in y_g compared to π_p employed in OPS-P. Consequently, the BG response in OPS-S appears more steady and less prone to fluctuations than in OPS-P. The adoption of π_s as a control law in OPS-S results in a more steady BG response, as evidenced by lower variability and fewer instances of BG values falling outside the desired target range, in comparison to the utilization of π_p in OPS-P.

When examining the standard of care strategies (Step and 202), it becomes apparent from both Table I.5 and Figure I.6 that they fall short in terms of performance compared to the other strategies, particularly regarding Time in Range (TIR). Notably, The 202 method has the poorest TIR statistics among all the strategies evaluated. Additionally, the Step strategy has a mean Time Above Range 2 (TAR2) higher than the defined target threshold. Regarding the ESC strategy, Figure I.5 highlights shows that it converges faster than OPS-S, OPS-P, and Step. However, upon examining the results in Table I.5 and the corresponding violin plots in Figure I.6, it becomes clear that the ESC strategy performs inadequately in terms of hypoglycemia management, with the mean Time Below Range 1 (TB1) exceeding the 4% target threshold.

6 Conclusion and Future Work

In this paper, a new approach which does not rely on a physiological model based on online optimization is proposed for long-acting insulin titration in T2D subjects. The proposed method combines a time-varying optimization scheme with a gradient estimate based on noisy function evaluations to tune a chosen feedback control law. The developed method can be used with SMBG measurements and/or CGM measurements. Using simulations with different T2D models, the method was compared to different titration schemes under different scenarios with

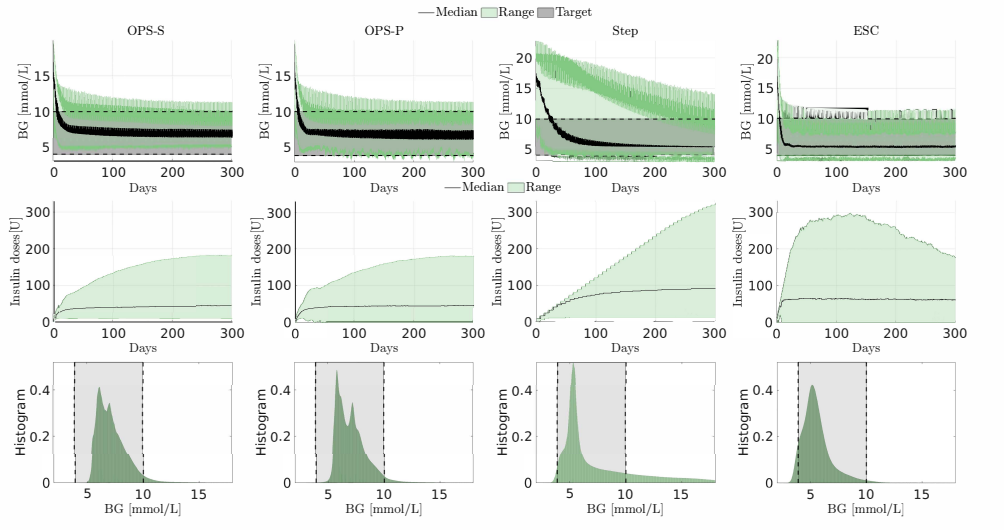

Fig. I.5: Simulation results for OPS-S, OPS-P, Step, and ESC with Model 1, Model 2, and Model 3. The plots on the second row are normalized histograms for all the glucose readings with $T_m = 5$ [min] among the 1500 simulated subjects. The 95–5 PR is the difference between the 95_{th} percentile and the 5_{th} percentile.

Table I.5: Statistics for different scenarios and algorithms (red numbers indicate values outside the target range).

	Mean TIR	std TIR	Mean TBR1	std TBR1	Mean TBR2	std TBR2	Mean AG	std AG
Target [5]	> 70%		< 4%		< 1%		< 8.6 [mmol/L]	
OPS-S	96.2%	3%	0%	0%	0%	0%	7.2	0.72
OPS-P	96.82%	2.1%	0.01%	0.15%	0%	0%	7.1	0.63
OPS-NA	94.64%	4.4%	0.02%	0.4%	0%	0%	7.2	0.7
OPS-SMBG	97.11%	2%	0.6%	1.75%	0%	0%	5.9	0.7
OPS-RLS	83.6%	28.87%	0.25%	2.4%	0.02%	0.33%	8	2.19
Step	78.48%	21.92%	1.38%	0%	0.01%	0%	7.47	2.46
202	77.43%	14.94%	1%	2.89%	0%	0.02%	7.78	6.46
ESC	92.61%	6.92%	5.67%	7.1%	0.17%	0.72%	5.62	0.71

	Mean TAR1	std TAR1	Mean TAR2	std TAR2	Mean Insulin	Mean GV	std GV	Mean GMI	std GMI
Target [5]	< 25%		< 5%			< 36%		< 7%	
OPS-S	3.2%	3%	0.5%	0.4%	47.33 [U]	16.4%	4%	6.46%	0.32%
OPS-P	2.72%	2.01%	0.4%	0.4%	49	17.5%	3.7%	6.4$	0.3%
OPS-NA	4.48%	3.51%	0.9%	0.9%	51.82 [U]	19.7%	3.9%	6.44%	0.31%
OPS-SMBG	1.86%	1.33%	0.4%	0.4%	64.6 [U]	21.77%	5.08%	5.87%	0.3%
OPS-RLS	10.87%	19.7%	5.33%	1%	34 [U]	16%	4.8%	6.81%	0.95%
Step	1.15%	12.2%	8.61%	10.97%	90.76 [U]	32.7	5.55%	5.56%	1.07%
202	17.43%	12.05%	4.11%	5.05%	47.6 [U]	30.94%	8.67%	6.69%	0.72%
ESC	1.3%	1.2%	0.5%	0.4%	71.49 [U]	25.06%	5.74%	5.75%	0.31%

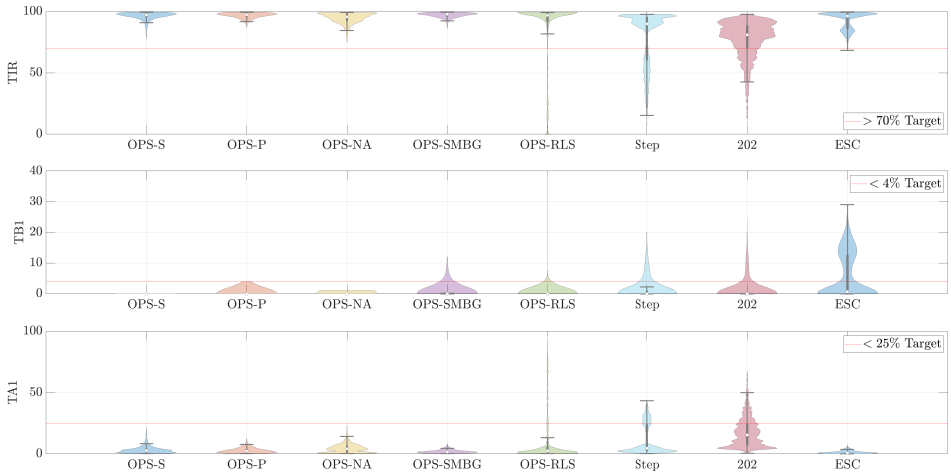

Fig. I.6: Violin plots for the metrics TIR, TB1, and TA1 with the different methods.

respect to the glucose management measures in Table G.4. The performance of the strategy under different scenarios was assessed based on the simulation results. The developed strategy was shown to have better statistics for the glucose management metrics when compared with the other titration methods. Additionally, the developed strategy demonstrated good performance under conditions of intra-subject variations and non-adherence to insulin. As two of the titration strategies were standard of care titration strategies, this indicates that the proposed strategy can be further developed to be implemented in a clinical setting. Moreover, Two different methods for obtaining a gradient estimate were used. The one-point residual feedback based method was shown to have better statistics for the glucose management metrics than the RLS method for our application and simulations. Additionally, the relatively simple computational steps for the proposed online optimization scheme makes it suitable to be implemented on computationally constrained devices such as an average smartphone. It is important to note that the simulation study in this paper did not include certain realistic factors, such as sensor malfunctions and different types of meals and exercises. Nonetheless, the outcomes derived from these simulations provide initial means to evaluate the effectiveness of insulin dosing strategies. It is worth noting that our simulation study utilized three different models and a wider range of real-world situations than previous studies exploring dosing algorithms in the management of type 2 diabetes. As a result, the results from this study provide valuable insights into the effectiveness of insulin dosing algorithms for T2D. Future work involves deriving theoretical guarantees for the proposed strategy, and validating the strategy against other high fidelity T2D simulation models such as [29] and against more real-life scenarios. Simulation validation, as it is common in the literature for diabetes (see for example [2, 3, 6, 8, 9]), will pave the way for the strategy to be tested and validated in a clinical setting.

A RLS with Directional Forgetting

Finding the value $\hat{\psi}$ that minimizes

$$\sum_{i=0}^{j} \lambda^{j-i} \left(\mathrm{z}(i) - \boldsymbol{\phi}(i)^T \hat{\psi}\right)^{\mathrm{T}} \left(\mathrm{z}(i) - \boldsymbol{\phi}(i)^T \hat{\psi}\right),$$

with $\lambda \in (0, 1]$ acting as a forgetting factor, is the goal of the recursive least squares estimation with directional forgetting. When compared to older data, the forgetting factor is utilized to emphasize newer information. This makes it useful for estimating time varying parameters such as the gradient $g(j)$. However, it is known that in the absence of persistent excitation in $\phi(j)$ (see [30] for more details), the covariance $P := \mathbb{E}\left[(\psi - \hat{\psi})^T(\psi - \hat{\psi})\right]$ cannot be bounded. We can ensure persistence excitation by adding a small dither to our control law parameters $\hat{\theta}(j)$. Moreover, we use the directional forgetting RLS technique presented in [31] to guarantee the boundedness of the covariance matrix regardless of the persistent excitation requirement. The recursive estimation is summarized in Algorithm 9. Note that the algorithm includes an update step for the information matrix $R(j)$ separately from $P(j)$ to avoid computing $P^{-1}(j)$ in the calculation of $\bar{P}(j)$ and $M(j)$.

Algorithm 9: RLS with directional forgetting

Input: Estimates $\hat{\psi}(j-1)$ with covariance matrix $P(j-1)$ and $R(j-1) = P^{-1}(j-1)$, regressor $\boldsymbol{\phi}(j)$ and measurement $\mathrm{z}(j)$, forgetting factor $\lambda \in (0, 1]$, and a threshold ϵ_ϕ (chosen to be in the order of the minimum added dither) to stop forgetting when $\|\boldsymbol{\phi}(j)\| < \epsilon_\phi$.

Output: $\hat{\mathrm{g}}(j)$ as a component in $\hat{\psi}(j)$, $P(j)$ and $R(j)$.

if $\|\boldsymbol{\phi}(j)\| \geq \epsilon_\phi$ **then**

  $\bar{P}(j) = P(j-1) + \frac{1-\lambda}{\lambda}\left(\boldsymbol{\phi}(j)R(j-1)\boldsymbol{\phi}^{\mathrm{T}}(j)\right)^{-1}\boldsymbol{\phi}^{\mathrm{T}}(j)\boldsymbol{\phi}(j)$

  $M(j) = (1-\lambda)\frac{R(j-1)\boldsymbol{\phi}(j)\boldsymbol{\phi}^{\mathrm{T}}(j)}{\boldsymbol{\phi}^{\mathrm{T}}(j)R(j-1)\boldsymbol{\phi}(j)}$

else

  $\bar{P}(j) = P(j-1)$

  $M(j) = 0$

$K_f(j) = \bar{P}(j)\boldsymbol{\phi}(j)\left(1 + \boldsymbol{\phi}^{\mathrm{T}}(j)\bar{P}(j)\boldsymbol{\phi}(j)\right)^{-1}$

$\hat{\psi}(j) = \hat{\psi}(j-1) + K_f(j)\left(\mathrm{z}(j) - \boldsymbol{\phi}^{\mathrm{T}}(j)\hat{\psi}(j-1)\right)$

$P(j) = \bar{P}(j) - \bar{P}(j)\boldsymbol{\phi}(j)\left(1 + \boldsymbol{\phi}^{\mathrm{T}}(j)\bar{P}(j)\boldsymbol{\phi}(j)\right)^{-1}\boldsymbol{\phi}^{\mathrm{T}}(j)\bar{P}(j)$

$R(j) = (\mathrm{I} - M(j))R(j-1) + \boldsymbol{\phi}(j)\boldsymbol{\phi}^{\mathrm{T}}(j)$

The matrix M in the RLS strategy applies the forgetting factor λ on a subspace of the column space of the information matrix R, for details, see [31].

References

[1] T. Kadowaki, H. Jinnouchi, K. Kaku, M. L. Hersløv, J. Hyllested-Winge, and S. Nakamura, "Insulin degludec in a simple or stepwise titration algorithm in a japanese population of patients with type 2 diabetes: a randomized, 26-week, treat-to-target trial," *Diabetology international*, vol. 8, no. 1, pp. 87–94, 2017.

[2] T. B. Aradóttir, D. Boiroux, H. Bengtsson, J. Kildegaard, M. L. Jensen, J. B. Jørgensen, and N. K. Poulsen, "Model predictive control for dose guidance in long acting insulin treatment of type 2 diabetes," *IFAC Journal of Systems and Control*, vol. 9, p. 100067, 2019.

[3] D. Krishnamoorthy, D. Boiroux, T. B. Aradóttir, S. E. Engell, and J. B. Jørgensen, "A model-free approach to automatic dose guidance in long acting insulin treatment of type 2 diabetes," *IEEE Control Systems Letters*, vol. 5, no. 6, pp. 2030–2035, 2020.

[4] M. Al Ahdab, T. Knudsen, J. Stoustrup, and J.-J. Leth, "An online stochastic optimization approach for insulin intensification in type 2 diabetes with attention to pseudo-hypoglycemia (in press)," in *2022 IEEE 61th Conference on Decision and Control (CDC)*, 2022.

[5] R. I. Holt, J. H. DeVries, A. Hess-Fischl, I. B. Hirsch, M. S. Kirkman, T. Klupa, B. Ludwig, K. Nørgaard, J. Pettus, E. Renard *et al.*, "The management of type 1 diabetes in adults. a consensus report by the american diabetes association (ada) and the european association for the study of diabetes (easd)," *Diabetes Care*, vol. 44, no. 11, pp. 2589–2625, 2021.

[6] A. El Fathi, C. Fabris, and M. D. Breton, "Titration of long-acting insulin using continuous glucose monitoring and smart insulin pens in type 1 diabetes: A model-based carbohydrate-free approach," *Frontiers in Endocrinology*, vol. 12, 2021.

[7] W. Karush, "Minima of functions of several variables with inequalities as side conditions," in *Traces and Emergence of Nonlinear Programming*. Springer, 2014, pp. 217–245.

[8] L. Magni, D. M. Raimondo, L. Bossi, C. Dalla Man, G. De Nicolao, B. Kovatchev, and C. Cobelli, "Model predictive control of type 1 diabetes: an in silico trial," 2007.

[9] J. Garcia-Tirado, J. P. Corbett, D. Boiroux, J. B. Jørgensen, and M. D. Breton, "Closed-loop control with unannounced exercise for adults with type 1 diabetes using the ensemble model predictive control," *Journal of process control*, vol. 80, pp. 202–210, 2019.

[10] T. K. Ritschel, A. T. Reenberg, and J. B. Jørgensen, "Large-scale virtual clinical trials of closed-loop treatments for people with type 1 diabetes," *IFAC-PapersOnLine*, vol. 55, no. 23, pp. 169–174, 2022, 9th IFAC Conference on Foundations of Systems Biology in Engineering FOSBE 2022.

[11] A. Borri, G. Pola, P. Pepe, M. D. Di Benedetto, and P. Palumbo, "Symbolic control design of an artificial pancreas for type-2 diabetes," *IEEE Transactions on Control Systems Technology*, vol. 30, no. 5, pp. 2131–2146, 2021.

[12] T. B. Aradóttir, H. Bengtsson, M. L. Jensen, N. K. Poulsen, D. Boiroux, L. L. Jensen, S. Schmidt, and K. Nørgaard, "Feasibility of a new approach to initiate insulin in type 2 diabetes," *Journal of diabetes science and technology*, vol. 15, no. 2, pp. 339–345, 2021.

[13] S. Vlaski, E. Rizk, and A. H. Sayed, "Tracking performance of online stochastic learners," *IEEE Signal Processing Letters*, vol. 27, pp. 1385–1389, 2020.

[14] A. S. Bedi, P. Sarma, and K. Rajawat, "Tracking moving agents via inexact online gradient descent algorithm," *IEEE Journal of Selected Topics in Signal Processing*, vol. 12, no. 1, pp. 202–217, 2018.

[15] Y. Zhang, Y. Zhou, K. Ji, and M. M. Zavlanos, "A new one-point residual-feedback oracle for black-box learning and control," *Automatica*, vol. 136, p. 110006, 2022. [Online]. Available: https://www.sciencedirect.com/science/article/pii/S000510982100532X

[16] X. Chen, Y. Tang, and N. Li, "Improve single-point zeroth-order optimization using high-pass and low-pass filters," in *International Conference on Machine Learning*. PMLR, 2022, pp. 3603–3620.

[17] A. Simonetto, E. Dall'Anese, S. Paternain, G. Leus, and G. B. Giannakis, "Time-varying convex optimization: Time-structured algorithms and applications," *Proceedings of the IEEE*, vol. 108, no. 11, pp. 2032–2048, 2020.

[18] Y. Tang, K. Dvijotham, and S. Low, "Real-time optimal power flow," *IEEE Transactions on Smart Grid*, vol. 8, no. 6, pp. 2963–2973, 2017.

[19] C. Kelley and E. Sachs, "Quasi-newton methods and unconstrained optimal control problems," *SIAM Journal on Control and Optimization*, vol. 25, no. 6, pp. 1503–1516, 1987.

[20] J. Zhuang, T. Tang, Y. Ding, S. C. Tatikonda, N. Dvornek, X. Papademetris, and J. Duncan, "Adabelief optimizer: Adapting stepsizes by the belief in observed gradients," *Advances in neural information processing systems*, vol. 33, pp. 18 795–18 806, 2020.

[21] M. A. Ahdab, M. Papež, T. Knudsen, T. B. Aradóttir, S. Schmidt, K. Nørgaard, and J.-J. Leth, "Parameter estimation for a jump diffusion model of type 2 diabetic patients in the presence of unannounced meals," in *2021 IEEE Conference on Control Technology and Applications (CCTA)*, 2021, pp. 176–183.

[22] S. E. Engell, T. B. Aradóttir, H. Bengtsson, M. Ekelund, and J. B. Jørgensen, "Glucose response to fast-and long-acting insulin in people with type 2 diabetes," *IFAC-PapersOnLine*, vol. 54, no. 15, pp. 496–501, 2021.

[23] M. Al Ahdab, J.-J. Leth, T. Knudsen, P. Vestergaard, and H. G. Clausen, "Glucose-insulin mathematical model for the combined effect of medications and life style of type 2 diabetic patients," *Biochemical Engineering Journal*, vol. 176, p. 108170, 2021.

[24] M. Ahdab, T. Knudsen, and J.-J. Leth, "State space temporal gaussian processes for glucose measurements," in *2022 European Control Conference (ECC)*. United States: IEEE, 2021, pp. 1277–1282.

[25] *In vitro diagnostic test systems: requirements for blood-glucose monitoring systems for self-testing in managing diabetes mellitus*. International Organization for Standardization, 2003.

[26] D. Rodbard, "Characterizing accuracy and precision of glucose sensors and meters," *Journal of diabetes science and technology*, vol. 8, no. 5, pp. 980–985, 2014.

[27] P. Colmegna, K. Wang, J. Garcia-Tirado, and M. D. Breton, "Mapping data to virtual patients in type 1 diabetes," *Control Engineering Practice*, vol. 103, p. 104605, 2020.

[28] MATLAB, *version R2022a*. Natick, Massachusetts: The MathWorks Inc., 2022.

[29] R. Visentin, C. Cobelli, and C. Dalla Man, "The padova type 2 diabetes simulator from triple-tracer single-meal studies: In silico trials also possible in rare but not-so-rare individuals," *Diabetes technology & therapeutics*, vol. 22, no. 12, pp. 892–903, 2020.

[30] A. Goel, A. L. Bruce, and D. S. Bernstein, "Recursive least squares with variable-direction forgetting: Compensating for the loss of persistency [lecture notes]," *IEEE Control Systems Magazine*, vol. 40, no. 4, pp. 80–102, 2020.

[31] L. Cao and H. Schwartz, "A directional forgetting algorithm based on the decomposition of the information matrix," *Automatica*, vol. 36, no. 11, pp. 1725–1731, 2000.

Paper J

Entropy for Optimal Control on a Simplex with an Application to Behavioral Nudging

Mohamad Al Ahdab, Torben Knudsen, Jakob Stoustrup, and John Leth

The paper has been published in the
IEEE Control Systems Letters, vol. 7, pp. 2797-2802, 2023.

The layout has been revised.

Abstract

We study the utilization of the entropy function of inputs in solving an Optimal Control Problem (OCP) with linear dynamics and inputs constrained to a variable-sized simplex in which the size is also an input. By using the entropy function as part of the objective functional in the OCP, we are able to derive a closed-form solution. Additionally, we present an example of how the studied OCP can be applied to choose between nudging techniques to discourage a specific behavior, such as non-adherence to medication, through the lens of behavioral momentum theory.

1 Introduction

Optimal control problems (OCPs) are concerned with finding an optimal input trajectory for a dynamical system which maximizes or minimizes an objective functional while satisfying specific constraints. A class of problems in which the input trajectory is constrained to be on a simplex arises in many applications such as portfolio optimization in finance, resource allocation in energy systems, mixing chemicals in chemical reactions, and when the control input is a discrete probability distribution. The use of entropy in the objective for continuous-time dynamics has been studied in works of [1] and [2]. In [1], the authors analyzed the use of the entropy function for stochastic linear optimal control problems. As for the work in [2], the authors derived a class of Hamilton–Jacobi–Bellman (HJB) equations for optimal control problem in which the input is a probability measure. The optimization in the mentioned papers is performed over a probability measure with the dynamics having inputs drawn from the probability measure, and the optimal control problem considers averaged dynamics with respect to the probability measure in addition to averaged objective terms with respect to the probability measure. In this paper, we consider an OCP with linear time-varying dynamics and an input vector $\boldsymbol{u}$ constrained to a simplex of size $v > 0$ with v being an input itself. In particular, we show how the use of the entropy function in the objective in addition to a linear objective in state, a linear objective in $\boldsymbol{u}$, and a quadratic objective in v will yield a closed-form solution using the necessary conditions of the maximum principle with Arrow type sufficient conditions [3]. Although setting $v = 1$ in our setup will make our problem a special case of those considered in [1, 2], these works do not explicitly address and solve the case of a discrete probability measure with continuous linear time-varying dynamics and a linear objective function, as we do in this paper. Moreover, we introduce the size of the simplex as an additional optimization input, which further expands the scope of the problem. Furthermore, we present an example on how the OCP of interest in this paper can be used to schedule different nudging techniques using behavioral momentum theory [4] to discourage an unhealthy behavior in people. Behavioral momentum theory suggests that behaviors that are reinforced more frequently are more resistant to changes in the environment. With this theory, we model the dynamics of the average rate of a target behavior by a linear model, with the average rate of a reinforcement being a parameter.

To discourage an unhealthy behavior, we introduce different nudges to the behavior as inputs to the OCP framework. In the context of our framework, we represent the probabilities of selecting the nudges as inputs belonging to a simplex, with the size of the simplex representing their overall rate. Our objective is to optimize the choice of different nudges and their average

rate to minimize the average rate of the targeted behavior, while also considering the cost of each nudge and ensuring a diversity of nudges.

The use of computational and machine learning techniques have recently been investigated for the design of nudges for medical care professionals such as in [5] and to encourage patients to adhere to their prescribed medicine in [6]. Additionally, the work in [7] considers the optimal design of nudges within a Markov decision process framework derived from resource-rational analysis. In this paper, we consider the problem of choosing between nudges while minimizing their average rate within a continuous optimal control framework derived from behavioural momentum theory. Our work offers an alternative framework and perspective for the problem of behavioral nudging in healthcare. We hope that our discussion in this paper can be one of the early works towards the application of control theory concepts in behavioral nudging of people in healthcare.

The summary of the contributions of this paper is as follows

- We derive closed-form solution for an OCP with inputs constrained to a simplex in which the size of the simplex itself is also another input.
- We present examples of how the OCP of interest and behavioral momentum theory can be used to assist in the choice of different nudging techniques aimed at discouraging an undesired behaviour, such as non-adhering to medication. To our knowledge, this is the first time control theory techniques have been used in connection with behavioral momentum theory.

2 Notations

All vectors are considered as column vectors. We let $[a, b]$ denote the closed interval from a to b, and $[a\ b]$ denote the row vector with coordinates a and b. The symbols $\boldsymbol{I}_n$ and $\mathbf{0}_{n\times m}$ are used to denote the $n \times n$ identity and the $n \times m$ zero matrix, respectively. The symbol $\mathbf{1}_n$ is used to denote the n-dimensional column vector of 1s. The symbols $\geq_e, >_e$ are used for element-wise $\geq$ and $>$. For $\boldsymbol{u} \in \triangle_n^v := \left\{\boldsymbol{u} \in \mathbb{R}^n_{\geq 0} \mid \|\boldsymbol{u}\|_1 = v\right\}$, we write the entropy function as $\phi(\boldsymbol{u}) = -\sum_{i=1}^n u_i \ln(u_i)$ and we take $0\ln(0) := 0$. For $\boldsymbol{u} \in \triangle_n^v$ and $\boldsymbol{w} >_e 0$, we write the Kullback–Leibler (KL) divergence (relative entropy) as $D_{KL}(\boldsymbol{u} \,||\, \boldsymbol{w}) = \sum_{i=1}^n u^i \ln\left(u^i/w^i\right)$. We use $\exp_e(\boldsymbol{x})$ and $\ln_e(\boldsymbol{x})$ for the element-wise exponential and logarithm of a vector $\boldsymbol{x}$, respectively.

3 Solution of the Optimal Control Problem

In this section, we first present the OCP of interest in 3.1, and derive an explicit solution for it in 3.2.

3.1 Problem Setup

To define the OCP of interest (OCPv) in this work, we begin by defining

$$L\left(\boldsymbol{x},\boldsymbol{u},v,t\right):=\frac{1}{\eta}\phi(\boldsymbol{u})+\boldsymbol{c}^{\mathrm{T}}(t)\boldsymbol{u}+\boldsymbol{d}^{\mathrm{T}}\boldsymbol{x}+qv^{2},$$

and $\boldsymbol{S}(\boldsymbol{x}):=\boldsymbol{e}^{\mathrm{T}}\boldsymbol{x}$, with $\eta>0$, $\boldsymbol{c}(t)\in\mathbb{R}^{n_u}$ being continuously differentiable, $\boldsymbol{d}\in\mathbb{R}^{n_x}$, and $\boldsymbol{e}\in\mathbb{R}^{n_x}$. The OCP in this paper has the following form

$$\max_{\boldsymbol{u},v}\int_{t_0}^{t_f}L\left(\boldsymbol{x}(t),\boldsymbol{u}(t),v(t),t\right)dt+S\left(\boldsymbol{x}(t_f)\right) \tag{J.1a}$$

$$\dot{\boldsymbol{x}}(t)=\boldsymbol{A}\boldsymbol{x}(t)+\boldsymbol{B}(t)\boldsymbol{u}(t),\ \boldsymbol{x}(t_0)=\boldsymbol{x}_0, \tag{J.1b}$$

$$v(t)-\mathbf{1}^{\mathrm{T}}\boldsymbol{u}(t)=0,\ \boldsymbol{u}(t)\geq_e 0,\ v(t)\geq 0. \tag{J.1c}$$

Note that for the case in which v is set to 1, the inputs $\boldsymbol{u}$ will be constrained to the unit simplex $\triangle_{n_u}^1$. Also note that $B(t)$ is assumed to be an explicit function of time t e.g., see below (J.11).

3.2 Closed-Form Solution

In order to find the solution for OCPv, we use the necessary conditions of the maximum principle. To summarize the necessary conditions, it is convenient to define the Hamiltonian function for our problem

$$H\left(t,\boldsymbol{x},\boldsymbol{u},v,\boldsymbol{\lambda}\right)=\tilde{L}(\boldsymbol{x},\boldsymbol{u},v,t)+\boldsymbol{\lambda}^{\mathrm{T}}\left(\boldsymbol{A}\boldsymbol{x}+\boldsymbol{B}(t)\boldsymbol{u}\right), \tag{J.2}$$

for all $(t,\boldsymbol{x},\boldsymbol{u},v,\boldsymbol{\lambda})\in[t_0,t_f]\times\mathbb{R}^{n_x}\times\mathbb{R}^{n_u}\times\mathbb{R}\times\mathbb{R}^{n_x}$, where $\boldsymbol{\lambda}$ is called the adjoint variable[1]. The necessary conditions for the tuple $\left(\boldsymbol{x}^*(t),\boldsymbol{u}^*(t),v^*(t)\right)$, $t\in[t_0,t_f]$, to be a solution of the OCP in (J.1) are summarized as follows

$$\left(\boldsymbol{u}^*(t),v^*(t)\right)\in\underset{\boldsymbol{u}\in\triangle_{n_u}^v,v\geq 0}{\operatorname{argmax}}\ H\left(\boldsymbol{x}(t),\boldsymbol{u},v,\boldsymbol{\lambda}(t),t\right), \tag{J.3a}$$

$$\dot{\boldsymbol{\lambda}}(t)=-\boldsymbol{H}_{\boldsymbol{x}}\left(t,\boldsymbol{x}^*(t),\boldsymbol{u}^*(t),v^*(t),\boldsymbol{\lambda}(t)\right), \tag{J.3b}$$

$$\boldsymbol{\lambda}(t_f)=-\boldsymbol{S}_x(t_f) \tag{J.3c}$$

From the maximality condition (J.3a), we get (see Appendix A)

$$\left(\boldsymbol{u}^*(t),v^*(t)\right)=\underset{\boldsymbol{u}\in\triangle_{n_u}^v,v\geq 0}{\operatorname{argmax}}\ H\left(\boldsymbol{x}(t),\boldsymbol{u},v,\boldsymbol{\lambda}(t),t\right), \tag{J.4a}$$

$$\boldsymbol{u}^*(t)=v^*(t)\frac{\exp_{\mathrm{e}}\left(\eta\boldsymbol{B}^{\mathrm{T}}(t)\boldsymbol{\lambda}(t)+\eta\boldsymbol{c}(t)\right)}{\mathbf{1}^{\mathrm{T}}\exp_{\mathrm{e}}\left(\eta\boldsymbol{B}^{\mathrm{T}}(t)\boldsymbol{\lambda}(t)+\eta\boldsymbol{c}(t)\right)}>_e\mathbf{0}, \tag{J.4b}$$

$$v^*(t)=\frac{-\mathrm{W}_0\left(-2q\eta\exp\left(-1\right)\mathbf{1}^{\mathrm{T}}\exp_{\mathrm{e}}\left(\eta\boldsymbol{B}^{\mathrm{T}}(t)\boldsymbol{\lambda}(t)+\eta\boldsymbol{c}(t)\right)\right)}{2q\eta}, \tag{J.4c}$$

[1]The adjoint variable λ_0 in $H(t,\boldsymbol{x},\boldsymbol{u},v,\boldsymbol{\lambda},\lambda_0)=\lambda_0 L(\boldsymbol{x},\boldsymbol{u},v,t)+\boldsymbol{\lambda}^{\mathrm{T}}\left(\boldsymbol{A}\boldsymbol{x}+\boldsymbol{B}(t)\boldsymbol{u}\right)$ is set to $\lambda_0=1$ since the end-point $\boldsymbol{x}(t_f)$ is free [3].

where W_0 is the principal branch of the Lambert W function. Letting

$$\left(\boldsymbol{u}^0, v^0\right) := \mathrm{argmax}_{\boldsymbol{u}\in\triangle_{n_u}^v, v\geq 0} H\left(\boldsymbol{x}, \boldsymbol{u}, v, \boldsymbol{\lambda}, t\right)$$

, we get that $(\boldsymbol{u}^0, v^0)$ is $(\boldsymbol{u}^*, v^*)$ for a given $\boldsymbol{\lambda} \in \mathbb{R}^{n_x}$, which is a unique solution due to the strict concavity of H in $(\boldsymbol{u}, v)$. Substituting $(\boldsymbol{u}^0, v^0)$ in the Hamiltonian we get that $H(\boldsymbol{x}, \boldsymbol{u}^0(\boldsymbol{x}, \boldsymbol{\lambda}, t), v^0(\boldsymbol{x}, \boldsymbol{\lambda}, t), \boldsymbol{\lambda}, t)$ is an affine function in $\boldsymbol{x}$ which is concave. Additionally, since $\boldsymbol{S}(\boldsymbol{x})$ is also concave in $\boldsymbol{x}$, the necessary conditions (J.3) are sufficient (Arrow type sufficient conditions [3]). Now using the adjoint equation (J.3b) together with the transversality condition (J.3c), we get

$$\dot{\boldsymbol{\lambda}}(t) = -\boldsymbol{A}^{\mathrm{T}}\boldsymbol{\lambda}(t) - \boldsymbol{d},\ \boldsymbol{\lambda}\left(t_f\right) = \boldsymbol{e}. \tag{J.5}$$

Referring to [8], we can obtain the solution to (J.5) as[2]:

$$\boldsymbol{\lambda}(t) = \boldsymbol{M}_A(t)\boldsymbol{e} + \boldsymbol{M}_d(t), \tag{J.6}$$

where

$$\begin{bmatrix} \boldsymbol{M}_A(t) & \boldsymbol{M}_d(t) \\ \boldsymbol{0}_{1\times n_x} & 1 \end{bmatrix} = \mathrm{e}^{\boldsymbol{M}\left(t-t_f\right)}, \boldsymbol{M} = \begin{bmatrix} -\boldsymbol{A}^{\mathrm{T}} & -\boldsymbol{d} \\ \boldsymbol{0}_{1\times n_x} & 0 \end{bmatrix}.$$

Substituting the adjoint solution (J.6) in (J.4), we get the solution

$$\boldsymbol{u}^*(t) = v^*(t)\frac{\exp_{\mathrm{e}}\left(\zeta(t)\right)}{\boldsymbol{1}^{\mathrm{T}}\exp_{\mathrm{e}}\left(\zeta(t)\right)} >_e \boldsymbol{0}, \tag{J.7a}$$

$$v^*(t) = \frac{-\mathrm{W}_0\left(-2q\exp(-1)\eta\boldsymbol{1}^{\mathrm{T}}\exp_{\mathrm{e}}\left(\zeta(t)\right)\right)}{2q\eta}, \tag{J.7b}$$

$$\zeta(t) := \eta\boldsymbol{B}^{\mathrm{T}}(t)\left(\boldsymbol{M}_A(t)\boldsymbol{e} + \boldsymbol{M}_d(t)\right) + \eta\boldsymbol{c}(t). \tag{J.7c}$$

Remark 3.1. *For the case when v is set to 1 and it is not optimized over, the solution $\boldsymbol{u}^*$ can then be shown to be $\boldsymbol{u}^* = \frac{\exp_e\left(\zeta(t)\right)}{\boldsymbol{1}^{\mathrm{T}}\exp_e\left(\zeta(t)\right)}$ by following the same procedure to obtain (J.7a). Moreover, if $\boldsymbol{d} = \boldsymbol{e} = \boldsymbol{0}$ and $\boldsymbol{c}(t) = \boldsymbol{c}$, then the solution (J.7) is a constant input $\boldsymbol{u}^* = \exp_{\mathrm{e}}(\eta\boldsymbol{c})/\boldsymbol{1}^{\mathrm{T}}\exp_{\mathrm{e}}(\eta\boldsymbol{c})$. Additionally, if the inputs are weighted equally (i.e., $\boldsymbol{c} = c\boldsymbol{1}$ for some scalar $c \in \mathbb{R}$), then the solution simplifies to $\boldsymbol{u}^* = \frac{1}{n_u}\boldsymbol{1}$. This is the well-known solution for the maximum entropy on a simplex.*

Remark 3.2. *Incorporating the entropy function into the objective of OCPv encourages the utilization of all available inputs, as the resulting solution, as shown in equation (J.7), is always non-zero. This encourages diversification in the inputs, which can be advantageous in certain applications where exploring diverse solutions is desirable or in situations where one or more*

[2]Note that for a non-singular $\boldsymbol{A}$, we can write $\boldsymbol{M}_A(t) = \exp\left(\boldsymbol{A}\left(t-t_f\right)\right)$, and $\boldsymbol{M}_d(t) = \boldsymbol{A}^{-1}\left(\boldsymbol{M}_A(t) - \boldsymbol{I}\right)\boldsymbol{d}$.

inputs could potentially lose their effectiveness, such as in the case of a faulty actuator. Using only a linear term for the inputs in the objective of OCPv will yield a bang-bang solution in step (J.4). Additionally, if we use a quadratic term $-\boldsymbol{u}^{\mathrm{T}}(t)\boldsymbol{Q}\boldsymbol{u}(t), \boldsymbol{Q} \geq 0$ *for the inputs in place of the entropy function, then the problem in (J.4) becomes a standard quadratic optimization problem (StQP). However, determining explicit solutions for StQPs is known to be NP-hard [9], even though efficient algorithms are available. In contrast, despite the need to evaluate a matrix exponential for* $\boldsymbol{M}_A$ *and* $\boldsymbol{M}_d$*, computing the explicit solution in (J.7) can be more efficient to implement in many scenarios (e.g., when* $\boldsymbol{A}$ *is diagonal). Moreover, if we intend to implement (J.7) recursively, as demonstrated in 4.4, the matrix exponential need only to be evaluated once. Finally, obtaining an explicit solution may prove valuable for conducting further theoretical analyses of the implemented solution's dynamics.*

Remark 3.3. *The solution to OCPv can be used in a receding horizon fashion by recursively estimating the dynamics parameters and solving the OCP for a fixed horizon (see 4.4 for an example). To ensure that the inputs between the solutions are close to each other, we introduce a relative entropy objective* $-\eta_p^{-1}\exp\left(-\rho\tilde{t}\right) D_{KL}\left(\boldsymbol{u}(t) \,||\, \boldsymbol{u}_p\right)$ *with* $\rho > 0$*,* $\eta^{-1} < \eta_p^{-1}$*, and* $q_p \exp\left(-\rho\tilde{t}\right)\left(v(t) - v_p\right)^2$ *where* $\tilde{t} := t - t_0$*,* $|q_p| < |q|$*, with* $q_p \leq 0$*. The values* $\boldsymbol{u}_p, v_p$ *are the last inputs from the previously computed solution. In this case, the solution in (J.4) becomes*

$$\boldsymbol{u}^*(t) = v^*(t)\frac{\exp_{\mathrm{e}}\left(\boldsymbol{\gamma}(t)\right)}{\mathbf{1}^{\mathrm{T}}\exp_{\mathrm{e}}\left(\boldsymbol{\gamma}(t)\right)}, \tag{J.8a}$$

$$\begin{aligned} v^*(t) = \frac{-1}{2\bar{q}(t)\bar{\eta}(t)}\mathrm{W}_0\Big(&- 2\bar{q}(t)\bar{\eta}(t)\mathbf{1}^{\mathrm{T}}\exp_{\mathrm{e}}\left(\boldsymbol{\gamma}(t)\right) \\ &\exp\left(-2\bar{\eta}q_p\exp\left(-\rho\tilde{t}\right) - 1\right)\Big), \end{aligned} \tag{J.8b}$$

$$\begin{aligned} \boldsymbol{\gamma}(t) := \bar{\eta}(t)\boldsymbol{B}^{\mathrm{T}}(t)\boldsymbol{\lambda}(t) + \bar{\eta}(t)\boldsymbol{c}(t) \\ + \bar{\eta}(t)\eta_p^{-1}\exp\left(-\rho\tilde{t}\right)\ln_e\left(\boldsymbol{u}_p\right), \end{aligned} \tag{J.8c}$$

where $\bar{\eta}(t) = \frac{1}{\eta^{-1} + \eta_p^{-1}\exp\left(-\rho\tilde{t}\right)}$*, and* $\bar{q}(t) = q + q_p\exp\left(-\rho\tilde{t}\right)$*.*

4 Example with Behavioral Momentum Theory

In this section, we will present a simple model derived from the principles of behavioral momentum theory. The model takes the form of $\dot{x}(t) = \boldsymbol{B}(t)\boldsymbol{u}(t)$, with $\mathbf{1}^{\mathrm{T}}\boldsymbol{u}(t) = v(t)$ and will be described in detail in 4.1. We will then proceed to use this model to solve OCPv for various scenarios in 4.2, 4.3, and 4.4.

4.1 Behavioral Momentum Model

Behavioral momentum theory provides a quantitative basis for the idea that the rate of a behavior, which has been reinforced frequently in the past is more resistant to change with disruptions than if it has been reinforced less frequently [4, 10]. In the works of [4, 10],

mathematical representations for behavioral momentum theory were introduced and validated with data obtained from different experiments. In this paper, we use a simple continuous-time version based on an averaged model from [4, 10]. Let $\beta(t) \in \mathbb{R}_{\geq 0}$ be the average rate of occurrence for a specific behavior per unit time and define $x(t) := \log_{10}\big(\beta(t)\big)$, then the change $x(t) - x(t_1)$ with $\Delta t := t - t_1 \geq 0$ is modelled with respect to disruptions and reinforcers as $x(t) - x(t_1) = \frac{-\delta(t)}{\sqrt{r(t)}}\Delta t$, where $r(t) \in \mathbb{R}_{\geq 0}$ is the average rate of a reinforcer, and $\delta(t) = b(t)v(t)$ with $v(t) \in \mathbb{R}_{\geq 0}$ being the average rate of disruption events, and $b(t) \in \mathbb{R}_{\geq 0}$ being an effect factor for the disruption events. The value $\sqrt{r}$ represents a "behavioral inertia", a higher average reinforcer rate would require a higher average rate for the effect of disruptions δ to change the behaviour. Dividing by Δt and taking the limit for $\Delta t \to 0$, we obtain

$$\dot{x}(t) = \frac{-1}{\sqrt{r(t)}}\delta(t). \tag{J.9}$$

Consider now that for a disruption happening with an average rate of $v(t)$, the disruption can be of n_u different types with a probability $\bar{u}_i$ of being of type i with an effect factor b_i. In that case, $\delta(t)$ in (J.9) becomes

$$\delta(t) = v(t)\boldsymbol{b}^{\mathrm{T}}(t)\bar{\boldsymbol{u}}(t), \tag{J.10}$$

with $\bar{\boldsymbol{u}}(t) \in \triangle^1_{n_u}$ and $\boldsymbol{b}(t) \in \mathbb{R}^{n_u}_{\geq 0}$. Here, the i_{th} component $\bar{u}_i(t) \geq 0$ of $\bar{\boldsymbol{u}}(t)$ can also be understood as the average rate of a type of disruption with respect to the other types in $\delta(t)$ (average rate ratio). Note that the sum $\sum_{i=1}^{n_u} v(t)\bar{u}_i(t) = v(t)$. The value $v(t)$ is usually desired to be small enough to avoid what is known as alert fatigue [11]. Alert fatigue is when the rate of disruptions is high enough that the disruptions will lose their effect. Note that the model (J.9) with (J.10) can be written in the form of the model of OCPv (J.1b) by introducing $v(t)$ in the constraint (J.1c):

$$\dot{x} = \frac{-1}{\sqrt{r(t)}}\boldsymbol{b}^{\mathrm{T}}(t)\boldsymbol{u}(t), \mathbf{1}^{\mathrm{T}}\boldsymbol{u}(t) = v(t), \tag{J.11}$$

where $\boldsymbol{B}(t) = \frac{-1}{\sqrt{r(t)}}\boldsymbol{b}^{\mathrm{T}}(t)$.

Remark 4.1. *For a better understanding of the averaged representation and how to obtain* (J.10)*, consider the Poisson Compound Process* $\Pi(t)$ *defined as*

$$\Pi(t) = \sum_{k=1}^{P(t)} \frac{-1}{\sqrt{r(T_k^-)}}\boldsymbol{b}^T(T_k^-)\boldsymbol{W}_k, \tag{J.12}$$

where $P(t)$ *is a Poisson process representing the number of disruptions (jumps) up until time* t *with rate* $v(t)$*,* T_k^- *is the pre-disruption time value of the* k_{th} *random disruption type,* $\boldsymbol{W} = \boldsymbol{W}_k$ *is an IID stochastic process where* $\boldsymbol{W}_k$ *represents the type of the* k_{th} *disruption such that* $\boldsymbol{W}_k \in \mathcal{W} = \{\boldsymbol{w}_1, \ldots, \boldsymbol{w}_{n_u}\}$ *with* $\boldsymbol{w}_i$ *being a vector of zeros except for the* i_{th} *element being 1 and* $\mathbb{P}(\boldsymbol{W}_k = \boldsymbol{w}_i) = \bar{u}_i$*. Taking the expectation of* $\Pi(t)$ *(Chapter 5 in [12]) will give us*

$$\mathbb{E}\left[\Pi(t)\right] = \int_0^t v(s)\frac{-1}{\sqrt{r(s)}}\boldsymbol{b}^T(s)\bar{\boldsymbol{u}}(s)ds, \tag{J.13}$$

which is equivalent to $x(t)$ in (J.9) with $\delta(t)$ being chosen as in (J.10). This interpretation also gives us a method to apply the disruptions in real life by simulating (J.12).

In this paper, we will consider nudges as intentional disruptions that can change the reinforcement contingencies associated with a behavior and we will examine three different examples. The first one in section 4.2 deals with a case when $v(t)$ is fixed to be 1 (see Remark 3.1) and $\boldsymbol{b}$ is constant. The second case in section 4.3 is when $v(t)$ is optimized over, and the third case in section 4.4 is when $\boldsymbol{b}(t)$ is time-varying compared with a receding horizon setting. It is important to note that the examples discussed are simplified abstractions. The intention of presenting the examples is to show how the solution of OCPv in this paper can potentially be used for behavior nudging with elements from behavioral momentum theory. In all of the figures, we will report $\beta(t) = 10^{x(t)}$ and $\bar{\boldsymbol{u}}(t) = \frac{1}{v(t)}\boldsymbol{u}(t)$. The code for generating the results can be found on `https://gitlab.com/aau-adapt-t2d/nudging_entropyocp`.

4.2 Case with a Constant Rate of Nudges

Consider a case in which a diabetic subject is not following their prescribed medication regimen, such as failing to administer the correct dose of insulin or taking a lower or higher dose than what was prescribed due to some constant average rate of a reinforcer $r = 7$ [1/Week]. Here the reinforcer could be inconveniences of administering the dose and/or economical burden. Assume that we have three different types of disruptions: $\bar{u}_1$ being the probability of sending dose reminder text messages to the subject with an effect of $b_1 = 0.2$, $\bar{u}_2$ being the probability of sending personalized encouraging text messages to the subjects (e.g., reminding them about the importance of their health to their family) with an effect of $b_2 = 0.3$, and $\bar{u}_3$ being the probability of a phone call from a medical staff reminding them about the importance of their health with an effect of $b_3 = 0.4$. Our case study assumes that having a call from a medical staff is the most effective method while sending unpersonlized reminders is the least effective. Additionally, consider that we desire to fix the rate of nudges to a constant $v = 1$ [1/Week]. Phone calls from medical staff can be costly and labor intensive. To account for this, we define a linear cost for the different options $\boldsymbol{c} = -[0.1\ 0.5\ 1]^{\mathrm{T}}$ giving a higher cost for $\bar{u}_3$ and a lower cost for $\bar{u}_1$. A higher cost for $\bar{u}_2$ than the cost for $\bar{u}_1$ is used since the second type of nudges requires obtaining personal information regarding the subjects and formulating specific text messages for them. This cannot be easily automated when compared to just sending dose reminders with $\bar{u}_1$. Additionally, we choose $d = e = -2$ to lower $x(t)$ within a time horizon $t_f = 24$ [Week]. Finally, we select $\eta = 1$ for the entropy function. Figure J.1 shows the results of applying the solution in (J.7) with $v = 1$ compared to a solution to the problem obtained numerically by using forward-Euler with a discretization step $T_d = 0.01$ to discretize the dynamics, lift the problem, and then solve it using SDP3 [13] with CVX [14]. The numerical solution matches the closed-form solution which further validates it. We can see from the solution that the reliance on medical staff and personalized reminders is higher at the beginning than text reminders but slowly decreases with time to reduce the burden on the medical staff. Additionally, none of the nudging techniques have a zero contribution at any point of time and there is always a mix between all of them ((J.4b) will always be strictly positive). In figure J.2, we compare our closed-form solution with a numerical solution obtained using a quadratic cost $-\boldsymbol{u}^{\mathrm{T}}\boldsymbol{u}$ instead of

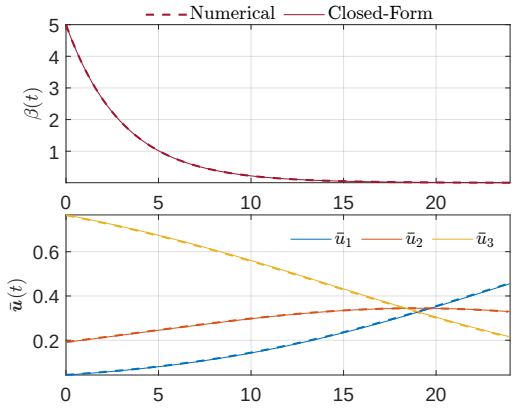

Fig. J.1: Numerical solution (dashed) against the closed-form solution (solid) for OCPv with constant $v = 1$.

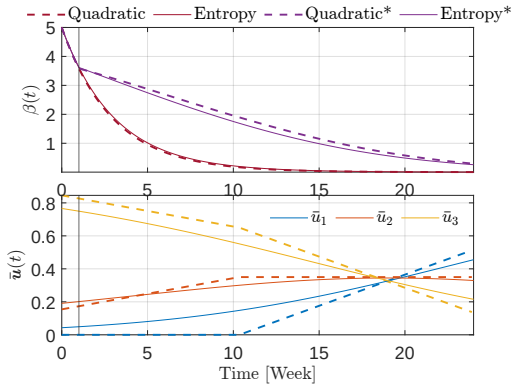

Fig. J.2: Comparison between the quadratic objective case (dashed) and the entropy objective case (solid) in OCPv.

the entropy in OCPv. Additionally, we simulate the response $\beta(t)$ in a case where the medical staff become unavailable after the first week rendering $b_3 = 0$ in simulation only and not in the calculation of the input nudges. We can see from the figure how the input nudges with the entropy objective are smoother than the ones calculated with a quadratic cost. Additionally, we see that for the quadratic cost case, the text reminders were not used at all until almost 10 weeks from the beginning of the scheduling of nudges. This is not preferable since it is desired for the subject to be more acquainted with the different nudging techniques as early as possible to handle technical and personal difficulties from the beginning. The average rate of the behaviour $\beta(t)$ for both the quadratic objective case and the entropy objective case are very similar. For the case when $b_3 = 0$, the entropy objective case has a lower $\beta(t)$ curve over

time than the curve obtained with the quadratic objective. This is expected since maximizing the entropy encourage the use of all the available resources which offers robustness in case of the sudden absence of one resource or more.

4.3 Case with a Time-Varying Nudge Rate

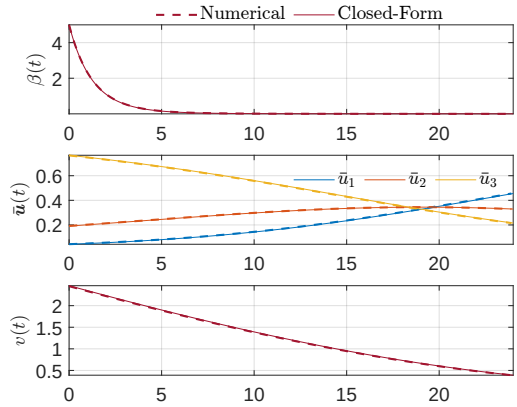

Fig. J.3: Numerical Solution (dashed) against the closed-form solution (solid) for OCPv.

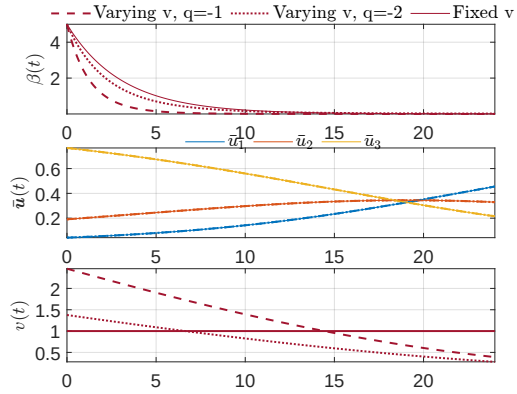

Fig. J.4: Comparison between the solutions with varying v with $q = -1$ (dashed), $q = -2$ (dotted), and with a fixed rate $v = 1$ (solid).

We consider in this section the same case in the previous section 4.2 but when we desire to optimize over $v(t)$. Figure J.3 shows the results when we choose $q = -1$ against a numerical solution obtained using CVX and SDP3. We observe from figure J.3 that the numerical solution matches the closed-form solution which further validates it. We notice from the solution that

the rate of nudges v at the beginning has a value greater than 2 [1/Week], and phone calls from medical staff have the highest share of the different types of nudges. Afterwards, the nudge rate v decreases to be below 1 [1/Week] throughout the solution while the reliance on text reminders is increasing to finally be the nudge with the highest contribution. Allowing v to vary gives the opportunity to lower it while the average behavioral rate $\beta(t)$ is decreasing, which prevents overburdening the subject with nudges that could lead to alert fatigue. In figure J.4, we compare the solutions when $v = 1$ with two cases of varying v with $q = -1$ and $q = -2$. We can see from the figure that for both of the cases of varying v, the average rate $\beta(t)$ decreases faster than the case of a fixed rate due to v starting with a value greater than 1. Additionally, we observe that the inputs $\bar{\boldsymbol{u}}$ are identical for all the cases with $\bar{u}_3$ being the highest at the beginning and the lowest towards the end. Notice how increasing $|q|$ will make v starts at a lower value which helps to reduce the risk of alert fatigue from the beginning.

4.4 Receding Horizon Case

In this section, we demonstrate how the solution of OCPv can be used in a receding horizon fashion to adapt to changes in the parameters of the model. We introduce "feedback" by utilizing recursively estimated values of the model's parameters for the computation of a new scheduling scheme. We choose $\rho = 5, q_p = 0.5q$, and $\eta_p = 10\eta$ in (J.8) for the receding horizon solution. For the simulation, we consider a case in which the effect b_3 of a phone call from the medical staff vanishes for a while during treatment according to $b_3(t) = 0.4 - 0.4\sigma(10(t-10)) + 0.4\sigma(10(t-18))$. Additionally, we consider a case in which the subject pays less attention to text messages on their phone over time captured by modifying the effects b_1 and b_2 according to $b_1(t) = 0.2\left(\frac{1}{2} + \frac{1}{2}\mathrm{e}^{-0.2t}\right)$ and $b_2(t) = 0.3\left(\frac{1}{2} + \frac{1}{2}\mathrm{e}^{-0.2t}\right)$. We simulate a case in which we have a perfect knowledge about $\boldsymbol{b}(t)$ (Nominal), and for a case in which we have an estimate of the effect of nudges. For the receding horizon case, we consider that every week t_j such that $t_j - t_{j-1} = 1$ [Week], $j \in \mathbb{Z}$, we obtain an estimate $\hat{\boldsymbol{b}}(t_j) = \boldsymbol{b}(t_j - 2/7) + 0.25\|\boldsymbol{b}(t_j - 2/7)\|_2\boldsymbol{\xi}(t_j)$ with $\boldsymbol{\xi}(t_j) \sim \mathcal{N}(\boldsymbol{0}, \boldsymbol{I})$[3]. The solution of the receding horizon for each week then uses a constant $\hat{\boldsymbol{b}}(t_j)$ for the entire week with $t_f = 24$ [Week]. The figure in J.5 shows the results. We can see from the results that the open loop response of β with the perfect knowledge of $\boldsymbol{b}(t)$ compared to the one with the receding horizon and imperfect knowledge of $\boldsymbol{b}$ are very similar. As for the inputs, we can see how they are affected by the noise and the delay during the simulation. Despite the presence of noise and delay, the receding horizon solution is able to follow the trend of the optimal open-loop solution for the case of a perfect knowledge of $\boldsymbol{b}(t)$.

[3]Several techniques could be used to obtain estimates of the model parameters with data. The data can contain the frequency of the undesired behaviour, feedback from the subject regarding the effectiveness of the different nudges, and data on how the subject responds to nudges such as the number of times they answer phone calls or read text messages (see [6]). Since the use of these techniques is out of the scope for this paper and the goal of this section is to demonstrate how receding horizon could work, we used a random additive error with a delay of two days to simulate estimation errors.

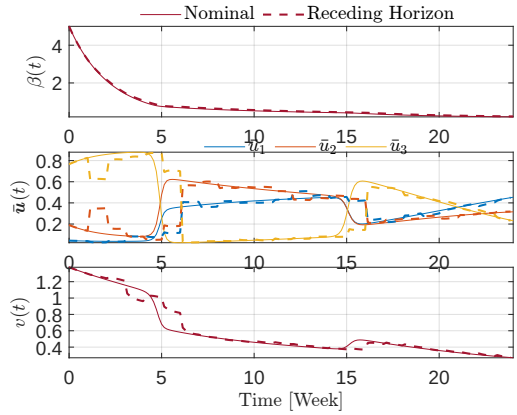

Fig. J.5: Solution for the Nominal case with a perfect knowledge of $\boldsymbol{b}(t)$ (solid) and a receding horizon case (dashed).

5 Conclusion and Future Work

We presented an OCP in which the inputs are constrained to a variable-sized simplex, with the size being another input to optimize over. We showed that with the inclusion of the entropy function in the objective, it is possible to derive closed-form solutions when the dynamics are linear, and the objectives are linear on the states and the simplex inputs, and quadratic on the size of the simplex. A possible future research direction is to study a more general class of OCPs with entropy and simplex constraints. We also demonstrated how the formulated OCP can potentially be used in conjunction with behavioral momentum theory in the help of scheduling nudges to discourage unhealthy behaviors, such as non-adherence to medication. This work is a starting point for utilizing control theory methods with the behavioral momentum theory for nudging design. Future work will focus on incorporating more complex behavioural momentum models, comparing this framework with different frameworks such as the one in [7], performing and developing system identification for behavioural momentum models, and applying the solutions in a real-life setting using a receding horizon approach.

A Maximization with Entropy

Consider $\boldsymbol{u} \in \triangle_{n_u}^{v}$ with $v \geq 0$. We will derive the solution for the following problem

$$\left(\boldsymbol{u}^*, v^*\right) = \underset{\boldsymbol{u} \in \triangle_{n_u}^{v}, v \geq 0}{\operatorname{argmax}} \frac{1}{\eta}\phi(\boldsymbol{u}) + \boldsymbol{\alpha}^{\mathrm{T}}\boldsymbol{u} + qv^2, \tag{J.14}$$

where $\eta > 0, q < 0$, and $\boldsymbol{\alpha} \in \mathbb{R}^{n_u}$. Define first the Lagrangian on $\operatorname{int}\left(\triangle_{n_u}^{v}\right) \times \mathbb{R}_{\geq 0}$ as

$$L = \frac{1}{\eta}\phi(\boldsymbol{u}) + \boldsymbol{\alpha}^{\mathrm{T}}\boldsymbol{u} + qv^2 + \boldsymbol{\lambda}^{\mathrm{T}}\boldsymbol{u} + \mu v + \zeta\left(v - \mathbf{1}^{\mathrm{T}}\boldsymbol{u}\right), \tag{J.15}$$

where $\boldsymbol{\lambda} \geq_e 0, \mu \geq 0$, and ζ are Lagrange multipliers. We proceed by writing the Karush–Kuhn–Tucker (KKT) conditions [15] which are sufficient since the problem is concave

$$\frac{-1}{\eta}\ln_e(\boldsymbol{u}) - \frac{1}{\eta}\mathbf{1} + \boldsymbol{\alpha} + \boldsymbol{\lambda} - \zeta\mathbf{1} = 0, \tag{J.16a}$$

$$2qv + \mu + \zeta = 0, \tag{J.16b}$$

$$\boldsymbol{u} \geq_e 0,\ u_i\lambda_i = 0,\ \forall i \in \{1, \ldots, n_u\}, \tag{J.16c}$$

$$v \geq 0,\ \mu v = 0, \tag{J.16d}$$

$$\mathbf{1}^{\mathrm{T}}\boldsymbol{u} = v. \tag{J.16e}$$

Since we are considering $\operatorname{int}\left(\triangle_{n_u}^{v}\right) \times \mathbb{R}_{\geq 0}$, we get $\boldsymbol{\lambda} = \mathbf{0}$ and $\mu = 0$ from (J.16c), (J.16e), and (J.16d). From (J.16a) we get $\boldsymbol{u} = \exp_e(\eta\boldsymbol{\alpha} - \mathbf{1} - \eta\zeta\mathbf{1}) >_e 0$. From (J.16b), we have $\zeta = -2qv$ which we substitute back in $\exp_e(\eta\boldsymbol{\alpha} - \mathbf{1} - \eta\zeta\mathbf{1})$ and use (J.16e) to get

$$\begin{aligned}\mathbf{1}^{\mathrm{T}}\exp_e(\eta\boldsymbol{\alpha})\exp(-1)\exp(2q\eta v) &= v,\\ \Rightarrow -2q\eta v\exp(-2q\eta v) &= -2q\eta\exp(-1)\mathbf{1}^{\mathrm{T}}\exp_e(\eta\boldsymbol{\alpha}).\end{aligned} \tag{J.17}$$

Equation (J.17) is in the form of $y\exp(y) = x$ with $x > 0$ ($q < 0$). The solution of this equation is known to be the principle branch of the Lambert W function $y = \mathrm{W}_0(x)$. With the Lambert W function, we solve (J.17) for v to obtain

$$v^* = \frac{-\mathrm{W}_0\left(-2q\eta\exp(-1)\mathbf{1}^{\mathrm{T}}\exp_e(\eta\boldsymbol{\alpha})\right)}{2q\eta} \tag{J.18a}$$

$$\boldsymbol{u}^* = \frac{v^*\exp_e(\eta\boldsymbol{\alpha})}{\mathbf{1}^{\mathrm{T}}\exp_e(\eta\boldsymbol{\alpha})}. \tag{J.18b}$$

Since the objective function in (J.14) is strictly concave on $\triangle_{n_u}^{v} \times \mathbb{R}_{\geq 0}$, then (J.18) is the unique maximizer on $\triangle_{n_u}^{v} \times \mathbb{R}_{\geq 0}$.

References

[1] H. Wang, T. Zariphopoulou, and X. Y. Zhou, "Exploration versus exploitation in reinforcement learning: A stochastic control approach," *Available at SSRN 3316387*, 2019.

[2] J. Kim and I. Yang, "Maximum entropy optimal control of continuous-time dynamical systems," *IEEE Transactions on Automatic Control*, 2022.

[3] A. Seierstad and K. Sydsaeter, *Optimal control theory with economic applications*. Elsevier North-Holland, Inc., 1986.

[4] B. D. Greer, W. W. Fisher, P. W. Romani *et al.*, "Behavioral momentum theory: A tutorial on response persistence," *The Behavior Analyst*, vol. 39, pp. 269–291, 2016.

[5] Y. Chen, S. Harris, Y. Rogers *et al.*, "Nudging within learning health systems: next generation decision support to improve cardiovascular care," *European Heart Journal*, vol. 43, no. 13, pp. 1296–1306, 2022.

[6] B. D. Horne, J. B. Muhlestein *et al.*, "Behavioral nudges as patient decision support for medication adherence: the encourage randomized controlled trial," *American Heart Journal*, vol. 244, pp. 125–134, 2022.

[7] F. Callaway, M. Hardy, and T. Griffiths, "Optimal nudging for cognitively bounded agents: A framework for modeling, predicting, and controlling the effects of choice architectures," Jan 2022. [Online]. Available: psyarxiv.com/7ahdc.

[8] C.-T. Chen, *Linear system theory and design*. Saunders college publishing, 1984.

[9] K. G. Murty and S. N. Kabadi, "Some np-complete problems in quadratic and nonlinear programming," Tech. Rep., 1985.

[10] J. A. Nevin and T. A. Shahan, "Behavioral momentum theory: Equations and applications," *Journal of Applied Behavior Analysis*, vol. 44, no. 4, pp. 877–895, 2011.

[11] B. S. Last, A. M. Buttenheim *et al.*, "Systematic review of clinician-directed nudges in healthcare contexts," *BMJ open*, vol. 11, no. 7, p. e048801, 2021.

[12] F. B. Hanson, *Applied stochastic processes and control for jump-diffusions: modeling, analysis and computation*. SIAM, 2007.

[13] K.-C. Toh, M. J. Todd, and R. H. Tütüncü, "Sdpt3—a matlab software package for semidefinite programming, version 1.3," *Optimization methods and software*, vol. 11, no. 1-4, pp. 545–581, 1999.

[14] M. Grant and S. Boyd, "CVX: Matlab software for disciplined convex programming, version 2.2," http://cvxr.com/cvx, Jan. 2020.

[15] W. Karush, "Minima of functions of several variables with inequalities as side conditions," in *Traces and Emergence of Nonlinear Programming*. Springer, 2014, pp. 217–245.

ISSN (online): 2446-1628
ISBN (online): 978-87-7573-651-5

AALBORG UNIVERSITY PRESS